2021

MASS SPECTROMETRY METHOD DEVELOPMENT FOR THE DISCOVERY AND CHARACTERIZATION OF SECONDARY METABOLITES

Zachary Kelley
University of Kentucky, zachkelley64@yahoo.com
Author ORCID Identifier:
https://orcid.org/0000-0002-7076-5450
Digital Object Identifier: https://doi.org/10.13023/etd.2021.282

STUDENT AGREEMENT:

I represent that my thesis or dissertation and abstract are my original work. Proper attribution has been given to all outside sources. I understand that I am solely responsible for obtaining any needed copyright permissions. I have obtained needed written permission statement(s) from the owner(s) of each third-party copyrighted matter to be included in my work, allowing electronic distribution (if such use is not permitted by the fair use doctrine) which will be submitted to UKnowledge as Additional File.

I hereby grant to The University of Kentucky and its agents the irrevocable, non-exclusive, and royalty-free license to archive and make accessible my work in whole or in part in all forms of media, now or hereafter known. I agree that the document mentioned above may be made available immediately for worldwide access unless an embargo applies.

I retain all other ownership rights to the copyright of my work. I also retain the right to use in future works (such as articles or books) all or part of my work. I understand that I am free to register the copyright to my work.

REVIEW, APPROVAL AND ACCEPTANCE

The document mentioned above has been reviewed and accepted by the student's advisor, on behalf of the advisory committee, and by the Director of Graduate Studies (DGS), on behalf of the program; we verify that this is the final, approved version of the student's thesis including all changes required by the advisory committee. The undersigned agree to abide by the statements above.

Zachary Kelley, Student

Dr. Bert Lynn, Major Professor

Dr. Yinan Wei, Director of Graduate Studies

MASS SPECTROMETRY METHOD DEVELOPMENT FOR THE DISCOVERY AND CHARACTERIZATION OF SECONDARY METABOLITES

DISSERTATION

A dissertation submitted in partial fulfillment of the
requirements for the degree of Doctor of Philosophy in the
College of Arts and Sciences
at the University of Kentucky

By
Zachary David Kelley
Lexington, Kentucky
Director: Dr. Bert C. Lynn, Professor of Chemistry
Lexington, Kentucky
2021

https://orcid.org/0000-0002-7076-5450

ABSTRACT OF DISSERTATION

MASS SPECTROMETRY METHOD DEVELOPMENT FOR THE DISCOVERY AND CHARACTERIZATION OF SECONDARY METABOLITES

Secondary metabolites are organic compounds produced by an organism for reasons other than growth and development. In plants, secondary metabolites generally act as defense agents produced to deter predators and inhibit other competitive species. For humans, these compounds can often have a beneficial effect and are pursued and utilized as natural pharmaceuticals. The development of sensitive, high-throughput analytical screening methods for plant derived metabolites is crucial for natural pharmaceutical product discovery and plant metabolomic profiling. Here, metabolomic profiling methods were developed using a microfluidic capillary zone electrophoresis device and evaluated against traditional separation approaches. An alkaloid screening assay was constructed to analyze transgenic mutant plant extracts for novel metabolites. Putatively identified novel features were detected, elucidated, and then isolated and purified for pharmaceutical evaluation. Additionally, methods for the analysis of polyphenolic plant-derived secondary metabolites, such as cannabinoids, were also developed and evaluated. In this case, the occurrence of cross-instrumental variation was addressed, given the tight legal restrictions regarding commercialization the products in question. Lastly, the microfluidic CZE-MS methods were further applied for both primary and secondary metabolite profiling in a DMPK assay. This assay was developed to inclusively monitor metabolic changes as a response to varying concentrations of a therapeutic in circulation. The metabolomic methods developed and evaluated in this work displayed high sensitivity, efficiency, and accuracy and can be utilized across a wide variety of applications.

KEYWORDS: Mass Spectrometry, Capillary Electrophoresis, Alkaloids, Secondary Metabolites, Metabolomics

Zachary Kelley

(Name of Student)

7/16/2021

Date

MASS SPECTROMETRY METHOD DEVELOPMENT FOR THE DISCOVERY AND CHARACTERIZATION OF SECONDARY METABOLITES

By
Zachary David Kelley

Dr. Bert C. Lynn
Director of Dissertation

Dr. Yinan Wei
Director of Graduate Studies

07/16/2021
Date

Dedicated to

Amanda, Barry, and my family,
My never-ending sources of love, support, and encouragement throughout this voyage.

ACKNOWLEDGMENTS

First of all, I would like to sincerely thank my advisor, Dr. Bert C. Lynn, for his patience, guidance, encouragement, and friendship throughout the last five years. Through his thought-provoking teachings and constant push for me to continuously ask "why?", I truly feel that I have immensely grown as both a scientist and as a person. I have no doubts in my mind that I picked the perfect advisor for my graduate program and will be forever grateful for my time in his research group. I look forward to continuing our relationship as colleagues and catching up in the future at the annual ASMS meetings.

I would also like to thank my committee members, Dr. Mark A. Lovell, Dr. Stephen M. Testa, and Dr. Brian C. Rymond for their support and constructive feedback through-out the years. Even through a project change and the challenges of a pandemic, they always took the time to help guide me in the right direction and push me to widen my scientific skillset. Additionally, many thanks to everyone at Naprogenix LLC, especially Dr. John Littleton and Dr. Trent Rogers, for supporting me with a research assistantship throughout most of my graduate career. My time with the company has been invaluable and has opened the doors to so many opportunities already.

I am also very thankful for my colleagues in the Lynn lab, both past and present, for their friendship and support. From teaching each other and learning about our cultural differences to working through complicated experiments and instrumental issues, I will also look back on our time together with fondness and I can't wait to see what the future has in store for everyone. Special thanks to my other graduate school colleagues and the

Chemistry Department faculty and staff for further enriching my time in the program as well.

I will also be forever thankful for my wonderful family and friends. Between the early morning calls with my mom, Laura, during our morning commutes to the weekly Tuesday night chats with my dad, Stephen, I never felt far from my family or unsupported, despite the long distance between us. To all of my siblings, both by birth and by marriage, for the laughs when I needed them most and their advice during the tough decisions. To my friends for making Kentucky feel like home and always making me feel welcomed and appreciated. I am extremely fortunate to have so many wonderful people in my life and I truly cherish all of you.

Lastly, I would like to thank my partner through it all, Amanda. Graduate school is challenging, but she made it is so much easier through her constant encouragement, understanding, and love. She believed in me every day, even when I didn't believe in myself, and gave me a reason to keep pushing on when I wanted to quit. I am truly blessed to have such a wonderful partner and will be eternally grateful for everything that she has done and sacrificed for me to help me through this journey. Having her by my side is one of the main reasons that I have made it this far and I can't wait to see what adventures the future has in store for us next.

TABLE OF CONTENTS

LIST OF TABLES

LIST OF FIGURES

LIST OF ABBREVIATIONS AND SYMBOLS

ABC	Acid-Base Chloroform
ABCXC	Acid-Base Chloroform-Xylene-Chloroform
ACN	Acetonitrile
ADME	Administration Distribution Metabolism Excretion
APCI	Atmospheric Pressure Chemical Ionization
API	Atmospheric Pressure Ionization
APPI	Atmospheric Pressure Photoionization
BGE	Background Electrolyte
CBC	Cannabichromene
CBD	Cannabidiol
CBDA	Cannibindiolic Acid
CBDV	Cannabidivarin
CBG	Cannabigerol
CBN	Cannabinol
CE	Capillary Electrophoresis
CEC	Capillary Electro-Chromatography
CHCl3	Chloroform
CI	Chemical Ionization
CID	Collision-Induced Dissociation
CRM	Charged Residue Model
CZE	Capillary Zone Electrophoresis
DDA	Data-Dependent Analysis
DEA	Drug Enforcement Agency
EI	Electron-Impact Ionization
EOF	Electroosmotic Flow
EPA	Environmental Protection Agency
ESI	Electrospray Ionization
FIA	Flow-Injection Analysis
FT-ICR	Fourier-Transform Ion Cyclotron Resonance
FWHM	Full-Width At Half Max
GC	Gas Chromatography
HCD	Higher-Energy Collision Dissociation
HCl	Hydrochloric Acid
hDAT	Human Dopamine Transporter
HESI	Heated Electrospray Ionization
HETP	Height Equivalent of the Theoretical Plate
HPLC	High Pressure Liquid Chromatography
HRAM	High Resolution Accurate Mass
IEM	Ion-Evaporation Model
ITP	Isotachophoresis
LC	Liquid Chromatography

LE	Leading Electrolyte
LOQ	Limit Of Quantification
m/z	Mass-To-Charge Ratio
MALDI	Matrix-Assisted Laser Desorption Ionization
mCPBA	Meta-Chloroperoxypbenzioc Acid
MDL	Method Detection Limit
MEKC	Micellar Electrokinetic Chromatography
MeOH	Methanol
MS	Mass Spectrometry
MS/MS	Tandem Mass Spectrometry
MT	Migration Time
NaCl	Sodium Chloride
NCE	Normalize Collision Energy
PFPP	Perfluorophenylpropyl
pHPLC	Preparative High Performance Liquid Chromatography
PK	Pharmacokinetics
PRM	Parallel Reaction Monitoring
QIT	Quadrupole Ion Trap
QqQ	Triple Quadrupole Mass Spectrometer
QuEChERS	Quick-Easy-Cheap-Effective-Rugged-Safe
RP	Resolving Power
RSD	Relative Standard Deviation
RT	Retention Time
SIM	Single Ion Monitoring
SIMS	Secondary Ion Mass Spectrometry
SPE	Solid Phase Extraction
SUD	Substance Use Disorder
TCM	Traditional Chinese Medicine
TE	Trailing Electrolyte
THC	Tetrahydrocannabinol
THCA	Tetrahydrocannabinolic Acid
THCV	Tetrahydrocannabivarin
TIC	Total Ion Current
tITP	Transient Isotachophoresis
TSG	Tetrahydroxystilbene Glucoside
uHPLC/UHPLC/UPLC	Ultra-High Pressure Liquid Chromatography
UV	Ultraviolet
WT	Wild Type
ZCI	Zipchip Interface

CHAPTER 1. INTRODUCTION

Background

The term "natural products" refers to the class of chemical compounds arising from biological sources of production ranging from simple bacteria to complex plants, fungi, and animals. These chemical entities arise from both primary and secondary metabolic pathways. Natural products have been used medicinally across the world for thousands of years, with recorded uses dating back as far as 2600 BC in Mesopotamia.[1–3] Though diverse in origin, it has been reported that over 50% of natural products commercially available for a variety of uses are plant derived secondary metabolites.[3–6] These plant-derived natural products are also the foundation behind a majority of traditional Chinese medicines (TCM).[2,7] Organic and medicinal chemists have found interest in these novel metabolites and extensively investigate their chemical properties and pharmacological activities. These investigations of natural products have motivated method development for new practical separation techniques, structure elucidation experiments, and synthetic methodologies that now constitute the foundations of modern organic, analytical, and medicinal chemistry. This interest in natural products has been both academic and driven by the potential industrial impact of their complex biosynthesis and application.[7] Natural products are commonly commercialized as dyes, industrial fibers, adhesives, oils, waxes, flavors, fragrances, and, most importantly, pharmaceuticals.[2,7] Recognition of the potential biological activity associated with a myriad of natural products has fueled the current focus of this field, specifically, the search for new pharmaceuticals, antibiotics, and pesticides. This field is also a source of many analytical challenges. The complex nature of these metabolites paired with the wide variety of compounds with subtly

different variations to their structures all found within the same organism greatly complicate the analysis and characterization of these compounds. These complexities and similarities also complicate downstream purification for pharmacological testing and production. The focus of this work is to develop new metabolomics-centered analytical methods for the discovery and characterization of several types of secondary plant metabolites.

Secondary Metabolites and Metabolomics

The metabolic products produced by all living organisms are classified as either primary or secondary metabolites. Primary metabolites are fairly conserved across all living organisms and consist of groups of small molecules that are crucial for survival such as nucleic acids, amino acids, and lipids.[7] Secondary metabolites are organic molecules that are not necessarily essential to the normal growth or development of an organism.[7] While primary metabolites have a key role in the survival of the species, the absence of secondary metabolites does not result in immediate death, but rather in long-term impairment of the organism's survivability, as they often play an important role in defense. There is some ambiguity in the classification, however, as many primary and secondary metabolites share biosynthetic pathways or similar base structures. Secondary metabolites are produced by all types of organisms, but the most commonly discussed secondary metabolites are those produced by plants.[7–10] Most plant secondary metabolites, such as terpenes, phenolic compounds, and alkaloids are classified based on their biosynthetic origin or key chemical functional groups. Figure 1.1 displays some common examples of terpenes, phenolics, nitrogen-based compounds (alkaloids), and

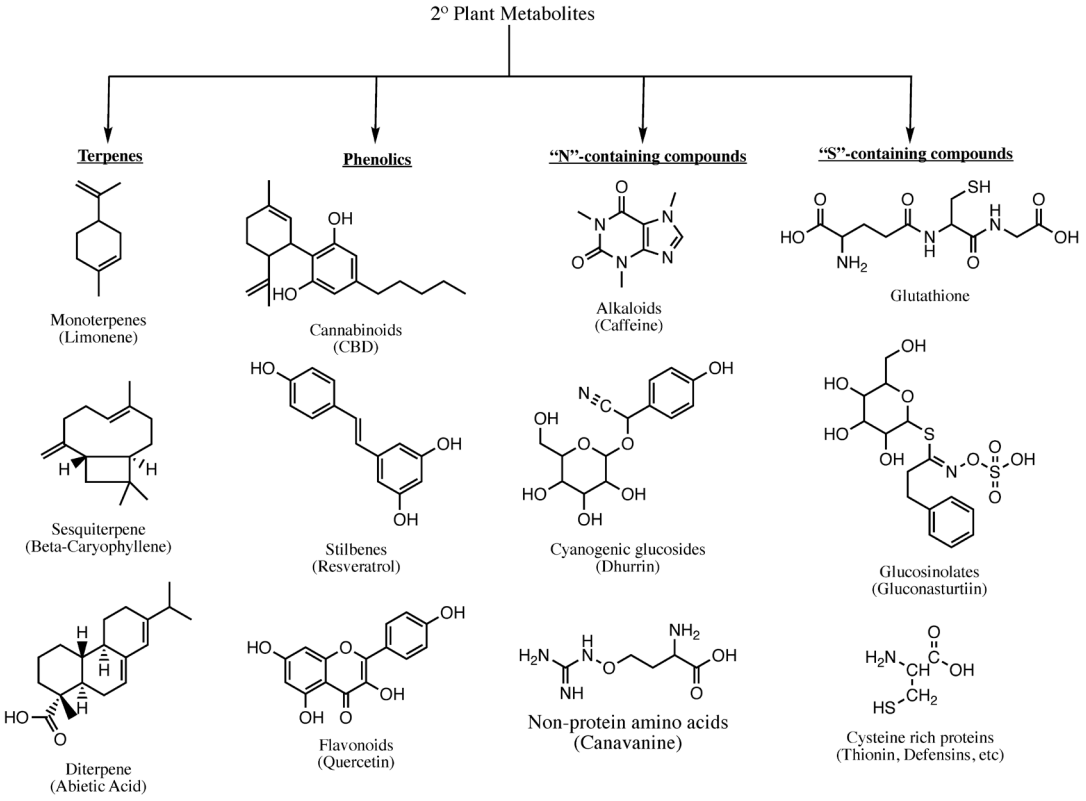

Figure 1. 1 Common classes of secondary plant metabolites with representative examples.

sulfur-based compounds. Terpenes, the largest class with over 25,000 known compounds, consist of varying combinations of isoprene subunits, with subclasses based on the number of subunits. Terpenes are highly volatile compounds often associated with the scent of a plant (pinene, limonene, myrcene, linalool, etc). Phenolic compounds, though less diverse with approximately 8000 identified secondary metabolites, make up a larger portion of the total biomass of plants due to lignin falling under the category. This subclass also contains more homologous secondary metabolites conserved across numerous species such as various stilbenes, flavonoids, anthraquinones, and tannins. Lastly are the more exotic nitrogen or, less common, sulfur containing compounds. These metabolites are usually derived from amino acids, specifically in the case of true alkaloids, and are the most heterologous of secondary metabolites.[11] Despite the vast diversity of these secondary metabolites, both within and between classes, similarities can be observed in their biosynthesis (Figure 1.2). Primary biosynthetic pathways, such as the shikimate, phenylpropanoid, and polyketide pathways, are fairly conserved across species, with differences not usually occurring until the later enzymatic conversions.[12]

The role of many of these metabolites in plants has been a subject of debate as there are multiple plausible explanations for their presence. Several hypotheses have been presented: 1) they are the byproducts of mutations and are not harmful or beneficial, 2) they are an example of "evolution in progress" in that they are the result of the organism attempting to make new functional metabolites, 3) they are waste products, 4) further expanding on 2), the enzymes responsible for their production are the result of prophylactic measures to ensure primary metabolism is unhindered, 5) they formerly had a functional role that has since been defunct, and lastly, and most likely, 6) they have

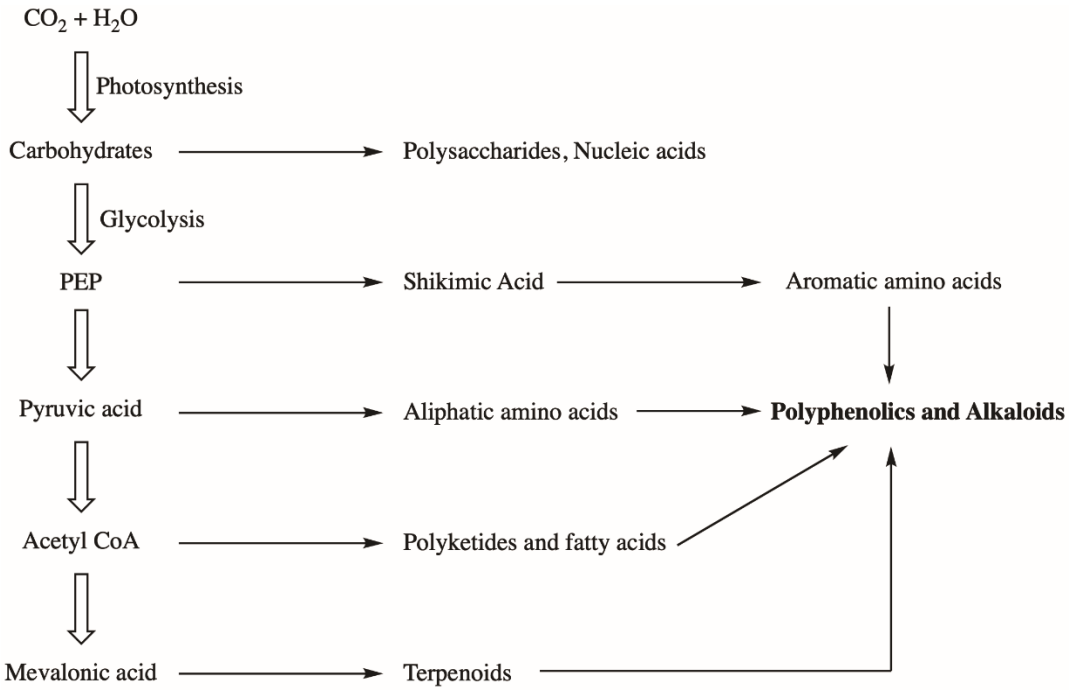

Figure 1. 2 Simplified biosynthetic pathway for the sources of polyphenolic and alkaloid secondary metabolites.

resulted as evolutionary responses to aid in the survival of the plant by acting as attractors or deterrents.[13,14] It is also likely that all six hypotheses are true to an extent, however the sixth would confer the most evolutionary advantage. As attractors, such as pigments or fragrances, these metabolites could function to attract for pollinators or be secreted in resins as defense agents to trap predators and insects.[14,15] As deterrents, bitter taste as well as antibiotic and antimicrobial activities are often associated with many secondary metabolites. A defense-centric evolutionary impact can also be inferred in that environmental stressors, such as microbial exposure, UV light, temperature, and chemical exposure can often affect the relative expression rate of these metabolites.[16]

The activity and application associated with these plant secondary metabolites has been of interest to humans for centuries. Traditional Chinese Medicine (TCM) texts, such as the The Chinese Materia Medica (1100 B.C.), list various plant-based treatments in the form of ointments, tinctures, and extracts.[2] Unfortunately, many of the both beneficial and determinantal effects discovered before the advent of modern science were the result of trial and error driven by the growing necessity of curing new diseases and ailments.[17] Modern controlled *in vitro* and *in vivo* assays have since reduced the risk behind testing the efficacy of these metabolites and have allowed scientists to uncover the specific sources of the activity. These scientific advances have resulted in not only a massive academic field, especially in eastern cultures, focusing on understanding how ancient remedies, such as those found throughout TCM, function, but also in the development of lead compounds with industrial application and as treatments for many diseases and conditions. Figure 1.3 shows an example of three out of the thousands of naturally derived compounds, of varying complexity, that see use in both industry and as

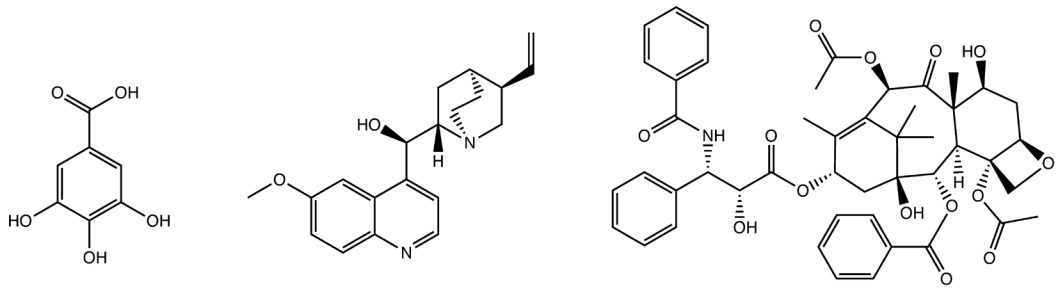

Gallic acid - polyphenolic
Chemical Formula: $C_7H_6O_5$

Quinine - Alkaloid
Chemical Formula: $C_{21}H_{28}N_2O_2$

Paclitaxel - Taxane class of diterpene
Chemical Formula: $C_{47}H_{51}NO_{14}$

Figure 1. 3 Common industrial and pharmaceutical natural products.

pharmaceuticals. Gallic acid, a simple acidic, phenolic secondary metabolite, is widely utilized as a dye, an excellent base molecule for organic synthesis, and even as a treatment for reducing coronary arterial disease and arterial thrombosis.[18] Quinine, a more complex quinoline alkaloid approved by the FDA in 2004 for pharmaceutical use, had been used for centuries for the treatment of malaria, fever, indigestion, mouth and throat diseases and cancer.[2,7,19] Increasing in complexity, paclitaxel (Taxol®) isolated from the bark of *Taxus brevifolia,* has been widely utilized as a chemotherapeutic agent for the treatment of ovarian, esophageal, breast, lung, cervical, and pancreatic cancer.[2,4,17,19–24] Despite paclitaxel's complexity, the application of the metabolite has caused the demand to exceed what is practical in terms of natural isolation (~2g per treatment requires the bark of six 100-year-old trees versus 50,000 treatments annually), therefore synthetic and semi-synthetic methods have been developed.[2,19] The demand for these naturally-derived products has increased exponentially over the past few decades, owing to the success of therapeutics like paclitaxel and the avoidance of complex organic synthesis to design lead compounds for initial testing. Additionally, the public desire for more "natural" consumer products has further compelled interest in refocusing research towards identification and application of these metabolites.

Not all aspects of the secondary metabolite natural product field are positive, however. Drug abuse has plagued society throughout the history of both modern and ancient medicine. Almost all commonly abused drugs (Figure 1.4) are of natural origin. The most historically well-known abused natural products would be those derived from the alkaloid, morphine, produced by the opium poppy, *Papaver somniferum.* Morphine is a schedule II-controlled substance that acts on the opioid receptors and is a powerful

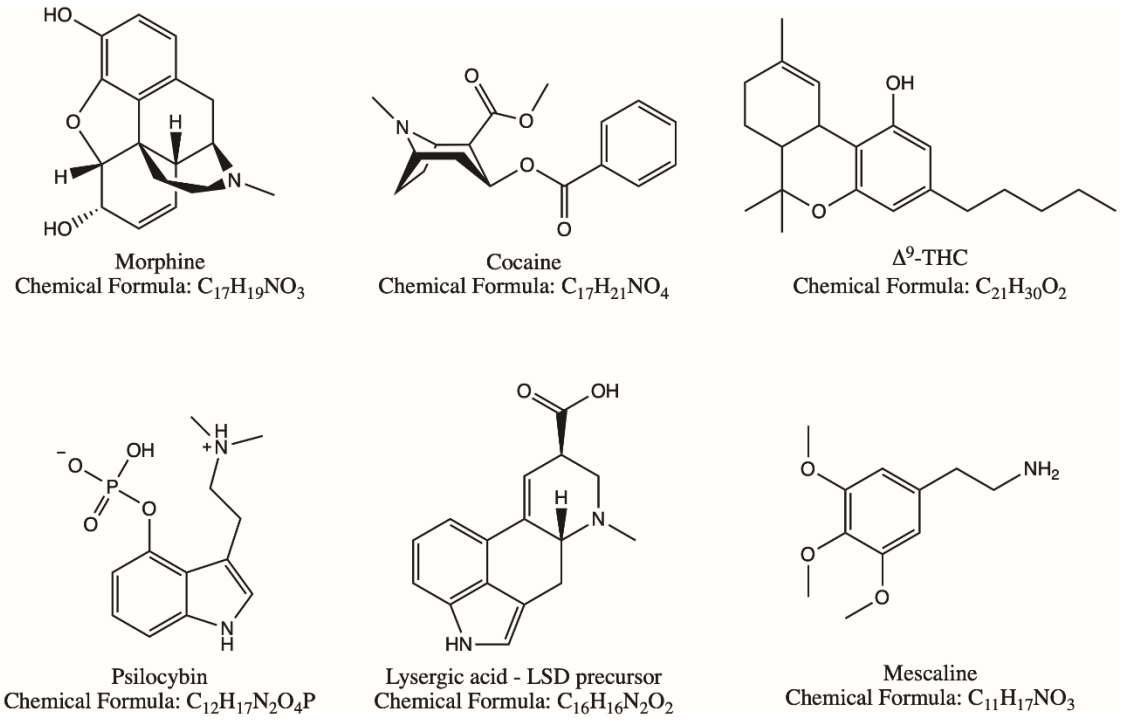

Figure 1. 4 Secondary plant metabolites often abused as recreational drugs.

narcotic analgesic and highly addictive drug of abuse. It is also the precursor to heroin, diacetylmorphine, a schedule I-controlled substance twice as potent as its precursor.[16,22] Cocaine is a tropane alkaloid derived from the leaves of *Erythroxylon coca*. It is a schedule II-controlled topical anesthetic, potent central nervous system stimulant, and adrenergic blocking agent.[16,22] Cannabinoids, such as Δ^9–THC, are a unique class of secondary metabolites derived from the buds of various *Cannabis* plant species, such as *Cannabis sativa* and *Cannabis indica*. Various schedules (III-V) are assigned to the cannabinoids, however, they are not considered to be of high risk for abuse and have been legalized for reactional use in several states. Psilocybin (fungal secondary metabolite derived from various members of the genus *Psilocybe*), lysergic acid (precursor to LSD, or "acid", derived from ergot fungus and found in the seeds of various flowering plants), and mescaline (protoalkaloid found in the peyote cactus, *Lophophora williamsii*) all hallucinogenic or psychedelic schedule I-controlled substances.[7,22] Despite the risk of abuse, the beneficial applications of secondary metabolite natural products maintain the necessity for the continued effort and investigations in regards to these complex and novel metabolic entities.

The discovery and characterization of these complex metabolites presents an analytical challenge. When testing for possible activity, inclusive whole plant extracts or simple partitions of the extracts are screened in a high-throughput manner. If activity is observed, analytical chemists are then tasked with the difficult process of generating inclusive metabolite profiles of the whole or fractionated extracts to determine the molecular constituents that may be the source of the activity. The generation of these metabolite profile is the basis for the field of metabolomics (Figure 1.5).

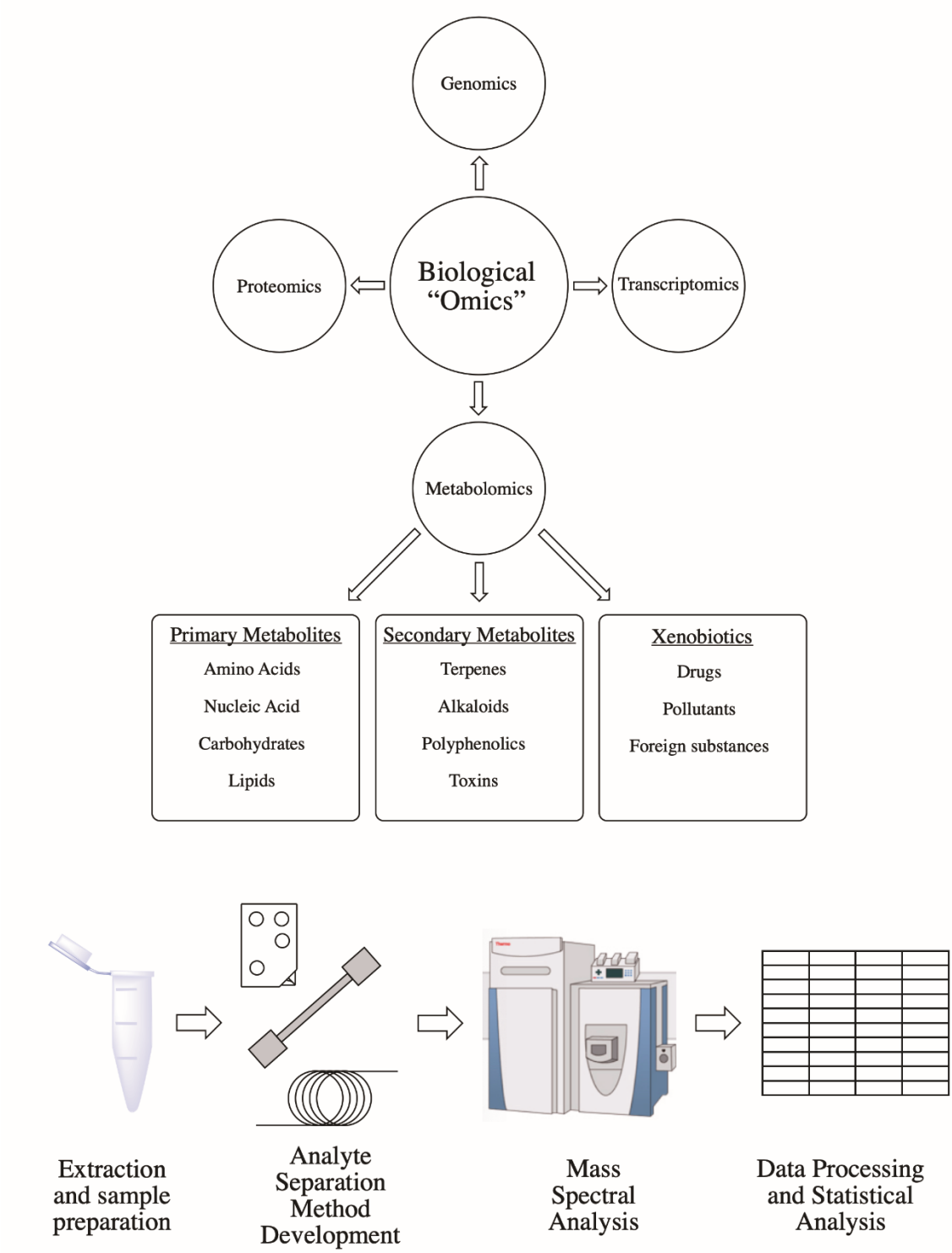

Figure 1. 5 Metabolomics, a branch of the "-omic" sciences, and the general workflow for metabolomic profiling.

Metabolomics is a branch of the "-omic" sciences defined as the "systematic study of the unique chemical fingerprints that specific cellular processes leave behind."[25–27] When paired with the other "-omic" sciences, such as genomics, transcriptomics, and proteomics, metabolomics can provide information in regards to the phenotypic expression of different organisms, especially plants. The analytical targets of these analyses are largely primary and secondary metabolites with molecular weights less than 1500 Da.[26] Comprehensive metabolomic profiling assays typically focus on dividing the metabolome into subsets of metabolites, usually based on compound polarity, common functional groups, or structural similarity. From there, specific sample preparation or extraction methods and analytical procedures are developed and optimized for each subset.[25,26] This leads to a patchwork effect when attempting to discuss an organisms entire metabolome. Focused efforts have been placed on developing new and efficient separation and analytical techniques to aid in the deconvolution of these complex datasets. With over 6,500 common known metabolites recorded, these analyses can be cumbersome and complicated.[25] Metabolomic databases, such as METLIN - developed by the Scripps Research Institute, have been developed to aid in the process and, as of 2021, consist of over 850,000 entries. The primary analytical tools used for metabolomic profiling consist of a form of chromatographic or electropherographic separation (gas chromatography -GC, liquid chromatography – LC, or capillary electrophoresis – CE) coupled to mass spectrometry. As new metabolomics methods are developed and technological advancements are made in the field of mass spectrometry, metabolomic profiles will become more and more pivotal to our understanding of an organism's metabolic expression and aid in the discovery of new and novel secondary metabolites.

Mass Spectrometry

The framework for what we now know as modern mass spectrometry was first laid by Sir J. J. Thompson with his discovery of the electron in 1897 and description of an analytes mass-to-charge ratio, or "m/z".[28,29] Over a decade later in 1912, Thompson invented the first mass spectrometer, then known as the "parabola spectrograph".[28] In the century since its invention, the field of mass spectrometry has seen numerous revolutionary advancements, furthering the technology to a point where it is regularly applied across nearly every scientific discipline. To better understand the magnitude of these advancements, for example, the improvement of mass resolution can be examined. A mass spectrometer's resolving power is described as the ability of the instrument to separate two mass spectral peaks and is calculated by analyzing the ratio of an analytes' mass to the width of the observed mass spectral peak.[28] Thompson's parabola spectrograph had a resolving power (RP) of approximately 13, meaning that an ion at m/z 150 would have a mass spectral peak ranging ~11.5 mass units from approximately m/z 144 to m/z 156.[28] Modern instruments, such as the widely utilized Thermo Q Exactive High Resolution Accurate Mass (HRAM) orbitrap mass spectrometer (RP=140,000) or the Bruker Scimax (RP= 20,000,000) would detect the same mass peak with widths less than 0.001 and 0.000001 respectively. The continued evolution, development, and wide application of this analytical tool has further strengthened mass spectrometry as one of the most useful and important analytical tools in modern science.

Though a variety of different types of mass spectrometers have been developed, their general working principle is fairly conserved. Samples and analytes are delivered to the instrument using an external device such as an LC, GC, or a simple syringe pump.[30]

Upon delivery, the analytes are ionized, using a variety of ionization sources, and introduced into the mass spectrometer. Ionization source selection is dependent on the nature of the sample matrix and chemical properties of the analytes themselves. Upon ionization, the newly formed ions are separated by a mass analyzer. The mass analyzer is the section of the instrument responsible for the instruments' resolving power and they are significantly more diverse than the ionization sources. Modern instruments often employ more than one of these components, aiding to their higher resolving powers and allowing them to be utilized for controlled fragmentation of selected ions, thus providing structural information of the analytes as well. Following separation of the ions by the analyzers, the ions strike a detection plate inducing an electron cascade, in the case of an electron multiplier, and the amplified response is converted into the aforementioned mass-to-charge ratio (m/z). In addition to these components, a complex high vacuum system is employed throughout the mass spectrometer to maintain a "mean-free path" to allow the ions to travel through to the detector uninterrupted. These high vacuum systems can reach pressures often as low as 10^{-10} mbar. A general block diagram of a mass spectrometer can be seen in Figure 1.6. The following sections will discuss the finer details of some of these mass spectral components to further elucidate the inner workings of these complex instruments.

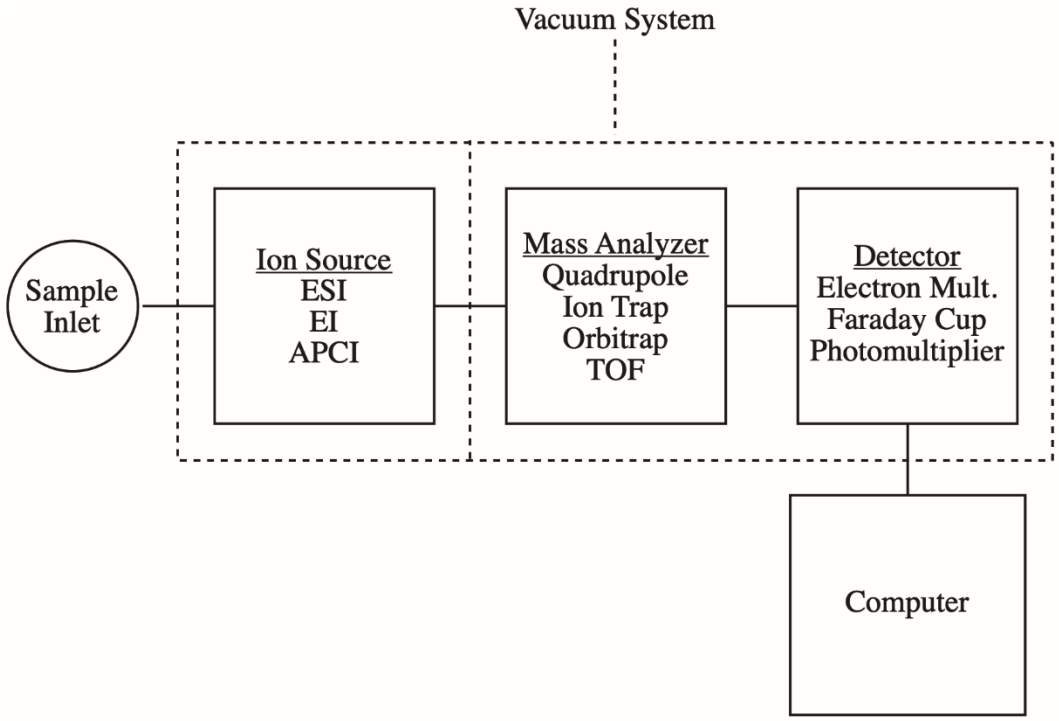

Figure 1. 6 Mass spectrometer block diagram.

1.1.1 Ionization Sources

As stated above, analytes must be ionized prior to their separation by the mass analyzer. There are a number of ionization techniques employed by modern mass spectrometers and the choice is usually dependent on the particular experiment, specifically, if a prior form of separation is in place (i.e. LC or GC) and the physical nature of the analyte. Ionization sources can be generally grouped by the phase requirements of the analytes for proper ionization. Electron ionization (EI) and chemical ionization (CI) require analytes to be in the gas phase under vacuum for ionization using electrons emitted by a heated filament.[28,30,31] These methods are generally employed for GC applications and result in fragmentation of the analytes into fragment ions, classifying these as "hard ionization methods". Other, more niche, ionization methods, like MALDI (matrix-assisted laser desorption ionization) and SIMS (secondary ion mass spectrometry), employ lasers or primary ion beams to 'desorb' sample molecules that ionize in the subsequent gas phase from a solid surface, such as a MALDI target. These sources are better suited for higher mass analytes (>500). The work found in this dissertation centers around the use of atmospheric pressure ionization (API) methods, specifically, electrospray ionization (ESI). API methods are considered to be "soft" ionization methods, in that the analytes are usually detected as intact ions resulting from either protonation/deprotonation or cation/anion adduct formation, depending on the polarity of the source.[32–35] Aside from ESI, atmospheric pressure chemical ionization (APCI) and atmospheric pressure photoionization (APPI) are also classified as API methods. In APCI, a coronal discharge is used to ionize a reagent gas which then interacts with and subsequently ionizes the desolvated analytes through interactions such

as a proton transfer.[28,30,33] In APPI, a hydrogen or krypton discharge lamp is used to produce 10-10.6 eV photons to ionize analytes that have ionization energy below that of the emitted photon.[30] Both APPI and APCI are fairly similar and only differ in the usage of a photon source rather than the coronal discharge. The method primarily used in this work, however, is ESI. John Fenn first developed ESI in 1988 and subsequently was awarded a Nobel Prize in 2002 for his contributions.[28,30,32] It is arguably the most widely utilized ionization source in modern mass spectrometry applications, especially when coupling liquid chromatography. In ESI, analytes within a solution are pumped through a stainless-steel emitter, or "spray needle", that is held at a higher potential in regard to the inlet of the mass spectrometer. As the solvent solution is pumped through the needle, the applied potential causes a "Taylor cone" to form as a combinatorial result of the dipole of water in the solvent solution and repulsion of the cations/anions dissolved in solution depending on the polarity of the applied potential. In addition to the applied potential, a stream of nitrogen gas is also supplied to aid in aerosolization and desolvation of the solvated analytes into ions. Droplets are emitted from the tip of the Taylor Cone as a result of increasing charge density. The droplets consist of both charged species (protons and cations for positive ion mode) and solvated analytes and move toward the inlet of the mass spectrometer, driven by both the supplied nitrogen stream and the potential difference. The subsequent mechanism of ESI in which the droplets convert to single ionized analytes has been explained using two separate models, though it is likely that the actual mechanism is a combination of both models. The first model, the Ion Evaporation Model (IEM – Figure 1.7) states that, as the droplets evaporate as a function of the desolvation process, the charge density increases.

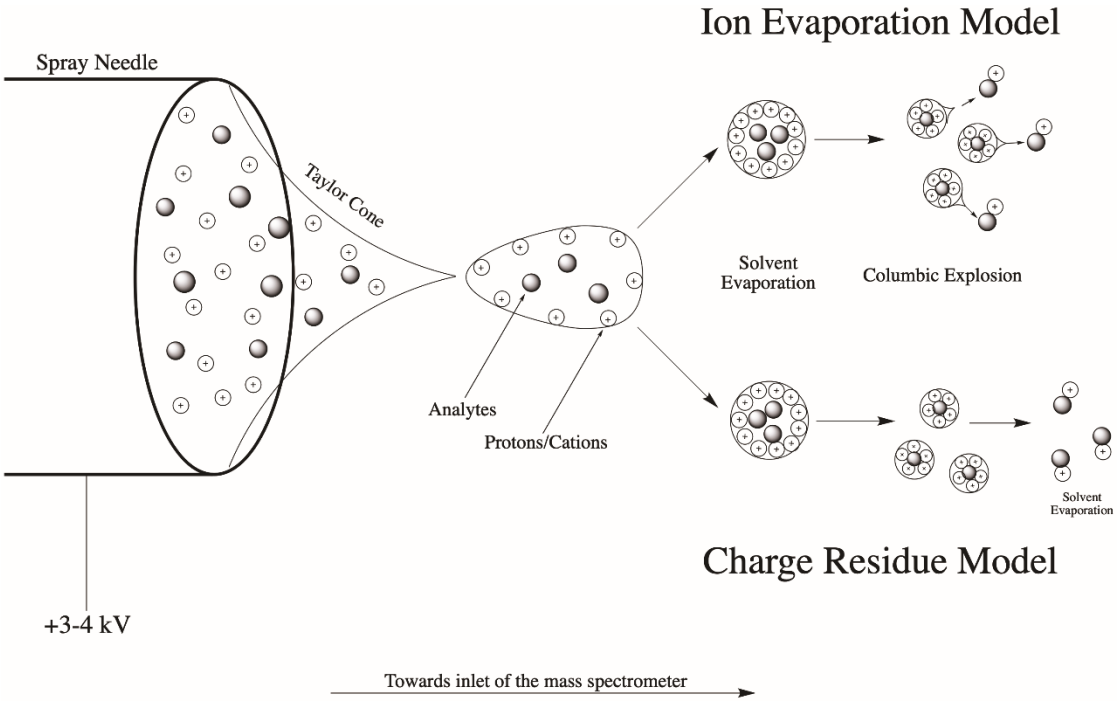

Figure 1. 7 Electrospray ionization diagram displaying both the ion evaporation model (IEM) and the charged residue model (CRM).

Once the charge density has reached a point known as the Rayleigh limit, the repulsion of the like-charged ions overcomes the surface tension of the droplet and analyte ions are ejected in a similar manner to how the droplets are ejected from the Taylor Cone.[28,30,32–35] For the second model, the Charged Residue Model (CRM – Figure 1.7), when the Rayleigh limit has been reached, it is believed that the droplets undergo serial fissions as a result of coulombic explosions. These sequential fissions continue until only single analyte ions remain and enter the gas phase.[1,3,5-8] The electrospray process is widely applicable and can be utilized at a variety of flow rates ranging from mL/min to nL/min depending on the application and the parameters in place.[30]

1.1.2 Mass Analyzers

Mass spectrometers are usually classified in terms of their mass analyzers. The two main classes of analyzers are "beam" analyzers, such as magnetic sector, quadrupole, and time-of-flight analyzers, and "trapping" analyzers, such as ion trap, ion cyclotron resonance, and orbitrap analyzers. Within each class, however, the difference between analyzers is vast and certain metrics must be utilized to make accurate comparisons. These metrics are the mass range limit, the analysis speed, the transmission of ions, the mass accuracy, and the resolving power (described above).[28] Mass range limit and analysis speed are fairly self-explanatory, the mass range limit describes the operating window in which ions can be measured and the speed is a measure of how long it takes to measure the ions in that range. Transmission describes the ratio of ions that enter the instrument versus the amount that make it all the way to the detector due to more mechanical loss, such as collisions with transfer lenses. This is not to be confused with

the “duty cycle” which describes the proportion of time that a system is active within a given period. For example, if a wide m/z window is being analyzed but only single m/z’s are transmitted at a time, the duty cycle will be low.[30] The transmission of an instrument is a direct function of the instruments design whereas the duty cycle is a function of the applied parameters (full scan vs single ion monitoring- SIM, 100% duty cycle). Mass accuracy is directly related to the resolving power of the mass analyzer. An analyzer with low resolving power will also have low accuracy. The mass accuracy is derived from the difference between $m/z_{observed}$ and $m/z_{expected}$ on a ppm or mmu scale. The mass analyzers primarily used in this work are quadrupoles and orbitraps.

Quadrupole mass analyzers are currently among the most popular analyzers installed in modern mass spectrometers and are often utilized in tandem with other analyzers. Figure 1.8 displays the general setup of a quadrupole mass analyzer. The analyzer consists of four parallel metal rods connected pairwise to combination of RF (V) and DC voltages (U) with the pairs being 180^{o} out of phase from each other. [30,36–38] At a given RF and DC voltage, only ions of a certain m/z are allowed to pass through and reach the detector. Ions traveling through the z-axis will experience the electric field and be transmitted if their trajectories are stable in the xy plane and do not exceed r_0 (Figure 1.8). For a beam of positively charged ions traveling in the xz plane, as the x electrodes cycles between a positive and negative potential, ions will oscillate from being focused toward the center axis (positive potential) to moving towards the rods (negative potential). The y electrodes operate with an equal potential in magnitude but 180^{o} out of phase from the x electrodes.

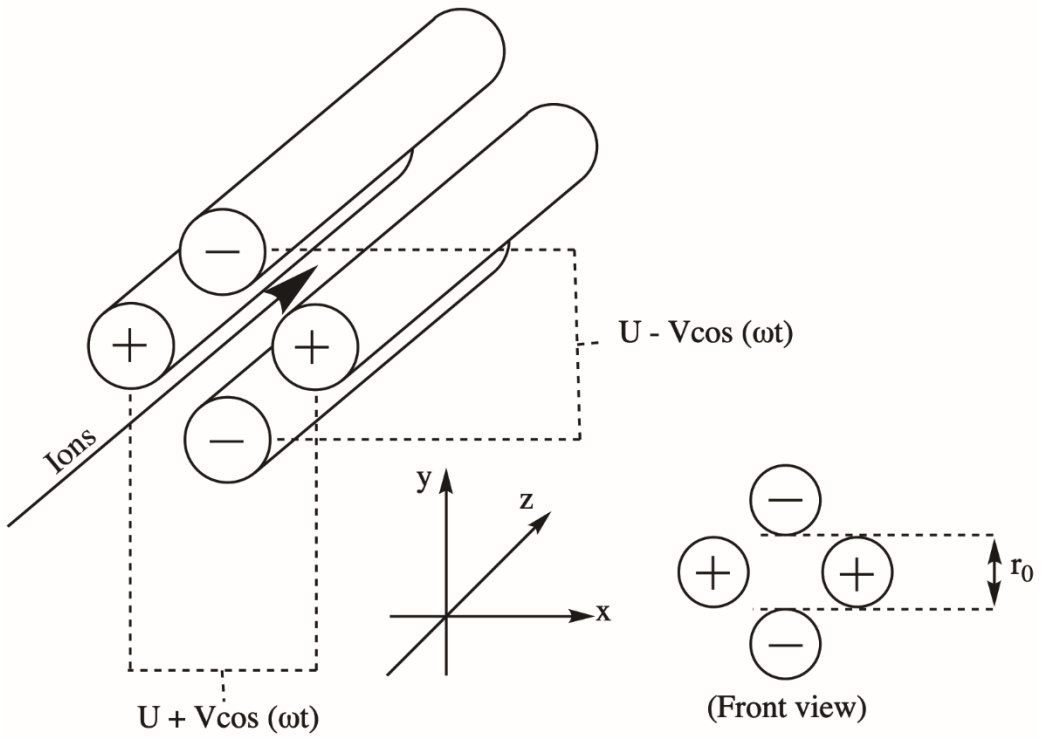

Figure 1. 8 Quadrupole mass analyzer.

Through this, ions are filtered based on their m/z. This motion is better describe using the following equations:[28,30,36–38]

The force of the applied electric fields in the x and y axes are define as:

$$F_x = m\frac{d^2x}{dt^2} = -ze\frac{\partial\phi}{\partial x}$$

$$F_y = m\frac{d^2y}{dt^2} = -ze\frac{\partial\phi}{\partial y}$$

Where ze is the charge and ϕ represents the applied potentials and are defined as:

$$\phi_0 = +(U - V\cos\omega t)\ \ and\ \ -\phi_0 = -(U - V\cos\omega t)$$

$$\phi_{(x,y)} = \phi_0(x^2 - y^2)/r_0^2 = (x^2 - y^2)(U - V\,cos\,\omega t)/r_0^2$$

Further rearrangement and differentiating leads to the Paul equation named after the scientist who pioneered the mass analyzer in the 50s:

$$\frac{d^2x}{dt^2} + \frac{2ze}{mr_0^2}(U - V\cos\omega t)\,x = 0$$

$$\frac{d^2y}{dt^2} + \frac{2ze}{mr_0^2}(U - V\cos\omega t)\,y = 0$$

While these equations describe the trajectory of an ion at a given m/z, further information is required to truly understand the stable trajectory on an ion through the quadrupoles. Here, incorporation of the Mathieu equation is employed:

$$\frac{d^2u}{d\xi^2} + (a_u - 2q_u\cos 2\xi)\,u = 0$$

Where u is either x or y (with signs changing respectively) and $\xi^2 = \frac{\omega^2 t^2}{4}$.

Finally, implementation of the above equations can be used to plot the stable combinations of applied RF and DC voltages for an ion at a given m/z to have a stable trajectory through the mass analyzer, as depicted in Figure 1.9 where:

$$a_u = \frac{8zeU}{m\omega^2 r_0^2} \quad and \quad q_u = \frac{4zeV}{m\omega^2 r_0^2}$$

As depicted in Figure 1.9, the specific combinations of different DC (U) and RF (V) voltages are the driving factors behind the stable trajectory. The area under the triangular region corresponds to the combinations of U and V in which a specific m/z is stable, however, not all m/z's stability diagrams superimpose, as seen in the above equation. The dashed line stability curves in Figure 1.9 represent other m/z's stable trajectories. The "scan line" denotes the slope at which U and V are ramped. The angle of the slope can be adjusted to increase or decrease the resolution of ions with differing m/z's, which is inversely proportionate to the signal intensity. Quadrupoles generally have a working m/z limit of 4000 and a maximum resolution of 2000.[30] Additionally, the usage of RF only and no application of DC voltages allows for the passage of all ions with no resolution. This is referred to as an "ion guide" and is used to focus or transmit ions in larger, complex mass spectrometers. Quadrupoles are the most robust and cost-effective mass analyzers and are widely employed. Further aiding to their recent wide-spread adoption, modern mass spectrometers automatically make the RF and DC voltage adjustments for the operator depending on their desired m/z limits, easing their usage for less experienced users and making them more accessible to a wider audience.

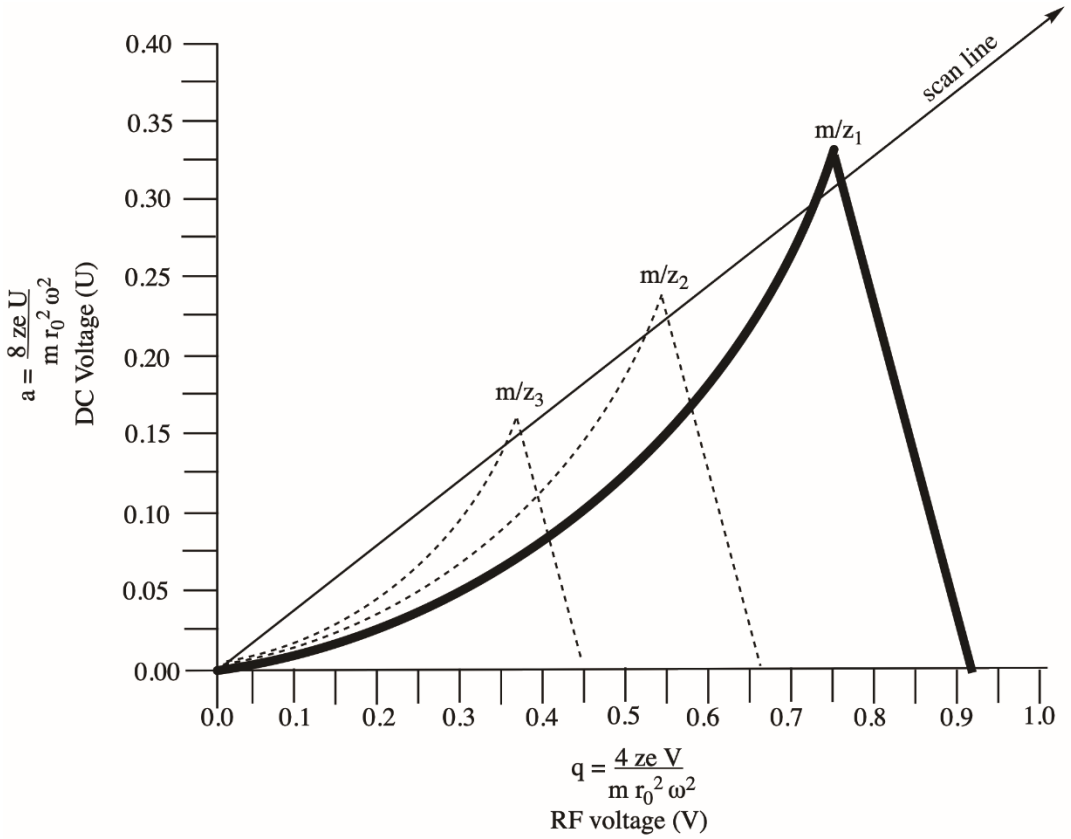

Figure 1. 9 Mathieu stability diagram describing the stable trajectory of an ion through the quadrupole mass analyzer.

Another mass analyzer that, recently, has become increasingly popular is the orbitrap. First developed by Makarov in 1999 and commercialized in 2005, the orbitrap is an electrostatic ion trap that uses the axial harmonic motion of ions to determine the m/z.[30,39] The orbitrap, as depicted in the lower left side of the box diagram of the Thermo Fisher Q Exactive in Figure 1.10, consists of a pair of electrodes, shaped like a barrel cut in half, with a central spindle electrode in the z axis. In the case of positive ion mode detection, ions are injected through a hole in the outer electrode (ground), attracted by a negative kV voltage applied to the spindle. Once injected into the orbitrap, the ions adopt a circular/oval trajectory around the central spindle and oscillate along the z-axis as defined by the following:

$$U_{(r,z)} = \frac{k}{2}\left(z^2 - \frac{r^2}{2}\right) + \frac{k}{2}(R_m)^2 \ln\left(\frac{r}{R_m}\right) + C$$

Where r and z are the cylindrical coordinates, C is a constant, R_m is the radius, and k is the field curvature. The above equation can be utilized to derive how ions at a given m/z move within the orbitrap in an axial and radial direction, as well as their rotational frequency, however, only the frequency of the axial oscillations (ω) is dependent on the m/z of a given ion:

$$\omega = \sqrt{\left(\frac{z}{m}\right)k}$$

The axially rotation of the ions generates an image current as the ions rotate around the center electrode and oscillate between the two halves of the outer electrode. The image current generated as the ions axially oscillate while maintaining their orbital trajectories is then amplified and converted into corresponding m/z signals using a Fourier transform.

Orbitraps offer one of the highest resolutions among mass analyzers, rivaled only by FT-ICR analyzers, with the highest achievable resolution of 250,000.

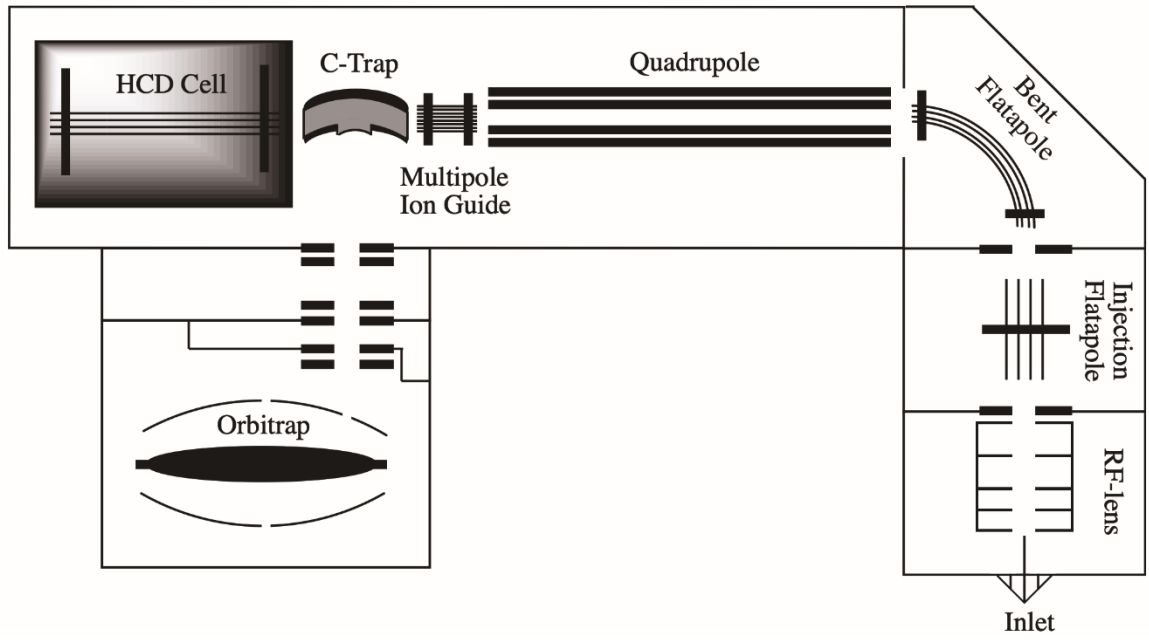

Figure 1. 10 Thermo Q Exactive High Resolution Accurate Mass (HRAM) orbitrap mass spectrometer block diagram.

Orbitraps also offer high mass accuracy as well, with the use of internal calibrants (lock masses) resulting in low single digit to sub-ppm accuracies. Drawbacks of the analyzer arise from the reduction in scan speed as resolution increases as the resolving power is proportional to the time in which the oscillations are recorded. At low resolution (17,500), ~8-10 scans can be performed in a second while at high resolution (140,000), only 1-2 scans can be acquired. Additionally, orbitraps, like FT-ICR analyzers, require ultra-high vacuum for optimal performance (10^{-10} mbar). [28,30,39–42]

The Thermo Q Exactive High Resolution Accurate Mass (HRAM) orbitrap mass spectrometer, depicted in Figure 1.10, was the orbitrap instrument utilized in this work. It is composed on a series of quadrupoles acting as either mass filters or ion guides (multipoles and flatpoles) followed by a "C-trap" that is used to collect and store packets of ions to either be pumped into an HCD cell for MS/MS fragmentation (see below) or pulsed directly into the orbitrap for mass analysis. The implementation of the C-trap also increases the duty cycle of the particular instrument as ion packets can be collected concurrently while the orbitrap is being utilized for mass analysis. At the low resolution end of the instrument (17,500), the duty cycle can approach up to 90% depending on the mass window utilized. The C-trap is functionally an RF-only quadrupole that employs varying potentials to collect, store, and thermally equilibrate ion "packets" prior to ramping the potential to pulse them to either the detector or the collision cell. The high mass resolution of the Q Exactive paired with it's high efficiency and speed make it an invaluable tool for untargeted global metabolomics.

1.1.3 Tandem Mass Spectrometry

Tandem mass spectrometry (MS/MS) is broadly defined as "the acquisition and study of the spectra of ions following m/z selection" and is usually coupled to a method of activation and molecular fragmentation.[30] The primary application of MS/MS experiments is to use fragmentation patterns to provide structural elucidation of select precursor ions. Tandem mass spectrometry can be divided into two main categories: MS/MS in space or MS/MS in time. Tandem in space MS/MS instruments, such as beam-type triple quadrupole mass spectrometers (QqQ) have specified regions for ion selection (uppercase "Q") and ion fragmentation (lower case "q", the reaction region). Whereas tandem in time MS/MS instruments, such as trapping-type quadrupole ion-traps (QIT), are capable of performing both the isolation and fragmentation in the same mass analyzer. Fragmentation mechanisms vary from instrument to instrument, but the most commonly used mechanism is collision induced dissociation (CID). In CID, selected ions are accelerated by an electric field to a high kinetic energy level. Neutral gas molecules (He, N_2, Ar) pumped into the fragmentation chamber, prior to the ion selection process, collide with the precursor ions and the kinetic energy is converted into internal energy. Once resonantly excited, the precursor ions will undergo fragmentation, generally at the site of the most labile bond, through either homolytic fragmentation or heterolytic fragmentation. In homolytic fragmentation, each fragment retains one of the electrons associated with the corresponding most-labile bond. In heterolytic fragmentation, the electrons remain with only one of the fragments. Following fragmentation, the ions equilibrate and generally do not undergo further fragmentation as the applied excitation potential is specific to the precursor ions. [28,30,31]

In this work, the Q Exative HRAM orbitrap mass spectrometer was used for MS/MS experiments. The Q Exactive employs a type of CID known as "higher-energy collisional dissociation" (HCD). Conversely to traditional CID in an ion trap, HCD is non-resonant and can often cause both labile and stronger bonds to break during the fragmentation process. Because of this, more extensive fragmentation patterns can be observed when using HCD. Additionally, whereas CID in ion traps is performed in time, HCD acts more like MS/MS performed in space. Product ions are not equilibrated by collision cooling as they are in ion traps and can undergo further fragmentation as the process is not a slow ramping process like it is with ion traps. As depicted in Figure 1.10, selected ions are collected in the C-trap and then pulsed into the HCD-cell for fragmentation. After a period of time, the resulting fragments are then pulsed back into the C-trap, recollected, and then pulsed into the orbitrap for mass detection.[28,41–46]

Separation Science

The integration of front-end separation techniques to mass spectrometry has become increasingly common since the initial coupling of ion mobility in the late 30s and gas chromatography in the late 50s.[28,30] Since then, high performance liquid chromatography (HPLC) and capillary electrophoresis (CE), among others, have also joined the classification of "hyphenated techniques" coupled to mass spectrometry. These separation methods aid in quantitation and discovery in separating complex mixtures so that analytes can be measured independently by the mass spectrometer. Separations provide a number of advantages in that time-resolved mass spectra can be acquired, sample analyses can be automated, matrix effects can be reduced, structural/stereo-

isomers can be distinguished, and relative or absolute quantitation can be performed.[30,31,47–49] For the work performed in this dissertation, method development primarily employed HPLC and CE separation methods, described in detail below.

1.1.4 Liquid Chromatography

Liquid chromatography (LC) is a chromatographic method that utilizes the chemical characteristics of analytes in solution and how they interact with a solid "stationary phase" packed in a stainless-steel column for separation. Flow rate and station-phase characteristics are used to broadly define the type of LC used. Higher flow rates (100-1000 μL/min) and larger particle sizes (>5 μm) and column inner diameters (abbrev. ID, >2.1 mm) define standard high performance liquid chromatography (HPLC). A reduction in particle size (<2,5 μm) , ID (1-2.1 mm) , and flow rates (<400 μL/min) defines ultra high performance liquid chromatography (stylized as uHPLC, UHPLC, or UPLC depending on manufacturer, UHPLC used in this dissertation). Further decreases in the aforementioned parameters define capillary liquid chromatography (Cap-LC) and nano liquid chromatography (Nano-LC), though the difficulty associated with their implementation makes them less widely used. Aside from the column, an external and easily changed part of an LC, LCs are modular instruments. These modules vary between instruments and applications, however, the average LC consists of a solvent reservoir system, a binary or quaternary pump, a solvent degasser, an autosampler, and a column oven/housing unit. Mobile phase, the solution pumped through the system responsible for changing how analytes react with the stationary phase, is pumped from the reservoir, mixed and degassed, and delivered to the column. The common effluent is

then routed to the ion source of the mass spectrometer (usually an API source, such as ESI) and mass spectral detection is performed. The mobile phase selection is dependent on the stationary phase and analytes being separated. For “reversed phase” (RP) stationary phases (Figure 1.11), water and an organic solvent such as acetonitrile or methanol are used. Separations are performed using either sloping gradients (changing ratios of aqueous and organic) or isocratic gradients (fixed ratios), depending on the type of separation being performed. The separation is performed as a function of how the analytes interact with the stationary phase and how they partition in and out of it versus the mobile phase. Stationary phases can also be selected based on specific chemical characteristics of the function group coupled to the silica particles that make up the stationary phase packing material (Figure 1.11). A fairly nonpolar analyte, for example, would be injected in a mixture onto the column under high aqueous mobile phase conditions. Under these conditions, the nonpolar analyte is going to be in equilibrium partitioning in and out of the stationary as it moved down the column, with the equilibrium favoring the stationary phase, or it being “retained”. As the gradient changes to a higher organic concentration in the mobile phase, the equilibrium will begin to shift towards favoring or being equal with the mobile phase. This principle allows this given analyte to be separated from more polar analytes that would not have interacted as favorably with the stationary phase under high aqueous conditions.[30,31,47–49]

Two theories can be examined when evaluating chromatographic separations in terms of separation “plates” as a function of equilibrium, Plate theory and Rate theory.[47,50,51] The plate theory assumes instantaneous equilibrium at each integral separation layer or “plate”. Generally, the number or plates is used to make this

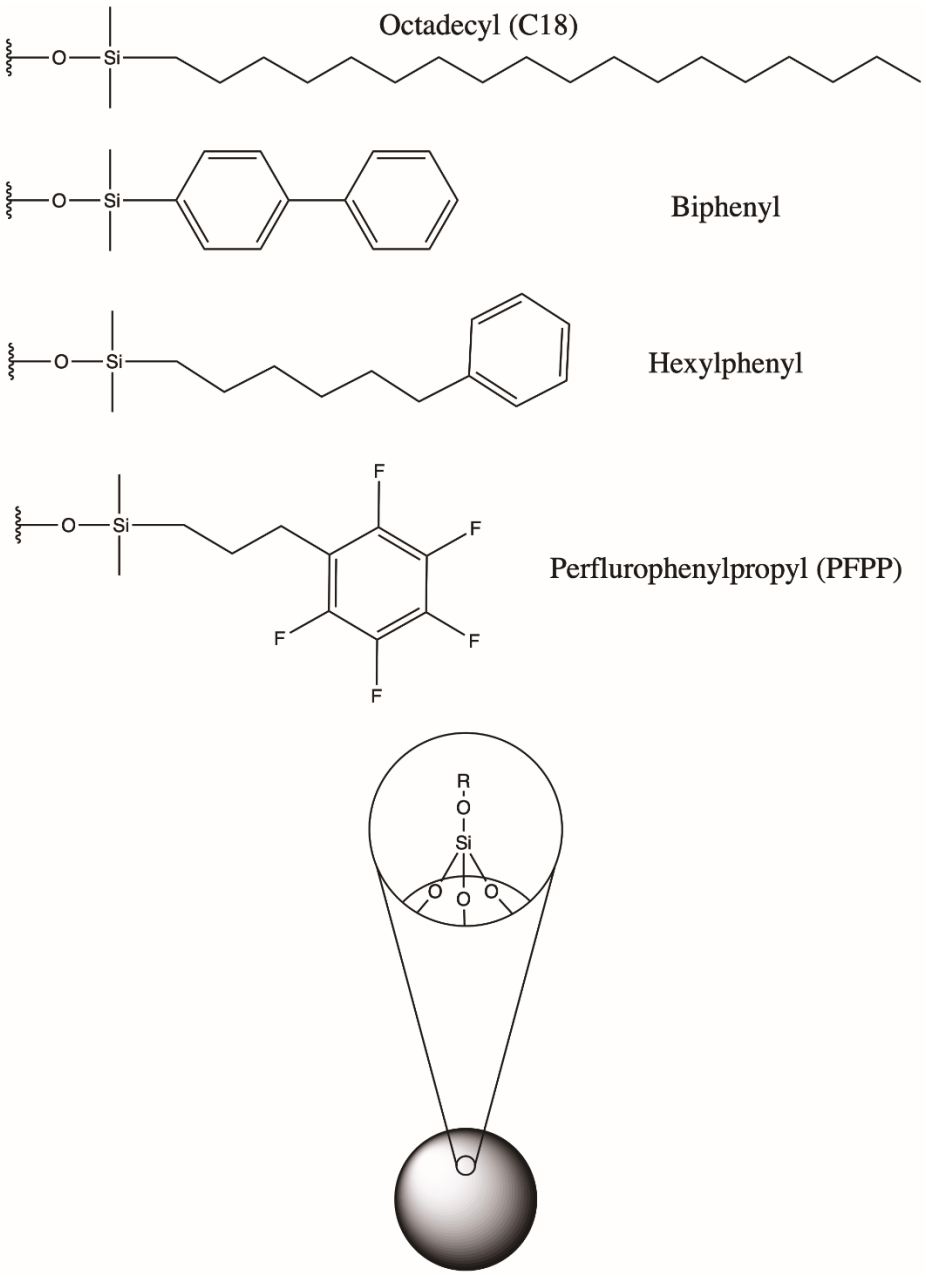

Figure 1. 11 Examples of several reversed-phase HPLC column packing materials.

assessment and, theoretically, the more plates, the better the separation. The number of plates (N) can be calculated based on the retention time (t_R) and full width at half of the maximum height ($w_{1/2}$) of a peak:

$$N = 5.55\,(\frac{t_R}{w_{\frac{1}{2}}})^2$$

From here, the height equivalent of the theoretical plate (HETP) can be calculated as a function of the number of plates (N) and the length of the column (L):

$$HETP = \frac{L}{N}$$

The HETP can also be calculated using the rate theory, however, here kinetic factors are taken into account when equilibrium is established rather than it being understood as instantaneous.[50,51] Here, the van Deemter equation is utilized:

$$HETP = A + B + C$$

Where A, eddy diffusion $= \lambda_i d_p$: (factor of the packed bed x particle diameter)

Where B, longitudinal (axial) diffusion$= 2\gamma \frac{D_M}{u}$: (obstruction factor (usually 0.5) x diffusion coefficient/velocity of the mobile phase)

And where C, the resistance to mass transfer $= c \frac{{d_p}^2}{D_M} u$

Rearranged and simplified as:

$$HETP = \lambda_i d_p + \frac{D_M}{u} + c \frac{{d_p}^2}{D_M} u$$

Plotting these parameters results in the van Deemter plot, which can be utilized to identify the best operating conditions for a given column. Generally, the lower the HETP, the more equilibrium partitions the analyte will experience and the better the separation will be.[50,51]

1.1.5 Capillary Electrophoresis

Electrophoresis is a type of separation method based on the rate in which charged species migrate as a function of an applied electric field.[31,52,53] Electrophoretic separations can be performed on both the macro and micro scales, with the former being performed using a solid (paper) or semisolid (gel) medium and the latter being performed using buffer solution-fused silica capillaries. This microscale electrophoresis method is known as capillary electrophoresis (CE). This separation technique, though not as widely applied as LC methods, has been utilized by a number of industries due to its high resolving power (100,000+ theoretical plates – A and C factors of the van Deemter equation are eliminated), separation speed, and low sample volume requirements (nL range).[52–55] A standard CE instrument setup can be seen in Figure 1.12 (top). Briefly, a fused silica capillary with an ID <100 μm is used to bridge two buffer reservoirs containing a background electrolyte solution (BGE). In the case of positively charged analytes, a positively charged electrode is placed in the origin side BGE reservoir and a negatively charged electrode is placed in the detector side BGE reservoir. The capillary is filled with the BGE driven by both an applied pressure and an applied potential. Once filled, the origin side of the capillary is placed in a sample vial containing a sample solvated in either BGE or a differing electrolyte solution depending on the application.

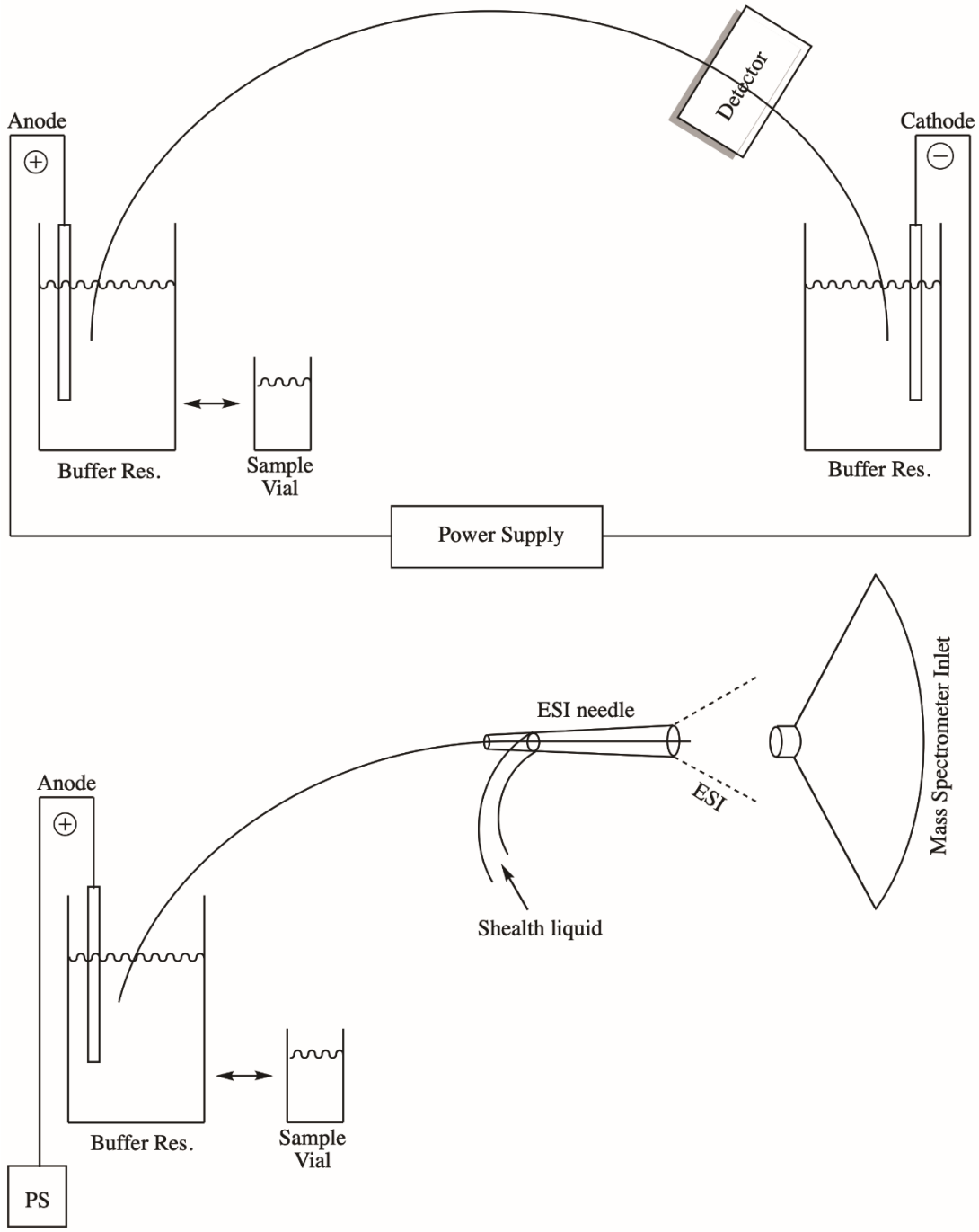

Figure 1. 12 (Top) Standard capillary electrophoresis block diagram. (Bottom) Capillary Electrophoresis coupled to mass spectrometry.

The sample is injected either electrokinetically (voltage-driven), hydrodynamically (pressure-driven), or using both for a short period of time – i.e. 20 sec = ~ 5 nL. Following injection, the origin side of the capillary is reinserted into the origin side BGE reservoir and a high voltage is applied, initiating the separation. In standard CE experiments, a window is burned into the polyamide coating of the fused silica so a detector (UV, PDA, Fluorescence) can be implemented on opposite end of the capillary from the origin. Alternatively, rather than a reservoir on the detector end, CE can be easily coupled to a mass spectrometer with the inlet at ground acting as the cathode. The capillary is integrated into housing tubing within the mass spectrometer's ionization source allowing for a bulk solution (1-5 μL/min) to be supplied at the end of the capillary for electrospray ionization.[52,54–57]

Separations via CE can be performed many ways such as standard capillary zone electrophoresis (CZE), isotachophoresis (ITP), miceller electrokinetic chromatography (MEKC), and capillary electrochromatography (CEC). In this work, only CZE and ITP were applied (discussed below).[31,52] The driving factors behind CE-based separations are electrophoretic and electroosmotic flow.

Electrophoretic flow (Figure 1.13 – bottom left) describes how ions migrate as a response to the applied potential.[52] The electrophoretic mobility (μ_{ep}) is directly proportional to velocity (ν_{ep}) at which the ion moves in an applied electric field (E_{app}) and inversely proportional to the frictional retarding force of the ion, which is a function of the ion's size and shape and the viscosity of the BGE, as shown in the following:

$$\nu_{ep} = \mu_{ep} E_{app} = \mu_{ep} \frac{E_f}{F_f} \quad where \;\; E_f = qE \; and \; F_f = -6\pi\eta r\nu$$

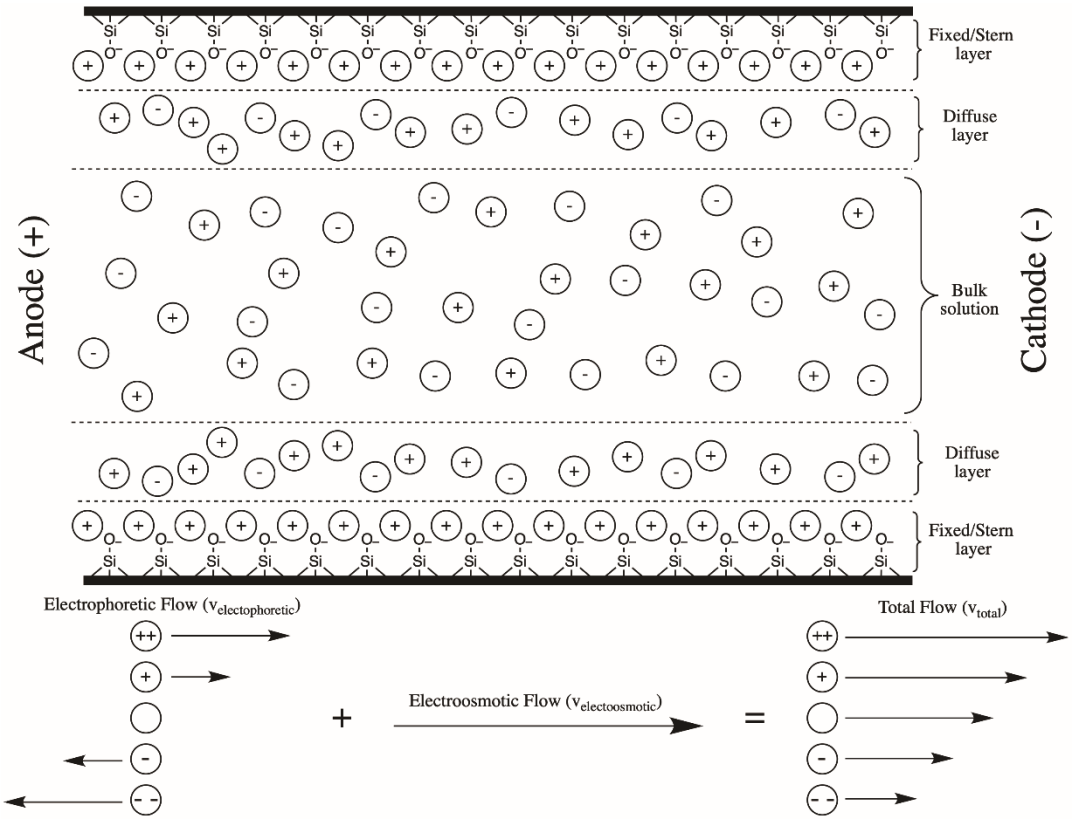

Figure 1. 13 (Top) Fixed and diffuse layers of capillary electrophoresis, making up the "double layer" responsible for electroosmotic flow. (Bottom) Total flow of an analyte is the summation of its electrophoretic mobility and the electroosmotic flow.

Where E_f is the electrical field strength, q is the charge of the ion, r is the ion's radius, ν is the ion's velocity and η is the solution viscosity. For the case in which positively charged analytes are of interest, the BGE is acidic, and the origin side is positively charged, analyte cations will exhibit a forward moving electrophoretic mobility toward the detector, neutral analytes will not migrate, and analyte anions will migrate towards the origin anode.

Electrophoretic mobility is not the only driving force behind CE. Electroosmotic flow (EOF) also occurs and is the result of the formation of an electric double layer forming between buffer cation/anions and the silanol groups of the fused silica capillary. Following an initial wash with a high pH solution, such a NaOH, the surface silanols are deprotonated and negatively charged. Buffer cations, once introduced into the capillary, interact with the negatively charged silanols and form the fixed or "Stern" layer (see Figure 1.13). The cations only partially neutralized the negative charge of the capillary walls so a second, cation-rich layer, called the diffuse layer, forms and the two layers make up the aforementioned electric double layer. The cations in the double layer migrate toward the cathode and the ensuing motion generates a "bulk flow" phenomenon. This phenomenon also causes the solution to adopt a wall flow/flat profile as opposed to the parabolic profile observed from pressure-induced flow. The magnitude of the EOF is generally greater than the electrophoretic flow so even negatively charged analytes have a resulting net flow towards the cathode (Figure 1.13 – bottom middle and bottom right). The velocity of the EOF (ν_{eo}) is defined as:

$$\nu_{eo} = \mu_{eo} E_{app} = \frac{\epsilon \zeta}{\eta} E$$

Where ε is the dielectric constant of the buffer and ζ is the zeta potential.

The zeta potential describes the potential of the double layer on the capillary wall. It is a function of the pH of the BGE and is reduced as the pH decreases and the number of cations in solution increases.

The apparent mobility (μ_{app}) of an analyte is the result of the summation of it's electrophoretic and the electroosmotic flow of the solution with the apparent velocity (ν_{app}) being a function of the apparent mobility and the applied field:

$$\mu_{app} = \mu_{ep+}\, \mu_{eo}$$

$$\upsilon_{app} = \mu_{app} E$$

1.1.6 Microfluidic Capillary Zone Electrophoresis

The work performed in this dissertation involved the utilization of a microfluidic CZE-MS devices called the ZipChip. First designed in 2008 and later fabricated and commercialized by 908devices in 2016 for research use, this microfluidic CZE-MS device has been reported in literature for a variety of uses including the identification of post-translationally modified peptides, analysis of antibody conjugates and viral capsid proteins, and for the detection and quantification of pathogenic metabolites in marine life.[58–65] This devices (Figure 1.14) consists of an etched rectangular glass slide with three wells (S, B, and SW) connected by corresponding channels to an intersection with a long serpentine separation channel. The serpentine channel meets with another well-sourced channel (P) at the corner of the glass chip. Injections into this device are hydrodynamic. Pressure is then applied to the "S" well to load the sample into the cross intersection by

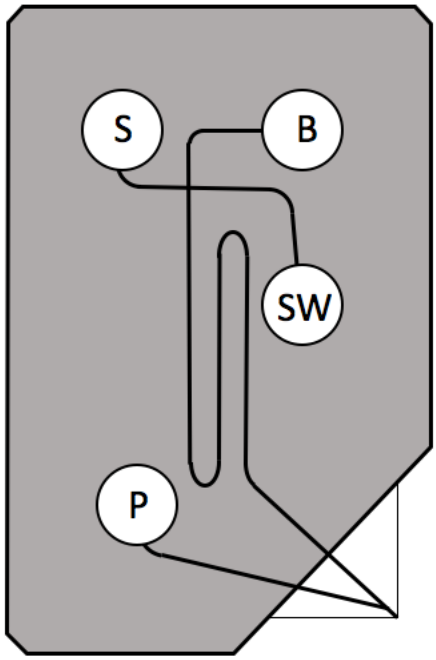

Figure 1. 14 The 908 Devices "ZipChip" microfluidic CZE-MS device. Consists of an etched piece of glass with channels connecting to four wells: S - sample well, B - background electrolyte well, SW - sample waste well, and P - pressurized ESI spray well.

pumping it to the waste well (SW) and also concurrently applied at the "B" well, filled with BGE, to begin the formation of a sample plug in the beginning of the serpentine separation channel. After a period of time corresponding to a specified injection volume, pressure is exclusively applied to the "B" well to clear the channel intersection and endcap the sample plug in BGE. A subsequent potential is applied and the sample is electrophoretically separated through the serpentine channels before meeting with the "P" channel where bulk flow and an additional potential is provided to produce electrospray from the corner of the chip (Figure 1.15). Aside from the difference in scale of this device (10 cm separation channel) compared to traditional CZE (often >40-50 cm), this device also employs transient isotachophoresis (tITP, described below) for its separation mechanism.[58–61] Additionally, for the standard HS or HR variety chips (10 cm vs 22 cm separation channel), the walls of the channels are chemically modified with aminopropylsilane effectively reducing the zeta potential to 0 as no negatively charged silanols exist for the double layer to form. This effectively eliminates the EOF, leaving tITP as the only separation mechanism. Isotachophoresis (ITP) is a type of preconcentrating electrophoretic mobility method driven by the usage of leading (LE) and trailing (TE) electrolytes. Ideally, analytes will have an intermediate ionic mobility compared to the LE (high mobility) and TE (low mobility). Once the potential is applied, the analytes will stack in between the LE and TE interface and focus as they migrate. While a reduction in separation efficiency is observed, if separation is observed at all, the compaction of the analyte band greatly increases the signal intensity and narrows the peak width. The lack of separation is obviously not ideal, however, the analyte band compaction and subsequent signal increase is a desirable feature of ITP, which lead to the

development of tITP. In tITP, the sample is dissolved in a solution containing the leading electrolyte and the BGE has relatively low conductivity. Upon the application of the high voltage, the analytes briefly travel with the LE, stacking behind it and preconcentrating/focusing, before the LE breaks away. Once the LE has broken away, the analytes are then able to be electrophoretically separated. The utilization of the tITP phenomenon greatly increases the sensitivity of the method and, coupled with the low flow rates associated with CE compared to HPLC, makes this method ideal for detection of trace analytes in complex mixtures. Another important factor for this device is its speed. Standard analyses can be performed in 3-6 minutes depending on the chip (HS vs HR) and applied field strength. This speed does not come at the cost of separation efficiency and the device is reproducibly capable of separating all 20 canonical amino acids with baseline resolution in less than 1.5 minutes.

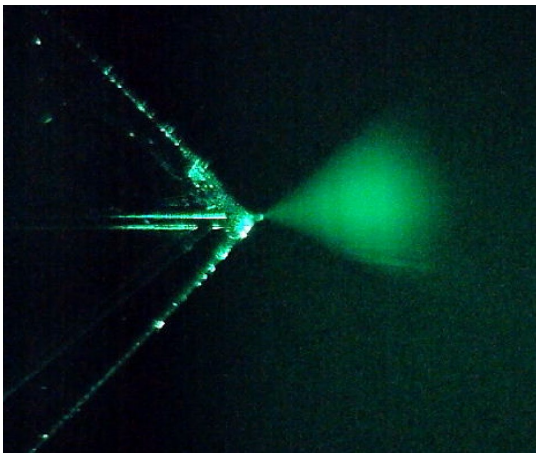

Figure 1. 15 Still image of the ESI corner of the ZipChip while spraying.

CHAPTER 2. THE ANALYSIS AND CHARACTERIZATION OF TRANSGENIC LOBELIA CARDINALIS ALKALOIDS VIA HPLC-MS AND CZE-MS

Segments of this dissertation chapter are taken from: Kelley, Z. D.; Rogers, D. T.; Littleton, J. M.; Lynn, B. C. "Microfluidic Capillary Zone Electrophoresis Mass Spectrometry Analysis of Alkaloids in Lobelia Cardinalis Transgenic and Mutant Plant Cell Cultures." *Electrophoresis* 2019, 40 (22), 2921–2928[66]

Introduction

Alkaloids, as stated in chapter 1, are a class of secondary metabolites characterized by the presence of at least one basic nitrogen.[67,68] The class is further divided in to subsets regarding origin and nitrogen arrangement. The "typical" or "true" alkaloids are derived from amino acid precursors, such as tryptophan and histidine, and contain a type of heterocyclic nitrogen motif, as depicted in Figure 2.1, or a primary amine while still being of amino acid origin (see mescaline – tyrosine derived in Figure 1.4).[68,69] Additionally, there are "atypical" or "pseudo" alkaloids that, while sometimes still of amino acid origin, their nitrogen is the result of transamination.[69] The biosynthetic pathways (simplified, Figure 2.2) for the synthesis of both typical and atypical alkaloids can often be tremendously complex, often involving 20+ enzymatic steps and with multiple diverging intermediate steps, leading to individual plant species producing a diverse variety of metabolites sharing similar central motifs.[70,71,72] Given the diversity of alkaloids as a whole, the role of these metabolites in plants is also multifaceted. They can be utilized as predator defense/determent agents, nitrogen stores, nonspecific basic catalysts, anti-oxidants, and even as waste product or reactionary byproducts.[67,70,73,74] Adding to the diversity of these molecules, the formation of an informal interaction of the heterocyclic nitrogen with a free oxygen, an "N-oxide"

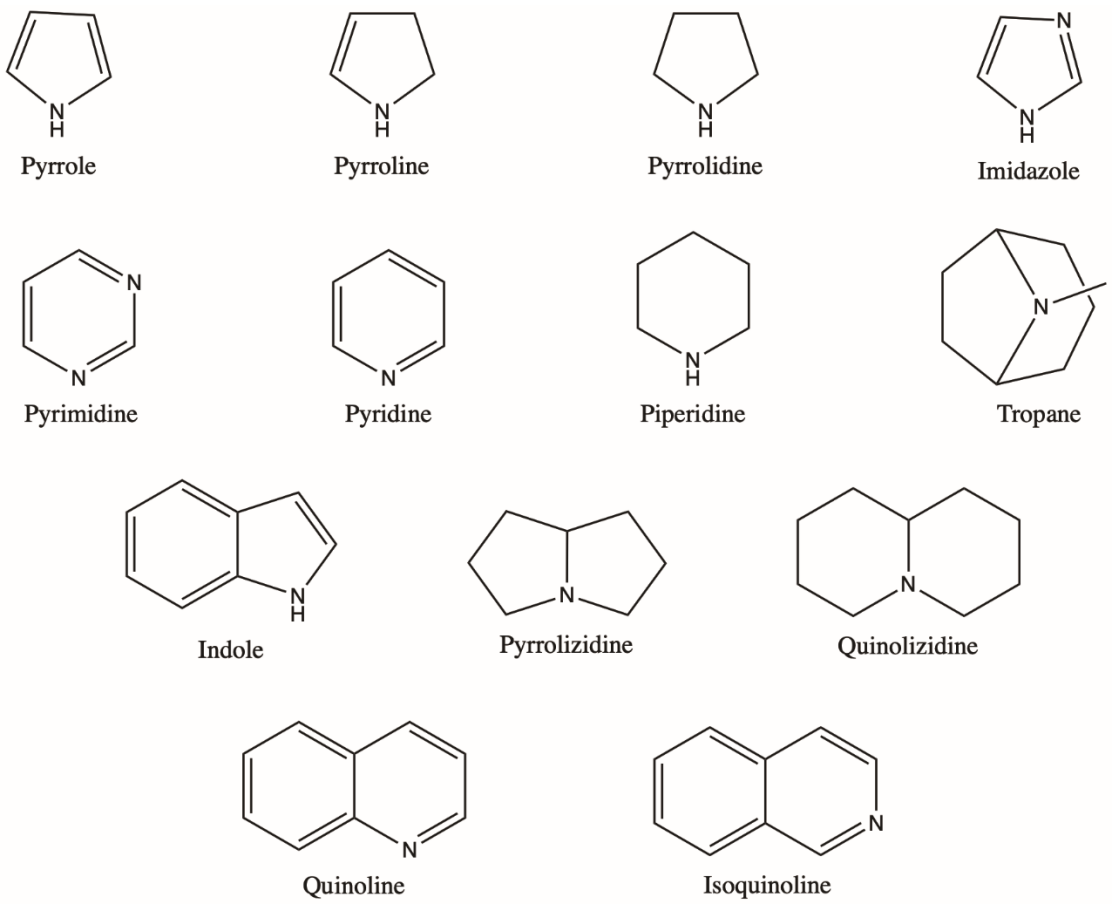

Figure 2. 1 Common alkaloid central heterocyclic nitrogen motifs.

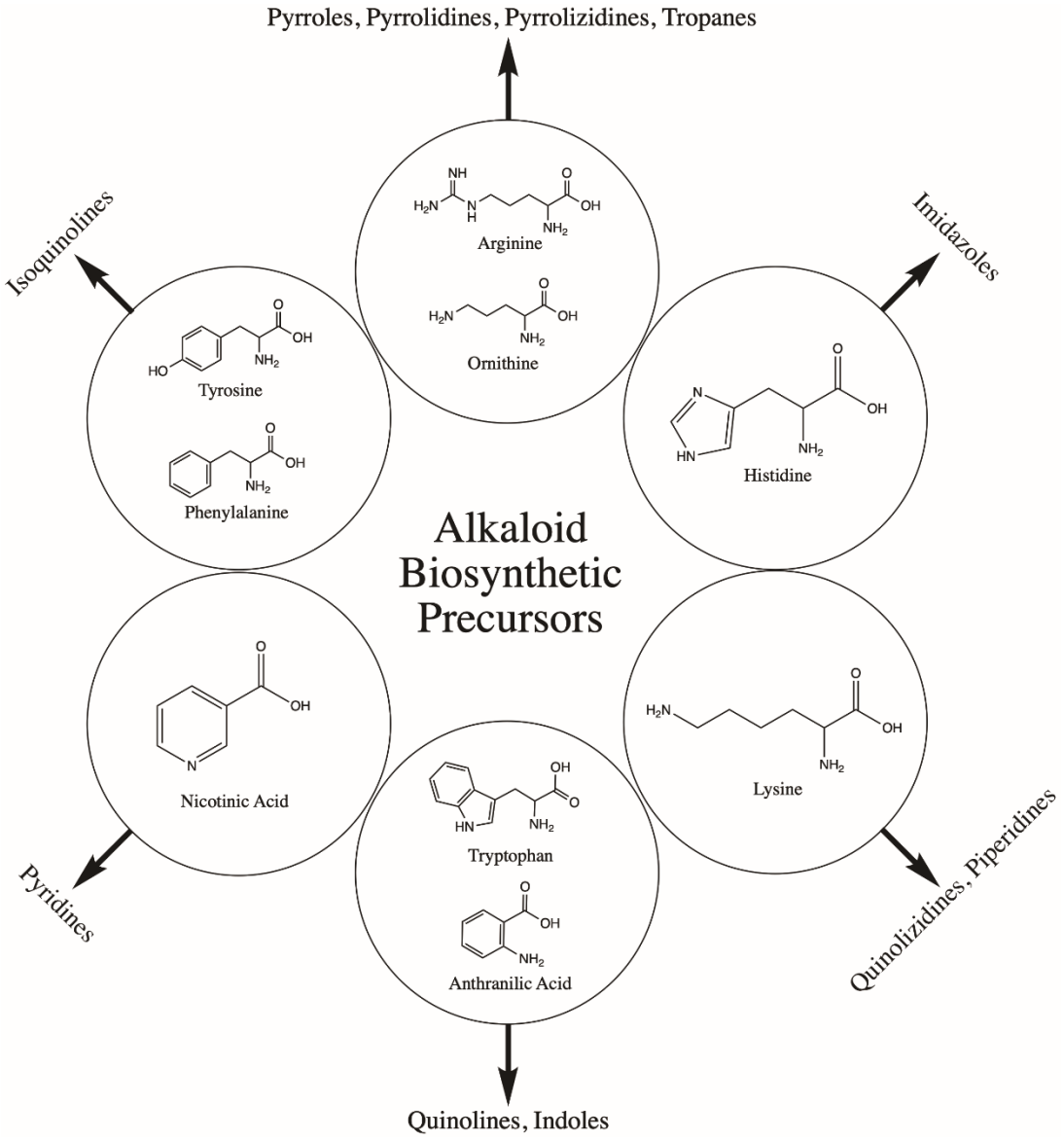

Figure 2. 2 Simplified biosynthetic origins of selected classes of alkaloids.

interaction, is also common to aid in the aqueous solubility and transport of the metabolites throughout the plant.[2,75,76,29,77]

In addition to their role in plants, this diverse class of secondary metabolites is also of interest to humans for pharmacological applications as "natural" pharmaceuticals. The medicinal application of alkaloids can be seen in a wide variety of current products including quinine (Figure 1.2), an antimalarial, reserpine, an antihypertensive, and vincristine, an antitumor-agent.[78,79] Additionally, many addictive or chronically abused stimulants and hallucinogens, such as nicotine, morphine and its derivatives, and cocaine, are also found within this group. Given their vast pharmaceutical applications paired with their complex structures that would be difficult to reproduce synthetically, these metabolites are often extracted, purified, and tested for pharmacological activity across a variety of targets.

The alkaloids in question for this chapter are those found in the cardinal flower, *Lobelia cardinalis* (Figure 2.3 - left). *Lobelia cardinalis* produces a binitrogenous alkaloid, lobinaline (decahydro-1-methyl-5,7-diphenyl-6-(3,4,5,6-tetrahydro-2-pyridinyl)-quinoline - $C_{27}H_{34}N_2$ – Figure 2.4), recently shown to have inhibitory activity on the human dopamine transporter (hDAT).[72,80–82] Another member of the *Lobelia* genus, *Lobelia inflata* (Figure 2.3 – right) produces an alkaloid of proposed biosynthetic origin, lobeline, which has also been reported to have similar activity.[83–85] Other than the hypothesis that lobeline and lobinaline share a biosynthetic precursor, sedamine, very little is known about *L. cardinalis* and its other secondary metabolites as few publications involving the plant have been produced since the 1960s.[83,86–88]

Figure 2. 3 *Lobelia cardinalis* (left) and *Lobelia inflata* (right). (Free use images. Image sources: pixabay.com, daledbet (cardinalis) and KatarzynaTyl (inflata)).

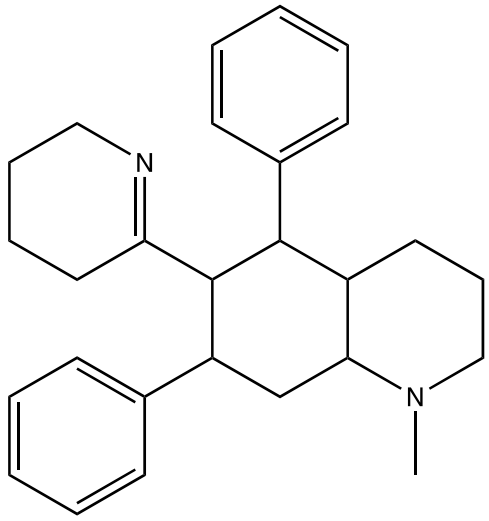

Figure 2. 4 Lobinaline - decahydro-1-methyl-5,7-diphenyl-6-(3,4,5,6-tetrahydro-2-pyridinyl)-quinoline - $C_{27}H_{34}N_2$.

A natural pharmaceutical company based out of Lexington, KY, Naprogenix LLC, discovered this hDAT inhibitory activity in the mid-2000s.[81,82] The focus of their activity screen centered around the search for atypical hDAT inhibitory secondary metabolites that could be used as low-to-zero-abuse liability cessation aids for people suffering from substance use disorders (SUD).[89] Naprogenix has since genetically modified *L. cardinalis* to produce hairy root cultures expressing the human dopamine transporter (hDAT) using *Agrobacterium rhizogenes*-mediated transformation. The cultures were then further mutated via activation-tagging mutagenesis by the insertion of viral enhancer sequences into the hairy root cultures genome to induce random gain-of-function mutations.[81,82] These transgenic mutants were selected on media containing MPP+ (1-methyl-4-phenylpyridinium) which is accumulated intracellularly by activity of the hDAT and targets the mitochondrial oxidative phosphorylation mechanism. This selection process is visualized in Figure 2.5. The hypothesis is that surviving progeny hairy roots were predicted to contain up-regulated or novel secondary metabolites with hDAT inhibitory activity. To test this, analytical methods were developed to identify those specific metabolites that are increased in MPP+-resistant mutants relative to wild type (WT). Here, samples of the surviving hairy root cultures were propagated, harvested, extracted, and then analyzed using the both LC-MS and a microfluidic CZE-MS device. Metabolomic profiles were generated from the analyses and used for determination of lead compounds to be targeted for the pharmacological screening as potential therapeutics for people suffering from SUDs. Novel metabolites were structurally characterized using tandem mass spectrometry (MS/MS) analyses and then selected compounds were purified using a variety of extraction and purification methods.

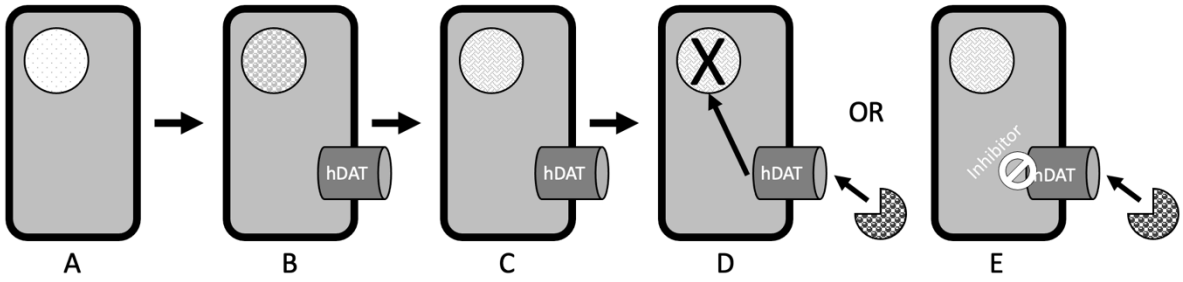

Figure 2. 5 Naprogenix mutant transgenic *Lobelia cardinalis* selection workflow. A) Hairy root *L. cardinalis* plant cell. B) Transgenic *L. cardinalis* expressing the human dopamine transporter. C) Transgenic *L. cardinalis* post activation tagging mutagenesis. D) Cell death following exposure to MPP+ if no hDAT inhibitory metabolites are present or E) Cell survival if hDAT inhibitory metabolites are present.

Materials, Methods, and Instrumentation

2.1.1 Extraction Protocol and Sample Preparation – Liquid-Liquid Extractions

Both field grown *Lobelia cardinalis* plant material and mutant hairy cultures/culture extracts were provided by Naprogenix Inc. Field grown plant material was provided as dried, ground, and homogenized biomass. The biomass was extracted in 5 to 25 g batches using 200 mL of ACS grade methanol per 5 g of plant material. Extractions were performed overnight (approximately 18 hours) in Erlenmeyer flasks with constant stirring. The solvent from the biomass extraction was recovered via vacuum filtration, reduced via rotary evaporation, and stored at 4^{o} C. Transgenic hairy root cultures were provided as methanolic extracts and prepared by Naprogenix Inc as stated: Briefly, hairy root cultures were collected, rinsed to remove media with sterilized water, and lyophilized. The lyophilized roots were ground to a fine powder and transferred to a glass vial. The root powder was extracted with 5mL of MeOH per 100 mg of roots, and the vials were agitated for 24 h. The methanolic extraction was repeated three times. The combined extracts were centrifuged at 20,000xg. The supernatant was collected and stored in a freezer at -20^{o} C until analyzed.

Prior to analysis or preparative HPLC separation, methanolic extracts underwent liquid-liquid partitioning. The field grown plant material methanolic extracts were pooled and diluted with ACS grade methanol (Fisher Scientific) to a concentration of 500±50 mg of extracted material per 100 mL of methanol (final concertation of ~5 mg/mL) and 100 mL aliquot was transferred to a 2 L separatory funnel. The methanolic extracts were further diluted with 200 mL of DI water and 25 mL of 1N HCl to a total volume of 325

mL. Following the addition of aqueous acid, a liquid-liquid partition was performed 4X with 400 mL of $CHCl_3$ per partition. To break emulsions that appeared during the initial partitioning of more concentrated extracts, a saturated NaCl solution was added in 10 mL aliquots until the emulsion separated. Following each partition, the organic $CHCl_3$ layer was collected in a 1 L round bottom flask and the $CHCl_3$ was recovered via rotary evaporation. The remaining residue following rotary evaporation was discarded. The aqueous acid extract layer was then made basic (pH 12) using 50 mL of 1N NaOH. The basic aqueous solution was allowed to equilibrate at room temperature for 30 minutes and was then partitioned 4X with 400 mL of $CHCl_3$ per partition. The $CHCl_3$ layer was collected in a 500 mL round bottom flask and the volume was reduced via rotary evaporation. Following volume reduction, the basic $CHCl_3$ extract was reconstituted in 50 mL of ACS grade MeOH, 100 mL DI water, and 20 mL of HCl, total volume of 170 mL, and transferred to a 1 L separatory funnel. The aqueous acid extract was partitioned 2X with 250 mL of histological grade xylenes. The xylenes layer was removed and discarded. The aqueous acid extract layer was then made basic (pH 12) using 40 mL of 1N NaOH and was extracted as listed above 2X with 200 mL of $CHCl_3$ with the organic layer being collected after each partition. The resulting basic $CHCl_3$ extract, hereafter referred to as the "ABCXC extract", was collected, reduced to dryness via rotary evaporation, and stored in the freezer at -18^{o} C.

2.1.2 HPLC – Analytical and Preparatory Scale

Following liquid-liquid partitioning, dried ABCXC extracts were reconstituted in appropriate volumes of HPLC-grade MeOH at concentrations specific to the method being employed. For general analytical HPLC analysis, the extracts were diluted to

approximately 1 mg/mL. For preparative HPLC separations, the extracts were diluted to 250 mg/mL. Both preparative and analytical HPLC experiments were performed using an Agilent 1100 series binary solvent pump coupled to an Agilent 1100 series VWD for UV detection. Injections were made using a Rheodyne injector with a 10 µL PEEK sample loop for analytical HPLC analyses (5 or 10 µL injections) or a 200 µL stainless steel sample loop for preparative separations (50, 100, or 200 µL injections). For both separation procedures, the 260 nm channel was monitored on the VWD detector. Analytical separations were performed using a Kromacil Eternity XT 5 µm C18 column (4.6x150 mm). Preparative separations were performed using two different stationary phase pHPLC columns; for bulk separations, a Phenomenex Luna 10 µm C18 column (10x100 mm) was used, for high selectivity separations, a Restek Pinnacle BiPh 5um biphenyl column (10x150 mm) was used. For analytical separations, a binary gradient was employed over a 20 minute separation at a rate of 1 mL/min consisting of optima grade water (solvent A) and optima grade acetonitrile (solvent b) (Fisher Scientific), both with 0.1% formic acid, starting at 5% B for 2.5 minutes, increasing linearly to 95% B by 12 minutes, being held at 95% B until 16 minutes, and then returning back to starting conditions, 5% B, by 18 minutes for equilibration. Preparative separations were performed using column-specific isocratic gradients. For the C18 column, 25% B at a rate of 5 mL/min was used for the entire 10 minute preparative separation. For the biphenyl column, 10% B at a rate of 5 mL/min was used for the entire 10 minute preparative separation. Both preparative columns were washed with 100% ACN w/ 0.1% for 20 minutes after every four preparative separations and were equilibrated at their respective organic content percentages for five column volumes following washings.

Fractions corresponding to analyte peak elutions were collected during the pHPLC separations. The collected fractions were basified to pH ~12 with 1N NaOH and extracted with an equal volume of $CHCl_3$ exhaustively. The $CHCl_3$ was removed under a stream of dry nitrogen and the purified material was stored in a freezer in sealed glass vials at -18° C.

2.1.3 UHPLC-MS

Samples analyzed via UHPLC-MS were prepared several ways depending on the nature of the analysis being performed. Prior to the extraction protocols listed above, raw methanol extracts of both field grown plant material and transgenic hairy root material were analyzed to establish a baseline for comparison post-liquid-liquid partitioning. Aliquots of the methanolic extracts were diluted to 1 mg/mL with optima grade methanol. An additional dilution was made to approximately 50 ug/mL in 1 mL of the appropriate solvents corresponding to the HPLC gradient starting conditions (listed below). Chromatographic separations were achieved using a Shimadzu Nexera X2 modular UHPLC system (Torrance, CA) consisting of the following modules: SIL-30AC, LC-30AD, CTO-20A, CBM-20A, and DGU-20A) coupled to either a Restek Pinnacle DB Biphenyl UHPLC column (1.9 µm, 2.1x50 mm) or a Kromacil Eternity XT C18 UHPLC column (2.5 µm, 2.1x50 mm). For the use of the Biphenyl column, chromatographic separation was achieved over 20 minutes using solvent A (0.1% formic acid) and B (0.1% formic acid in ACN) at 300 µL/min in a gradient flow method consisting of solvent B at 20% for 2 minutes, increasing linearly to 95% by 14 minutes, being held at 95% until 17 minutes, and then returning to starting conditions by 18 minutes for equilibration. For the use of the C18 column, chromatographic separation was achieved

over 20 minutes also using solvent A (0.1% formic acid) and B (0.1% formic acid in ACN) at 400 µL/min in a gradient flow method consisting of solvent B at 5% for 2.5 minutes, increasing linearly to 95% by 12 minutes, being held at 95% until 16 minutes, and then returning to starting conditions by 18 minutes for equilibration. The UHPLC-MS analyses were performed on a ThermoScientific Q Exactive High Resolution Accurate Mass (HRAM) Orbitrap mass spectrometer. MS parameters for UHPLC separations consisted of a scan range of 150 to 2000 m/z, a resolution of 140,000, microscans set to 3 (~1.7 scans per second), and an AGC target of 3e6. Electrospray ionization was achieved using a sheath gas flow of 15 L/min, a spray voltage of +3500, an inlet capillary temperature of 350 ºC, a HESI probe temperature of 280 ºC. Additionally, initial exploratory analyses were performed using a Hewlett-Packard series 1100 HPLC with an Agilent 300Extend-C18 column coupled to a Hewlett-Packard ESI-LCMSD. Chromatographic separations were performed over 36 minutes using solvents A and B listed above at 750 µL/min in a gradient flow method consisting of solvent B at 10% for 5 minutes, increasing linearly to 90% by 28 minutes, being held at 90% until 30 minutes, and then returning to starting conditions by 32 minutes for equilibration. MS parameters for these exploratory separations consisted of a scan range of 100 to 600 m/z. Electrospray ionization was achieved using a sheath gas flow of 12 L/min, a spray voltage of +3500, and a nebulizer gas temperature of 300 ºC.

2.1.4 Microfluidic CZE-MS analysis

Dried methanolic extracts of wild type (WT) hairy roots, virally transformed hDAT mutants (DAT+) hairy roots, and induced gain of function DAT+ mutants (MUT – mutant LOB479) of *L. cardinalis* hairy roots were obtained by Naprogenix Inc. Extracts

were prepared using a scaled-down version of the liquid-liquid partition listed above as follows: Aliquots of the dried extracts were weighed and reconstituted in MeOH to produce 1 mg/mL solutions. A 250 µL aliquot of each sample was diluted in 200 µL of optima H2O and acidified with 50 mM HCl to pH 2. The acidified extracts were partitioned with 500 µL of CHCl3 and the organic layer was removed. The pH of the aqueous layer was increased to pH 10 with 100 mM NaOH and extracted again with 500 µL of CHCl3. The organic layer was collected and reduced to dryness under a stream of dry nitrogen. The dried CHCl3 extracts were reconstituted in 250 µL of the 908 Devices metabolites diluent and transferred into autosampler vials with 300 µL inserts for analysis. Each sample was analyzed in triplicate.

Microfluidic CZE-MS analyses were performed using an HS variety ZipChip housed in the ZipChip Interface (ZCI) mounted to the inlet of the mass spectrometer. Each sample was delivered via an accompanying autosampler to the sample well and loaded into the sample channel for 24 seconds (5.00 nL - default HS Metabolites method). The sample set was analyzed using the predefined standard HS Metabolites method, field strength: 1000 V/cm, pressure assist start time: 2.00 minutes. All separations were performed for 3.00 minutes with approximately three minutes of pre-run time to transfer the sample from the autosampler to the ZCI. The background electrolyte was refreshed after every three samples. The ZCI was coupled to a ThermoFisher Q Exactive HRAM Orbitrap Mass Spectrometer (Thermo Fisher Scientific, Waltham, MA, USA). Acquisition parameters included a full scan range from m/z 70 to 600, mass resolution of 17,500, microscans set to 1 (~8 scans per second), sheath gas flow set to 2.0 psi, and an AGC target of 3e6. For comparison to traditional CE-MS, analyses were

performed on an abbreviated set of samples (triplicate sets of the WT and LOB479) using a Prince CE100 Capillary Electrophoresis system was coupled to a Finnegan LCQ Deca mass spectrometer. Electrophoretic separations were performed in a 67 cm fused silica capillary (Polymicro Technologies) with an ID of 50 µm and an OD of 186 µm. BGE for CE-MS (FA-BGE) was prepared as follow: 192.5 µL of formic acid was diluted to 100mL in optima H2O and then brought to pH 2.85 with 50mM ammonium formate solution. The capillary was prepared by flowing 1N NaOH, optima H2O, EtOH, and FA-BGE each for 3 minutes at 1000 mbar and then FA-BGE again for 20 minutes at 50 mbar with 25 kV applied. For sample analysis, the capillary was flushed with BGE for 3 minutes at 1000 mbar. Following flushing, the sample was loaded for 0.20 minutes at 100 mbar with 5 kV to mimic the sample loading conditions of the ZipChip. The separation was then performed over 20 minutes at 50 mbar with 25 kV applied. A sheath fluid consisting of 50/50 optima H_2O and isopropanol was flown at the tip of the capillary in the ESI source at 1.5 µL/min.

2.1.4.1 Analytical method validation – CZE-MS

A purified lobinaline standard was obtained using the preparative HPLC method listed above. The subsequent purified lobinaline standard was used to create a calibration curve for quantification of lobinaline in the plant extracts. Additionally, percent recovery and the method detection limit (MDL) were assessed using this standard. For percent recovery, following assessment of the lobinaline concentration naturally found in the plant extracts, a known amount of lobinaline was spiked into six samples of dry plant material. Spiked material was extracted and analyzed as stated above. The determined concentration of the spiked extracts was compared to the theoretical concentration in

order to assess the recovery percentage. For the MDL determination, the procedure established by the Environmental Protection Agency (EPA), EPA 821-R-16-006, was followed. Briefly, seven replicates of lobinaline spiked into surrogate matrices (*Sedum Acre* dried plant extracts) at ten times (100 nM) the suspected limit of detection (10 nM) were compared to seven blank surrogate extracts. This procedure was repeated on three separate days. The resulting concentrations of lobinaline in the spiked population was calculated and the standard deviation (S) of the concentrations was used in the following equation.

$$MDL_s = t_{(n-1,1-\alpha=0.99)}S_s$$

2.1.4.2 Data processing via MZmine2 software

MZmine2 data processing was performed as reported by Olivon et al. with modifications.[90] Data files (.RAW) were converted to .mzXML files using the open source MSConvert software prior to MZmine2 processing. For CZE-MS analyses, masses were detected from 0.70-2.50 minutes with an exact mass detector and a noise level of 1.0e5. The mass list was then filtered with an FTMS shoulder peak filter using the Gaussian function and a mass resolution of 17,500. Chromatograms were built from the filtered mass lists from 0.70-2.50 minutes with a minimum duration of 0.00 minutes, a minimum height of 1.5e6, and an m/z tolerance of 0.002. The resulting chromatogram lists were then deconvoluted using a local minimum search with the following parameters: a chromatographic threshold of 10.0%, a minimum RT of 0.01 minutes, a minimum relative intensity of 15.0%, a minimum absolute height of 1.0e6, a minimum ratio of peak top/edge of 5, and a peak duration range of 0.01 to 0.10. Following

deconvolution, the electropherograms were then deisotoped with an m/z tolerance of 0.002, RT tolerance of 0.1 absolutes minutes, and represented by the most intense ion. Alignment for comparison and data export was performed using the RANSAC alignment tool with tolerances consistent with previous processes along with a threshold value of 1 and the minimum number of points set to 10%. Aligned lists were then gap-filled for peaks with a 25% intensity tolerance and again with the m/z and RT range gap filler. Three separate peak lists were then produced corresponding to 1) all features detected, 2) features present in at least two of the replicates within the population, and 3) features found in all three replicates for each population. The above workflow was also followed for HPLC-MS/UHPLC-MS analyses, however time windows were adjusted to accommodate the longer run times and wider retention time windows.

2.1.4.3 Targeted and untargeted CZE-MS/MS analysis

For microfluidic CZE separations coupled to MS/MS experiments, the separation times were increased to 6.00 minutes and the initial applied field strength was reduced to 300 V/cm with a linearly increasing field strength gradient from 300 V/cm to 1000 V/cm over the 6.00 minutes. Pressure assist was initiated at the 3.00 minute mark. Untargeted MS/MS analyses were performed via the Xcalibur data-dependent acquisition (DDA, Full MS/dd-MS2) module. Briefly, full scan acquisitions were acquired as listed above. For the dd-MS2 parameters: a Top3 loop count with a 0.5 s dynamic exclusion was applied at 17,500 resolution with a 1e5 AGC target, 8e3 AGC minimum, 50 ms maximum IT, 2.0 m/z isolation window, and a fixed NCE of 30. Due to the ionization character of the alkaloids of interest, doubly charged ions and isotopes were also excluded. An exclusion list was also developed based on a blank full-scan analysis to prevent background ions or

those attributed to contaminants in the BGE or diluent from being selected by the Top3 experiment. Targeted MS/MS analyses were performed via the Xcalibur Parallel Reaction Monitoring (PRM) module. An inclusion list formulated based on the average (n=6) retention times and durations for seven of the ions of interest was applied. All applicable MS/MS parameters applied for the DDA were also applied for the PRM experiment. Fragmentation was induced with either 35 or 40 normalized collision energy (NCE). All analyses were performed in positive ion mode only, as stated previously.

Results and Discussion

2.1.5 Method Development and Characterization

To test the hypothesis that novel metabolites or changes in the observed metabolite regulation were the source of the *in vitro* hDAT inhibition observed by Naprogenix Inc, a metabolomics mass spectrometry-based analysis protocol was developed to compare wild type, field grown *L. cardinalis* to transgenic mutants expressing hDAT. Prior to mutant screening and metabolomic characterization, preliminary range finding experiments were performed to develop efficient extraction procedures of the plant material and reproducible chromatographic and electrophoretic separations methods. Compared to the other member of the *Lobelia* genus, *Lobelia inflata*, few articles have been published that focus on analyzing *L. cardinalis* since the 1960s.[72,80,86] Due to the relatively unknown nature of this plant, developing a putative "metabolites of interest" list to compare features observed across the mutant species was crucial. Initial HPLC-MS (Agilent MS) analyses of methanol extracts of whole plant material yielded mass lists consisting of few features aside from the primary metabolite

produced by *L. cardinalis*, lobinaline (Figure 2.4). It was theorized that a majority of the sample weight was contributed to chemical species outside of the analytical window such as high-mass molecules (fats/waxes, peptides/proteins, macromolecules and chlorophyll) or species better suited for different ionization methods such as negative ion mode ESI (ex. glucosides and acidic molecules). To address this, additional extraction methods needed to be employed prior to analysis in order to increase the signals of the putative metabolites of interest, the alkaloids, without concentrating the other interfering metabolites and possibly shortening the life of the HPLC components (blockages in transfer lines, insoluble buildup on the front end of the column, binary pump degradation due to pressure fluctuations, etc). Due to the basic nature of the nitrogen containing alkaloids, an acidic/basic extraction was developed. A variety of acid/base combinations and organic solvents were evaluated to determine the most effective, efficient, and reproducible extraction procedure (discussed in further detail in section 2.3.2.1). It was determined that, for analytical comparisons of the alkaloid containing fractions of the cultures, using HCl and NaOH as the acidic and basic components, respectively, and extracting with chloroform yielded the most comprehensive result. Following the development of the extraction method, the next issue to be addressed was the analytical separation method to be employed and coupled to the mass spectrometer.

2.1.5.1 UHPLC-MS method development and evaluation

Following the acid/base extraction, the plant extracts were enriched in alkaloids/basic analytes and in a suitable state for characterization. Up to this point, all range-finding analyses were performed on a nominal mass instrument (Aglient MS) with a solving power of approximately 800 based on the full width at half max (FWHM) for

an ion at m/z 400. Since little was known about the secondary metabolites produced by *L. cardinalis,* a high-resolution accurate mass (HRAM) instrument, with a resolution of 140,000 for an ion at m/z 400 and the capability to accurately determine the mass of an ion with higher precision (m/z 400 vs m/z 400.0000), was required to narrow down putative empirical formulas of unknown secondary metabolites. To address this, subsequent analyses were performed using the Thermo Q Exactive HRAM orbitrap mass spectrometer. To contribute further robustness to the analysis, chromatographic separations were performed using on a UHPLC system and column (Shimadzu Nexera) rather than an HPLC (Agilent 1100 series). The primary difference in UHPLC separations compared to HPLC separations is in the smaller particle size of the stationary phase material of the former compared to the latter used inside the column. Recalling that particle size is directly related to the A and C terms of the van Deemter equation, reducing the particle size from 5-10 µm (HPLC) to 1.9 µm (UHPLC) can have a drastic impact on the separation efficiency. As part of the instrument transition, column stationary phase was also evaluated. Preliminary investigations employed a column packed with a C18 stationary phase. Stationary phases consisting of phenyl ring or phenyl ring-like structures were evaluated to determine if pi-stacking interactions between the stationary phase and the phenyl rings of the lobinaline and lobinaline-like molecules would enhance separation efficiency. The stationary phases evaluated were biphenyl (BiPh), pentaflurophenylpropyl (PFPP), and phenylhexyl. The primary evaluation critique used was the separation of lobinaline ($C_{27}H_{35}N_2$ - m/z 387.2795) from what was originally theorized to be an oxidized form of lobinaline ($C_{27}H_{35}N_2O$ – m/z 403.2740 – Figure 2.6). A variety of mobile phase conditions, both isocratic and gradient flows, were

evaluated and examples of the most efficient separations observed can be seen in Figure 2.7. As displayed in Figure 2.7, in terms of peak shape, the C18 column was unparalleled presenting near baseline-resolved, gaussian distributed peaks. The BiPh column displayed improved separation between lobinaline and the putative N-oxide, however, the interaction with the stationary phase and the analytes resulted in band-broadening and very asymmetric peak shapes, which can complicate back-end data processing. For the PFPP and phenylhexyl columns, coelution of the two analytes and poor peak shape was observed independent of whether gradient or isocratic conditions were utilized. Under most chromatographic conditions, the analytes were retained on the PFPP and phenylhexyl columns for the duration of the analysis and elution was only observed at >90% organic (ACN with 0.1% formic acid). Due to the observations made during this comparison, it was determined that the C18 column was the most suitable stationary phase for the analyses. The coupling of the optimized UHPLC-HRAM-MS analysis to the acid/base extraction allowed for increased sensitivity and better separations of unknown secondary metabolites to begin fully characterizing the *l. cardinalis* extracts.

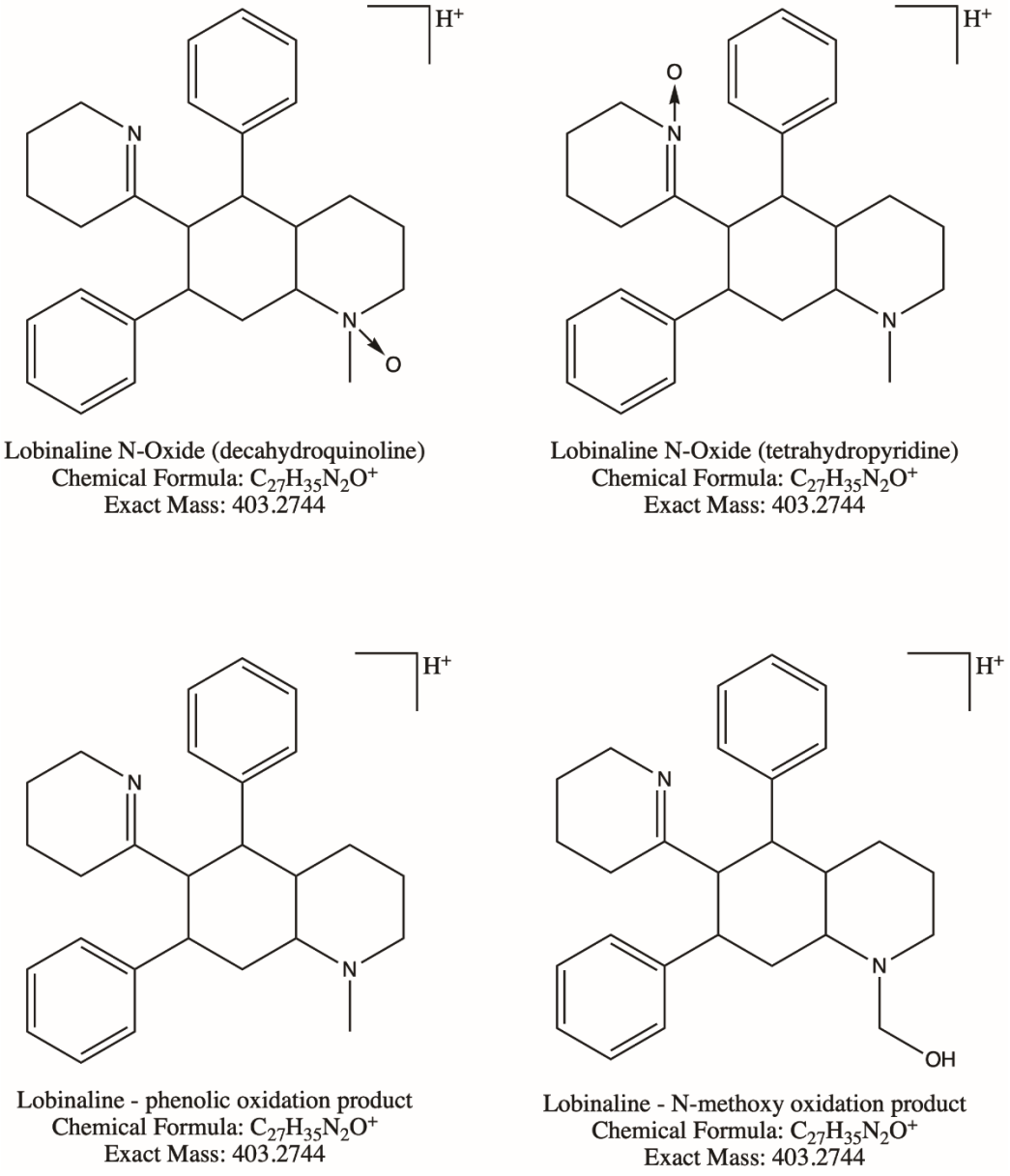

Figure 2. 6 Possible putative structures of the m/z 403.2744 ion used for the evaluation of the HPLC column separation efficiency evaluation.

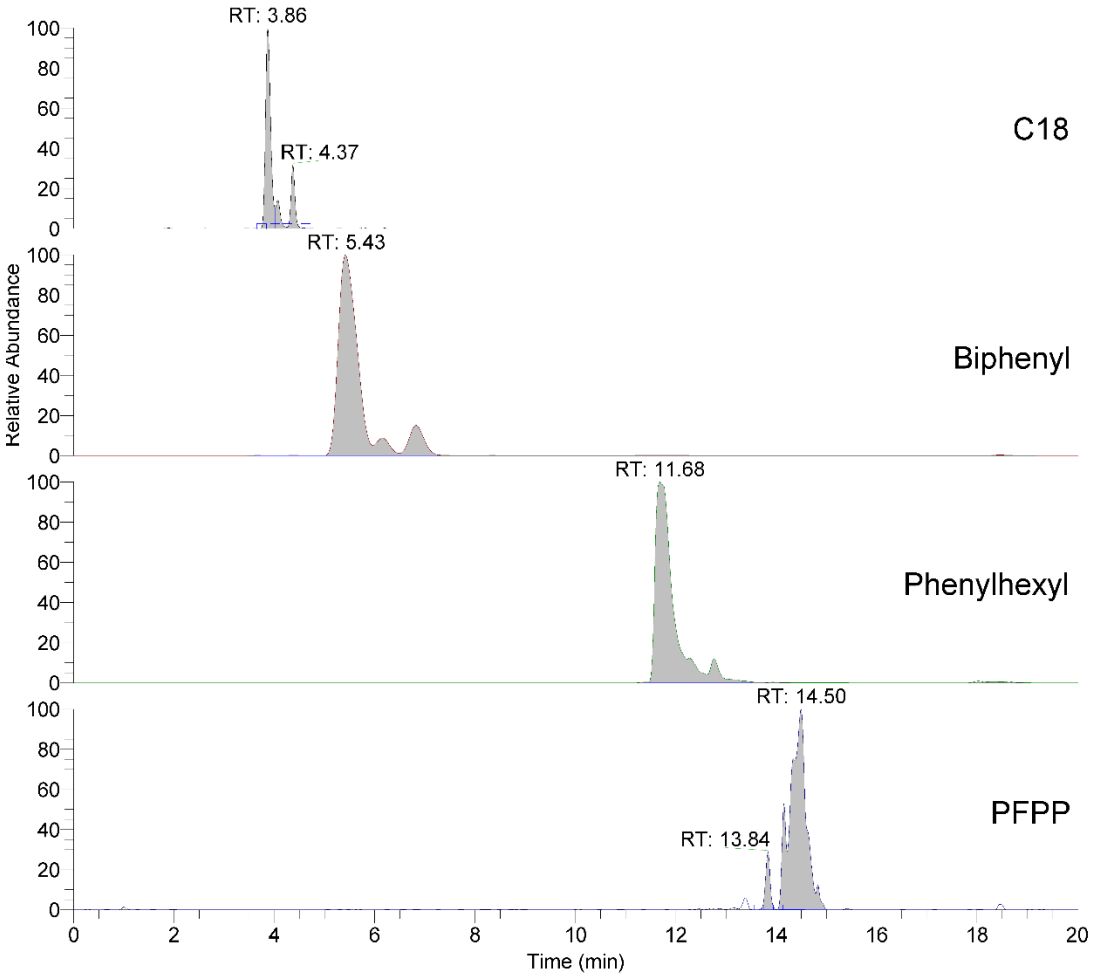

Figure 2. 7 Combined reconstructed ion chromatograms displaying the separation of lobinaline (m/z 387.2795) from the putative oxidation product (m/z 403.2744) using four different RP-HPLC columns.

2.1.5.2 Characterization of Wild Type versus Mutant Strains – UHPLC-MS

Though little primary literature exists regarding *L. cardinalis* metabolism, it is accepted that the plant produces lobinaline as a major secondary metabolite. Because of this, lobinaline content was utilized as the primary screening qualifier during preliminary GC-MS investigations performed by Naprogenix *et al.*[81,82] Mutant strains were characterized according to the quantified lobinaline content and then further categorized as a function of their lobinaline content compared to the observed DA uptake inhibition corresponding to each strain. Through their approach using GC-MS, they determined that, though lobinaline content contributed to the observed activity, it could not be responsible for 100% of the activity observed. The primary objective of our analyses was to determine what, if anything other than lobinaline, was responsible for the increased DAT inhibitory activity observed. In addition to the wild type and transgenic mutant culture extracts, a population in which only the empty viral cassette was inserted (DAT-) and a population in which hDAT was inserted but no gain-of-function mutations were induced (DAT+) were also provided as comparison populations that had not undergone selection.

Comparisons using UHPLC-MS primarily focused first on determining whether or not prevalent differences were readily evident in base peak chromatograms. No observable differences were noted between WT and the DAT- population, however, significant, baseline-resolved differences were apparent in DAT+ and further intensified in mutant strains compared to WT. Figure 2.8 displays stacked base peak chromatograms for WT, DAT+ and a mutant strain LOB479 using both the C18 and the BiPh columns. Note that all samples are produced using the same dry-weight mass of the methanolic

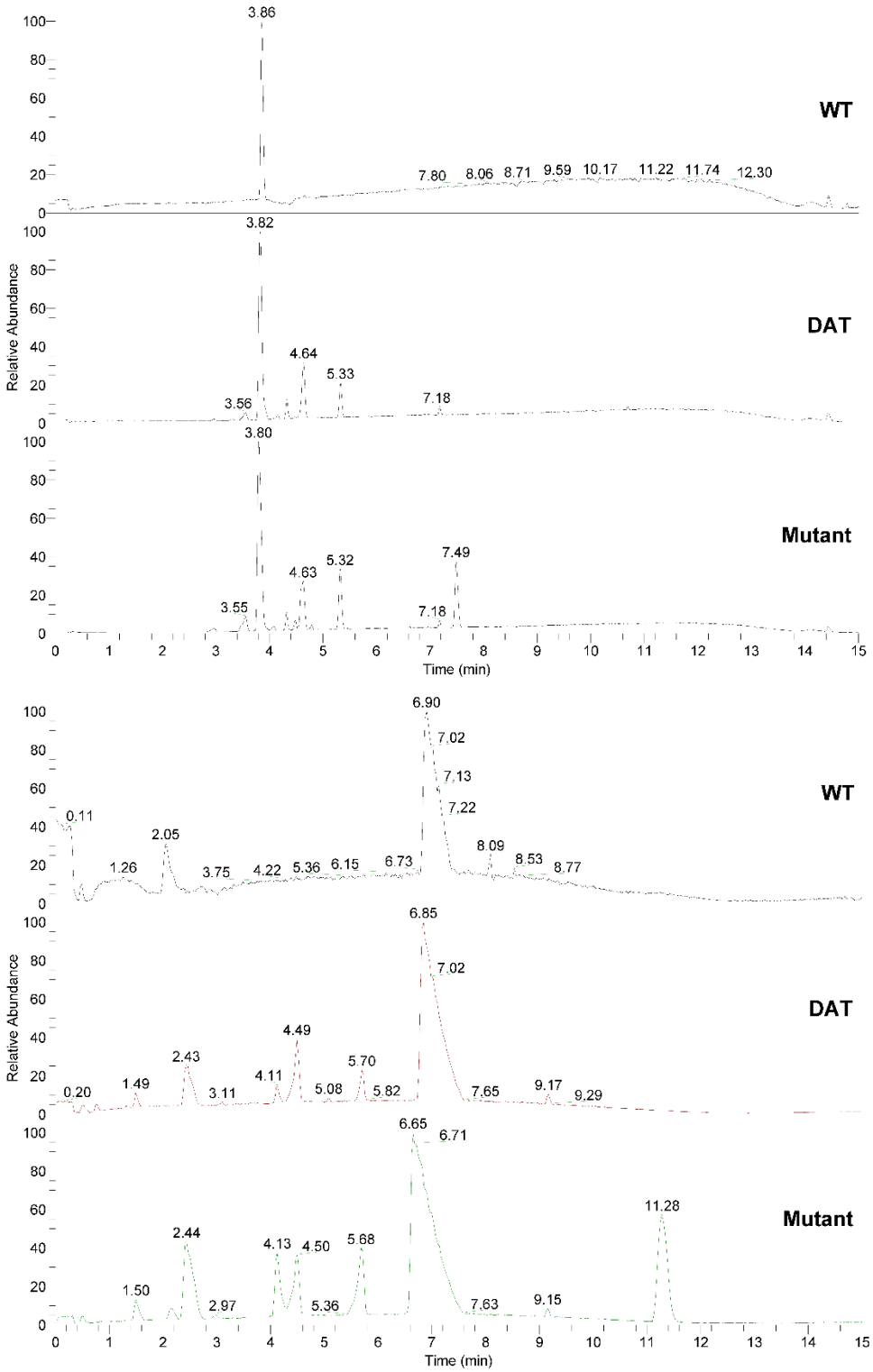

Figure 2. 8 (Top 3 traces): Base peak chromatogram of WT, DAT+, and Mutant *L. cardinalis* plant extracts using a C18 RP-HPLC column. (Bottom 3 traces): Base peak chromatogram of WT, DAT+, and Mutant *L. cardinalis* plant extracts using a biphenyl RP-HPLC column.

extract (1 mg/mL) so variations in responses of metabolites common to the sample-set are not attributed to differences in sample concentration, from a dry-weight basis. Focusing on the C18 base peak chromatograms, the major peak across all populations at ~3.8 minutes corresponds to lobinaline. The mass spectrum for lobinaline can be seen is Figure 2.9. Note that, in the mass spectrum for lobinaline, both the $[M+H^+]$ ion, m/z 387.2795, and the $[M+2H^+]$ ion, m/z 194.1436, can be seen in a ~1:2 ratio. This doubly charged phenomenon, attributed to lobinaline's the two basic nitrogen (pKa – simulated using Chemicalize software - tetrahydropyridine nitrogen: 9.06, N-methyldecahydroquinoline nitrogen: 10.22), was used as one of two motifs used to identify putative lobinaline-like molecules (discussed in further detail in section 2.3.2). The area counts for lobinaline increase 2-fold from WT to DAT+ and 5-10-fold from WT to the mutant strains. In addition to relative increases in lobinaline content, several other features were observed as baseline resolved peaks not readily apparent in WT cultures; 4.63 minutes – m/z 258.2426, 5.32 minutes – m/z 272.2583, 3.52 and 7.49 minutes – m/z 242.2115, and 4.31 minutes – m/z 403.2745 and m/z 202.1410. As stated in regards to the column selection process, the ion present at 4.31 minutes, m/z 403.2745, was putatively identified to have an empirical formula of $C_{27}H_{35}N_2O$ and displayed the same doubly-charged motif as lobinaline (z=+2: m/z 202.1410). This further indicated that it was likely a lobinaline-like molecule with the addition of an oxygen, such as an N-oxide, though additional chemical and mass spectrometry-based assays needed to be performed to provide further evidence for confirmation (see section 2.3.2.3). The data processing software, MZmine2, was utilized to process the data in an attempt to identify trace features not readily visible in the base peak chromatograms of the extract analyses,

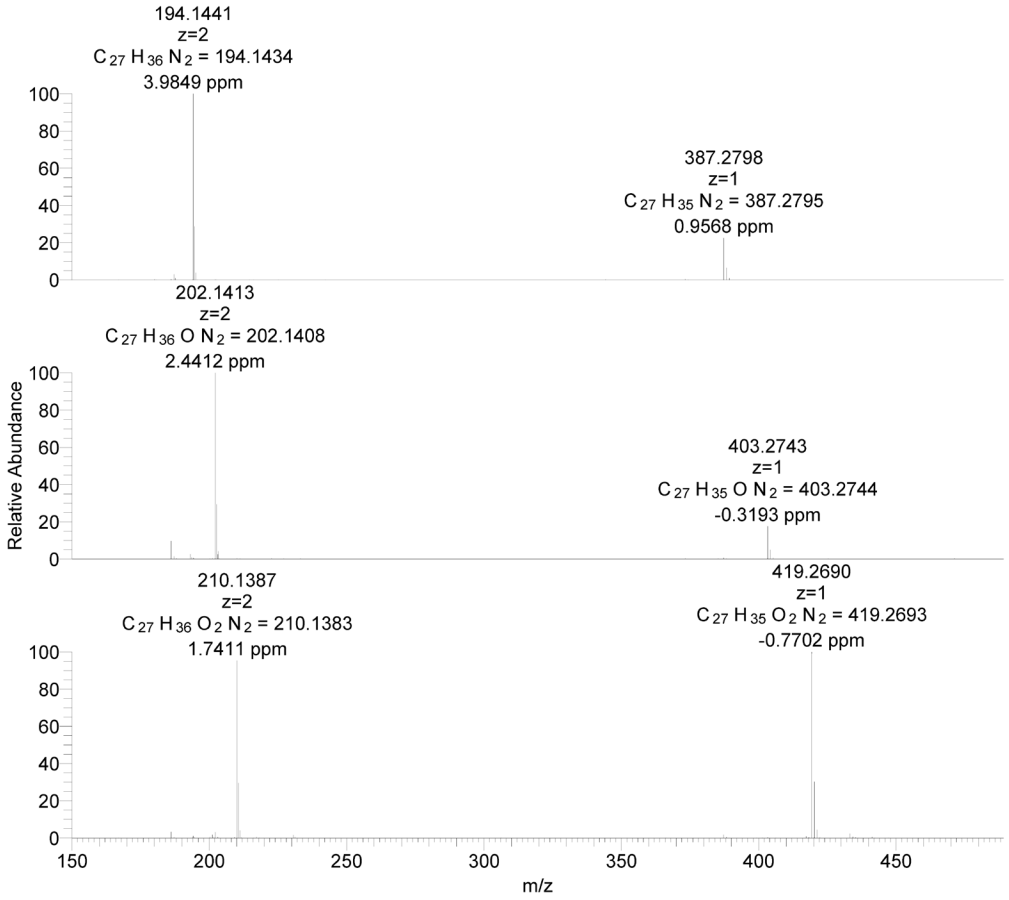

Figure 2. 9 Mass spectrum of lobinaline, m/z 387 (top), m/z 403 (middle), and m/z 419 (bottom) displaying both the single and doubly charged ions for all three analytes, a common motif of binitrogenous "lobinaline-like" alkaloids.

however, mainly due to variations in the baseline attributed to the chromatographic mobile phase gradient (see Figure 2.8, top trace, for example of this increase) and other inconsistencies, such variations in peak duration and peak asymmetries caused by interactions with the stationary phase, generating accurate peak lists representative of the WT and mutant cultures was not possible without significant, manual, post hoc correction. Additionally, the multiply charged nature of many of the analytes further complicated the process in that singly charged low mass species (~m/z 200) could be mistaken for the z = +2 species of higher mass ions (lobinaline z = +2: 194.1415), or vice versa. Though useful for qualitative identification of differences between the sample populations, such as the relative increase in lobinaline and its putative N-oxide, and initial development of peak lists containing features of interest, an alternative comparison method was necessary to determine the presence of trance analytes. To address the issues presented in the use of UHPLC-MS, the use of capillary electrophoresis was investigated due to the high sensitivity and separation efficiency associated with the technique and the reduced flowrate inducing a lower baseline, further aiding in chromatographic deconvolution. Also, since the primary focus of this analysis is on small, basic molecules, CE would be highly applicable as electrophoretic mobility is highly dependent on a molecule being charged in solution.

2.1.5.3 CZE-MS method development and evaluation

As an alternative approach to using UHPLC for separations and comparison, capillary electrophoresis was employed to semi-quantitatively assess the differences between mutant *L.* cardinalis and WT plant extracts. Both traditional “macro” CE-MS and microfluidic CZE-MS were evaluated for this approach (example base peak

electropherograms can been seen in Figure 2.10). Due to instrumental constraints with the "macro" CE-MS approach, i.e., incompatibility of the ionization source required to couple the CE instrument to the high-resolution mass spectrometer, the microfluidic CZE-MS approach was mainly utilized and the macro system was only employed to determine whether or not CE would be applicable to the analytes of interest. Preliminary CE-MS trials resulted in sharp, intense, and symmetrical peak-shapes for the ions of interest previously identified using the UHPLC-MS approach, but little information in regards to other secondary metabolites was observed, most likely due to the low sensitivity of the instrument the CE was coupled to. The electrophoretic characteristics observed of the analytes of interest, however, suggested that utilization of the CZE-MS would most likely be an effective. As depicted in Figure 2.10, the CZE-MS approach provided the same sharp, gaussian, and resolved peaks observed in the macro approach but also introduced other features that were previously unnoticed amongst the baseline noise. In addition, complex separations could be performed using the microfluidic CZE-MS (3 minutes plus sample delivery) approach ~5-7x faster than using the macro-CE approach (20 minutes plus sample delivery).

In order to make statistical comparisons, triplicate extracts from WT *Lobelia cardinalis* hairy roots were analyzed and compared DAT+ mutant culture extracts and extracts from a representative hDAT mutant culture that suggested to overproduce protective alkaloids other than just lobinaline. Example base peak electropherograms for each strain (WT, DAT+, and "Mutant") are shown in Figure 2.11. Prior to any data processing, notable differences were observed between the WT sample compared with the DAT+ and mutant samples as observed in the UHPLC-MS approach. Five additional

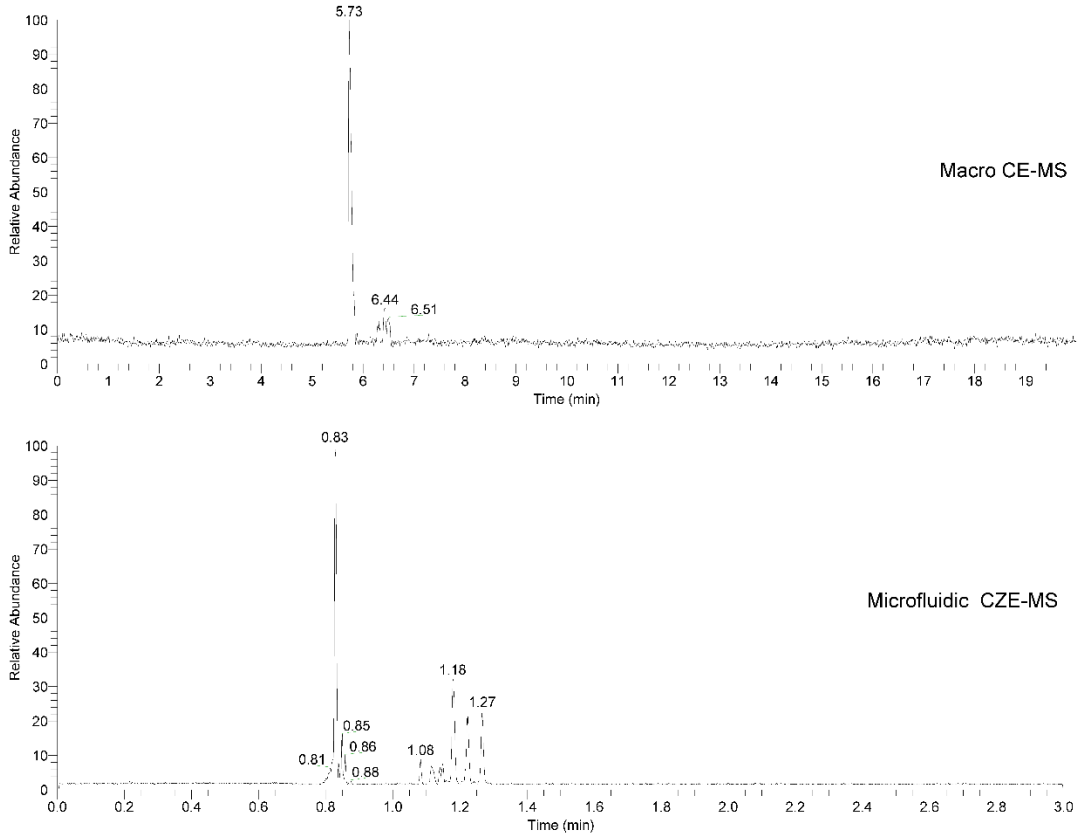

Figure 2. 10 Base peak electropherograms of the Mutant *L. cardinalis* extract using macro CE-MS (top) and microfluidic CZE-MS (bottom).

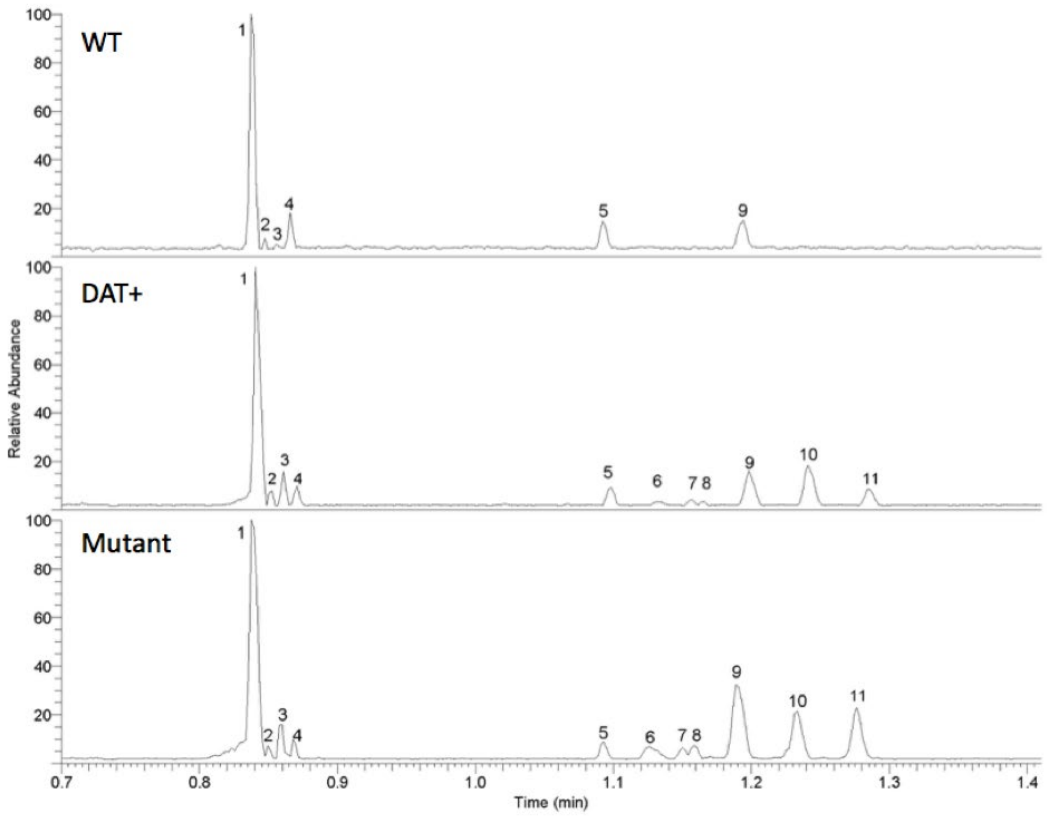

Figure 2. 11 Base peak electropherograms of WT, DAT+, and Mutant *L. cardinalis* extracts using the microfluidic CZE-MS approach.

peaks for the DAT+ and mutant were observable in the base peak electropherogram. It is also noteworthy that all of the observed peaks elute between the 0.7 and 1.5-minute marks making the entire separation approximately ten-times faster than the time required for a standard HPLC separation of similar material.

To assess the robustness of this approach, intra-day precision of the microfluidic CZE separation method was also evaluated. A WT extract was analyzed in analytical triplicate immediately preceding the first blank analysis of the day (t=0) and then again in triplicate approximately twelve hours later (t=12) with ~60 analyses in-between on the same HS chip. Twelve hours was chosen as the limit due to the manufacturer stating the BGE and diluents expire after twelve hours due to pH instability. For this assessment, the area count and retention time of the lobinaline (m/z 387.2795 – $C_{27}H_{35}N_2$) peak was compared. At t=0, the average lobinaline area count was $2.4e^{10}$ with an RSD of 14% and at t=12, the average area count was $2.5e^{10}$ with an RSD of 3%. Using a paired, two-tailed, student t-test ($\alpha = 0.05$) there was no statistical difference between these two means ($p=0.70$). A similar trend was observed in the average retention times of the lobinaline peak at 0.76 min (RSD = 1%) and 0.75 min (RSD = 2%) for the t=0 and t=12, respectively. Here, again, no statistical difference was observed via the t-test ($p=0.48$). This result suggests that the data acquired using this CZE-MS approach will not require the same post-hoc manual correction that the UHPLC-MS approach required during the data processing step.

2.1.5.4 MZmine2 data processing

The .RAW data files corresponding to the triplicate analyses of the WT, DAT+, and Mutant extracts were converted to .mzXML files and processed using the MZmine2 software following the workflow visualized in Figure 2.12 to increase the depth of metabolite coverage. Using MZmine2 as a data-mining software, peak lists were generated to allow for direct comparison between the strains both in the number of features detected and in area counts corresponding to each of those features. Prior to peak list generation, however, mass detection and chromatogram building must be performed. For this data set, a low noise level was set in order to ensure that low intensity signals corresponding to potential analytes in the samples were not discarded during processing. Any features associated with background noise that were included in the mass list due to the low noise level were processed out in a later step based on their peak duration. Here, the CZE-MS approach was considerably more advantageous than the UHPLC-MS approach as the baseline noise levels remain consistent throughout the analysis due to the ESI spray conditions remaining consistent. Masses were also only detected during the elution window starting with the elution of the leading electrolyte from the separation channels at approximately 0.70 minutes. Following mass detection and noise filtering, the resulting mass lists were converted into "chromatogram lists" for processing. Analyte band compaction during the separation and focusing process in the separation channels resulted in sharp, narrow electropherographic peaks with durations less than 0.1 minutes, therefore, the duration parameter in the chromatogram builder module was set to 0.0 minutes as the software utilizes single decimal increments. The resulting peak lists were then deconvoluted and deisotoped to remove the aforementioned background and noise-related features and any features that are part of an isotopic distribution. The filtered

electropherograms were then aligned using the RANSAC aligner tool to allow for direct comparison of each feature based on common retention times and peak durations. Any individual feature discarded in a prior process was then reclaimed using the gap-filling modules. Lastly, any feature not present in at least two replicates was filtered out using a peak list row filter.

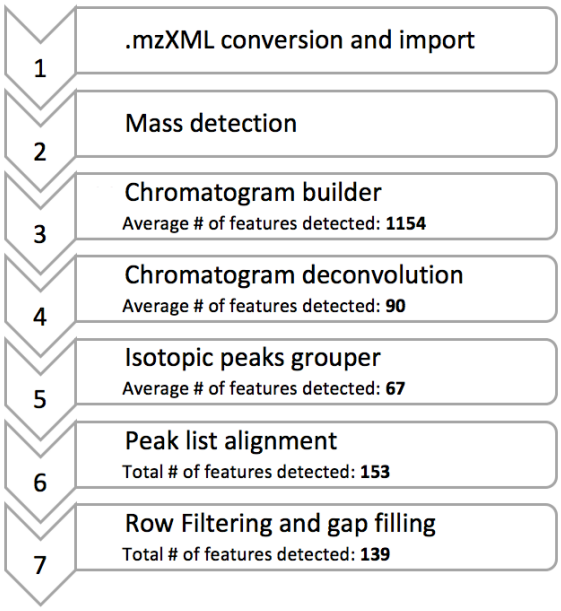

Figure 2. 12 MZmine2 workflow displaying the changes in the number of detected peaks after using each module.

2.1.5.5 Characterization of Wild Type versus Mutant Strains – CZE-MS

Using MZmine2, 139 unique, resolved peaks were detected that appeared in at least two replicates of the same sample. This strict filtering approach was utilized to reduce noise/spike related peaks and possible laboratory contaminants that were not common to all the samples, especially those within each triplicate set. The WT, DAT+, and mutant sample sets contained 136, 139, and 137 peaks, respectively observed in at least two of the triplicate samples (full feature list with associated area counts appendix 1). This master peak list was then used to select several known or putatively identified molecules of interest, such as those previously discussed, for a statistical comparison list. Lobinaline and lobinaline-like derivatives, henceforth referred to as "lobinalines" were initially set as top priority molecules due to the hDAT inhibitory activity of lobinaline reported previously.[81,82] The categorization of "lobinalines" was based on the calculated empirical formulas of the detected features and the common motif that they all share in the capability to become doubly charged molecules during electrospray ionization experiments. Figure 2.9 shows an example mass spectrum of lobinaline (Figure 2.9 – $C_{27}H_{34}N_2$ MW=386.2722, m/z for z: +1 = 387.2795, m/z for z: +2 = 194.1438), the putative N-oxide version of lobinaline (Figure 2.9B - $C_{27}H_{34}N_2O$, m/z for z: +1 = 403.2740, m/z for z: +2 = 202.1410) and the putative bi-N-oxide (Figure 2.9C - $C_{27}H_{34}N_2O_2$, m/z for z: +1 = 419.2693, m/z for z: +2 = 210.1387) displaying this common charge state motif. Additionally, features considered to share similar biosynthetic precursors to lobinaline, such as putative sedamine-like derivatives, and those found in relatively high abundance within the samples (i.e., visible in the base peak) were also added to the comparison list. Table 2.1 displays the final comparison list

of all the selected features with the corresponding average area count and relative standard deviation. Correlating putative structures, as suggested by MS/MS fragmentation patterns (discussed in more detail below), can be observed in Figure 2.13.

Average area counts for the lobinalines generally display an increasing trend from the WT to the mutant sample sets. This observation fits with the overarching hypothesis that lobinalines are protective agents against MPP+ toxicity used in *L. cardinalis* mutant selection. The observed abundance increases for the N-oxide (m/z 403.2740 – peak 3) and bi N-oxide (m/z 419.2693) versions of lobinaline are very promising since N-oxides tend to increase hydrophilicity, making both molecules excellent targets for further study.

Structures for both m/z 130.1595 (Figure 2.11/2.13 - peak 3) and m/z 200.2362 (Figure 2.11/2.13 - peak 4) are putative and drawn as primary amines for simplicity. Alternatively, secondary or tertiary amine structures would be equally probable. It should be noted that m/z 129 [$M^{+\bullet}$] has been previously reported in a methanolic plant extract analyzed by GC-MS therefore our observation of m/z 130.1595 [$M+H^+$] was not deemed a laboratory contaminant.[91] Lastly, the lobeline-like molecules, peaks 5-11 (Figure 2.11/2.13) also displayed a generally increasing trend. Though lobeline (8,10-diphenyllobelionol - $C_{22}H_{27}NO_2$), the primary alkaloid produced by *Lobelia inflata*, itself was not observed in these samples and has not been found in extracts of intact plant material of *L. cardinalis* in the past, both lobinaline and lobeline derive from similar precursors.[81]

Table 2. 1 Average area counts and %RSD for each of the most abundant features corresponding to the peaks in Figure 2.11.

	Feature m/z (charge)	Putative EF	Avg Area Count - WT	RSD	Avg Area Count - DAT	RSD	Avg Area Count - Mutant	RSD	NOTES
A1	373.2638 (z=1), 187.1359 (z=2)	$C_{27}H_{33}N_2$	8.16E+07	9%	9.09E+07	17%	1.79E+08	16%	lob. derivative
A2	387.2795 (z=1), 194.1415 (z=2)	$C_{27}H_{35}N_2$	1.75E+09	7%	3.45E+09	11%	5.23E+09	11%	Peak 1
A3	399.2822 (z=1), 200.1446 (z=2)	$C_{27}H_{35}N_2O$	7.28E+07	23%	1.57E+08	24%	1.60E+08	24%	Peak 2
A4	401.2587 (z=1), 201.1284 (z=2)	$C_{27}H_{33}N_2O$	9.42E+06	19%	4.61E+07	21%	6.53E+07	25%	lob. derivative
A5	403.2740 (z=1), 202.1410 (z=2)	$C_{27}H_{35}N_2O$	8.38E+07	11%	3.84E+08	19%	5.31E+08	20%	Peak 3
A6	415.2749 (z=1), 208.1415 (z=2)	$C_{27}H_{31}N_2O_2$	1.42E+07	17%	6.94E+07	23%	3.09E+07	23%	lob. derivative
A7	417.2537 (z=1), 209.1308 (z=2)	$C_{27}H_{33}N_2O_2$	6.61E+06	21%	2.35E+06	33%	3.91E+06	25%	lob. derivative
A8	419.2693 (z=1), 210.1383 (z=2)	$C_{27}H_{35}N_2O_2$	7.50E+05	16%	8.21E+06	20%	1.23E+07	30%	lob. derivative
B1	130.1595 (z=1)	$C_9H_{20}N$	1.43E+08	25%	1.51E+08	23%	1.72E+08	23%	Peak 4
B2	200.2363 (z=1)	$C_{13}H_{30}N$	1.78E+08	22%	2.03E+08	24%	2.19E+08	26%	Peak 5
C1	228.1967 (z=1)	$C_{13}H_{26}NO_2$	7.17E+07	25%	1.77E+08	22%	3.03E+08	22%	Peak 7
C2	242.2115 (z=1) isomer	$C_{14}H_{28}NO_2$	8.49E+07	29%	1.69E+08	25%	4.09E+08	25%	Peak 6
C2	242.2115 (z=1) isomer	$C_{14}H_{28}NO_2$	5.60E+07	24%	1.00E+08	21%	2.58E+08	25%	Peak 8
C2	242.2115 (z=1) isomer	$C_{14}H_{28}NO_2$	3.24E+08	20%	5.22E+08	21%	1.43E+09	21%	Peak 9
C3	258.2437 (z=1)	$C_{15}H_{32}NO_2$	1.03E+08	28%	8.22E+08	23%	1.28E+09	24%	Peak 10
C4	272.2574 (z=1)	$C_{16}H_{34}NO_2$	6.82E+07	25%	3.82E+08	24%	1.15E+09	25%	Peak 11
Note: Peaks corresponding to A1, A4, and A6-A8 are not visible in the base peak electropherogram, however they are molecules of interest due to their lobinaline-like structure									

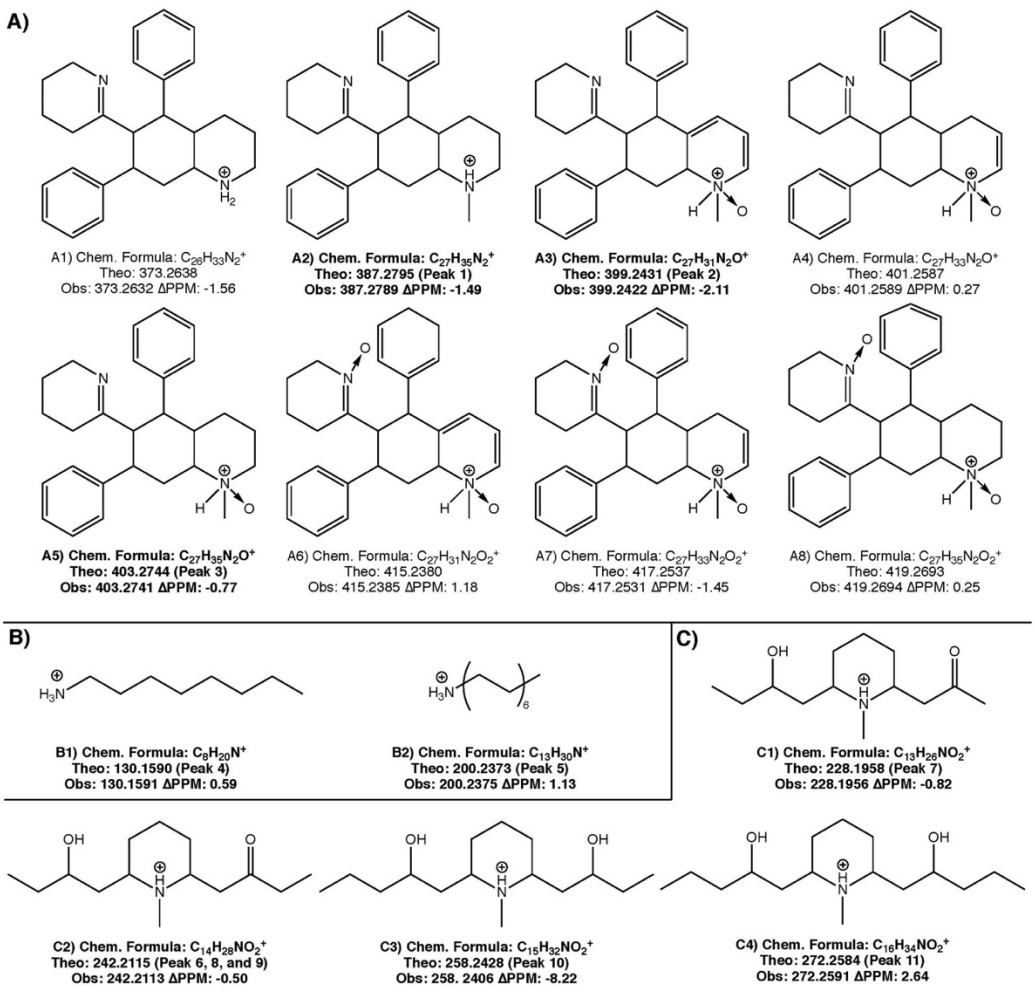

Figure 2. 13 Putative structures of interest. Group A represents lobinaline and lobinaline-like molecules. Group B consists of conjugated monoamines. Structures shown are putative as multiple varying chain lengths are possible for both molecules. Group C consists of lobeline-like molecules which are consistent with similar molecules found in other Lobelia species.

Molecules very similar to these have been reported in the literature to have activity both on the DAT and on nicotinic acetylcholine receptors (nAChRs)[17,18].

Preparative HPLC was used to isolate and purify a sample of lobinaline that was used to develop calibration standards for analysis using the microfluidic device (Figure 2.14). Based on the resulting calibration curve, the WT, DAT, and mutant extract samples were found to contain 83±13 μM, 168±13 μM, and 256±15 μM lobinaline, respectively (calculations for error in concentration values can be found in appendix 2). To translate these concentrations into a whole plant basis, 1.64 g (wet weight) of hairy roots yielded 68 mg of methanol extractable material or 4.14% of the total mass of extractables. Lobinaline comprised 3.2% of the methanol extractable material for WT or 0.13% of the plant (wet weight basis). Similarly, lobinaline comprised 6.5% of the methanol extractable material for DAT (0.27% plant basis), and 9.8% of the methanol extractable material for the mutant (0.41% plant basis).

Additionally, the purified standard was also used to assess both the percent recovery of the extraction method and the method detection limit. The percent recovery was determined to be 99±22% based on the recovery of lobinaline spiked into three separate WT samples and three separate mutant samples (6 total samples). The variation observed in the recovery is most likely due to percent moisture (not determined) in the plant material. For the MDL determination, lobinaline was spiked into powdered *Sedum acre* plant material at a concentration of 100 nM. Following the EPA guidelines for MDL determination, the MDL for this method was determined to be 74 nM. To make a global comparison with WT, variations in isolation, extraction, and analysis of all components must be controlled.

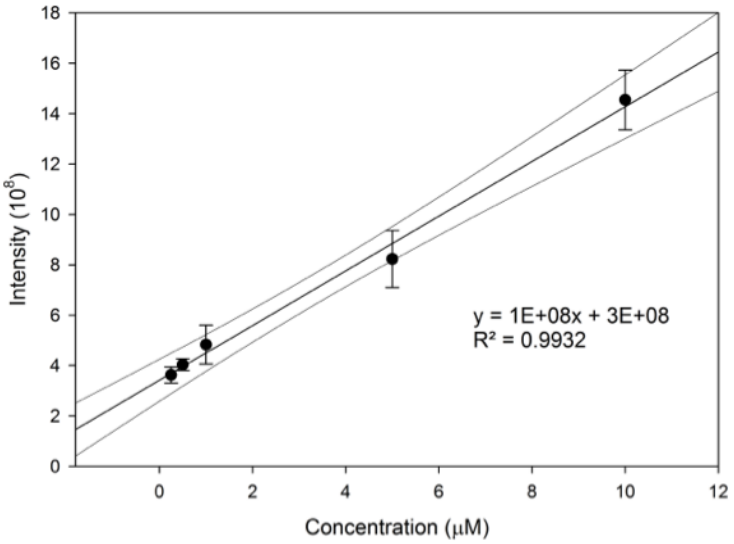

Figure 2. 14 Calibration curve for the quantitation of lobinaline.

Borrowing from quantitative western blot analysis, we evaluated the use of a "loading control" to normalize our data. All nine data sets (3 each from WT, DAT+, and mutant) were compiled and the variance for each of the detected peaks was calculated. The putative monoamine (m/z 200.2363 – peak 5) was found to have the lowest variance and was used as a normalization standard. Several bar graphs displaying normalized area counts for the prioritized features can be seen in Figure 2.15. Normalized area counts for all 139 features can also be seen in the appendix 1 list. Statistical analyses were performed on the prioritized list using the GraphPad Prism 8 software. Tukey's multiple comparison test was utilized as a post-hoc test for the selected features of interest. Statistically significant differences were observed for pairwise comparisons in fourteen of the sixteen prioritized features. Figure 2.15 also displays the post-hoc test result in significant differences denoted by stars (★) under the corresponding bar graphs. From the resulting data set and statistical analyses, multiple putative features have been selected as the potential source of the observed hDAT inhibitory activity.

Following the screening for ions of interest and evaluation of the microfluidic device, tandem mass spectrometry methods were developed to acquire evidence to support the putative structures. Here, both targeted and untargeted MS/MS was applied for analysis of the representative mutant plant extract (Mutant). Prior to any MS/MS experiments, adjustments to the separation method were made to increase the time in which ions were present to allow for adequate sampling of each ion. The applied field strength drives the separation event and analyte band compactions in the microfluidic chip therefore lower field strengths were utilized to broaden the analyte peaks. At the standard field strength of 1000 V/cm, for example, the lobinaline peak is 2.4 seconds

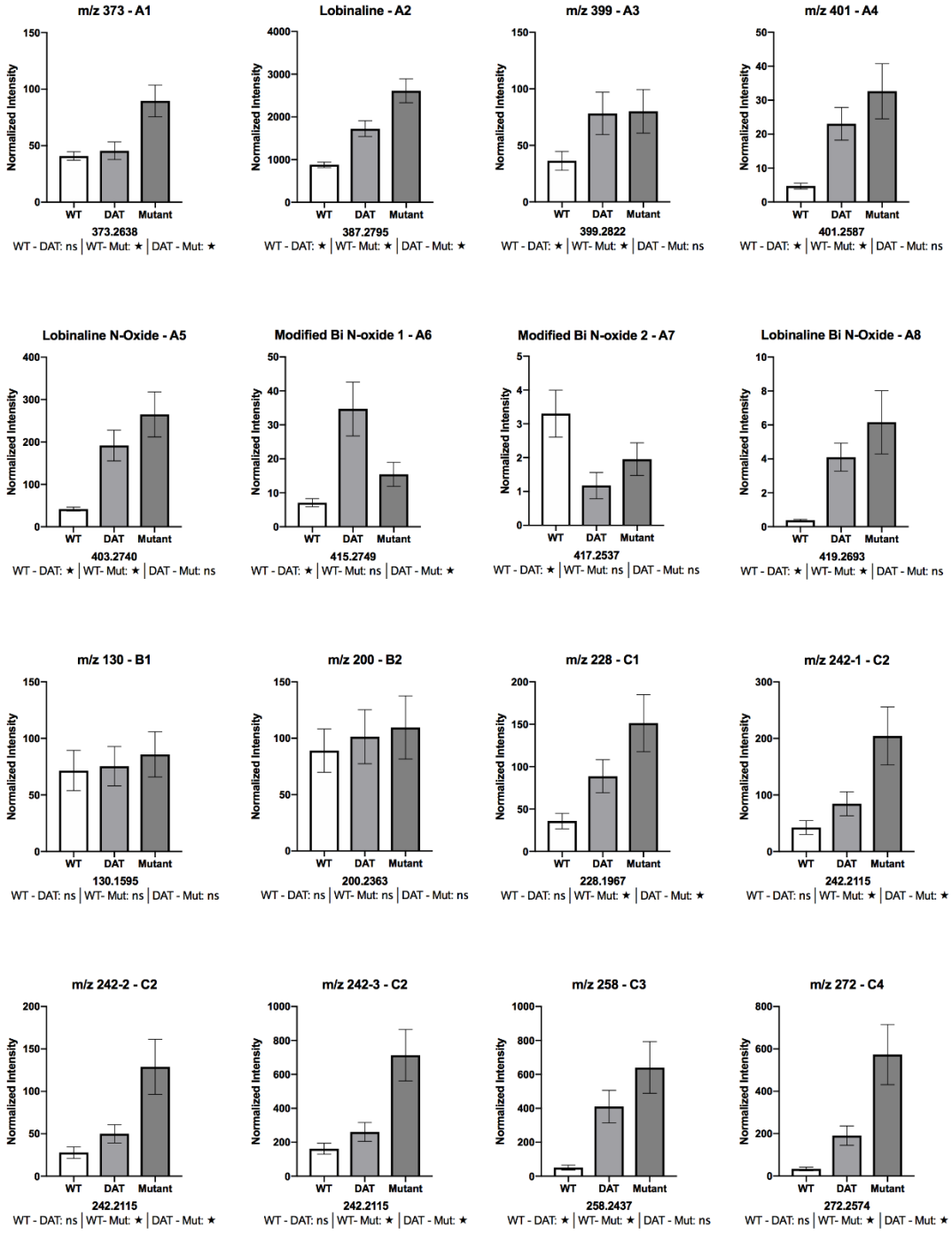

Figure 2. 15 Normalized area counts of the sixteen prioritized peaks - ★ denotes statistically significant based on post-hoc Tukey's multiple comparisons test (ns- not significant).

wide, approximately 21 scans, under the most inclusive MS acquisition parameters. Decreasing the field strength to 300 V/cm increases the peak to over 6 seconds wide consisting of 74 scans. This also changes the retention time, however, increasing it from 0.76 minutes to 2.87. Reducing the field strength to this level also caused the slower moving ions to remain within the separation channel during the allotted analysis time and elute in subsequent analyses, regardless of the application of the pressure assist feature. To address this, a field strength gradient was used. By increasing the field strength linearly from 300 to 1000 V/cm over the 6 minute separation, peak widths were at least doubled and no carry-over was observed. The development of this separation method allowed the data-dependent analysis (DDA – untargeted MS/MS) and parallel reaction monitoring (PRM – targeted MS/MS) experiments to be performed. For the targeted MS/MS PRM inclusion list development, seven of the ions of interest were selected: lobinaline and the mono- and bi- N-oxide versions and the lobeline-like molecule. Tandem spectra can be found in appendix 3. Six full scan acquisitions were acquired to record peak durations for each ion of interest. Using the average durations, the peaklist table was constructed to minimize multiplexing (cycling between more than four ions at once) while also preventing under-sampling (number of MS/MS scans for each ion: >5). To compare the efficiency of these parameters, the average number of MS/MS scans for each feature under both the PRM and DDA experiments was compared to the average number of scans in which that feature was present in the full scan acquisition. Table 2.2 displays this comparison.

Table 2. 2 Comparison of the number of times each feature was selected for both the targeted (PRM) and untargeted (DDA) MS/MS.

m/z (Identity)	FS	PRM-1	PRM-2	PRM-3	Average	Effciency (Avg/FS)	DDA-1	DDA-2	DDA-3	Average	Effciency (Avg/FS)
387 (A2)	30	15	13	14	14	47%	6	5	5	5	18%
403 (A5)	21	14	9	10	11	52%	3	2	1	2	10%
419 (A8)	19	11	10	0	7	37%	0	0	0	0	0%
228 (C1)	91	57	69	41	56	61%	12	9	6	9	10%
242 (C2-1)	37	23	26	0	16	44%	0	0	12	4	11%
242 (C2-2)	18	15	13	11	13	72%	0	5	7	4	22%
242 (C2-3)	30	20	21	21	21	69%	0	8	7	5	17%
258 (C3)	106	26	28	19	24	23%	13	11	10	11	11%
272 (C4)	95	24	26	15	22	23%	12	10	8	10	11%
						48%					12%

The PRM experiment resulted in >40% coverage of the ions compared to their prevalence in the full scan experiments. Those with <25% coverage most likely eluted from the separation channels during multiplexing events, specifically when alternating between three or four ions at once, or outside of the calculated window. The latter is more likely, due to retention time inconsistencies being prevalent in CE mobility experiments when the capillary walls do not have a permanent coating, which is the case for the employed device. Generally, with the PRM approach, under-sampling did not occur as each ion was analyzed more than five times with the exception of m/z 419 and the first eluting m/z 242 isomer in the third trial. Conversely, the DDA analysis did not yield similar results. Despite the usage of the exclusion list and a relatively short dynamic exclusion time, on average only five of the nine ions of interest were sampled adequately. In some cases, those with low abundance, such as m/z 419, were missed entirely. These results suggest that microfluidic CZE is better suited for the targeted MS/MS approach rather than the untargeted MS/MS approach, an aspect where UHPLC-MS outperforms CZE-MS. While useful for major metabolites with substantial peaks in the sample, the untargeted approach is not recommended for the identification of trace components via MS/MS with the microfluidic device as even broadened bands are missed by the selection algorithm.

The resulting findings from this analysis led to the hypothesis that the lobinaline N-oxide molecules, both the mono- and bi-N-oxides, were likely the source of the hDAT inhibitory activity. The reasoning behind this hypothesis is multifaceted. Primarily, novel inhibitory activity was observed by Naprogenix in their assays using lobinaline, however, lobinaline is a highly non-polar molecule and has very poor solubility in water (simulated Log K_{ow} = 4.8, XLOGP3 and 5.6, Chemicalize). The N-oxidation of alkaloids often

results in an increase in solubility. When performing their primary screening assays using whole plant extracts, a highly aqueous buffer was used. Since the mutant strains contain relatively higher quantities of the more hydrophilic lobinaline N-oxides, a higher concentration of the lobinaline-like alkaloids was available to interact with the transporter. Additionally, when characterizing their extracts, GC-MS was employed. The high temperature of the GC inlet will convert N-oxides back to the free-base forms, just as it would produce a dehydration product for an underivatized hydroxyl group. Due to the non-covalent nature of an N-oxide association, N-oxides cannot be derivatized. This aspect caused the N-oxide molecules to go undetected during their analyses leading to the impression that the activity was not attributed to lobinaline. As this newly discovered class of lobinalines was of interest for further hDAT inhibitory assays, and the concentration of this class of secondary metabolites was comparatively high compared to other identified metabolites, they were selected as the target of subsequent extractions, purifications, and characterization assays.

2.1.6 Extraction, Isolation, and Analysis of Lobinalines

As the lobinaline and lobinaline-like molecules were identified as the probable source of hDAT inhibitory activity, purification was required to produce high quality purified material to be used in further *in vitro* assays, performed by Naprogenix, to confirm if they are biologically active. Due to the high concentration of lobinaline in the plant (3.8% w/w of the methanol extracts of the WT plants), purification of lobinaline could be performed with relative ease using standard preparative HPLC methods.

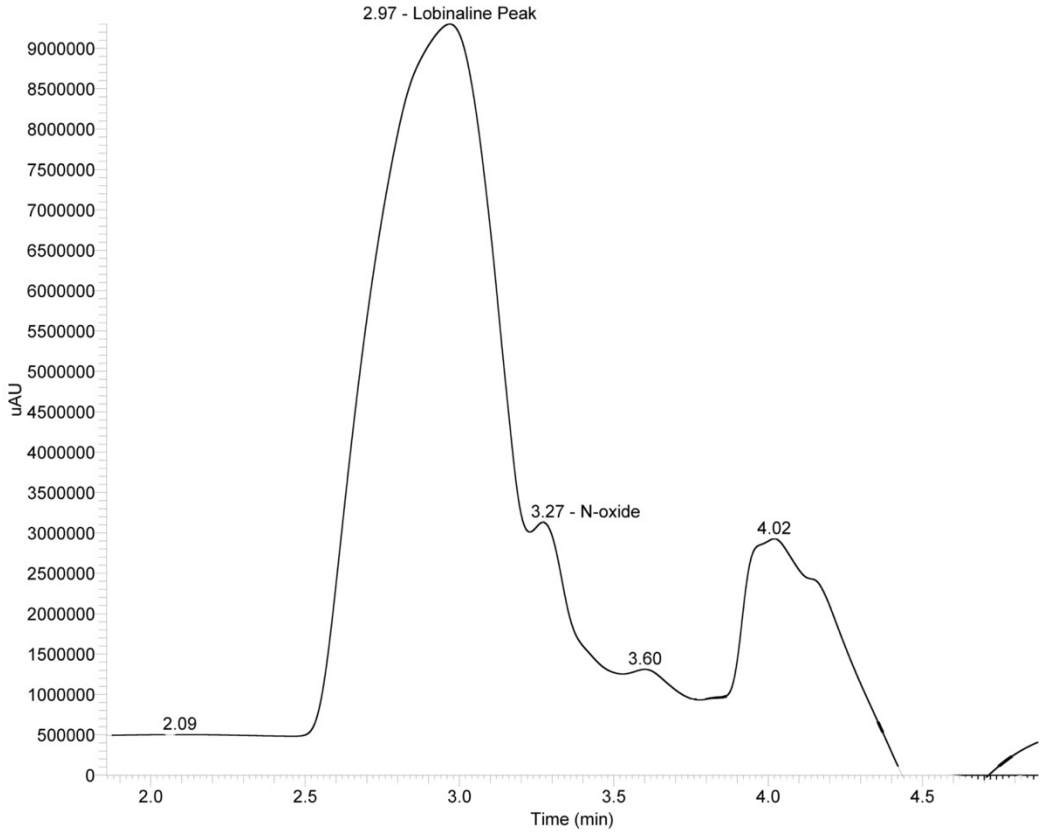

Figure 2. 16 HPLC chromatogram from the pHPLC purification of lobinaline and lobinlaine N-oxide using the C18 column and UV-Vis detection.

Following a large-scale acid/base chloroform partition, using a C18 preparative column and an isocratic gradient, >95% pure lobinaline can be obtained by collecting the leading half of the largest peak in the chromatogram (Figure 2.16). Two to three subsequent passes of the collected fraction through the column yields a >99% pure lobinaline standard. This, however, is not the case for the other lobinaline-like molecules. Assuming equal response factors given the similarities between the analytes, lobinaline is anywhere from ten to one thousand times more concentrated in the plant material than the other secondary metabolites. Additionally, pHPLC conditions provided inadequate separation of lobinaline from the other analytes of interest with the primary target, the mono-N-oxide, always eluting as a shoulder on the tail of the lobinaline peak (Figure 2.16). This aspect requires additional passes through the column to purify the N-oxide compared to the number required to purify lobinaline and, due to the comparatively lower concentration, results in low μg quantities once >90% purity is achieved owing to diminishing returns. To address this, modifications were made to the front-end liquid-liquid partitioning and reimplementation of the biphenyl column, at the preparative level, was applied.

2.1.6.1 Large-scale Extraction and Purification

In order to simplify the process of producing large quantities of purified material, specifically, purified lobinaline N-oxide, the liquid-liquid partitioning step was re-evaluated. Though the previous acid/base chloroform (ABC) method was ideal for analytical purposes, the concentration of lobinaline in the basic extract was at least one to two orders of magnitude higher than the other features of interest detected.

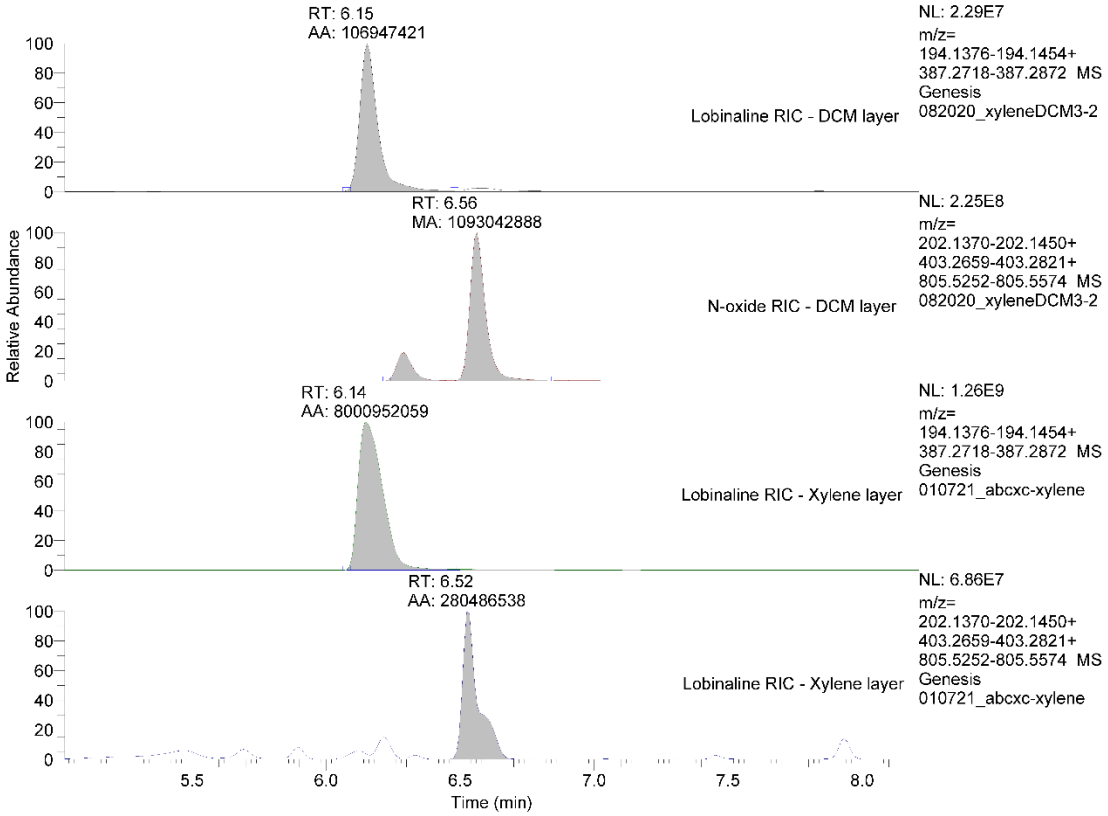

Figure 2. 17 (Top to bottom): RIC of lobinaline (m/z 387) in the DCM partition layer, RIC of the lobinaline N-oxide (m/z 403) in the DCM partition layer, RIC of lobinaline in the xylenes partition layer, and RIC of the lobinaline N-oxide in the xylene partition layer showing that the N-oxide is more concentrated than lobinaline in the DCM layer than it is in the xylene layer.

A series of modifications were tested and made to the workflow in order to selectively extract lobinaline from the target molecules. Organic solvents of varying polarity were evaluated against chloroform in terms of the relative ratios of the N-oxide to lobinaline as determined by UHPLC-MS analysis. The solvents evaluated were: methylene chloride, n-butyl chloride, diethyl ether, toluene, xylenes, and ethyl acetate. Most of the solvents (methylene chloride, n-butyl chloride, and diethyl ether) yielded near identical ratios of the N-oxide to lobinaline to the use of chloroform except toluene and xylenes with the latter, xylenes, resulting in ratios as high as 10:1, N-oxide to lobinaline (Figure 2.17 – top), though averaging between 0.5:1 and 1:1. Note that due to the high boiling point of xylene, it is used during the first half of the partition against aqueous acid, as the organic layer in that step is discarded. The basic partition is still performed with chloroform. This method is hereafter referred to as the "XC" partition. It is believed that increase in the ratio of the N-oxide to lobinaline is most likely attributed to not only the highly nonpolar nature of both of the phenyl ring-based solvent and lobinaline, but also to pi-stacking interactions between the two phenyl rings of lobinaline and the solvent itself. Analysis of the xylene layer displayed low levels of the lobinaline N-oxide compared to lobinaline (Figure 2.17 – bottom), confirming that, though this approach is not explicitly specific for lobinaline, the N-oxide group contributes significantly to the molecule's comparatively more polar nature and equilibrium favors the aqueous layer. Reproducibility, however, was difficult when using toluene/xylene as the initial organic partitioning solvent. The variation observed was believed to be due to the complexity of the matrix, consisting of fats/waxes, sugars, and chlorophyll, interfering with the system equilibrium during the pH changes and xylene partitioning step, i.e. formation of an emulsion. The ABC

partition, using chloroform for both the acidic and basic partition, consistently yielded reproducible results, as confirmed above during the CZE-MS method validation. Additionally, even when scaled-up, the end chloroform and basic aqueous layers were relatively clear aside from a deep yellow color observed in the aqueous layer. Conversely, the end aqueous base layer, when using xylene as the initial solvent for the acidic partition, was near opaque and brown/gold. In an attempt to address the irreproducibility of the partition, the ABC partition was coupled to the XC partition. For this approach, the chloroform from the basic ABC extraction was reduced to dryness and the residue was reconstituted in aqueous acid before undergoing the XC extraction – "ABCXC". To assess the reproducibility, a triplicate partition evaluation using the same stock extract and performed simultaneously yielded 0.35:1, 0.3:1, and 0.65:1, N-oxide to lobinaline. Though the resulting ratios were on the lower end of the distribution (average – 0.42:1 compared to 1:1-10:1 when using the XC method, alone), the end ABCXC chloroform fractions were more reproducible, concentrated in lobinalines at a manageable relative concentration, and contained few detected constituents outside of other members of the "lobinalines" and "lobeline" classes of compounds. The implementation of the ABCXC partition greatly reduced the difficulty associated with using pHPLC to separate the N-oxide from lobinaline, especially since few other analytes were present in the extracts. Additionally, as depicted in Figure 2.7, using an HPLC column with a biphenyl stationary phase displayed better separation of lobinaline from the N-oxide, though sacrificing peak shape. As separation is more significant for pHPLC, a biphenyl preparative column was also utilized to reduce the risk of diminishing returns resulting from coeluting peaks. Figure 2.18 displays an example of a standard separation

using the C18 pHPLC column (top) and the biphenyl pHPLC column (bottom). For the example C18 chromatogram, lobinaline elutes at 6.18 min and the N-oxide elutes and 6.38 min and for the example Biphenyl chromatogram, lobinaline elutes at ~4.75-5.5 min and the N-oxide elutes, with separation of two putative isomers, at 6.52 and 7.09 min. Under the applied conditions, the biphenyl column clearly outperforms the C18 for this specific application in that sufficient separation of the N-oxide from lobinaline is observed. Coupling of the ABCXC partitioning method to the use of the biphenyl preparative HPLC column has led to nearly 200 mg of pure, natural N-oxide and >1 g of pure, natural lobinaline, to be purified for characterization and pharmacological testing.

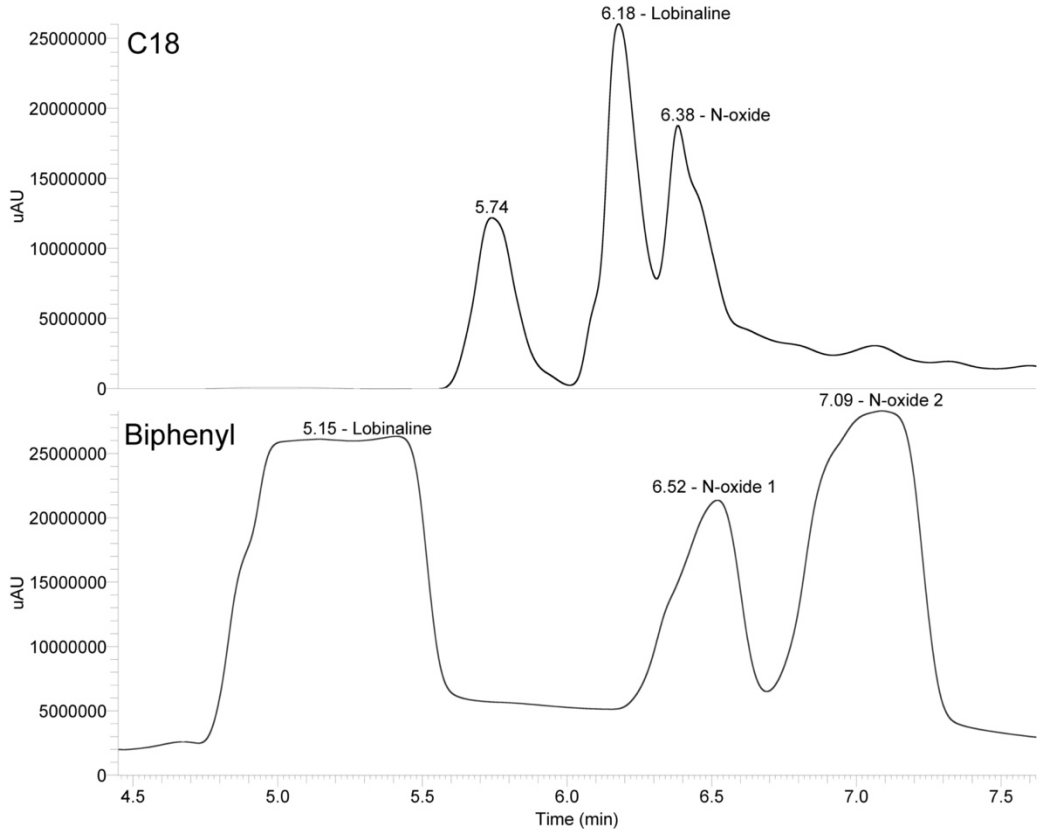

Figure 2. 18 (Top) Base peak chromatogram of the pHPLC purification of lobinaline and lobinlaine N-oxide using the C18 column post ABCXC partitioning. (Bottom) Base peak chromatogram of the pHPLC purification of lobinaline and lobinlaine N-oxide using the biphenyl column post ABCXC partitioning.

2.1.6.2 N-Oxide Characterization

Since little literature exists in regards to *L. cardinalis* secondary metabolites, initial classification of the previously undetected m/z 403.2740 ion as an "N-oxide" was hypothesized based on the calculated empirical formula. Supporting evidence of the oxygen being present in the molecule as part of an N-oxide interaction, rather than a hydroxyl, was provided through the lack of derivatization with BSTFA and, therefore, the ion not being detected via GC-MS, however, further evidence was required. Both chemical and analytical methods were employed to test this hypothesis.

For chemical reaction-based evidence, the first experiment performed was a reduction reaction using Zn dust and HCl. Though unable to unequivocally determine if the oxygen was present as an N-oxide and not a hydroxyl group, the Zn/HCl reaction was intended to confirm that that the oxygen was not involved in the ring structure of the molecule. Using a column purified standard of the putative N-oxide (~95%), the reaction resulted in near full conversion to the free base as depicted in Figure 2.19. Note that the retention time of the lobinaline produced in the reduction reaction matches the retention of the small lobinaline impurity detected in the "before" sample, suggesting homology of the two analytes. In addition to this reaction, the inverse was also performed in chemically converting lobinaline to the putative N-oxide. This reaction was performed using the peroxy acid metachloroperoxybenzoic acid (mCPBA). Due to the two basic nitrogen atoms in lobinaline, this reaction produced both the N-oxide of interest, a mono-N-oxide, and the bi-N-oxide (structure A8 in Figure 2.13, m/z 419.2693, z = +1/210.1382, z = +2).

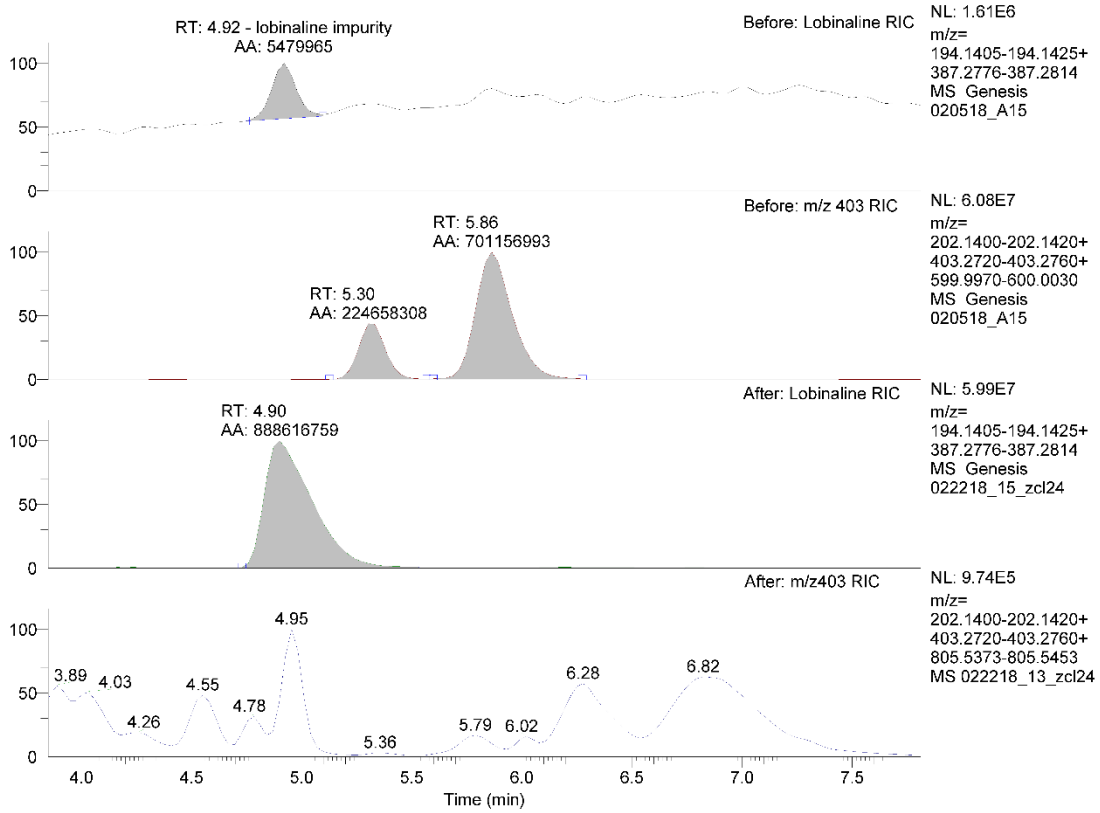

Figure 2. 19 (Top to bottom): RIC of lobinaline prior to Zn/HCl reduction of the N-oxide showing trace levels, RIC of the N-oxide prior to Zn/HCl reduction, RIC of lobinaline post-Zn/HCl reduction, RIC of the N-oxde post-Zn/HCl reduction showing trace levels.

This putative bi-N-oxide is also found in plant material, however, at concentrations 1-2 orders of magnitude lower than the mono-N-oxide and, therefore, several orders of magnitude lower than lobinaline. Figure 2.20 displays this reaction in four reconstructed ion chromatograms. The top trace, for simplicity, represents the "before" pure lobinaline sample with the channels corresponding to the mono and bi-N-oxides also selected showing that they are not present in the sample. The bottom three traces present lobinaline, the mono-N-oxide, and the bi-N-oxide respectively. As depicted, assuming a 1:1 relative response factor, the N-oxide signal is approximately $3/4^{th}$ that of lobinaline whereas it was not present in the before sample. In addition, the putative N-oxide produced has the same retention time as that of the natural N-oxide found in the plant material (Figure 2.21). This was also observed when another lab member, Masoumeh Dorrani, reacted pure lobinaline with hydrogen peroxide and ammonium bicarbonate. The reaction performed by lab member Dorrani yielded complete conversion of lobinaline to the putative N-oxide, and bi-N-oxide when coupled with a rhenium-based catalyst, and the resulting compounds have also been isolated for pharmacological testing to compare them to the results observed using natural N-oxide.

In addition to the aforementioned chemical confirmation experiments, several analytical experiments were also performed to characterize the putative N-oxide. The first regarded the hydrophobicity of the analyte. A common characteristic of N-oxides is increased hydrophilicity compared to their free-base counterparts. Lobinaline has a reported simulated Log K_{ow} of 4.8 (XLOGP3) and 5.6 (Chemicalize), inferring it is highly nonpolar and hydrophobic.

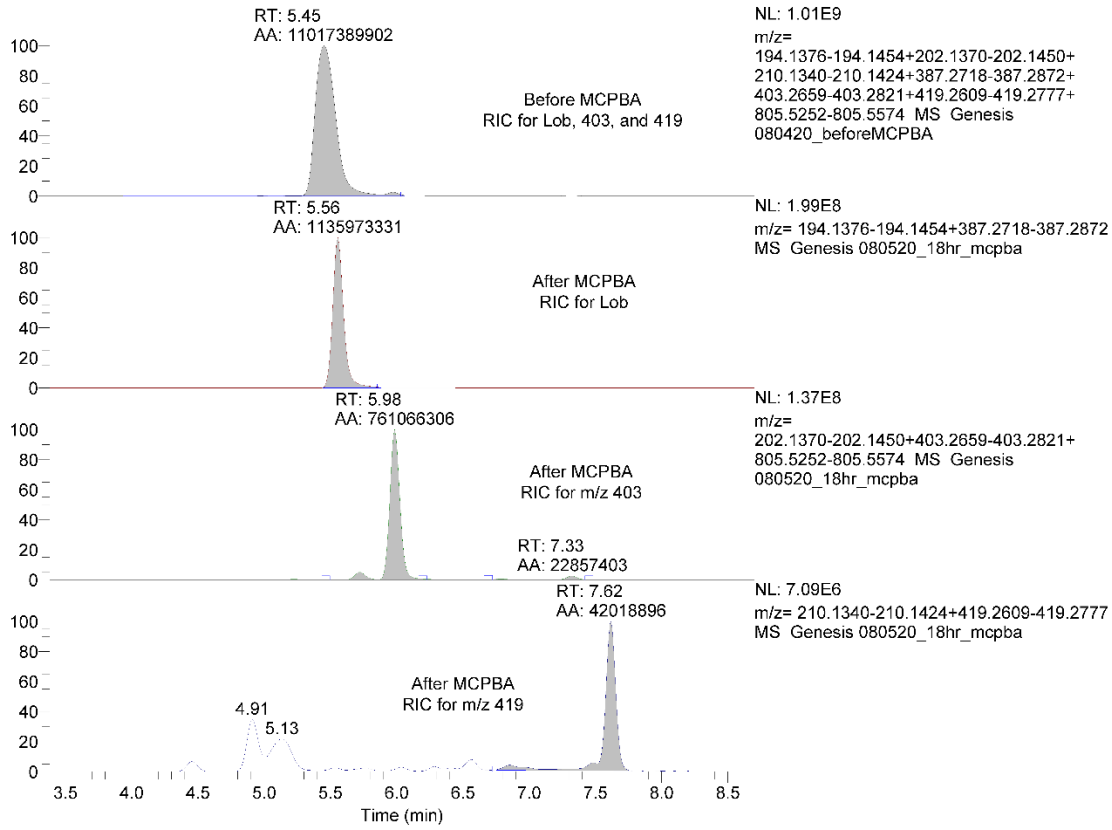

Figure 2. 20 (Top to bottom): combined RIC of lobinaline, lobinaline N-oxide, and lobinaline bi-N-oxide prior to mCPBA treatment showing one major peak, RIC of lobinaline post-mCPBA conversion, RIC of the lobinaline N-oxide post-mCPBA conversion, and RIC of the lobinaline bi-N-oxide post-mCPBA conversion.

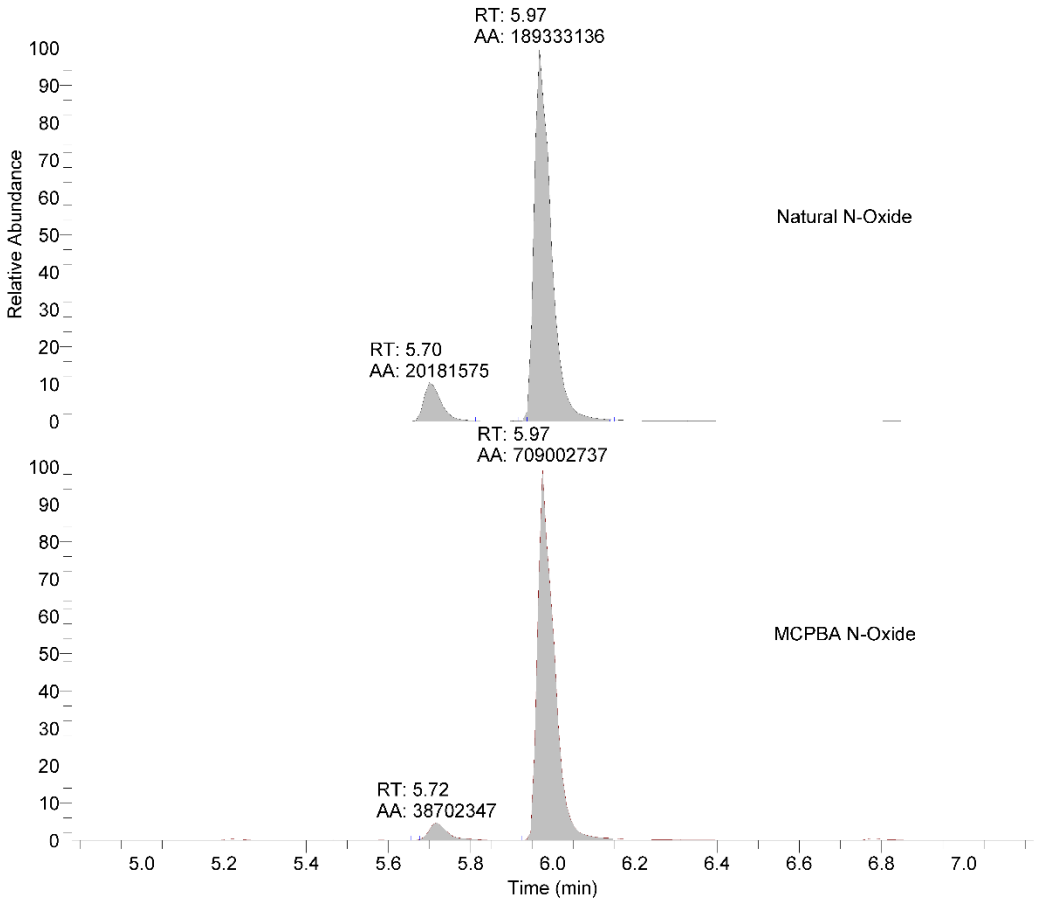

Figure 2. 21 Comparison of the RICs for the natural lobinaline N-oxide and the semi-synthetic lobinaline N-oxide.

The addition of an N-oxide would drastically increase the polarity of the molecule, comparable to that of a quaternary ammonium salt. To test this, the Log K_{ow} was determined following the OECD method 117 guidelines for Log K_{ow} determination via HPLC relative retention time using isocratic separations with varying organic percentages. The system was evaluated using a seven point calibration curve consisting of the experimental determined Log K_w values and the accepted Log K_{ow} values of 4-methylbenzyl alcohol, p-cresol, 4-methoxyphenol, ethylbenzene, anisole, benzyl benzoate, and benzyl alcohol – $R^2 = 0.9724$. Using this curve, the Log K_{ow} of the N-oxide was determined, from the observed Log K_w, to be 1.29 ± 0.19, drastically lower than that of lobinaline.

Tandem mass spectrometry was also utilized to characterize lobinaline and the putative N-oxide analytes. The fragmentation pattern of lobinaline was compared to the fragments produced from the N-oxide precursor ions in order to determine if any fragments could provide evidence to the location of the oxygen within their respective molecular structures. Though N-oxide bonds are generally the most labile bonds in the system, and therefore are usually dissociated immediately when subjected to MS/MS experiments, their presence could cause shifts in the relative abundances of observed fragment ions. Additionally, if the oxygen atoms were involved in a covalent bond rather than as an N-oxide, such as a hydroxyl/phenol or methoxy group, fragment species corresponding to those precursors would likely be present. Figure 2.22 displays stacked MS/MS spectra for lobinaline (top), m/z 403.2740 (middle), and m/z 419.2693 (bottom).

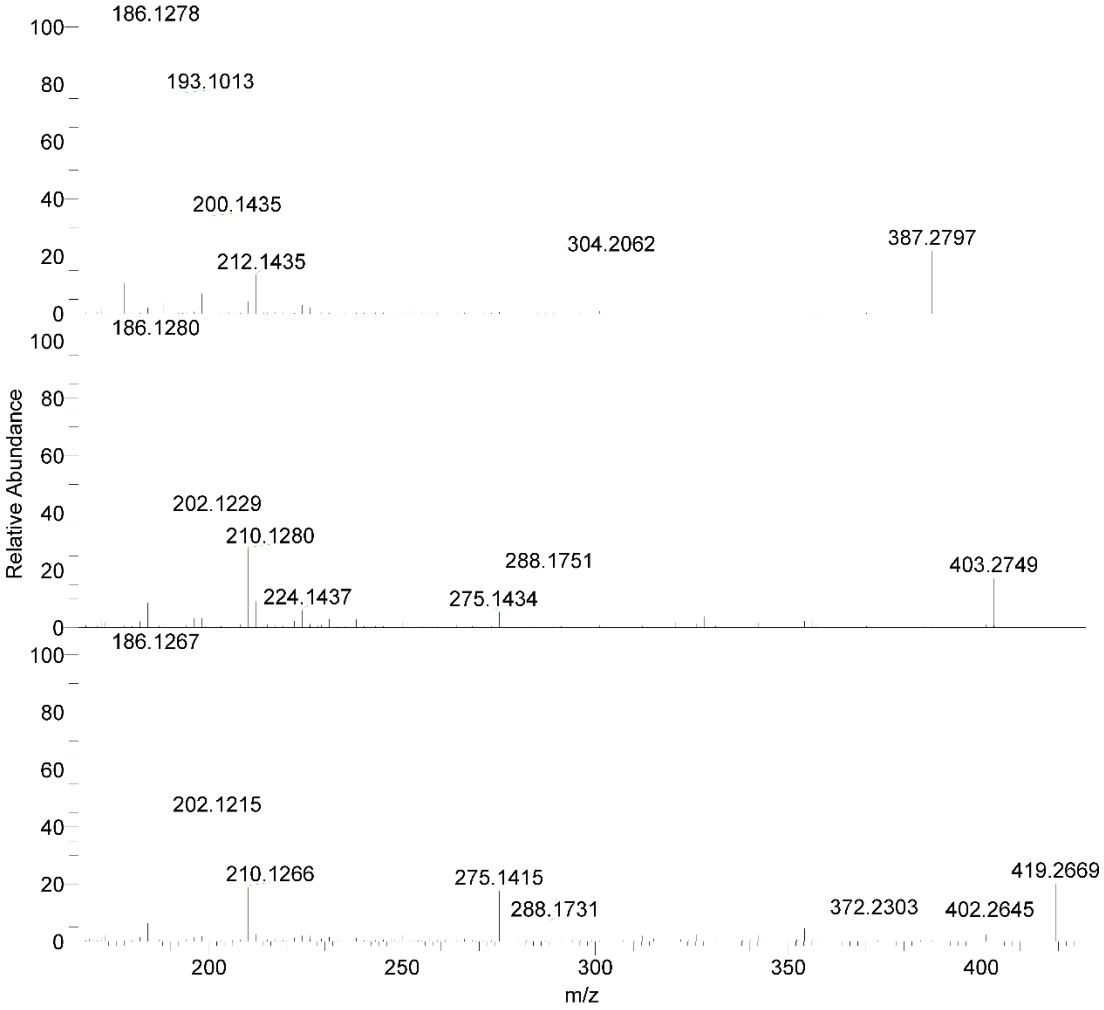

Figure 2. 22 Tandem MS/MS spectra of lobinaline (m/z 387 - top), the lobinaline N-oxide (m/z 403 - middle), and the lobinaline bi-N-oxide (m/z 419 - bottom).

As depicted in Figure 2.22, lobinaline displays a characteristic cross-ring cleavage through the decahydroquinoline ring resulting in the m/z 387 → 186 and m/z 387 → 200 fragmentations to be the predominant fragment ions observed. Additionally, m/z 387 → 304, representing the loss of the tetrahydropyridine ring is also observed as a major fragment along with a variation of the aforementioned cross-ring cleavage resulting in m/z 387 → 212. These possible fragmentation patterns can be seen in Figure 2.23. In viewing and comparing the MS/MS spectra of the three precursor ions, it appears that there are a number of different fragment ions in the N-oxide/bi-N-oxide spectra compared to the lobinaline spectrum, however, almost all of the ions overlap. The overt difference between the spectra is actually predominantly in the relative abundances of the ions rather than in their presence/absence. Lists of the top 50 fragment ions for each precursor were generated and compared using excel (only 2 decimals shown to account for slight variations in mass defects resulting from the loss of the lock mass during MS/MS experiments) – Table 2.3. Fragment ion lists were compared pair-wise (387 v 403, 387 v 419, and 403 v 419) and fragments that were not present in both sets were denoted as seen in table 2.3. Two of the differences can be attributed to the loss of water when the N-oxide bond is dissociated, 419 → 401 and 403 → 385. Again, possible structures for the fragments highlighted in table 2.3 can be seen in Figure 2.24. Interestingly, three low abundance fragment ions of the putative bi-N-oxide were calculated to each contain oxygen, m/z 419 → 372, 419 → 228, and 419 → 247.

Table 2. 3 MS/MS Fragmentation list for lobinaline (387), lobinaline N-oxide (403), and lobinaline bi-N-oxide

387 vs 403				387 vs 419				403 vs 419			
Frag, m/z	Rel. Abd	Frag, m/z	Rel. Abd	Frag, m/z	Rel. Abd	Frag, m/z	Rel. Abd	Frag, m/z	Rel. Abd	Frag, m/z	Rel. Abd
186.13	100.00	186.13	100.00	186.13	100.00	186.13	100.00	186.13	100.00	186.13	100.00
193.10	73.84	202.12	36.91	193.10	73.84	202.12	43.67	202.12	36.91	202.12	43.67
200.14	32.82	210.13	28.70	200.14	32.82	200.14	22.50	210.13	28.70	200.14	22.50
387.28*	19.03	200.14	25.38	**387.28***	19.03	210.13	18.53	200.14	25.38	210.13	18.53
304.21	18.33	288.18	20.79	304.21	18.33	275.14	16.10	288.18	20.79	275.14	16.10
212.14	13.71	**403.27***	20.63	212.14	13.71	**419.27***	14.95	**403.27***	20.63	**419.27***	14.95
178.08	11.05	212.14	9.17	178.08	11.05	***372.23***[9]	6.80	212.14	9.17	372.23	6.80
198.13	7.08	184.11	8.20	198.13	7.08	288.17	6.45	184.11	8.20	288.17	6.45
210.13	4.48	275.14	6.43	210.13	4.48	184.11	6.21	275.14	6.43	184.11	6.21
188.14	3.79	193.10	6.34	188.14	3.79	***402.26*****[*]**	5.83	193.10	6.34	***402.26*****[*]**	5.83
224.14	3.01	224.14	5.15	224.14	3.01	***385.26***[W]	4.57	224.14	5.15	385.26	4.57
184.11	2.07	302.19	4.86	184.11	2.07	***354.22***[4]	4.19	302.19	4.86	354.22	4.19
226.16	2.07	***328.21***[3]	3.73	226.16	2.07	169.10	3.82	328.21	3.73	169.10	3.82
276.17[1]	2.02	169.10	3.72	***276.17***[1]	2.02	212.14	2.47	169.10	3.72	212.14	2.47
199.14	1.75	290.15	3.15	199.14	1.75	290.15	2.42	290.15	3.15	290.15	2.42
290.19	1.72	198.13	3.05	290.19	1.72	***173.12***[6]	2.27	198.13	3.05	173.12	2.27
158.10	1.45	196.11	3.04	158.10	1.45	167.08	2.24	196.11	3.04	167.08	2.24
252.17	1.44	231.12	2.96	252.17	1.44	***326.19***[X]	2.24	231.12	2.96	326.19	2.24
172.11	1.43	***385.26***[W]	2.94	172.11	1.43	250.16	2.13	385.26	2.94	250.16	2.13
302.19	1.29	286.16	2.90	302.19	1.29	224.14	2.03	286.16	2.90	224.14	2.03
211.14	1.23	160.11	2.65	211.14	1.23	342.22	1.98	160.11	2.65	342.22	1.98
165.07	1.13	***354.22***[4]	2.59	165.07	1.13	314.19	1.97	354.22	2.59	314.19	1.97
167.09	1.02	238.16	2.50	167.09	1.02	155.08	1.95	238.16	2.50	155.08	1.95
170.10	0.98	356.24	2.42	170.10	0.98	174.13	1.94	356.24	2.42	174.13	1.94
169.10	0.85	158.10	2.35	169.10	0.85	198.13	1.94	158.10	2.35	198.13	1.94
155.09	0.79	167.09	2.33	155.09	0.79	226.12	1.94	167.09	2.33	226.12	1.94
274.16	0.79	300.18	2.31	274.16	0.79	312.17	1.92	300.18	2.31	312.17	1.92
301.18	0.76	***314.19***[5]	2.29	301.18	0.76	***401.26***[W]	1.89	314.19	2.29	401.26	1.89
196.11	0.67	155.09	2.28	196.11	0.67	328.20	1.83	155.09	2.28	328.20	1.83
185.12	0.62	***320.86***[X]	2.26	185.12	0.62	236.14	1.61	***320.86***[W]	2.26	236.14	1.61
300.17	0.62	194.14	2.10	300.17	0.62	158.10	1.57	194.14	2.10	158.10	1.57
191.09	0.58	172.11	2.09	191.09	0.58	286.16	1.57	172.11	2.09	286.16	1.57
281.20	0.55	222.13	1.95	281.20	0.55	182.10	1.53	222.13	1.95	182.10	1.53
171.12	0.54	156.08	1.93	171.12	0.54	231.12	1.53	156.08	1.93	231.12	1.53
156.08	0.49	250.16	1.93	156.08	0.49	196.11	1.50	250.16	1.93	196.11	1.50
181.10	0.45	182.10	1.80	181.10	0.45	172.11	1.48	182.10	1.80	172.11	1.48
171.10	0.43	304.21	1.78	171.10	0.43	200.11	1.40	304.21	1.78	200.11	1.40
217.10	0.43	***173.12***[6]	1.72	217.10	0.43	222.13	1.20	173.12	1.72	222.13	1.20
275.17	0.43	403.27	1.71	275.17	0.43	***228.14***[10]	1.18	403.27	1.71	228.14	1.18
194.14	0.40	***295.22***[7]	1.70	194.14	0.40	156.08	1.12	***295.22***[7]	1.70	156.08	1.12
200.11	0.37	***342.22***[8]	1.69	200.11	0.37	***247.11*****[***]**	1.07	342.22	1.69	***247.11*****[***]**	1.07
186.12	0.36	236.14	1.68	186.12	0.36	266.19	1.05	236.14	1.68	266.19	1.05
153.07	0.34	252.18	1.59	153.07	0.34	252.17	1.00	252.18	1.59	252.17	1.00
205.17	0.34	174.13	1.55	205.17	0.34	170.10	0.99	174.13	1.55	170.10	0.99
238.16	0.34	216.09	1.53	238.16	0.34	238.16	0.99	216.09	1.53	238.16	0.99
286.16	0.34	211.14	1.46	286.16	0.34	300.17	0.99	211.14	1.46	300.17	0.99
154.08	0.33	281.20	1.34	154.08	0.33	169.06	0.96	281.20	1.34	169.06	0.96
202.12	0.33	170.10	1.33	202.12	0.33	229.10	0.90	170.10	1.33	229.10	0.90
356.24	0.32	181.10	1.32	356.24	0.32	315.20	0.88	181.10	1.32	*315.20*	0.88
213.15[2]	0.30	274.16	1.32	***213.15***[2]	0.30	356.24	0.86	274.16	1.32	356.24	0.86

Numbers (1-10) correspond to fragment structures in Figure

* denotes precursor ions

** denotes fragment ion with mass greater than lobinaline and not associated to a loss of water

*** denotes fragment ion of bi-N-oxide with two oxygens (see text)

X denotes fragment ions of interest in which a putative empirical formula could not be generated

W denotes loss of water

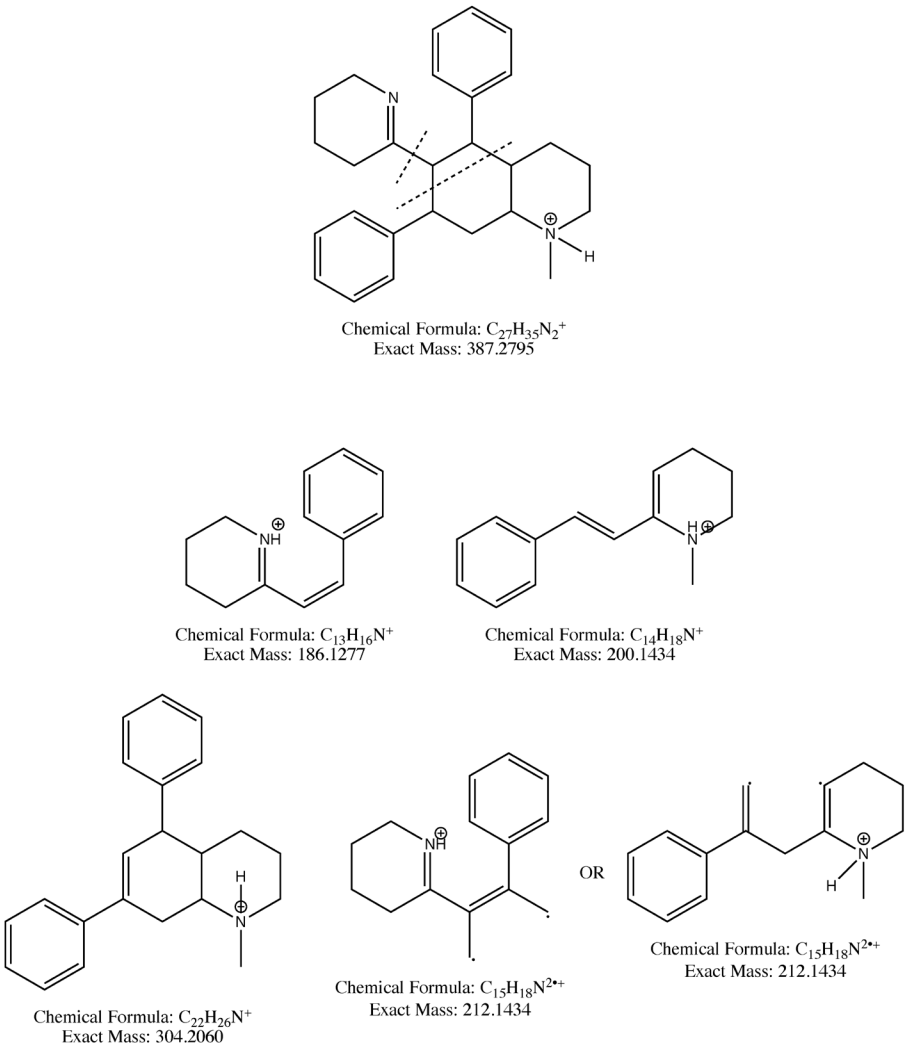

Figure 2. 23 Possible structures for the lobinaline MS/MS fragment ions.

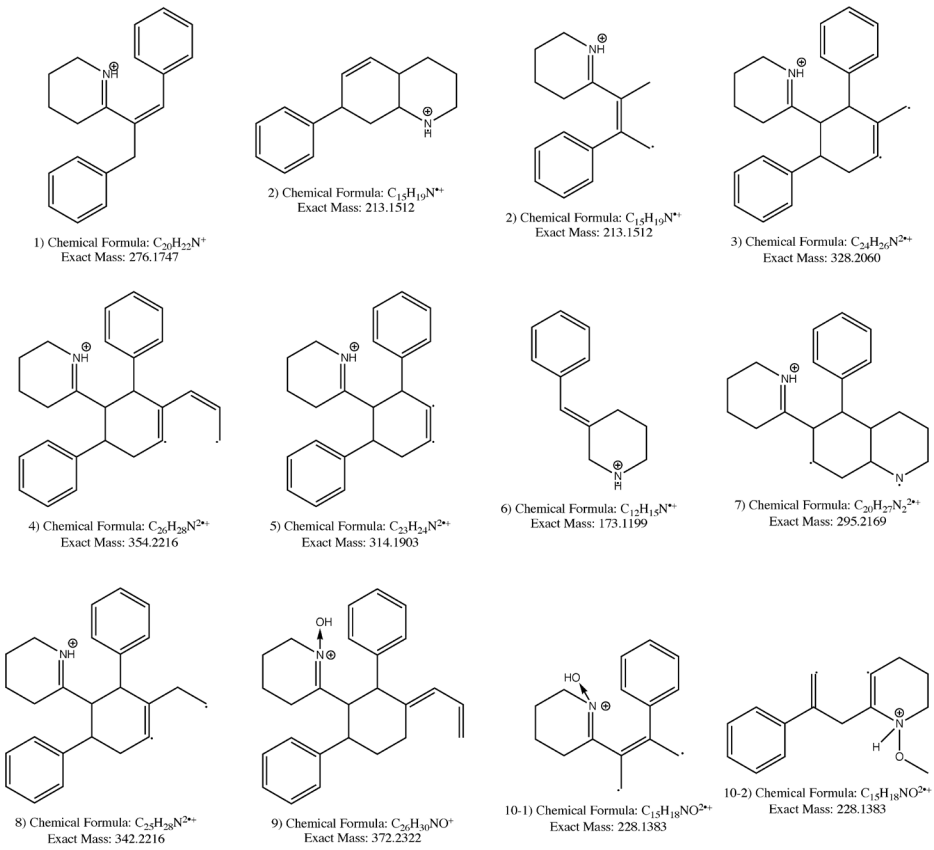

Figure 2. 24 Possible structures for the lobinaline N-oxide MS/MS fragment ions.

The m/z 372 (structure 9, Figure 2.24) and m/z 228 (structure 10-1 and 10-2, Figure 2.24) fragments, also present in the m/z 403 peak list, contained only one oxygen based on their calculated empirical formula and the m/z 419 → 247 fragment was calculated to contain two oxygens according to it's calculated formula. N-oxides can undergo 1,2 rearrangement, known as the Meisenheimer rearrangement, (structure 10.2, Figure 2.24) when exposed to a heat source, such as the HESI probe or the inlet capillary, therefore it is possible that the rearrangement could have occurred to stabilize the N-oxide interaction and produce those fragments, especially given their low relative abundance. Furthermore, if the oxygens were present as formal bonds, fragments corresponding to the characteristic cross-ring cleavage would likely be present with the addition of an oxygen. Though m/z 202.12 (m/z 186 + 16) is present for both N-oxides, it is also present in lobinaline, therefore it is likely not attributed to the addition of an oxygen, Likewise, a m/z 216 (m/z 200 +16) fragment is not present. Though not conclusive evidence to completely rule out the possibility of the oxygen atoms being involved in formal bonds, the lack of apparent fragmentation patterns consisting of the addition of oxygen compared to those found in lobinaline, as well as the supporting data collected from the semi-synthetic production of the N-oxide, supports the interactions being present as N-oxide bonds.

Conclusion

The aim of this chapter was to develop a metabolomic profiling method to characterize wild type and transgenic mutant *L. cardinalis* secondary metabolites. This was performed by developing an extraction and analysis protocol centering around the

utilization of a microfluidic CZE-MS device. This microfluidic CZE-MS device allowed for both a fast and sensitive high-throughput method for the screening of secondary metabolites, specifically plant alkaloids. Previous alkaloid MS screening assays traditionally rely on HPLC or GC as a separation method. These methods can be, not only time consuming, but also be unsuitable for the separation certain compounds and lack the capability of isomeric separation. Here, the utilization of the microfluidic chip displayed that more efficient separation can be achieved in approximately half the time or more compared with other methods. When coupled with processing software like MZmine2, the process is further streamlined resulting in a fast, comprehensive assay for plant secondary metabolites. These characteristics are particularly valuable for the use described here in which it is essential to rapidly compare alkaloid profiles in many different plant extracts in very small sample volumes. This method enables the identification and separation of novel putatively bioactive metabolites from transgenic mutant plant cells. The metabolites identified in this work, the lobinaline mono- and bi-N-oxide, have become a novel source of lead compounds for the pharmaceutical industry and are currently being tested for pharmacological activity.

CHAPTER 3. MASS SPECTROMETRY-BASED METHOD DEVELOPMENT FOR THE ANALYSIS OF PHENOLIC SECONDARY METABOLITES

Introduction

Phenolic plant metabolites are the most widely abundant secondary metabolites found within the plant kingdom and consist of a wide variety of subclasses, each with unique and specific roles.[11,92] The general requirement for the classification is an aromatic ring with an associated hydroxyl group (phenolic), however, many natural phenols are much more conjugated. Figure 3.1 displays generalized carbon backbones of simple monomeric phenolic secondary metabolites. In nature, these metabolites are often cyclic with bridging oxygens as well (see Figure 3.1 - C_6-C_3-C_6 flavonoid substructure), aiding to the diversity and complexity of the class. In addition to existing as single subunit metabolites, these molecules are also polymerized into varying sized polyphenolic oligomers such as procyanidins (2-3 flavonoids), tannins (5+ gallic acids linked to a glucoside with further conjugation), and lignin, one of the three primary structural components of woody plants (100+ varying linkages of three monolignol subunits). Aside from the structural aspect of phenolics in lignin, plant phenolics also act as defense agents against both biotic (antibiotic and antifeeding activity) and abiotic (antioxidant and UVB-blocking) insults.[11,92–94] Additionally, smaller phenylpropanol-derived phenols act as attractants for pollinators due to the color and scent that they confer to the plant.[11,94] Conversely to alkaloids, as seen in chapter 2, many monomeric phenolics can share a degree of homology between unrelated species.[94] Two examples of this would be resveratrol, a stilbene, and quercetin, a flavonoid, which can be found in a large variety of plants, many of which are commonly consumed by both humans and animals (grapes, berries, leafy greens, etc).[11,93–96]

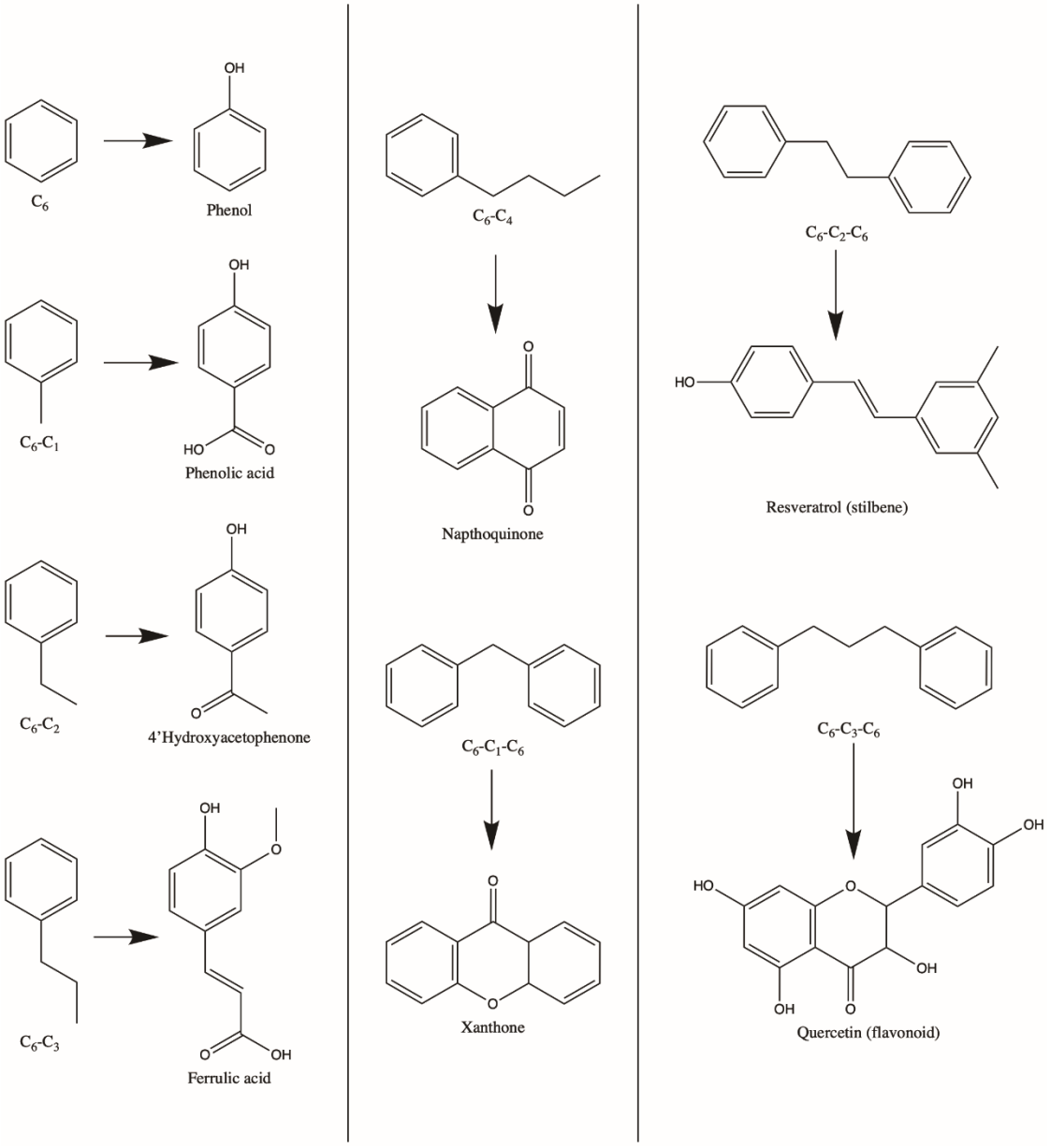

Figure 3. 1 Base carbon structures for phenolic secondary metabolites with examples.[97]

Aiding to the homology, most phenolics are generally biosynthesized through fairly conserved pathways.[94] The primary pathways include the shikimate pathway, converting shikimic acid to tyrosine or phenylalanine, followed by the phenylpropanoid pathway, which converts the resulting Tyr and Phe to courmaic or cinnamic acid, respectively, and the polyketide pathway. These biosynthetic pathways (Figure 3.2) generated most of the aforementioned phenolic classes such as flavonoids, stilbenes, and lignins (shikimate and phenylpropanoid) and anthraquinones (polyketide).

In addition to phenolic secondary metabolites roles in plants, they are also of interest to humans as natural pharmaceuticals, as discussed with alkaloids in chapter 2. Stilbene compounds have a variety of applications as antioxidants, as well as cancer chemo-preventive agents.[98,11] Flavonoids also have been evaluated as anti-cancer, anti-inflammatory, and cardiovascular disease therapeutics.[11,96,98] Additionally, most phenolic compounds all share a varying degree of antimicrobial activity, another desirable application of the metabolite class.[11,98] Their commonalities across various edible plants and fruits and existence in fruit-based beverages, such as wine, has led to their increased consumption in recent years due to the discovery of the benefits associated with them.[96] In recent years, another subclass of phenolic metabolites, the cannabinoids produced by the genus *cannabis*, have been the subject of much investigation and controversy.

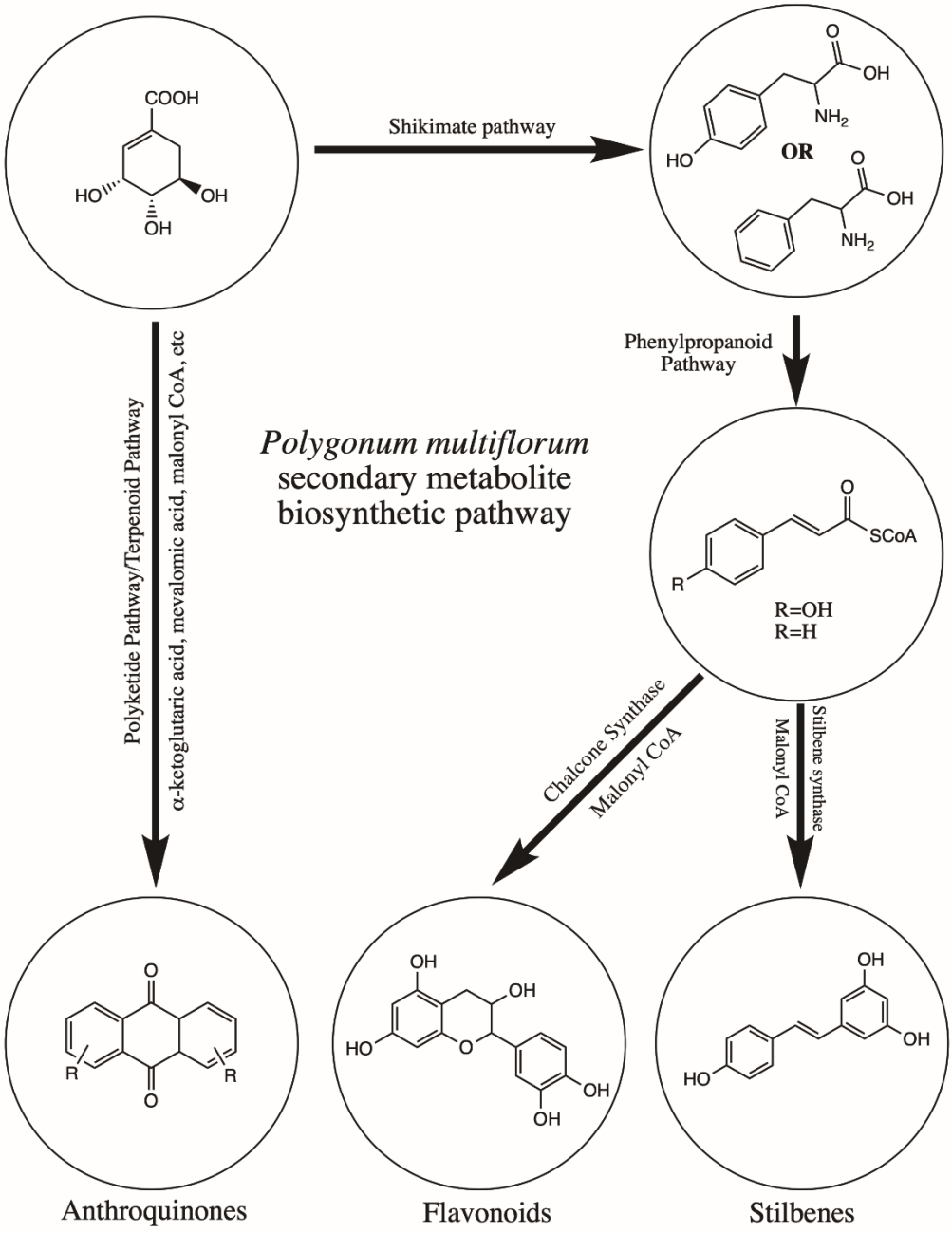

Figure 3. 2 Simplified biosynthetic pathway for the phenolic compounds of interest in this work.

Cannabinoids, the phenolic secondary metabolites of *Cannabis sativa, Cannabis indica,* and *Cannabis ruderalis,* have been increasingly the subject of much scientific, political, and ethical controversy, especially in the past decade. The most commonly studied and abundant cannabinoids (Figure 3.3) present in the *Cannabis* plant are cannabidiol (CBD), cannabigerol (CBG), cannabinol (CBN), cannabichromene (CBC), and Δ^9 -tetrahydrocannabinol (Δ^9THC) and their corresponding carboxylic acid precursors as they exist in the plant.[99–101] The medicinal aspect of cannabinoids has been the driving factor of their interest in recent years. Cannabinoids such as CBD, CBN, CBG, and CBC have shown degrees of activity including anti-inflammatory, analgesic, anticonvulsant, antipsychotic, and antibiotic activity, making the class very pharmacologically attractive as a whole.[95,99,101–104] Unfortunately, the reason for the controversy that has plagued the use of *Cannabis* throughout history is the psychoactive attributes of one of the primary cannabinoids, Δ^9THC.[99] This psychoactive attribute has led to legality constraints placed on *cannabis* cultivars. In states where the recreational use of *cannabis* is still illegal, such as here in KY, a legal classification of the plants is placed according to their Δ^9THC content. According to the 2018 KY farm bill, which legalized the use of specific *cannabis* products, *cannabis* extracts and products can be deemed as "hemp" products if they contain less than 0.3% Δ^9THC w/w%.[99,103,105,106] This determination can be made using a number of analytical techniques, mainly LC-UV, GC-MS, or LC-MS.[99,103] In accordance with the initial passing of the bill in KY, a mass influx of local testing companies were established to accommodate the equally large influx of cultivators and producers setting up in the state.

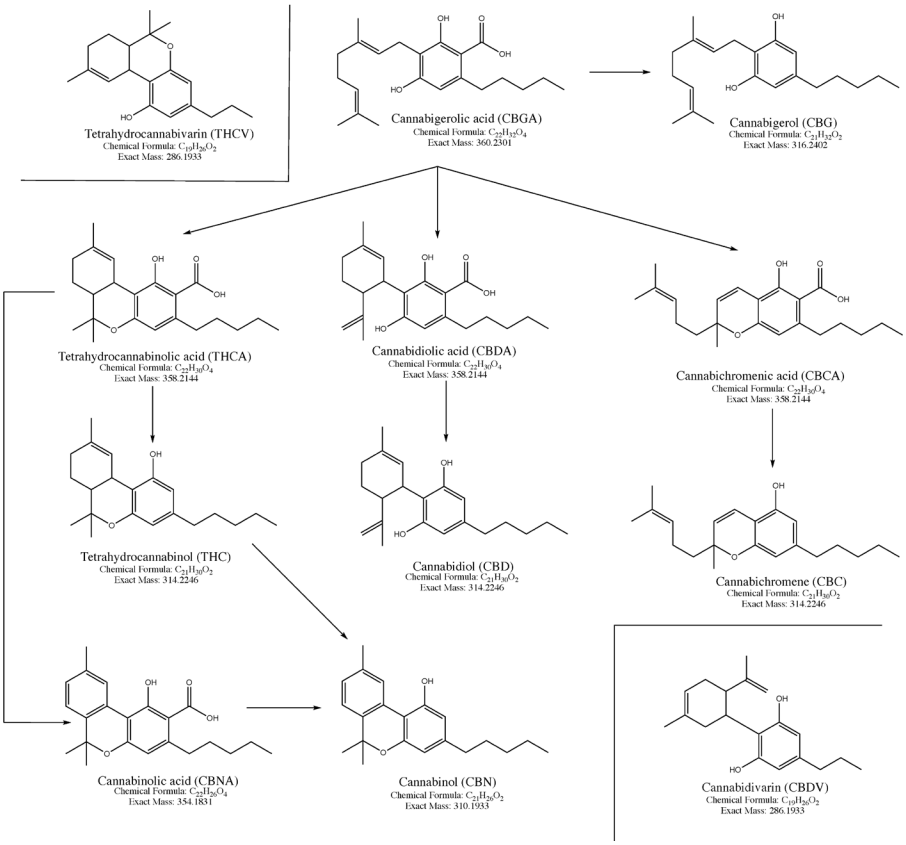

Figure 3. 3 Twelve of the cannabinoid class of phenolic secondary metabolites produced by *Cannabis* genus plants.

With no standardized analysis method and the only guideline being a Δ^9THC content limit, inter-lab variation quickly led to many products entering the market outside legal limitations due to poor analytical method construction, inexperience, and driving factors such as selected use of agencies consistently under-reporting results to drive produces to market. The focus of the first aspect of the work found in this chapter was to utilize example methods corresponding to the three commonly employed analytical approaches, LC-UV, GC-MS, and LC-MS. The hypothesis of this aspect of the chapter was that the sources of variation, specifically intra-laboratory and inter-instrumental variation, could be determined and reduced and, if reduction was not possible, then the mechanisms responsible could at least be understood and accounted for to minimize variation. Given that the cannabinoid industry is projected to be a $20+ billion dollar industry by 2022, it is absolutely crucial that accurate, reproducible, and sensitive methods are developed and adopted on a federal level to assist in the further ethical and scientific development of the industry.[99]

The second aspect of this chapter focuses more on the global metabolomic analysis of phenolics rather than just of a specific subclass like the cannabinoids. Here, the development of new analytical methods for the analysis of *Polygonum multiflorum* was performed. This research, also in collaboration with Naprogenix LLC (Lexington, KY) (see chapter 2), focuses on the characterization of *p. multiflorum* extracts in search of potential novel compounds resulting from the expression of alpha-synuclein in transgenic *p. multiflorum* hairy roots. Literature suggests that the phenolic compounds produced by *p. multiflorum* (Figure 3.4), such as TSG, emodin, and physcion, may present an inhibitory effect on the aggregation of alpha-synuclein into Lewy bodies,

which are believed to be one of the primary causes of Parkinson's disease.[107–109] In employing the transgenic plant technology described in chapter 2, Naprogenix is currently in the process of developing these transgenic *p. multiflorum* alpha synuclein hairy root cultures to develop novel therapeutics to potentially treat or halt the progression of the disease. As these cultures are still in development, the focus of this work was to analyze whole WT plant extracts to develop a baseline metabolomic database for future comparisons. In addition to database development, further development of CE-MS methods for the high-throughput characterization and analysis of these phenolic compound-rich extracts was also developed. Despite the chemical attributes of these metabolites making them unideal for electrophoretic separation, the hypothesis was that certain modifications could allow for the application of capillary electrophoresis for the analysis of these extracts. Both the potential downstream pharmaceutical application of this work and the analytical application of CE-MS for phenolic analytes, which are typically difficult to analyze via CE, are important aspects of the work performed in the second part of this chapter.

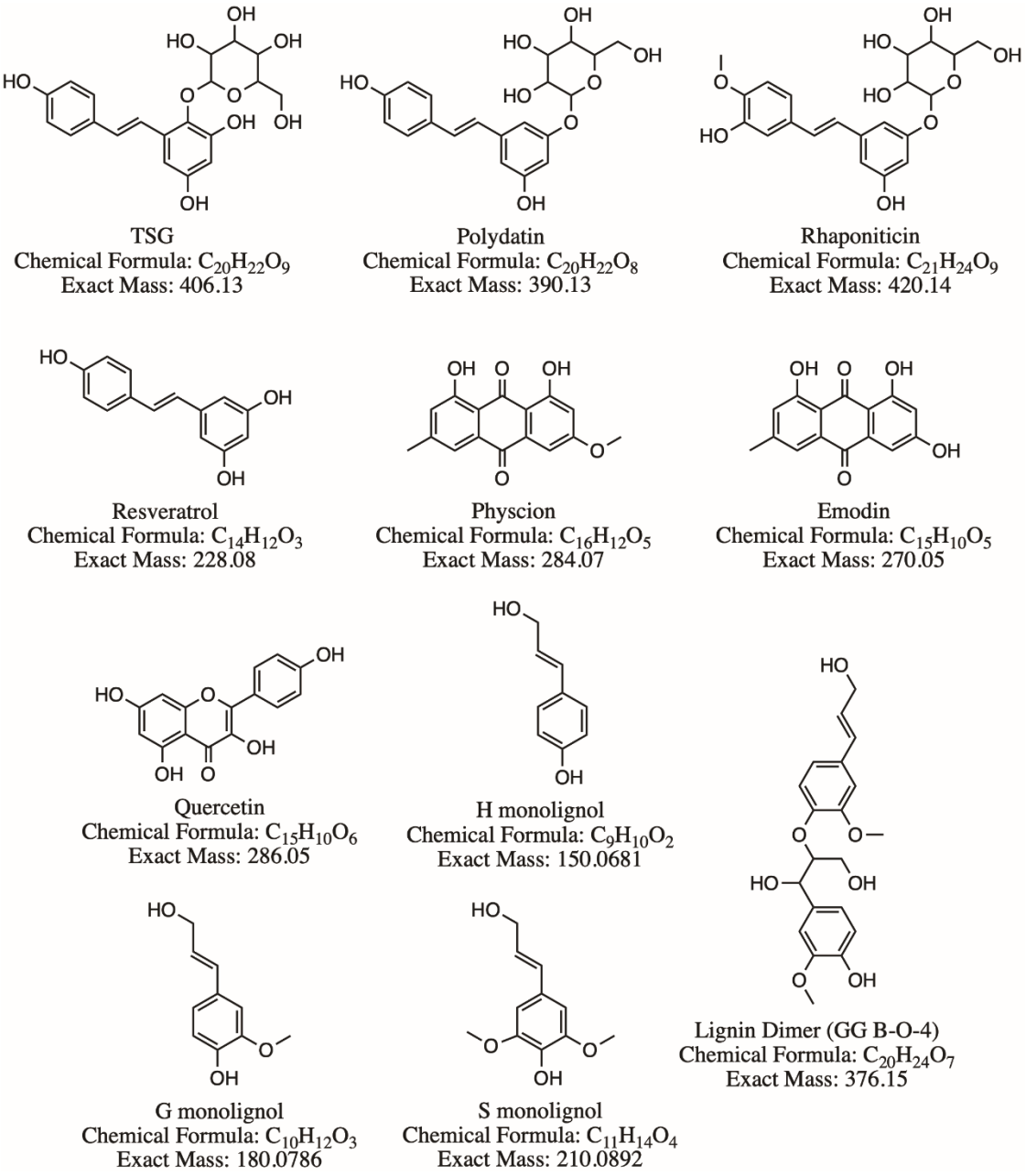

Figure 3. 4 Polyphenolic compounds of interest produced by *Polygonum multiflorum.*

Materials, Methods and Instrumentation

3.1.1 Cannabinoid Potency Testing Evaluation

Analytical cannabinoid reference standards, cannabidivarin (CBDV), tetrahydrocannabivarin (THCV), cannabichromene (CBC), cannabigerol (CBG), cannabinol (CBN), cannibindiolic acid (CBDA), cannabinidiol (CBD), tetrahydrocannabinolic acid (THCA), and Δ^8 and Δ^9-tetrahydrocannabinol (Δ^8/Δ^9-THC), were purchased from Caymen Chemical (Ann Arbor, MI) as 1 mg/mL solutions as defined by U.S. Drug Enforcement Administration (DEA) guidelines. Optima H_2O, acetonitrile, methanol and formic acid were purchased from Fisher Scientific (Waltham, MA). Hemp biomass and an ethanol hemp extract were donated by a local processor in Lexington, KY. Additional ethanol extracts were provided by Eastern Kentucky Extractions (Jenkins, KY). Three commercial CBD products were also obtained: a tincture gel pill and MCT oil tincture from Ananda Hemp (Cynthiana, KY) and a CBD lotion from BluLeaf Naturals (Lexington, KY).

Cannabinoid potency profiles were generated using three instrumental approaches: HPLC-UV, GC-MS, and UHPLC-MS. HPLC-UV analyses were performed using a Hewlett Packard 1100 series UV detector and binary pump coupled to a Rheodyne manual injector. Separations were performed using a Kromacil C18 column (4.6 x 150 mm) with a 5 μm particle size. An isocratic gradient consisting of 20% water with 0.1% formic acid and 80% ACN with 0.1% formic acid at 1.5 mL/min for 12 minutes was employed for the separation. For UV detection, 280 nm was monitored. GC-MS analyses were performed using a Hewlett Packard 6890 series GC coupled to an

Agilent 5973 MS detector. A DB-5HT column (15 meter, 0.10 μm film thickness, 0.250 mm ID) was used with an injector temperature of 260 ºC with a 50:1 split and a column over temperature gradient starting at 50 ºC for 3 minutes, increasing by 50 ºC to 100 ºC and then holding for 1 minute, then increasing by 15 ºC per minute to 280 ºC. The oven was held at 280 ºC for 5 minutes (22 minutes total) before returning to starting temperatures for the next analysis. For MS analysis, ions corresponding to the ten aforementioned standards were monitored in time dependent SIM mode in which the 5 most abundant fragment ions were used for quantitation. For UHPLC-MS analysis, separations were performed using a Shimazdu Nexera X2 UHPLC system with a Kromacil EternityXT C18 column (2.5 μm, 2.1x100 mm). The chromatographic separation consisted of solvent A (0.1% formic acid in H_2O) and B (0.1% formic acid in ACN) in a gradient flow method starting with solvent B at 55% for 2 minutes, increasing linearly to 95% over 6 minutes, being held at 95% for 2 minutes, and then returning to starting conditions for equilibration. The UHPLC-MS analyses were performed on a Thermo Scientific Q Exactive Orbitrap High-Resolution Accurate Mass (HRAM) Mass Spectrometer (Thermo Fisher Scientific, Waltham, MA, USA) equipped with a heated electrospray ionization (HESI) ionization source. Data acquisition was performed in the positive ion mode with a mass range of m/z 100-800 the following parameters: 10 L/min sheath gas flow and 4 L/min auxiliary gas flow, inlet capillary temperature of 280 ºC and auxiliary gas temperature (HESI probe temperature) of 280 ºC, 3kV spray voltage, scan resolution of 140,000 with a 3 Hz scan rate, a 3e6 AGC target, and a maxium IT of 200 μs.

For unprocessed sample preparation, dried hemp plant buds were ground with a mortar and pestle to a powder and extracted with ethanol exhaustively. The ethanol was filtered via vacuum filtration to remove residual insoluble biomass and reduced to dryness via rotary evaporation. The resulting extract was reconstituted in Optima methanol at 1 mg/mL and analyzed via HPLC-UV without further dilution (5 µL injections). For UHPLC-MS analyses, samples were further diluted to 10 µg/mL in 50/50 ACN/H_2O with 0.1% formic acid (5 µL injections). For GC-MS analysis, a 50 µL aliquot of the 1 mg/mL extract was reduced to dryness in an autosampler vial insert under a stream of nitrogen. The sample was reconstituted with 50 µL of a 50/50 BSTFA/pyridine solution and incubated for 20 minutes at 60 ^oC for derivatization. Following derivatization, the samples were analyzed without further dilution (5 µL injections). For processed sample preparation, 500 mg (wet weight) of ground biomass was dried in an oven at 60 ^oC for 30 minutes. The dried biomass was suspended in 5 mL of ACN with 2% formic acid in a 15 mL polypropylene tube. The suspension was diluted with 5 mL of DI water and shaken for 1 hour at room temperature. A QuEChERS extraction was performed using the Waters DisQuE AOAC method extraction salts (sodium acetate and magnesium sulfate). To the 10 mL solution, 1.5 g of the DisQuE salts were added. The extraction was vortexed for 1 minute and separated via centrifugation. The ACN layer was collected and filtered with a 0.22 µm nylon filter. The filtered ACN extract was then loaded onto a prewashed Waters Oasis HLB SPE cartridge. The first 500 µL of flow through from the cartridge was discarded and the remaining 4.5 mL of the "flow through" was collected and reduced to dryness under nitrogen. The SPE cartridge was washed with 3 mL of MeOH and the eluent was collected, added to the dried "flow-through" sample,

and also reduced to dryness. The dried, post-SPE extract was reconstituted in 5 mL of ACN and stored at -18 ºC overnight to precipitate fats and waxes in a "fat crash". The post-"fat crash" extract was dried under nitrogen then decarboxylated via heating in an oven at 120 ºC for 24 hours. Following the heat conversion, the samples were reconstituted as listed above and analyzed. Aliquots (50 µL) from each treatment step were also collected for quantitation to assess sample loss.

For potency profiles, calibrations curves were generated for the ten standards listed above spanning at least three orders of magnitude; 10 – 1000 µg/mL for GC and HPLC-UV, and 10 ng - 100 µg/mL for UHPLC-MS. Provided ethanol extracts were prepared for analysis as stated above for the ethanol extracts. The tincture encapsulated in the gel pill was removed with a syringe and transfer to an amber autosampler vial. Both the MCT tincture and gel pill tincture were diluted 1:10 (1:100 for UHPLC-MS). For the lotion analysis, the DisQuE extraction listed above was used, with modifications. Briefly, one "pump" of lotion (~2 mL, suggested usage amount) was suspended in 5 mL of DI H_2O in a 15 mL polypropylene tube. The aqueous sample was further diluted with 5 mL of ACN. Approximately 1.5 g of the DisQuE salts were added to the tube and the sample was vortexed for 1 minute. Following vortexing, the sample was centrifuged in a clinical centrifuge for 10 minutes. The top ACN layer was collected and stored overnight at -18 ºC to crash out any residual fats/waxes. The resulting ACN solution was reduced to dryness under nitrogen gas, reconstituted in 1 mL of optima MeOH, and diluted 1:10 for HPLC-UV and GC-MS (derivatized as stated above) analysis and 1:100 for UHPLC-MS analysis. Calculated concentrations were generated on a mg cannabinoid per 1 mg extract/product basis.

3.1.2 HESI Source Induced Degradation of CBDA and THCA

Prior to the performance of the degradation assay, the four cannabinoid standards were analyzed individually to confirm purity and again as a mixture via UHPLC-MS as stated above. Following purity confirmation via chromatographic separation, CBDA and THCA were analyzed individually to assess the rate of instrumental temperature-induced degradation. Each carboxylic acid cannabinoid was evaluated using both an infusion flow rate-based approach (5 μL/min – designated as "low flow rate") via direct infusion and an LC flow rate-based approach (300 μL/min – designated as "high flow rate") utilizing flow-injection analysis (FIA).

For the low flow rate analysis, the standards were individually infused at a concentration of 5 μg/mL in 50/50 ACN/H2O with 0.1% formic acid. Degradation induced by either the HESI probe or the inlet capillary was evaluated independently by varying the temperature of one component while holding the temperature of the other constant. For evaluation of the HESI probe, the inlet capillary temperature was held constant at 150 ºC while the HESI probe was incrementally increased from 50 ºC to 250 ºC in 25 ºC increments. Following each temperature increase, the system was allowed to reach equilibrium as determined by a stabilization in the TIC variation (<5% variation). Once stabilization was established, 15 scans were acquired and averaged to determine the ratio of the intact mass (m/z 359) to the degradation products (m/z 341 and 315). A similar approach was followed for the evaluation of degradation induced by the heat of the inlet capillary where the HESI probe temperature was held at ambient temperature, approximately 40 ºC, and the inlet capillary temperature was increased from 150 ºC to 300 ºC in 25 ºC increments.

For the high flow rate analysis, a flow injection analysis (FIA) approach was utilized by coupling a rheodyne injector to the line supplying a representative mobile phase, 50/50 ACN/H2O with 0.1% formic acid, to the mass spectrometer by the UHPLC as defined above. Again, both the degradation induced by the HESI probe and the inlet capillary were evaluated independently. For evaluation of the HESI probe, the inlet capillary temperature was held constant at 250 ºC, to accommodate for the desolvation required by increased flow rate, while the HESI probe was incrementally increased from 250 ºC to 400 ºC in 25 ºC increments. Three separate injections were performed at each temperature increment with time in-between to allow for the signals corresponding to the intact mass (m/z 359) to reduce to pre-injection baseline levels. Degradation rates were determined using the ratios of the area counts associated with the peaks corresponding to the intact carboxylic acid mass (m/z 359) and the two degradation products (m/z 341 and 315). The inlet capillary was evaluated using the same temperature increment patterns as the HESI probe (250 ºC to 400 ºC) with the probe being maintained at 250 ºC to accommodate the increased flow rate.

Additionally, solvent composition aiding in the rate of degradation under the high flow rate conditions was evaluated by analyzing the carboxylic acid cannabinoids in both 50:50 and 75:25 ACN or MeOH to H2O with 0.1% formic acid. For this analysis, only the HESI probe was evaluated with the inlet capillary temperature being held as 250 ºC while the probe was increased from 250 ºC to 400 ºC in 50 ºC increments.

3.1.3 *Polygonum Multiflorum* Extraction and Analysis

Standards of the following *P. multiflorum* secondary metabolites were purchased from Sigma Aldrich (St. Louis, MO): tetrahydroxystilbene glucoside (TSG),

rhaponiticin, polydatin, resveratrol, quercetin, emodin, and physcion. The following lignin model compounds were synthesized and provided by Lynn group member Poorya Kamali: H, G, and S monolignol, H, G, and S monolignol ethyl esters, and the G-β-O-4-G dimer. Commercial *p. multiflorum* plant material was provided by Naprogenix (Lexington, KY). The *P. multiflorum* plants were removed from the potting soil and the roots were cut from the stem. The stems and leaves (~250 mg) were rinsed with DI water and separated at the axial bud. For the root preparation, the branch roots were removed from the primary taproots and discarded. The taproot (100-200mg) was washed thoroughly with DI water and again with 50% EtOH to remove residual soil. The roots, leaves, and stems were cut into <1 cm sections and individually ground to a paste with a mortar and pestle and liquid nitrogen. The ground roots, stems, and leaves were extracted with up to 20 mL 80% EtOH (~10 mg/mL), individually, overnight on a magnetic stirrer. The extracts were centrifuged and filtered with a 0.22 μm syringe filter. Samples were analyzed both individually and pooled via UHPLC-MS analysis. Separations were performed using a Shimazdu Nexera X2 UHPLC system with a Kromacil EternityXT C18 column (1.9 μm, 2.1x50 mm). The chromatographic separation consisted of solvent A (H_2O) and B (ACN) in a gradient flow method starting with solvent B at 5% for 2.5 minutes, increasing linearly to 95% by 12 minutes, being held at 95% for 4 minutes, and then returning to starting conditions by 18 minutes for a 2 minute equilibration, 20 minutes total. The UHPLC-MS analyses were performed on a Thermo Scientific Q Exactive Orbitrap High-Resolution Accurate Mass (HRAM) Mass Spectrometer (Thermo Fisher Scientific, Waltham, MA, USA) equipped with a heated electrospray ionization (HESI) ionization source. Data acquisition was performed in the negative ion mode with

a mass range of m/z 100-1000 the following parameters: 10 L/min sheath gas flow and 4 L/min auxiliary gas flow, inlet capillary temperature of 280 ºC and auxiliary gas temperature (HESI probe temperature) of 280 ºC, 3kV spray voltage, scan resolution of 140,000 with a 3 Hz scan rate, a 3e6 AGC target, and a maximum IT of 200 µs. For targeted PRM MS/MS analyses, the above method was utilized and an inclusion list was generated based off of the observed RTs. Selected NCE levels were determined experimentally via infusion of the individual standards at 10 ug/mL concentrations in 50% methanol.

3.1.4 Dansylation of Polyphenolic Compounds

Cannabinoid and *p. multiflorum* standards were prepared at 1 mg/mL concentrations in MeOH with the exception of emodin and physcion which were prepared in acetone. For each dansylation reaction, 500 µL of the standard solution was added to a glass 1.5 mL autosampler vial with 250 µL of a 10 mg/mL dansyl chloride (approximately 5-fold molar excess) solution in ACN and 500 µl 50 mM Na carbonate buffer (pH 9.4). The reaction mixture was incubated at 60 ºC for 2 hours in a water bath. Following incubation, unreacted dansyl chloride was quenched with 5 µL methylamine and incubated, again at 60 ºC for 30 minutes. Once the reaction was quenched, the products were extracted with chloroform and ethyl acetate and reduced to dryness prior to analysis. The products were verified using UHPLC-MS and tandem mass spectrometry, as stated above, and via flow injection analysis, also as stated above – see "high flow-rate analysis". Dansylated standards were also analyzed via CE/CZE-MS using the 908 Devices ZipChip, see below.

3.1.5 Modified microfluidic CZE-MS

For modified microfluidic CE-MS analyses of unmodified and dansylated polyphenolic compounds, the 908 Devices Zipchip was employed. A prototype "bare" HR chip (HRB) in which the capillary walls were stripped of the aminopropyltriethoxy-silane coating was supplied by 908 Devices. For negative ion separation of unmodified polyphenolics, a basic BGE was developed consisting 10% isopropyl alcohol, 10 mM ammonium acetate, 0.04% ammonium hydroxide, pH 8.5. For lithium assisted positive ion separation, a Li-based BGE and sample diluent were developed consisting of 20% isopropyl alcohol, 10% ACN, 100 μM LiCl for the BGE and 80% methanol, 10 mM LiCl for the diluent. Basic separations were evaluated on the HRB chip using a field strength ranging from -145 V/cm to -100 V/cm with 1 nL sample injections. Li-assisted separations were evaluated on both the HS and HRB chips. For HS separations, field strengths employed ranged from 0 V/cm to 1000 V/cm with 1nL injections. For HRB separations, field strengths employed ranged from 0 V/cm to 500 V/cm with 0.5 nL injections. Pressure assist was utilized for all separations. All analyses were performed using a Thermo Q Exactive HRAM mass spectrometer with the same parameters as listed above except the mass range was adjusted to m/z 100 to 1000.

Results and Discussion

3.1.6 Cannabinoid Potency Testing Evaluation

The goal of the first part of this chapter was to evaluate the use of HPLC-UV, GC-MS, and UHPLC-MS in regards to their application for cannabinoid potency testing. As HPLC-UV is considered the "gold standard" for potency testing, the results from both

mass spectrometry-based approaches were compared to the HPLC-UV results in terms of calculated concentration accuracy, reproducibility, sensitivity, and selectivity.

Calibration curves were generated, using each approach, for quantitation of the selected cannabinoids (Figure 3.3) representing the most common and abundant cannabinoids found in CBD/cannabis products. Figures 3.5-3.7 display resulting chromatograms for samples containing equimolar concentrations of the cannabinoid standards (3.5 – HPLC-UV, 3.6 – GC-MS, 3.7 – UHPLC-MS). Representative calibration curves can also be seen for each method displaying CBD and THC. All three methods displayed great linearity for the calibration curves with R^2 values all greater than 0.95 with most greater than 0.99. Differences in limits of quantitation (LOQs) for each method were observed at this point with the HPLC-UV at 100 ng/mL, the GC-MS at 10 μg/mL, and the UHPLC-MS at 10 ng/mL. The UHPLC-MS method displayed the greatest sensitivity due to the high resolving power of the instrument allowing for the accurate mass detection and limiting the impact of noise-related mass peaks near the analyte's m/z. Due to the nature of the analytes, specifically the carboxylic acid cannabinoids, the sensitivity could have been further increased if the analysis was performed in negative ion mode, however, to maintain consistency with the industrial standard HPLC-UV method, which uses formic acid in the mobile phase, positive ion mode was selected.

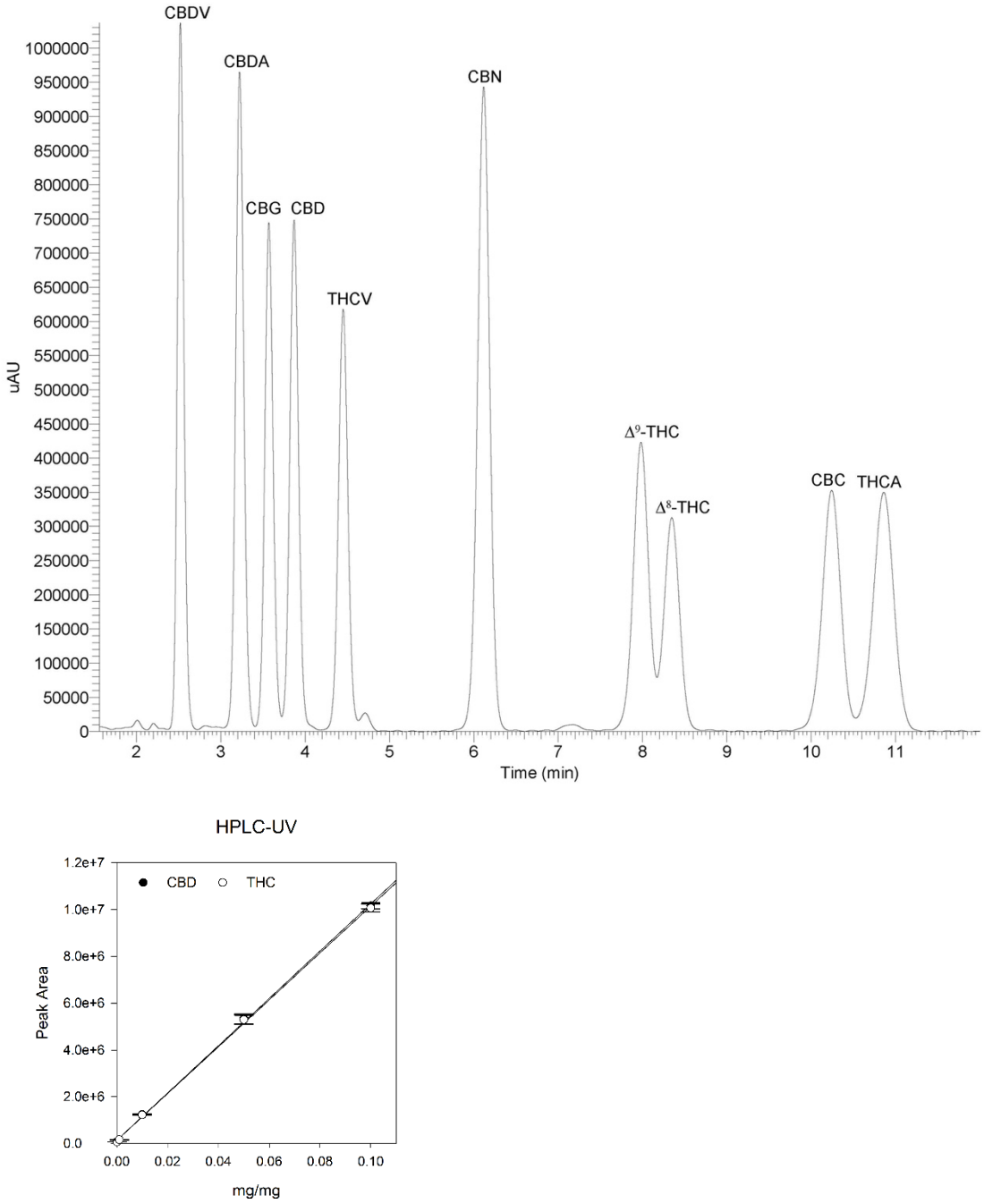

Figure 3. 5 (Top) Base peak chromatogram for the separation of ten cannabinoid standards using HPLC-UV detection. (Bottom) Calibration curve for THC and CBD displaying similar linear response factors for the two cannabinoid subclasses.

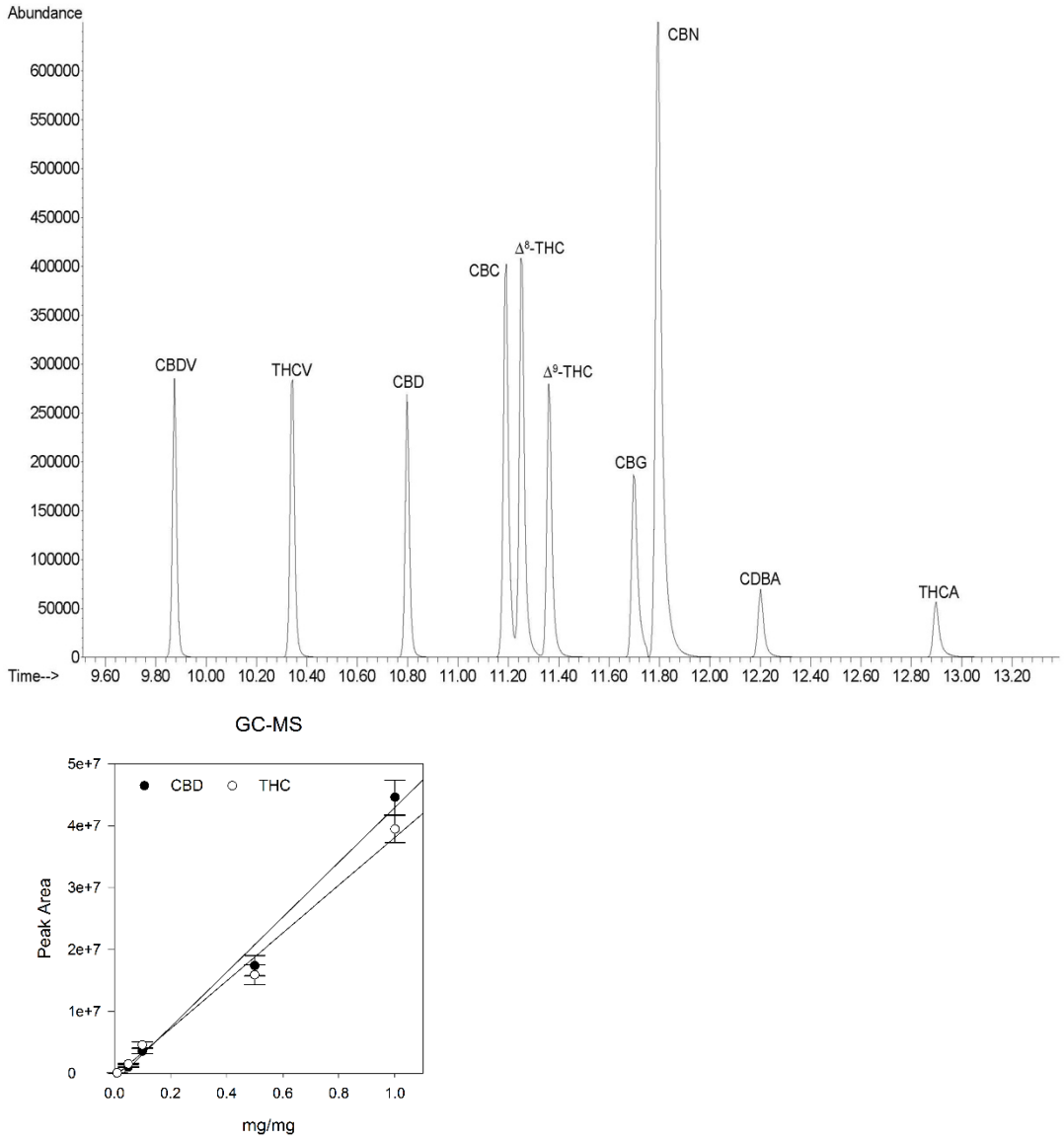

Figure 3. 6 (Top) Base peak chromatogram for the separation of ten cannabinoid standards using GC-MS detection. (Bottom) Calibration curve for THC and CBD displaying differing linear response factors for the two cannabinoid subclasses

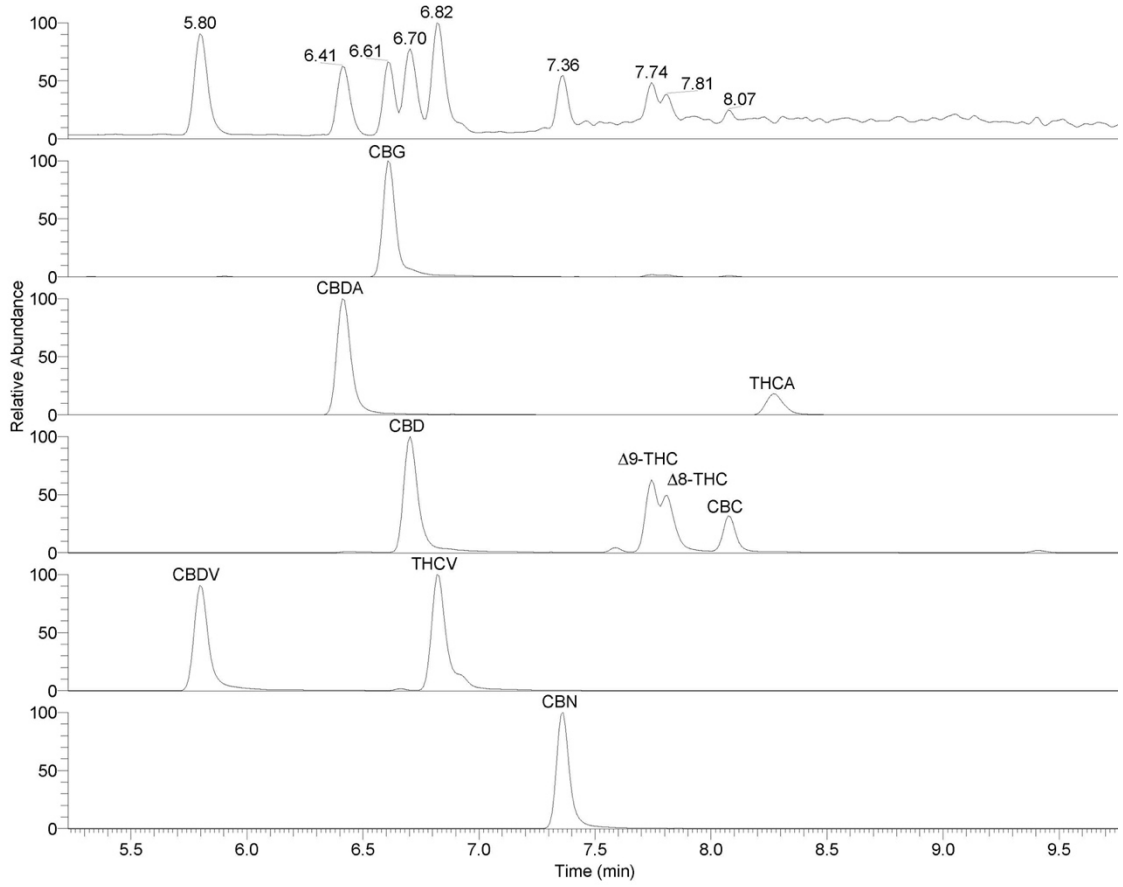

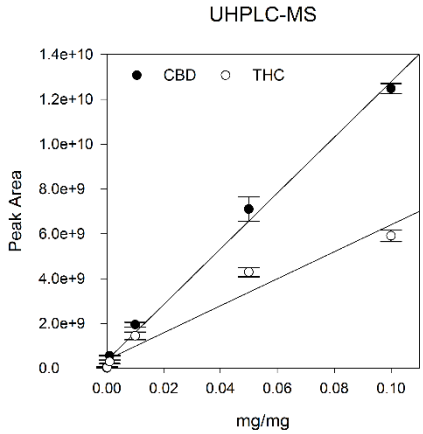

Figure 3. 7 (Top) Base peak chromatogram for the separation of ten cannabinoid standards using UHPLC-MS detection. (Bottom) Calibration curve for THC and CBD displaying differing linear response factors for the two cannabinoid subclasses.

Unexpectedly, the HPLC-UV approach appeared to be more sensitive than the GC-MS approach. A possible explanation for this could be the intense absorbance response of the cannabinoids at the selected wavelength, 280 nm, due to the aromatic ring moieties of the analytes. This could also be due to the high heat of the inlet of the GC causing degradation of the analytes. As depicted in Figure 3.6, at equimolar concentrations, the peaks corresponding to CBDA and THCA are much lower than those corresponding to their naturally decarboxylated counterparts, CBD and THC. Though the BSTFA derivatization (Figure 3.8) is intended to prevent decarboxylation, the reaction may not be as effective on the acids as it is for the phenolic -OH groups, thus leading to an easily dissociated, unprotected carboxylic acid. Differences were also observed in the selectivity of the chromatographic methods used, as well. At equimolar concentrations, baseline resolution of specific analytes could not be achieved, regardless of any method modifications tested. For both HPLC and UHPLC, the THC isomers could not be fully resolved from each other. Generally, for mass spectral approaches, this is less of an issue as RICs can be generated, as seen in Figure 3.7, but in this case, both analytes have the exact same m/z. From an application standpoint, Δ^8-THC is, on average, at trace levels in plant extracts, if present at all, therefore this drawback was not deemed to be detrimental for either method. The selectivity can be improved for the Δ^8/Δ^9 isomers, however, by altering the mobile phase conditions. This is not ideal as it drastically affects peak shape and selectivity of the method for other analytes (coelution, peak tailing, etc). In the event that Δ^8-THC is detected, the sample would need to be analyzed twice, once using the normal method, and again using the optimized method for Δ^8/Δ^9-THC separation.

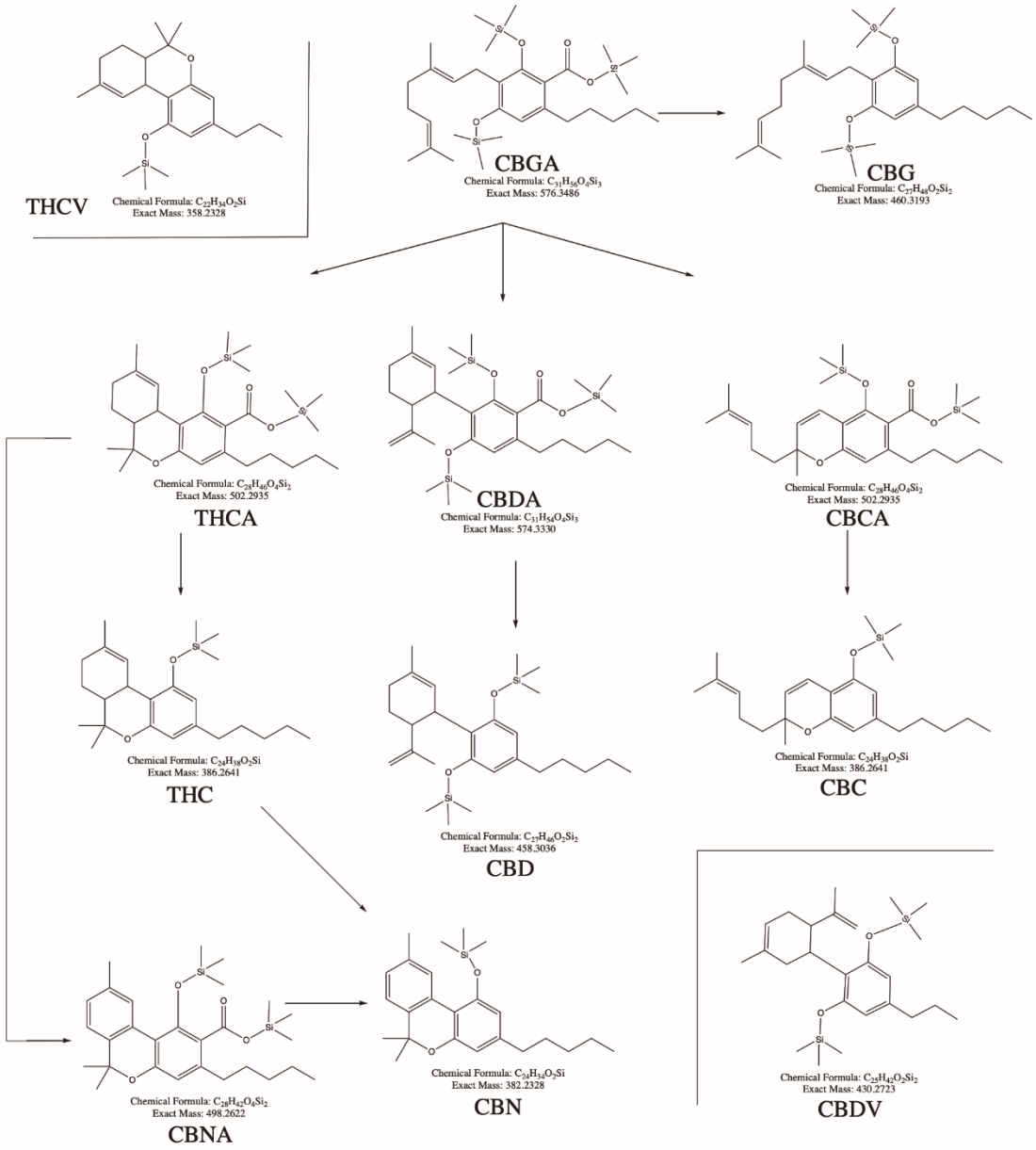

Figure 3. 8 BSTFA derivatized cannabinoid structures.

Additionally, it is worth noting that for GC-MS, CBC and Δ^8-THC coelute at higher concentrations. Though both analytes share the same m/z for their molecular ion ([M+•]= m/z 386), their fragmentation patterns differ, allowing for chromatographic deconvolution – CBC: m/z 386 → 304, 303, 246, 231; Δ^8-THC: m/z 386 → 343, 330, 303, 265, 246. The ionization process utilized by GC-MS, which induces this fragmentation, is ideal for the analysis of analytes like the cannabinoids. The phytocannabinoid family consist of several structural isomers (CBD/THC/CBC, CBDA/THCA/CBCA/, CBDV/THCV, etc), however, their fragmentation patterns can be found in common databases such as the NIST database to ease the process of identification and chromatographic deconvolution.

To assess reproducibility and potency profile accuracy, all three methods were applied to the EtOH extracts and commercial products. Table 3.1 displays the quantitation results, on a mg cannabinoid per mg extract/sample basis following analysis and corrections for dilutions. In terms of mg total cannabinoids per mg sample, the results were similar across all three methods with the exception of the GC-MS results in regard to the tincture and gel pill samples. Though both samples totaled the lowest in total cannabinoids, <50 ug/mg, the GC-MS results were nearly twice that observed for the HPLC-UV and UHPLC-MS methods. This can most likely be attributed to a matrix-effect as the samples were diluted, rather than extracted, from products containing high concentrations of oils like MCT oil. Compared to the other products, however, the calculated total cannabinoid profile of these two products was approximately 10X lower and predominantly composed of CBD.

Table 3. 1 Cannabinoid quantitation results for three extracts and three commercial products.

[illegible]	CBDV	RSD	CBDA	RSD	CBG	RSD	[illegible]	RSD	THCV	RSD	CBN	RSD	THC - delta9	RSD	THC - delta8	RSD	CBC	RSD	THCA	RSD	Total mg cannabinoids/mg
ETOH	ND	-	0.258	7%	ND	-	[illegible]	7%	ND	-	ND	-	ND	-	ND	-	ND	-	ND	-	0.401
Cma. Et 1	ND	-	ND	-	ND	-	[illegible]	7%	ND	-	ND	-	0.005	105%	ND	-	ND	-	0.089	6%	0.449
Cma. Et 2	ND	-	ND	-	ND	-	[illegible]	0%	ND	-	0.004	11%	ND	-	ND	-	ND	-	0.081	5%	0.501
Tinc.	ND	-	ND	-	ND	-	[illegible]	25%	ND	-	ND	-	ND	-	ND	-	ND	-	ND	-	0.021
Gel pill	ND	-	ND	-	ND	-	[illegible]	5%	ND	-	ND	-	ND	-	ND	-	ND	-	ND	-	0.004
Lotion	ND	-	0.058	7%	ND	-	[illegible]	5%	ND	-	ND	-	ND	-	ND	-	ND	-	0.008	25%	0.229
GC-MS	CBDV	RSD	CBDA	RSD	CBG	RSD	CBD	RSD	THCV	RSD	CBN	RSD	THC - delta9	RSD	THC - delta8	RSD	CBC	RSD	THCA	RSD	Total mg cannabinoids/mg
ETOH	ND	-	0.29	52%	ND	-	[illegible]	4%	ND	-	ND	-	0.02	5%	ND	-	ND	-	ND	-	0.41
Cma. Et 1	ND	-	ND	-	ND	-	[illegible]	22%	ND	-	ND	-	0.02	6%	ND	-	0.08	27%	ND	-	0.58
Cma. Et 2	ND	-	ND	-	ND	-	[illegible]	12%	ND	-	ND	-	0.02	10%	ND	-	0.08	16%	ND	-	0.63
Tinc.	ND	-	ND	-	ND	-	[illegible]	4%	ND	-	ND	-	ND	-	ND	-	ND	-	ND	-	0.04
Gel pill	ND	-	ND	-	ND	-	[illegible]	35%	ND	-	ND	-	ND	-	ND	-	ND	-	ND	-	0.06
Lotion	ND	-	0.06	21%	ND	-	[illegible]	13%	ND	-	ND	-	0.02	3%	ND	-	LOQ	-	ND	-	0.38
[illegible]LC-MS	CBDV	RSD	CBDA	RSD	CBG	RSD	CBD	RSD	THCV	RSD	CBN	RSD	THC - d9	RSD	THC - d8	RSD	CBC	RSD	THCA	RSD	Total mg cannabinoids/mg
ETOH	0.0001	11%	0.2404	12%	0.0059	18%	[illegible]	17%	ND	-	ND	-	0.0023	7%	ND	-	ND	-	ND	-	0.3445
Cma. Et 1	0.0005	2%	0.0002	5%	0.0284	3%	[illegible]	2%	ND	-	0.0009	5%	0.0077	6%	ND	-	0.0866	5%	ND	-	0.4858
Cma. Et 2	0.0003	1%	ND	-	0.0458	6%	[illegible]	1%	ND	-	0.0017	8%	0.0058	7%	ND	-	0.0072	6%	ND	-	0.5839
Tinc.	0.0002	3%	ND	-	ND	-	[illegible]	2%	ND	-	ND	-	0.0008	24%	ND	-	ND	-	ND	-	0.0023
Gel pill	0.0007	4%	ND	-	0.0002	12%	[illegible]	2%	0.0002	11%	ND	-	0.0014	18%	ND	-	ND	-	ND	-	0.0209
Lotion	ND	-	0.0508	4%	0.0107	6%	[illegible]	2%	ND	-	ND	-	0.0032	10%	ND	-	0.0083	5%	ND	-	0.2275

The primary application of the cannabinoid potency screenings performed by various testing agencies is to determine the legality of cannabis-products, as Δ^9-THC is considered an illicit substance. In order for a product to be considered legal in the state of KY, according to the 2018 Farm Bill, it cannot contain more than 0.3% total THC w/w%. For this calculation, the quantified mass of THCA is multiplied by 0.877 to take into account its conversion to Δ^9-THC in the body and added to the calculated THC concentration:

$$Total\ THC = \Delta^9 THC + (THCA \times 0.877)$$

A similar equation is used for CBD concentration calculations with its respective carboxylic acids. Table 3.2 displays the w/w% calculated for CBD and THC in the products using all three methods with this displayed graphically in Figure 3.9. For products like the in-house made EtOH extract and the commercial EtOH extracts, being slightly above the 0.3% total THC is common as the extracts will be further diluted when converted into final commercial products. An interesting trend was observed in that, for the HPLC-UV method, all the calculated total THC resulted from THCA whereas with both GC-MS and UHPLC-MS, no THCA was detected and only Δ^9-THC was detected at concentrations above the limit of quantification. For GC-MS, it is possible for interconversion of THCA to Δ^9-THC to occur in the inlet of the GC, as stated above, or decarboxylation during derivatization as the reaction is performed at an elevated temperature.

Table 3. 2 CBD and THC quantitation as w/w% for the extracts and samples. Red texts denotes THC w/w% greater than the legal limit for sale in the state of KY.

HPLC-UV	Total CBD w/w%	Total THC w/w%
ETOH	40.13%	0.00%
Com. Et 1	40.51%	3.94%
Com. Et 2	48.48%	1.00%
Tinc.	2.12%	0.00%
Gel pill	2.39%	0.00%
Lotion	22.65%	0.23%
GC-MS	Total CBD w/w%	Total THC w/w%
ETOH	38.97%	1.56%
Com. Et 1	53.29%	2.02%
Com. Et 2	58.13%	2.32%
Tinc.	3.64%	0.00%
Gel pill	4.65%	0.00%
Lotion	16.13%	1.64%
UHPLC-MS	Total CBD w/w%	Total THC w/w%
ETOH	33.61%	0.23%
Com. Et 1	43.03%	0.77%
Com. Et 2	47.34%	0.51%
Tinc.	1.19%	0.03%
Gel pill	1.74%	0.14%
Lotion	21.04%	0.32%

Figure 3. 9 (Top) CBD (left) and THC (right) w/w% percentages with error bars associated with standard deviation. (Bottom) CBD (left) and THC (right) w/w% percentages normalized to HPLC-UV results with error bars associated with standard deviation.

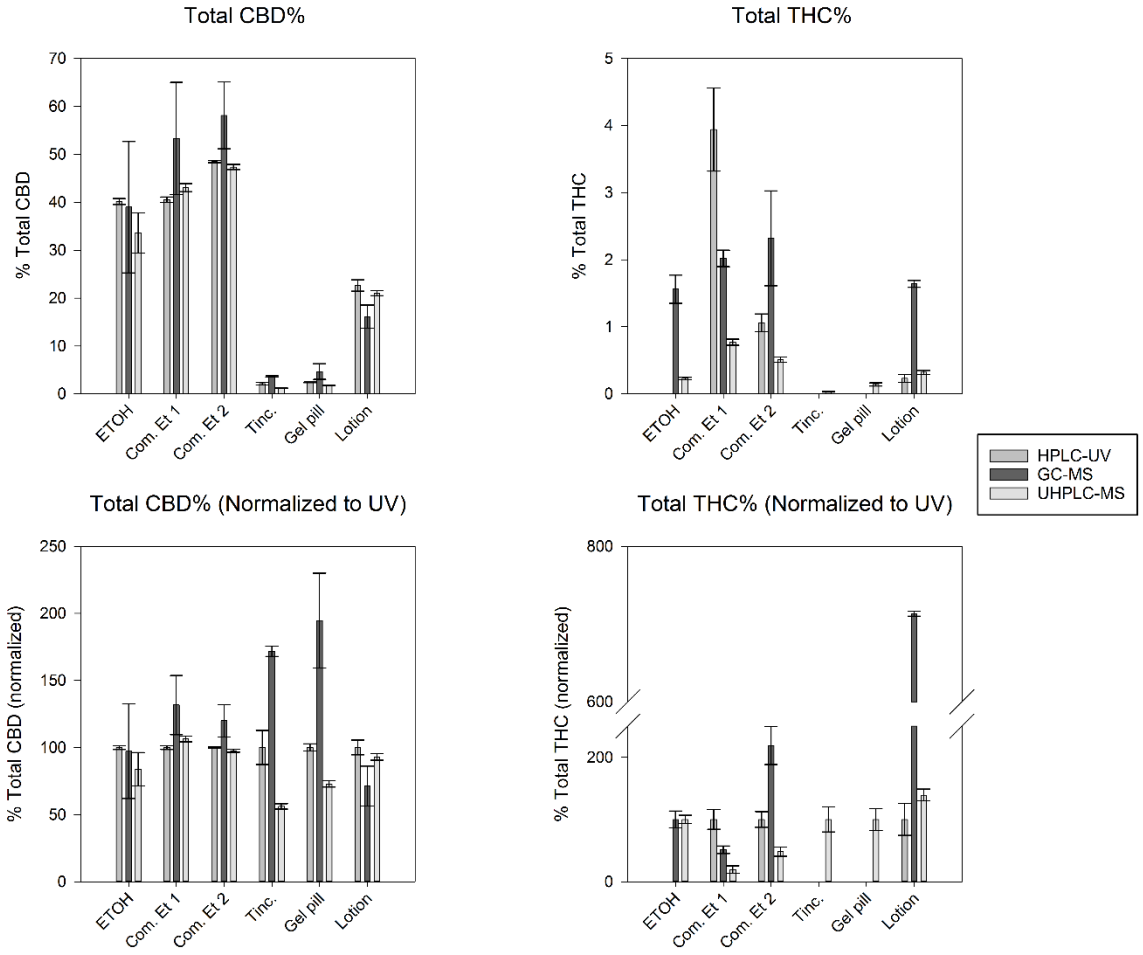

This would not be the case for UHPLC-MS, however, as any decarboxylation that would occur as a result of heat would be after chromatographic separation during the electrospray process, therefore it would not contribute to the observed THC response. As RICs were used for quantitation in UHPLC-MS, corresponding to the intact mass, any post-column degradation would have an effect on the observed THCA and CBDA response, however, discussed further in section 3.1.7. If post-column degradation were the case, as hypothesized, it would explain why the THC and CBD content, as determined by UHPLC-MS, is significantly lower than that calculated by the other two methods for a majority of the samples. As depicted in Figure 3.9, there is little agreement between the total CBD and total THC concentrations determined by each method, especially evident when normalized to the HPLC-UV results. Compared to GC-MS, HPLC-UV underrepresented CBD statistically ($p<0.05$) in all samples except the in-house extract and the lotion, and THC in the in-house extract (not detected), one of the commercial extracts, and greatly (7X) in the lotion. In using HPLC-UV to produce a potency profile for the lotion, the product would be considered legal to sell, however, according to the GC-MS results, the product contains 5X the legal concentration of total THC. Though likely more accurate for THC determination that HPLC-UV, the method lacked precision, as apparent in the relative size of the error bars in Figure 3.9. As stated previously, this is likely due to conversion of THCA to THC during the derivatization process and conversion of underivatized THCA to THC in the inlet of the GC causing inconsistent responses for both analytes. For UHPLC-MS potency profiling, the opposite is observed from GC-MS. The cannabinoid profiles were similar to those generated using HPLC-UV and the RSDs were all relatively low, suggesting both accuracy and precision

for this method, when compared to the HPLC-UV results. Here, again, we see that, for the lotion, the total THC concentration was determined to be outside the legal limit whereas it was below the limit when UV detection is used. The total THC content determined using the UHPLC-MS method may even be underrepresenting the THC content as THCA was detected using the UV method and not using the MS method, due to possible degradation or poor ionization efficiency.

Though standard HPLC with UV detection is preferred in the cannabis industrial for cannabinoid profiling, it is clear that it may not be an accurate enough method for determining low levels of THC in a product. Though deemed below the legal limit both by an accredited testing agency and using our HPLC-UV method, the CBD lotion was determined to have well over the legal concentration of total THC using both mass spectrometry-based methods. Unfortunately, the cannabinoid profiles generated using both of the MS approaches did not display statistical similarity, with the GC-MS potentially overestimating the results, with poor reproducibility, and the UHPLC-MS method, while more sensitive to the low-level cannabinoids like CBG and CBDV, potentially slightly underestimating the results. In order for accurate profiles to be generated, either ancillary methods need to be developed and employed to confirm results generated by the UV method, or the reason for the UHPLC-MS method underestimation needs to be determined and corrected. The latter is addressed in the section below.

3.1.7 Source-Induced degradation of CBDA and THCA

During initial investigations and cannabinoid profiling method assessments involving the carboxylic acid cannabinoids, THCA and CBDA, evidence of instrument-induced thermal degradation was observed. This was initially discovered when plotting

reconstructed ion chromatograms (RIC) of CBD and THC (m/z 315.2318) post analysis of a sample containing all four of the cannabinoids, CBDA, CBD, THCA, and Δ^9-THC. Two low intensity peaks corresponding to CBD and THC, m/z 315.2318, were observed to be co-eluting with the m/z 359.2216 peaks despite also being resolved as standalone peaks. This trend was confirmed when analyzing the carboxylic acid cannabinoid standards independently via UHPLC-MS. Upon further investigation of the mass spectrums of CBDA and THCA, an ion at m/z 341.2112 was also observed for both cannabinoids generating similar peaks to the carboxylic acids when plotted as a reconstructed ion chromatogram (Figure 3.10 - RICs, Figure 3.11 - example mass spectrum of THCA). The appearance of these two ions was hypothesized to be induced by the usage of high temperatures provided by the heated electrospray ionization (HESI) probe in aiding desolvation during the ionization process when coupling the UHPLC to the mass spectrometer. To determine the source of the degradation, the carboxylic acid cannabinoids were analyzed under various spray conditions to assess the rate in degradation.

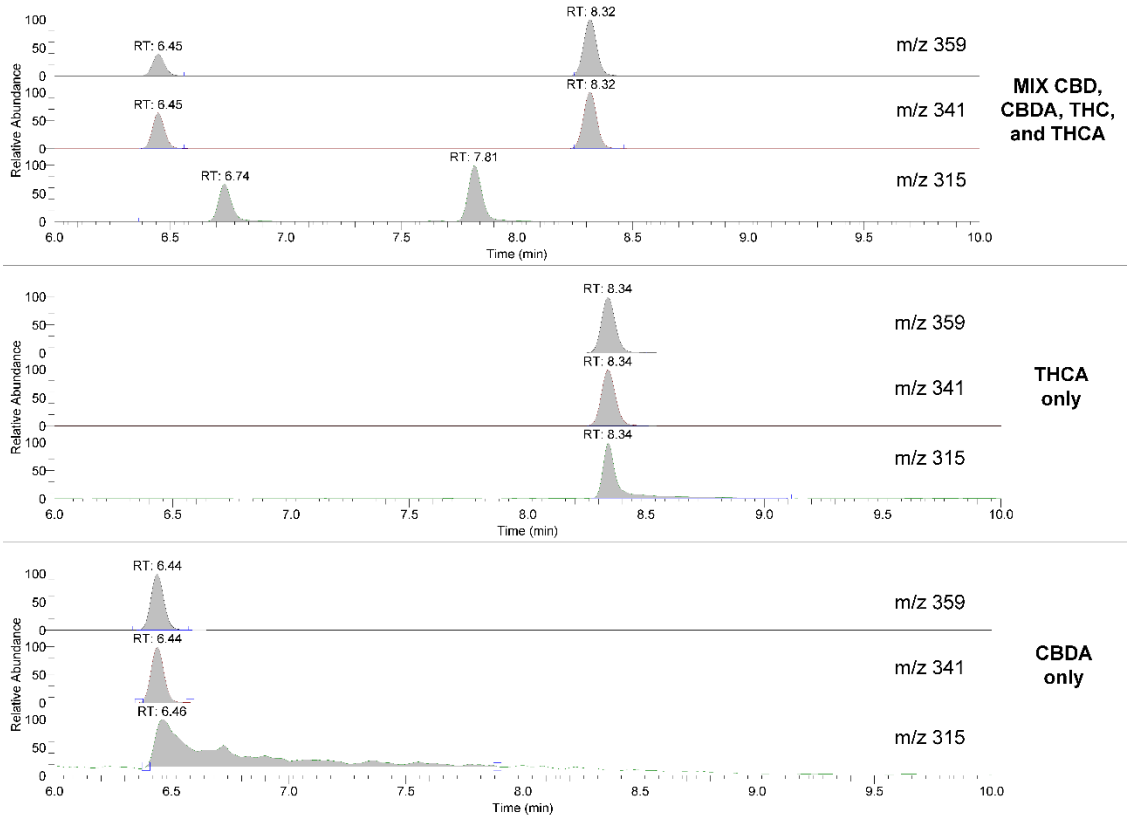

Figure 3. 10 (Top) RICs for m/z 359, 341, and 315 from a mix sample consisting of THCA, CBDA, CBD, and THC. (Middle) RICs for m/z 359, 341, and 315 from a sample consisting on THCA only. (Bottom) RICs for m/z 359, 341, and 315 from a sample consisting on CBDA only.

Figure 3. 11 Mass spectrum of the THCA peak displaying THCA (m/z 359), THC (m/z 315), and an unknown degradative product (m/z 341).

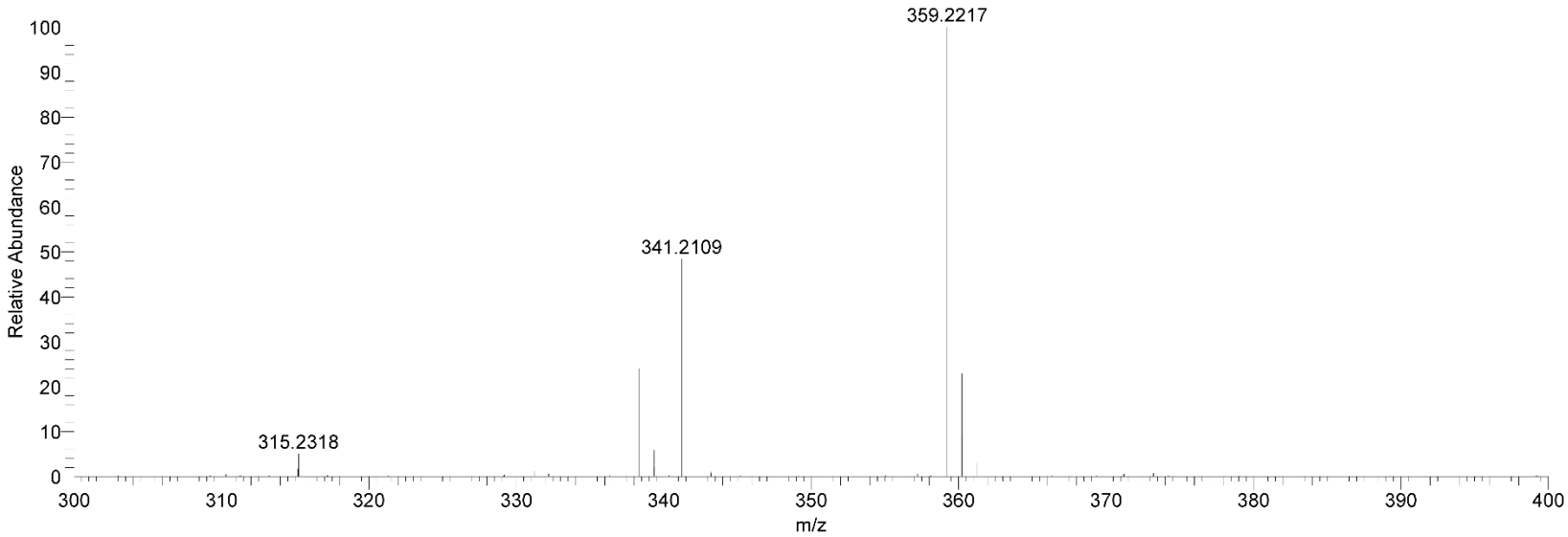

Evaluation of the rate of the instrument-induced degradation was first performed at low flow rates utilizing an "infusion" approach for assessment. Though infusion is not typical for cannabinoid profiling, the low flow rate (5 μL/min) through the HESI probe maximizes the time in contact with the heating element – approximately 13 seconds (0.22 minutes) for a 130 mm HESI probe. This approach was intended to elucidate the maximum extent degradation would occur when employing the HESI probe to aid in desolvation. The rate of degradation was determined by recording the ratio of the intensity of the intact mass ion to the intensities of the degradation product ions. Fifteen scans were acquired at each temperature increment to allow for adequate sampling when averaging the intensities. Perturbations in the total ion current (TIC) were present during the temperature increase and for a short time immediately following the temperature stabilization, therefore sufficient time was allotted at each temperature increment to allow for the TIC variation to stabilize to ~5% variation. In addition to the assessment of the HESI probe inducing degradation, the mass spectrometer inlet capillary temperature was also examined. For the inlet capillary assessment, the HESI probe temperature control was disengaged and allowed to reach ambient temperature, however, the probes' proximity to the inlet capillary prevented the probe temperature from reaching temperatures lower than ~40 ºC. Figure 3.12 displays graphs plotting the ratio of the degradation products to the intact carboxylic acid cannabinoids.

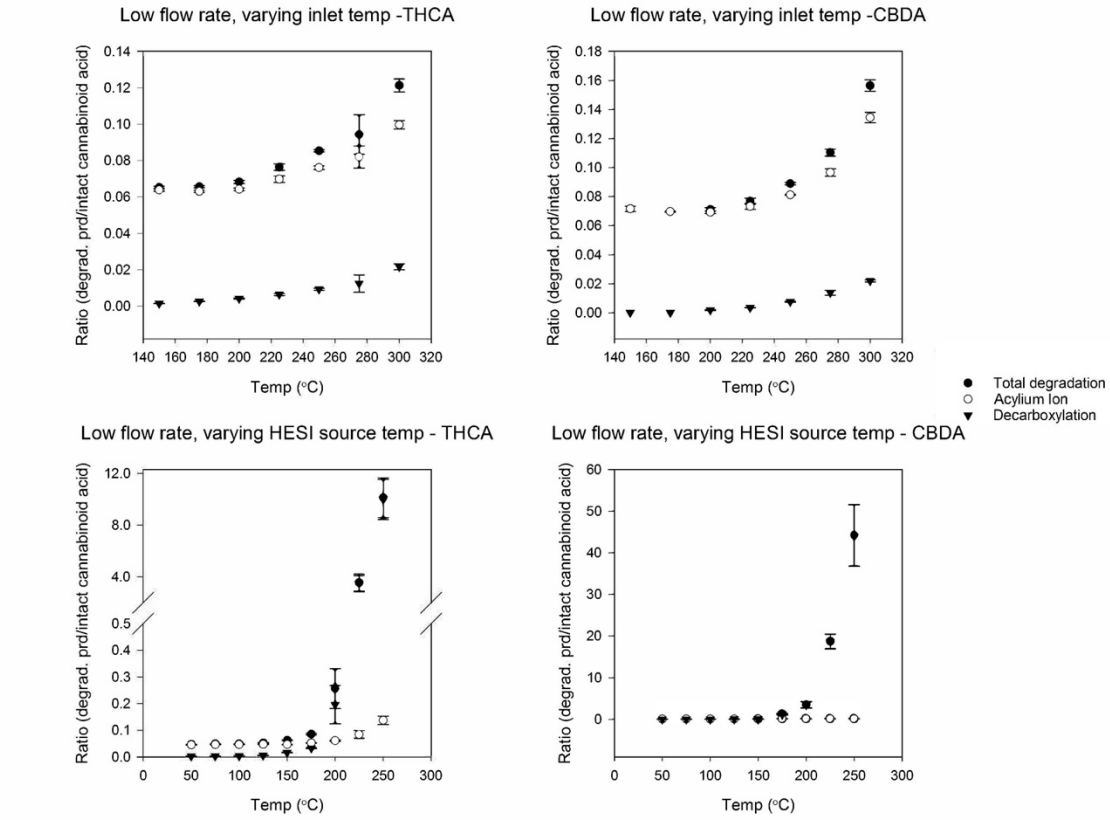

Figure 3. 12 Low flow rate (infusion) degradation analysis. Top left: THCA degradation with varying inlet capillary temperature. Top right: CBDA degradation with varying inlet capillary temperature. Bottom left: THCA degradation with varying HESI probe temperature. Bottom right: CBDA degradation with varying HESI probe temperature.

At low flow rates, varying the inlet capillary temperature resulted in minimal degradation of the carboxylic acids to their degradation products, even at the maximum temperature employed, 300 ºC. The highest observed ratio of the degradation products to the intact carboxylic acid was ~0.16:1 for CBDA. The slight upward increase in the degradation trend observed for the low flow inlet capillary experiment is believed to be due to an increase in response brought about by improved desolvation rather than by an increase degradation, though this is difficult to prove given that standards the degradation products representing the loss of H_2O (-18.0105) are not commercially available and the total degradation is largely attributed to an increase in their total signal. Conversely, the HESI probe had the opposite effect. Near the mid-temperature range, ~225 ºC, the decarboxylated product intensity increased with the ratio reaching as high as ~10:1 for THCA and ~50:1 for CBDA at the maximum temperature. The rate of the loss of H_2O remained relatively constant at higher temperatures when varying the HESI probe temperature. This product was believed to be the result of the loss of H_2O following protonation occurring at the carboxylic acid functional group (Figure 3.13), which would have dissociated at those temperatures, generating an acylium ion. Gas-phase conversion, at high temperatures, of carboxylic acids to acylium ions has been reported in literature, therefore it was hypothesized that the cannabinoid acids may be forming these ions during the high temperature electrospray and desolvation process.[110–113] To test this, MS/MS analyses were performed on the cannabinoid acids, their putative acylium ions, and their free forms to compare fragmentation patterns. Figure 3.14 displays all six tandem spectra with putative empirical formulae for selected fragments.

3.13 dehydration and decarb structures

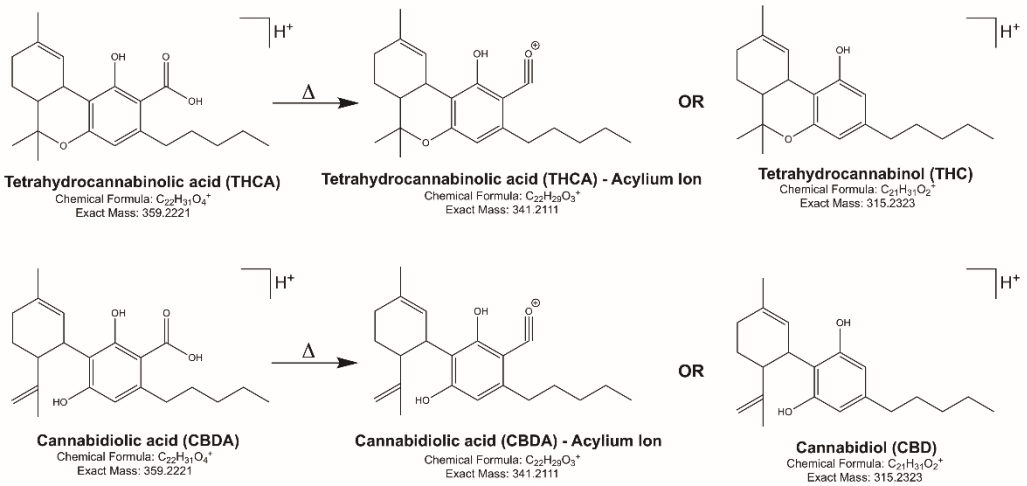

Figure 3. 13 THCA and CBDA (m/z 359) structures and their heat induced degradation products: the acylium ion (m/z 341) and the decarboxylated free cannabinoid (m/z 315).

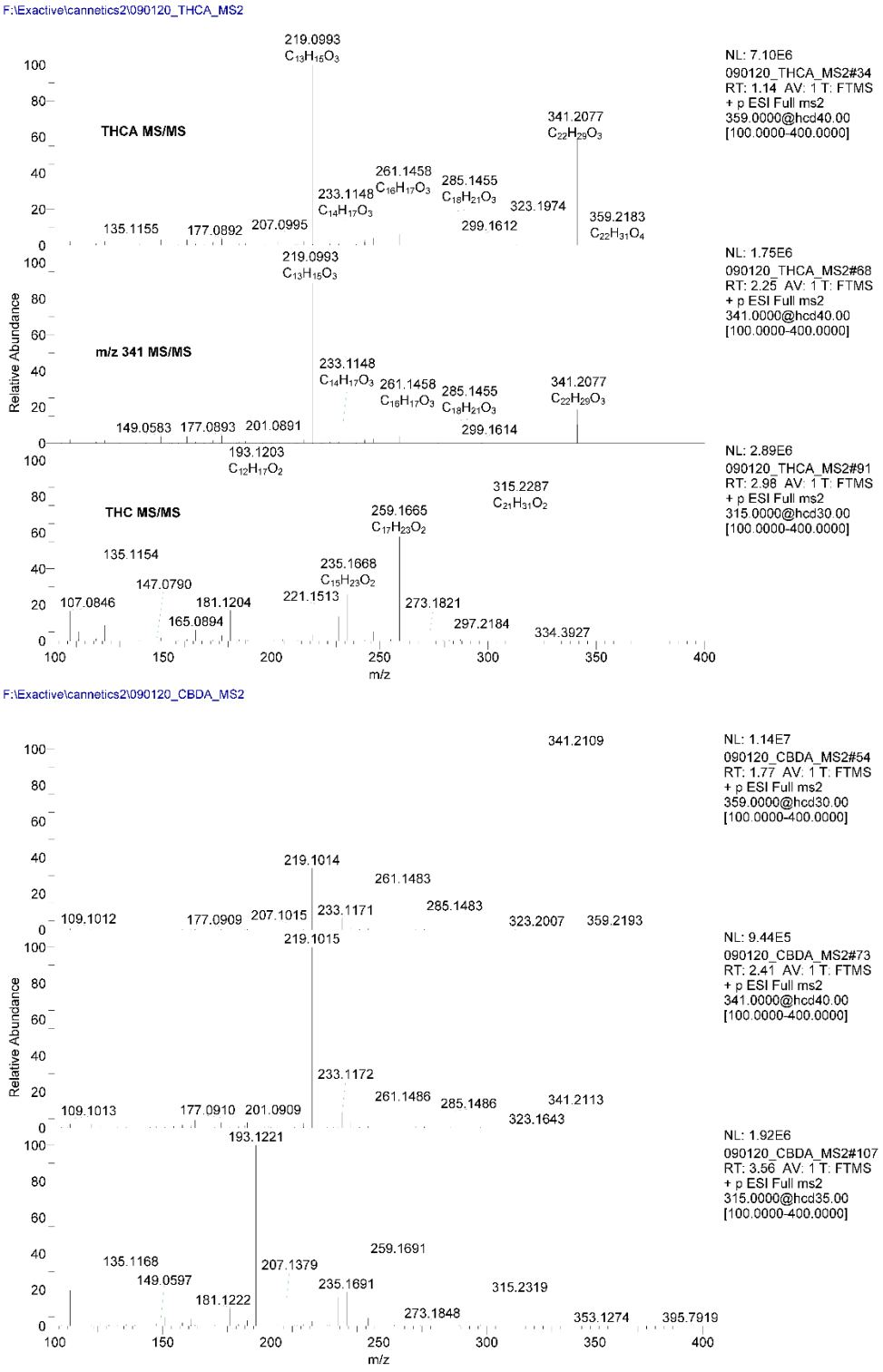

Figure 3. 14 MS/MS spectra of the cannabinoid acids (m/z 359) , the acylium ion (m/z 341), and the free cannabinoid (m/z 315) for THCA (top three traces) and CBDA (bottom three traces), respectively.

As this analysis was acquired using a HRAM mass spectrometer, empirical formulas are able to be generated for selected ions within 5 ppm of their theoretical mass. Fragmentation patterns for the carboxylic acids and the putative acylium ions displayed homology for both the THC and CBD classes of molecules. Note that most of the empirical formulas for the fragments ions corresponding to THCA, CBDA, acylium THC (aTHC), and acylium CBD (aCBD), have been calculated to contain three oxygen, while the fragments for THC and CBD mostly contain two. This would suggest that the phenolic -OH groups, shared by all six ions, are likely not the most labile bonds in the system and that the single oxygen loss in fragment species observed for THCA, CBDA, aTHC, and aCBD is likely attributed to the carboxylic acid. Carboxylic acids are usually extremely labile, as depicted in the loss of the -COOH frequently observed in the previous section, therefore it would be expected that the fragment ions observed during MS/MS analysis of THCA and CBDA would be calculated to contain only two oxygen atoms. Further evidence for this phenomenon can be observed in the following fragmentation pattern, observed for both CBD and THC species: THC/CBD: m/z 315.2320 ($C_{21}H_{31}O_2$) $\rightarrow$ 259.1691 ($C_{17}H_{23}O_2$) and CBDA/THCA: m/z 359.2216 ($C_{22}H_{31}O_4$) $\rightarrow$ 285.1486 ($C_{18}H_{21}O_3$), a difference of H_2O. The hydrogen atoms can be accounted for in that CBD/THC would have one hydrogen where the carboxylic acid attaches and the other would be lost in the acylium ($C{\equiv}O^+$) formation as the functional group is inherently charged and an [$M+H^+$] species would not exist. This evidence suggests that the occurring is actually due to the formation of an acylium ion during the gas-phase ionization process.

This approach, utilized for the evaluation of the HESI probe and the inlet capillary, was then applied to a higher flow rate (300 μL/min – Figure 3.15) to assess if their effects were evident on the carboxylic acid cannabinoids under conditions that emulate the industry standard approach for cannabinoid profiling using HPLC. At this flow rate, the time in which the analytes are in contact with the heating element of the HESI probe is greatly reduced from ~13 seconds (0.22 minutes) to ~0.2 seconds (0.004 minutes). To accommodate for the increased flow rate, the minimum temperature for both the HESI probe and the mass spectrometer inlet capillary were greatly increased (250 ºC) to prevent moisture interaction with the interior components (S-len) of the instrument. Flow injection analysis was utilized for this assessment allowing for area counts to be used for the ratio determination rather than averaged scan-to-scan ion intensities. The reduced time in contact with the HESI probe, even at the maximum employed HESI probe temperature, resulted in reduced rates of degradation, as anticipated. At the typical temperature ranges suggested for HESI probes at this flow rate, the ratio of the degradation products to the intact acids averaged at ~0.2:1 with the ratios reach as high as 0.4:1 at the maximum temperature. Contrary to the observations made during the infusion experiment, the inlet capillary temperature had an increased effect, especially for CBDA with ratios as high as ~4:1 for the acylium ion.

To further assess the carboxylic acid cannabinoid dehydration and acylium ion formation phenomenon, variations in solvent composition were also considered. Due to the non-polar characteristic nature of the cannabinoids, higher organic percentages in mobile phases are required to promote elution from standard reversed phase HPLC columns as demonstrated in UHPLC gradient mentioned previously.

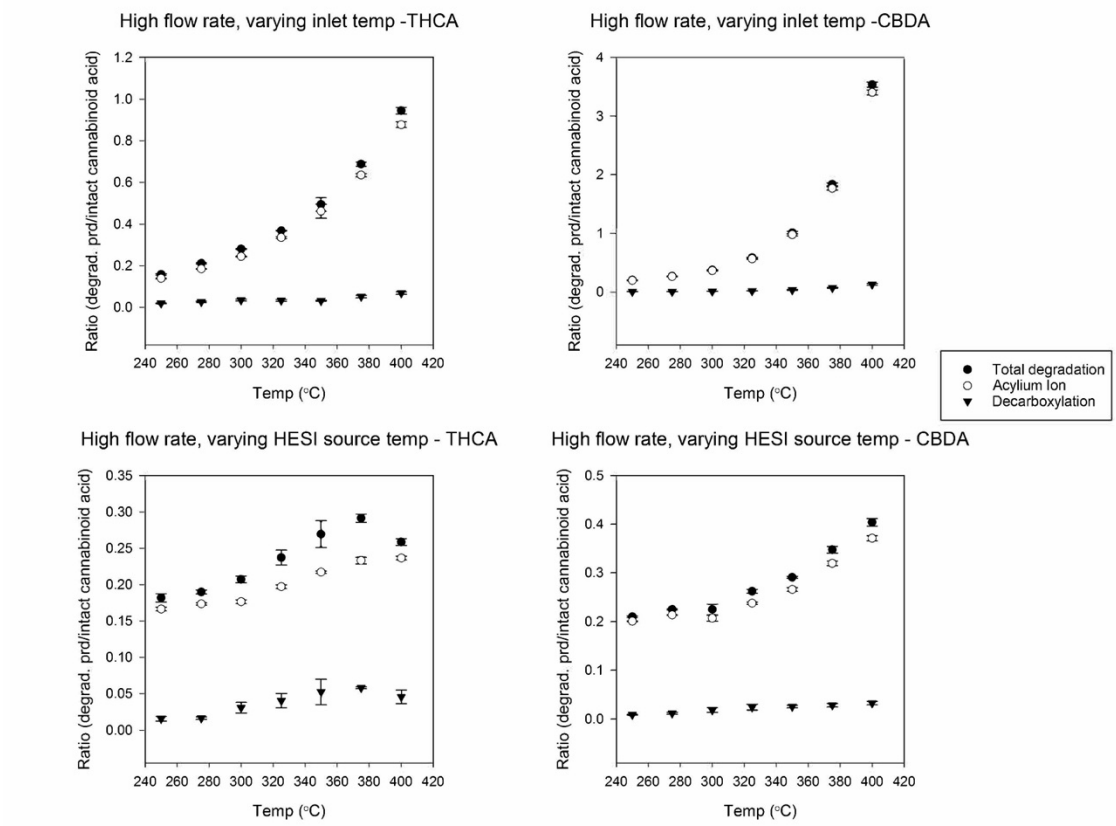

Figure 3. 15 High flow rate (LC flow) degradation analysis. Top left: THCA degradation with varying inlet capillary temperature. Top right: CBDA degradation with varying inlet capillary temperature. Bottom left: THCA degradation with varying HESI probe temperature.

Additionally, due to economic factors, methanol is often utilized as the organic component for HPLC separations rather than acetonitrile. Therefore, the high-flow rate experiment was repeated at a higher organic percentage, 75% ACN rather than 50%, and again with 50/50 and 75/25 MeOH: H_2O w/ 0.1% formic acid. Acetonitrile has a higher heat capacity (~92 J/mol*K than both water (~75 J/mol*K) and methanol (~81.5 J/mol*K) thus it was hypothesized that higher ACN percentages would reduce the rate of degradation for the ACN/water analyses however, the rate of degradation observed for the methanol/water experiments would be increased when compared. Figure 3.16 (ACN) and 3.17 (MeOH) displays the graphical representations of the degradation rates of the acids with varying mobile phases. As hypothesized, increased ACN concentrations reduced the degradation rates from 0.25:1 to 0.2:1 for THCA and 0.4 to 0.25 for CBDA, at the maximum temperature. The hypothesized outcome was not observed, however, for the MeOH experiment. Despite having a lower heat capacity than acetonitrile, the rates of degradation were not only lower than those observed when using acetonitrile, but also consistent across organic concentrations: THCA – 0.16:1 for both 50% and 75% MeOH, CBDA – 0.25:1 for both 50% and 75%. There are multiple possible explanations for this phenomenon. The first involves the protic nature of MeOH as opposed to the aprotic nature of ACN. Given that the solvent composition includes 0.1% formic acid, approximately pH 2.7, according to Shi and Middlemiss, the gas and liquid-phase conversion of carboxylic acids to acylium ions is driven towards the products at low pH, however, in the presence of an alcohol, such as methanol, a Fischer Esterification can occur.[113] This would result in the formation of a stable ester as opposed to or in conjunction with the formation of the acylium ion. For both acids, m/z 373.2373 would

be observed if formation of the ester occurs in the presence of methanol. This can be observed in Figure 3.18 wherein an example of the FIA series for CBDA in 75% methanol can be seen. The top three RIC traces represent CBDA, the ester ion, and the acylium ion, respectively. The bottom two traces show CBDA in 75% ACN displaying no evidence of the m/z 373.2373 ion outside of baseline noise. This ester ion appears at ratios as high as 0.06:1 for CBDA and 0.07:1 for THCA. Though low in comparison to the acylium ion and decarboxylated product, this observation adds an addition factor to be taken into consideration when quantifying cannabinoid acids. In addition to esterification, methanol also has a higher vaporization enthalpy, 38.3 kJ/mol versus 33.8 kJ/mol for ACN. During the electrospray process, ionization efficiency, which also contributes to signal intensity, is dependent on the rate of desolvation of the ions as charged species. As the formation of the acylium ion is hypothesized to be a gas-phase event, the reduced vaporization enthalpy would imply that, when using ACN, the analytes are desolvated earlier than they are when using MeOH. This would not only have an impact on the rate of acylium formation, it could also induce an artificial inflation of the observed ratios, as the relative signal intensities would be higher when using ACN than MeOH. The possible formation of the ester product and the acylium ion and the overall reduction in the signal response paired with the overall poor elutropic strength of MeOH (1 ε^o) compared to ACN (3.1 ε^o) would suggest that, though even at the lowest operating temperatures, the acylium ion appears, ACN is still the better suited solvent for cannabinoid profiling. As quantitation of the byproduct is currently not possible due to the lack of a commercial standard or method of synthesis, the best course of action would be for profilers to treat the acylium ion, and other degradative products,

as one would for the doubly and singly charged ions of a molecule possible of forming such species, in quantitation and use a summation of the area counts to represent the response of the molecule.

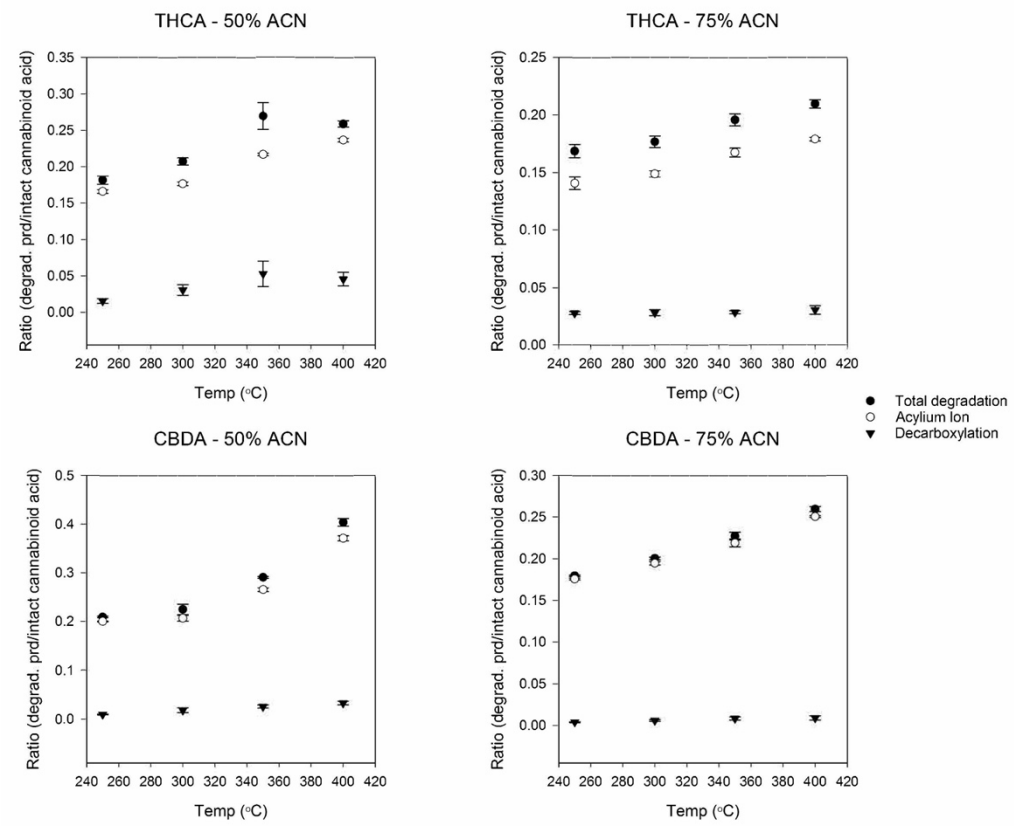

Figure 3. 16 ACN - High flow rate (LC flow) degradation analysis. Top left: THCA degradation with varying inlet capillary temperature at 50% ACN. Top right: THCA degradation with varying inlet capillary temperature at 75% ACN Bottom left: CBDA degradation with varying inlet capillary temperature at 50% ACN Bottom right: CBDA degradation with varying inlet capillary temperature at 75% ACN.

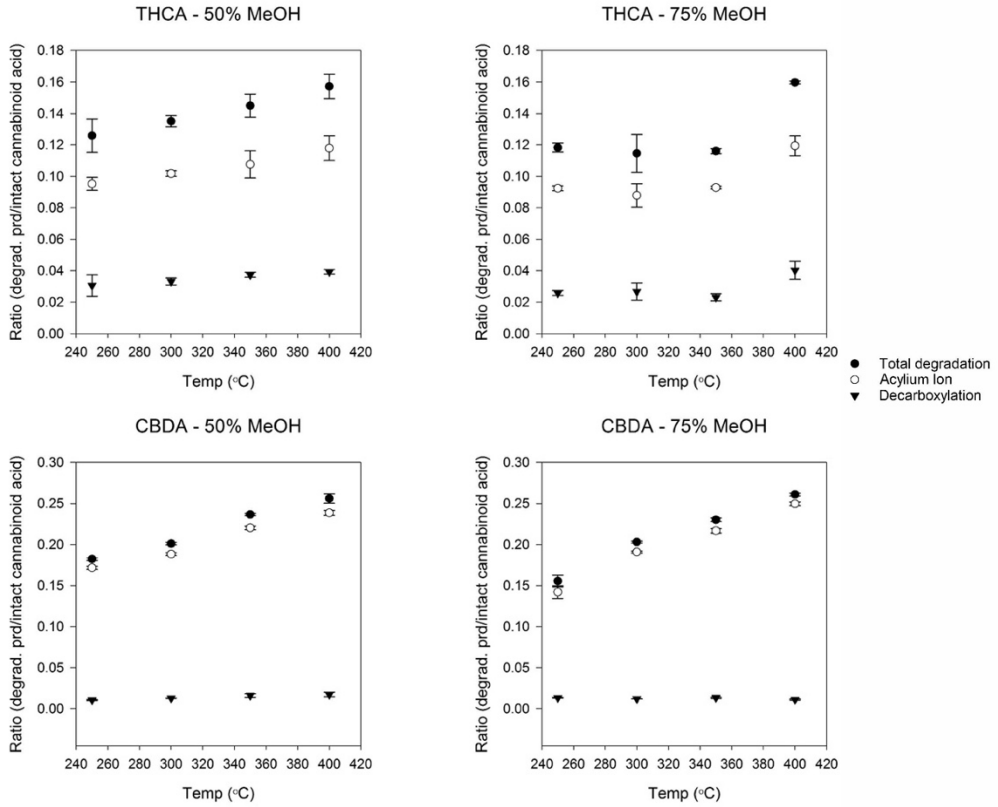

Figure 3. 17 MeOH - High flow rate (LC flow) degradation analysis. Top left: THCA degradation with varying inlet capillary temperature at 50% MeOH. Top right: THCA degradation with varying inlet capillary temperature at 75% MeOH Bottom left: CBDA degradation with varying inlet capillary temperature at 50% MeOH Bottom right: CBDA degradation with varying inlet capillary temperature at 75% MeOH.

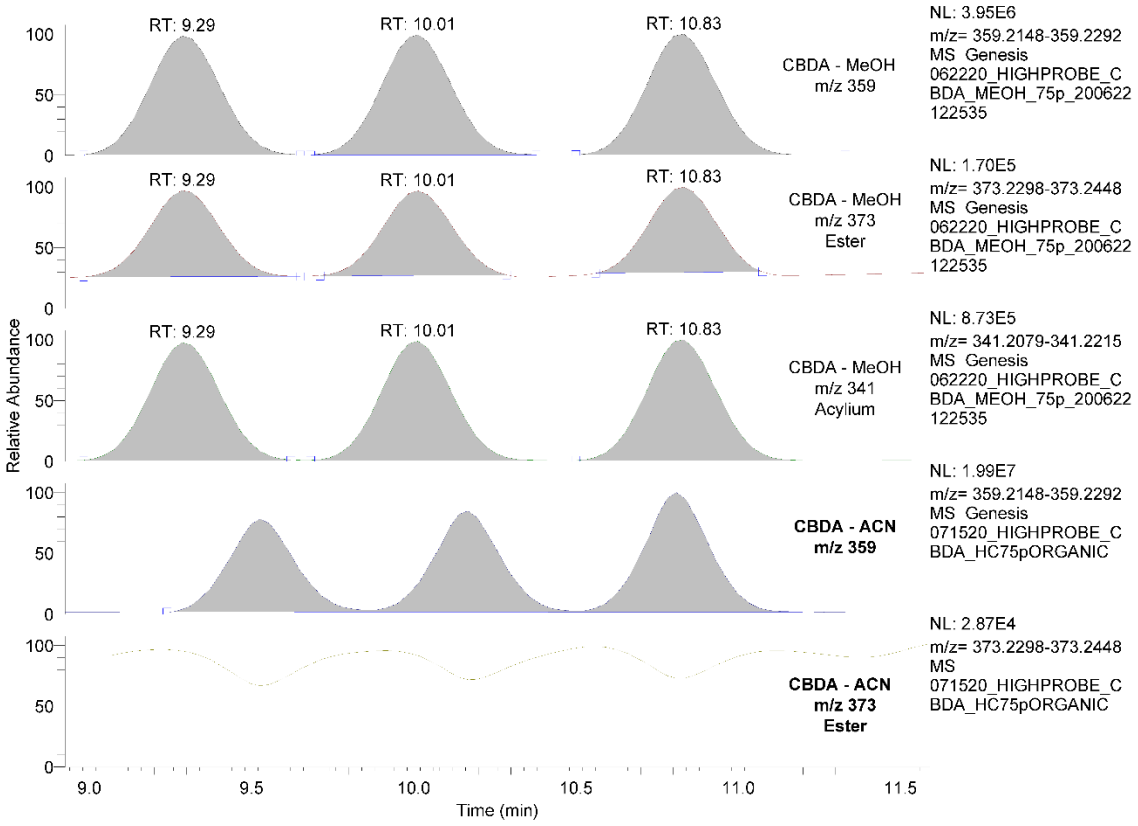

Figure 3. 18 (Top to bottom): Top three traces - FIA segment RIC for m/z 359 (CBDA), m/z 373 (putative CBDA methyl ester), and m/z 341 (acylium ion) for MeOH mobile phase. Bottom two traces – FIA segment RIC for m/z 359 (CBDA) and m/z 373 (methyl ester – baseline noise) for ACN mobile phase.

3.1.8 *Polygonum multiflorum* screening method development

In a similar manner to the work found in chapter 2, this chapter section focuses on the development of a screening method for plant extracts, In this case, those from *Polygonum mulitflorum*. It is hypothesized that *P. multiflorum* may produce secondary metabolites that interact with alpha-synuclein and may be used to treat Parkinson's disease.[107-109] Unlike with *L. cardinalis* in chapter 2*, p multiflorum* has been well characterized in literature and its main secondary metabolites are commercially available, however, difficulty can be encountered in the metabolomic analysis of *P. multiflorum* as most of its secondary metabolites are polyphenolics. Polyphenolics are nonpolar with poor aqueous solubility and exist as neutrals in most analytical applications. Though better suited for negative ion mode mass spectral analysis, the goal of this work was to develop an ancillary or alternative method that could be used to analyze both the polyphenolics and investigate other unknown metabolites using positive ion mode mass spectrometry.

Prior to advanced method development, seven commercial standards (trans-TSG, polydatin, rhaponiticin, resveratrol, emodin, physcion, and quercetin) were used to evaluate ionization methods and optimize UHPLC-MS separations, as extraction methods have already been thoroughly investigated in literature.[98] As stated previously, typically for polyphenolics, negative ion mode ESI to produce $[M-H]^-$ ions is employed. For this specific application, however, negative ion mode lead to multiple analytical issues such as enhancement of common contaminant signals (i.e. SDS and plasticizers), poor separation as organic modifiers are not typically used in HPLC separation, and poor MS/MS fragmentation. Poor MS/MS fragmentation is detrimental to this research as the

mutant *P. multiflorum* cultures that are to be developed and provided by Naprogenix and analyzed using this approach in the future will have undergone a similar mutation and selection process that the *L. cardinalis* cultures were in chapter 2. In doing so, it is possible that the cultures will produce novel secondary metabolites or upregulate previously trace secondary metabolites in response to the mutagenesis that will need to be characterized using tandem mass spectrometry. In work performed by fellow Lynn group lab members analyzing lignin monomers and dimers, i.e. polyphenolic compounds, the use of lithium chloride to produce $[M+Li]^+$ species has been successful in producing better MS/MS fragmentation patterns. In applying this technique, the *P. multiflorum* standards were analyzed using Li, Na, K, and NH_4 chloride salts to assess cationization efficiency, as well as fragmentation. Figure 3.19 displays an example of the MS/MS spectra of trans-TSG corresponding to the $[M-H]^-$, $[M+H]^+$, and $[M+Li]^+$ ions. As depicted in the Figure, little structural information can be derived from the $[M-H]^-$ and $[M+H]^+$ MS/MS spectra aside from the loss of the glucose yielding the free stilbene – $[M+H]^+$: $C_{14}H_{13}O_4^+$ - m/z 245.0808 and $[M-H]^-$: $C_{14}H_{11}O_4^-$ - m/z 243.0663. When performing the MS/MS experiments on the Li^+ adducts, an extensive fragmentation pattern can be seen, as observed during the lignin MS/MS analyses. In utilizing post-column addition of 10 mM chloride salts at 10 uL/min, the area counts corresponding to the standards forming adducts with the different cations was compared. Table 3.3 displays these area counts and also the area counts corresponding to the $[M-H]^-$ and $[M+H]^+$ ions. A decrease by over an order in magnitude can be observed when switching from negative to positive ion mode, thus limiting limits of quantification and detection when using positive ion mode.

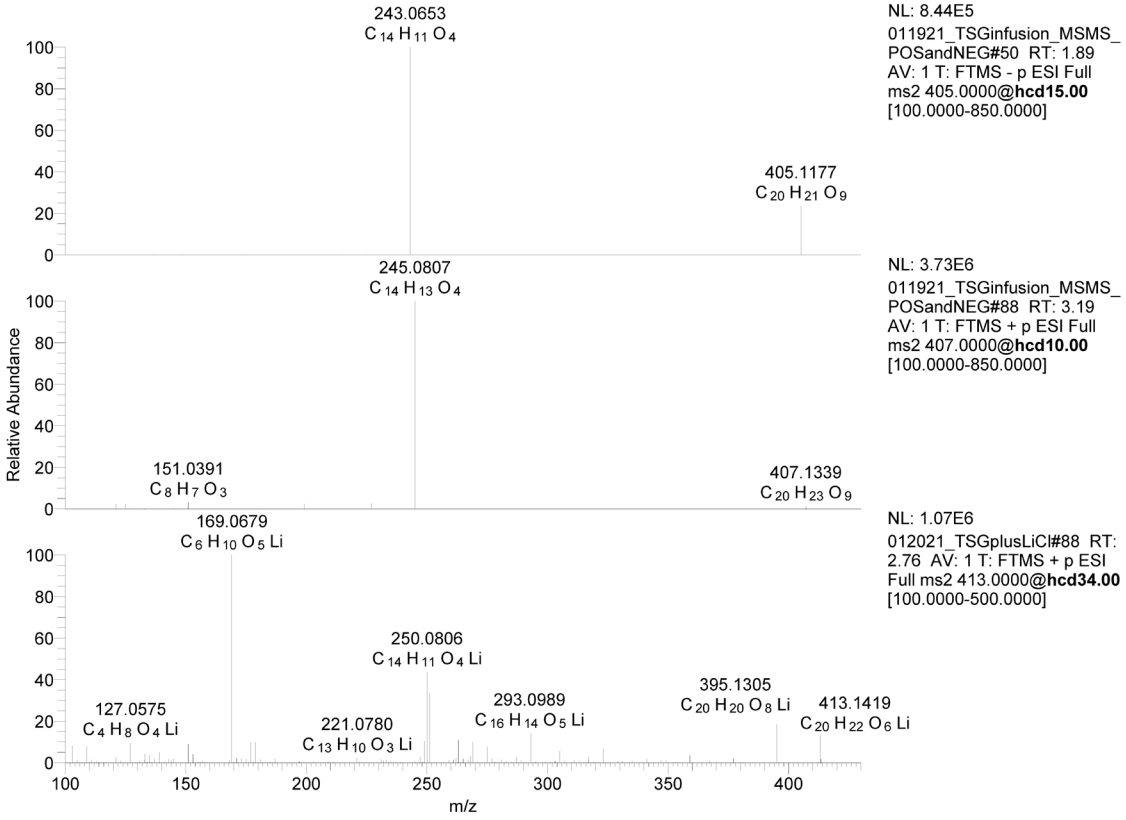

Figure 3. 19 MS/MS spectra for TSG: Top - $[M-H]^-$ at 15 NCE, Middle - $[M+H]^+$ at 10 NCE, and Bottom - $[M+Li]^+$ at 34 NCE.

Table 3. 3 Signal intensities for various polyphenols under differing ionization adduct conditions.

ID	M-H	M+H	M+Li	M+Na	M+K	M+NH4
TSG	5.8E+07	3.0E+06	2.4E+06	1.0E+06	1.7E+05	9.1E+04
Polydatin	6.4E+07	2.4E+06	2.4E+06	1.8E+06	1.0E+06	1.1E+06
Rhaponiticin	3.6E+07	1.0E+06	3.0E+06	1.7E+06	1.5E+06	1.9E+06
GG B-O-4	4.1E+07	1.2E+05	5.9E+07	8.0E+07	2.8E+07	1.6E+07
Resveratrol	1.6E+08	3.9E+06	0E+00	0E+00	0E+00	0E+00
Emodin	9.7E+08	3.1E+05	0E+00	0E+00	0E+00	0E+00
Physcion (7.4)	6.5E+06	2.2E+05	0E+00	0E+00	0E+00	0E+00
Physcion (10.3)	4.4E+07	2.8E+04	0E+00	0E+00	0E+00	0E+00
Quercetin	1.3E+07	2.6E+05	0E+00	0E+00	0E+00	0E+00

Additionally, cationization adducts were only observed for the stilbene glucosides, with Li+ being either the most responsive or similar in response to the [M+H+] species. This was expected, however, as the stilbenes and lignin dimers are very similar in structure. Interestingly, no interaction was observed for resveratrol with any of the cations, despite it being the free stilbene of polydatin. This would suggest that the Li^+ interaction is most likely either stabilized by the presence of the glucoside or the interaction is occurring with the glucoside exclusively. No cations outside of the $[M+H]^+$ ions were observed for the flavonoid or the anthraquinones, which may be explained by the fact that both classes are relatively planar molecules. This is not necessary problematic, however, as the flavonoids and anthraquinone standards produced more extensive fragmentation patterns at higher NCEs than the stilbenes and, in the event that putative novel flavonoids or anthraquinones are detected, they can be characterized without the requirement of adduct formation. Through this approach, screens would be performed once using negative ion mode, in order to ensure low concentration analytes are not missed, with standard UHPLC separations, and then again switching the polarity and using post column LiCl with a targeted MS/MS peak list to identify novel metabolites. Though applicable, the increased time resulting from the requirement of two analyses per sample makes this method less than ideal for high-throughput metabolomics screenings.

To establish a baseline peak list for downstream comparison, using compiled lists of known secondary metabolites found in *p. multiflorum*, trimmings of WT plants (~200 mg dry weight) were collected from Naprogenix, extracted, and analyzed. Using MZmine2 paired with METLIN and KEGG for database searching, an extensive peak list, consisting of over 120 identified primary and secondary metabolites, was constructed for

cross referencing in the event that novel peaks are detected. The list was broken down into analytes found in root, stem, leaf, and/or whole plant extracts, as well, to aid in prioritizing analyte procuration from specific tissue sections in down-steam extractions. This list can be seen in appendix 4.

In order to couple the analysis with characterization, specifically in a high-throughput manner, as utilized in Chapter 2, the use of CZE/CE-MS was explored for this application as well. Given that polyphenolics generally exist as neutrals at most pH's in solution, standard CE would be difficult to employ as neutrals would migrate with the EOF and not separate. High pH buffers could be employed for standard CE analysis, such as phosphate or borate BGEs, however such involatile salts can cause irreparable damage to mass spectrometers. For CE coupled to MS analysis, typically, positive ion mode acquisitions with low pH BGEs consisting of volatile salts are used. Extracts and standards were introduced to the ZipChip CZE-MS setup described in chapter 2 and the previously developed method was applied, as is. As expected, no peaks were observed. The cationic coating on the walls of the CZE HS chip effectively reduces the zeta potential and eliminates all electroosmotic flow. Additionally, since the analytes are neutral, no electrophoretic mobility is observed either. Pressure can be applied at the head of the BGE well to act as a "pseudo-electroosmotic" flow strictly in terms of providing a bulk flow in the separation channels. When pressure is applied at the origin side of the chip, the analytes are eventually forced out, concurrently, after approximately 10 minutes. This mass coelution is obviously disadvantageous as it greatly complicates any mass spectral data from being interpreted differently than an infusion or flow-injection analysis. Additionally, seemingly due to interactions with the wall coating increasing the

impacts of longitudinal diffusion, the pressure eluted peaks are multiple minutes wide and often result in carry-over, making quantitation, or even relative quantitation, difficult. To address this, collaboration with 908 Devices was established and the manufacturer provided a proto-type blank "HR" chip. Aside from being stripped of the cationic coating, the separation channel was also twice as long (10 cm vs 22 cm), overall making the application more akin to traditional CE. To correct for the added length, the maximum allowed applied field strengths are half that applicable to the HS chips: 500 V/cm vs 1000 V/cm. Though the switch to a bare chip allows for more "CE"-like, rather than CZE, separations and eliminates interactions with the wall coating, the analytes being neutral would still cause them all coelute with the reestablishment of the electroosmotic flow. Lithium chloride was added to the BGE and diluent, both independently and simultaneously, to test if interactions with the cation would allow for electrophoretic mobility to be observed. Though migratory and peak shape improvements were observed, as seen in Figure 3.20 for polydatin and rhaponitcin, the least and most conjugated stilbene glucosides respectively, the migration shifts were believed to be associated with Li cation migration rather than true Li adduct electrophoretic migration, causing the analytes to continue to coelute. Negative field strengths coupled with a NH_4OH separation BGE (pH 8.5) and diluent were also evaluated, however, only positive potentials can be applied to the ESI spray well of the chip requiring analyses to be acquired in the positive ion mode. Both Li and standard BGEs were tested in the spray well, however, no ions were detected regardless of applied voltages. It is possible that any electrophoretic migration occurring is quickly neutralized at the separation channel-spray channel intersection and the analytes are also neutralized in the process.

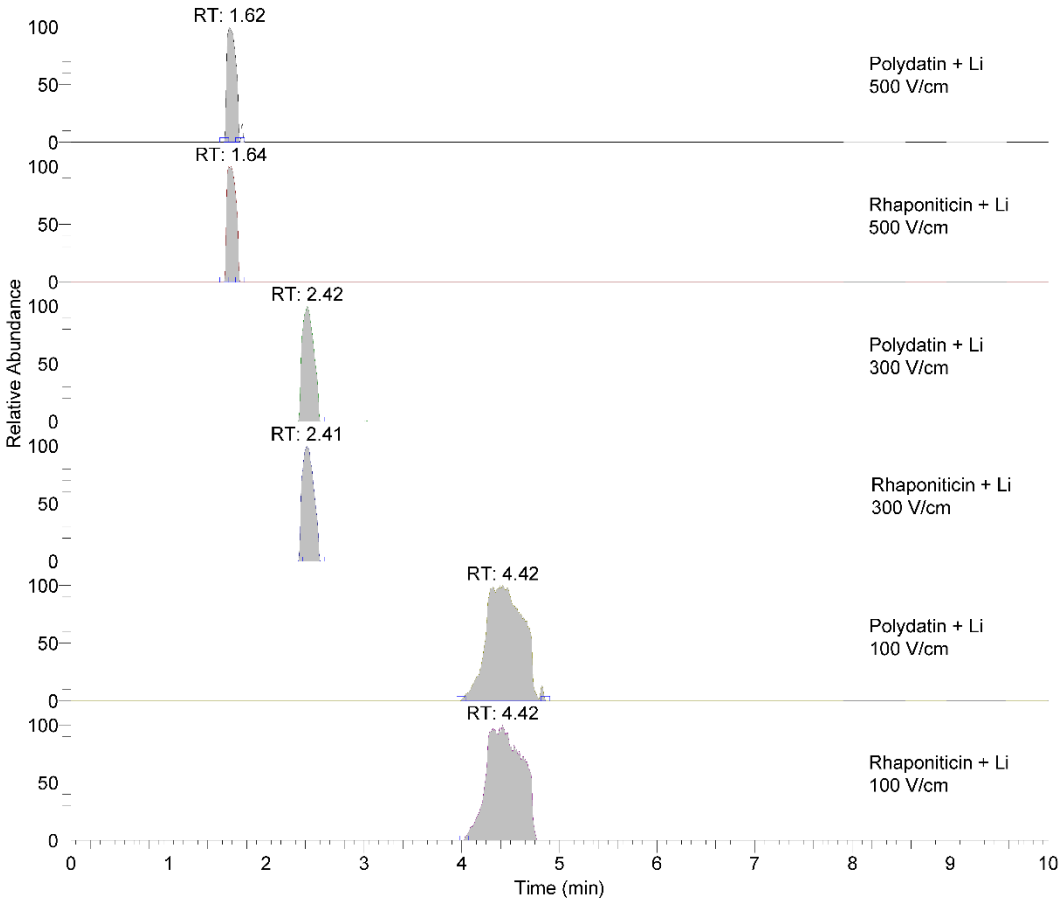

Figure 3. 20 Reconstructed electropherograms of $[M+Li]^+$ for polydatin and rhaponiticin at varying field strength voltages.

As no BGE, diluent, or surface modifications tested resulted in adequate separation of the analytes, modification of analytes was evaluated.

Borrowing from the common use of derivatizing analytes for GC-MS, derivatizing with dansyl chloride was investigated for this application. Dansyl chloride is commonly used as a fluorescence signal amplifier in protein analysis and reacts with primary amines and alcohols, under basic conditions, to produce sulfonamide or sulfoxide adducts with terminal tertiary amines. For this application, the tertiary amine of the dansyl group provided a cationization site (pKa 2.4) for positive ion separation and positive ion mode mass spectral analysis. Since previous work has been performed using the cannabinoids and dansyl chloride, also being phenolics, they first were evaluated to determine if electrophoretic separation was achievable with molecules that are generally highly non-polar, neutral, and poorly suited for positive electrophoretic separations.[114] Figure 3.21 displays the general dansylation reaction and Figure 3.22 displays both the cannabinoids, both monodansylated (A) and bidansylated, if possible (B), as well as the *p. multiflorum* metabolites, both monodansylated (C) and bidansylated, if possible (D). The reactions were performed using standards to assess reaction conditions and also on cannabis extracts as a surplus of extract material was available. The methods developed using the cannabis extracts will be applied to the *p. multiflorum* extracts when they are available in the future. Various reaction times, temperatures, and molar ratios were evaluated and it was determined that a 10-fold molar excess of dansyl chloride to reactant for 2 hours at 60 ºC resulted in >99% conversion to the monodansylated or bidansylated species based on the absence of signals corresponding to the reactants. By 2 hours, most analytes were

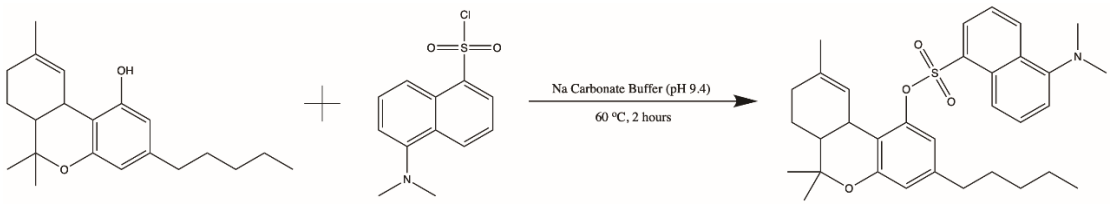

Figure 3. 21 Dansylation reaction with THC.

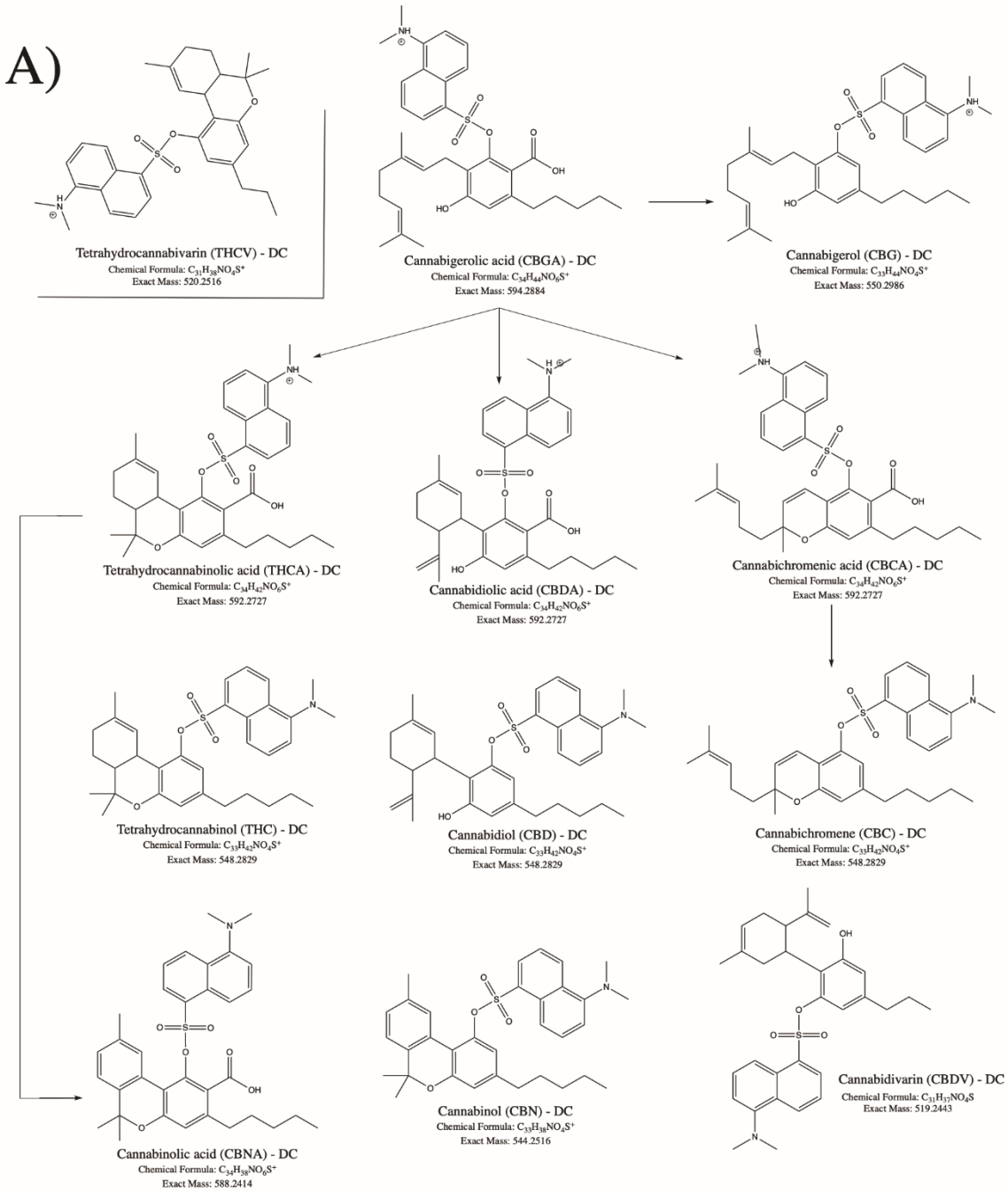

Figure 3. 22 – A) Structures and masses corresponding to mono-dansylated cannabinoids.

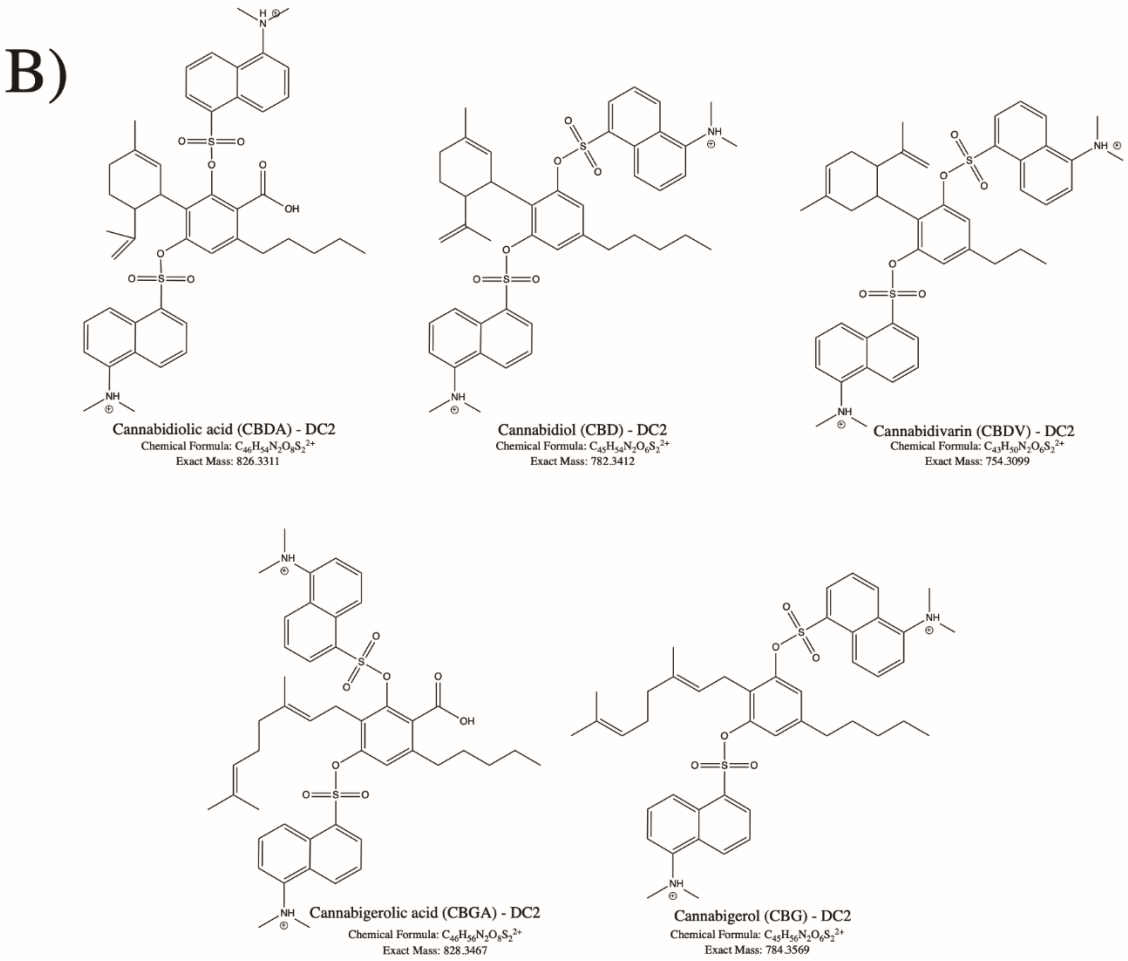

Figure 3. 22 – B) Structures and masses corresponding to bi-dansylated cannabinoids.

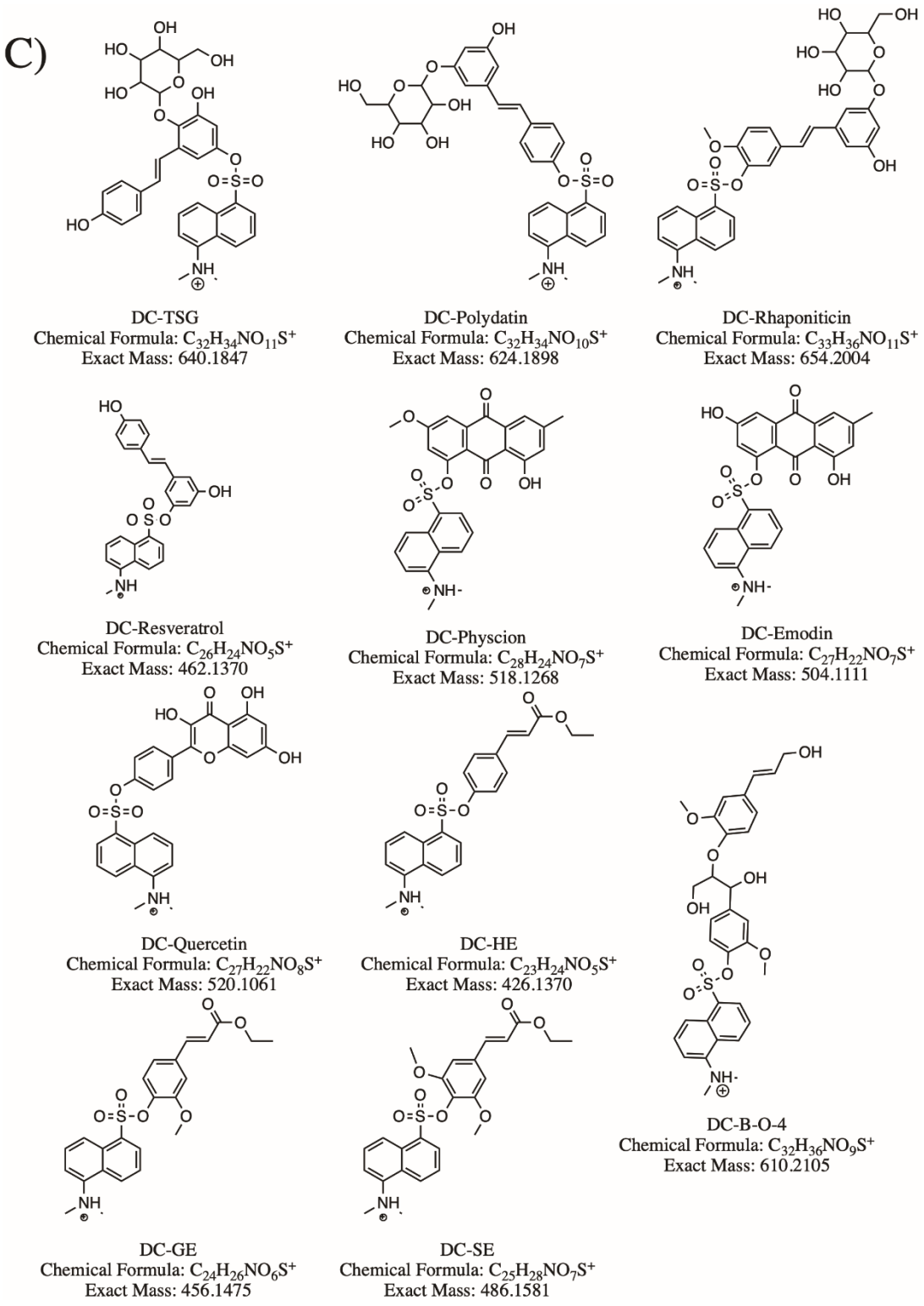

Figure 3. 22 – C) Structures and masses corresponding to mono-dansylated polyphenols.

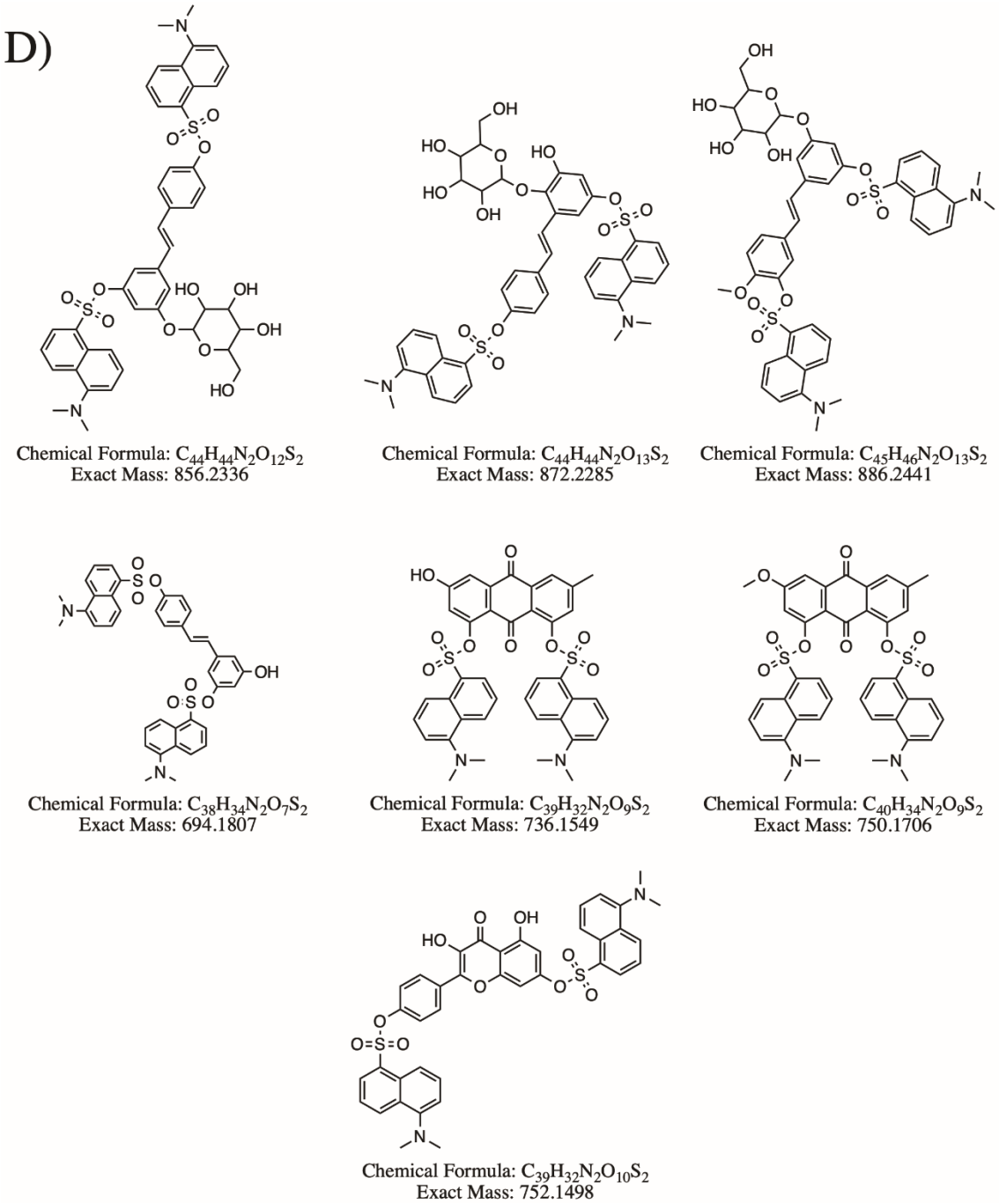

Figure 3. 22– D) Structures and masses corresponding to bi-dansylated polyphenols.

successfully monodansylated, however, for analytes like CBD and resveratrol containing hydroxyl groups with near equivalent pKa's, bidansylation was possible and observed. Initial evaluations of dansylated cannabinoid standards (A) as well as dansylated cannabinoid extracts (B), Figure 3.23, provided evidence of not only electrophoretic mobility, but adequate separation of the selected analytes as well. Peak shape degraded between the dansylated standards and the dansylated extract, most likely due to the extract undergoing minimal cleanup and processing prior to analysis. Though preliminary, this data provides evidence that this approach would likely be applicable to the *p. multiflorum* extracts in the future.

In order to adequately assess method development for the dansylated *p. multiflorum* CE-MS analysis, multiple separation and sample preparation conditions were evaluated, namely, sample diluent concentration, the usage of pressure assist, and the chip wall coating. Since the HS and HR chip channels are different lengths and the software prevents the same field strengths from being applied to different chips, retention time was not used as a comparison metric. Figure 3.24 displays RICs for the variously dansylated *polygonum* analytes using the HRB chip. Due to the multiple phenolic sites found on several of these analytes, like TSG, dansylation can occur at multiple locations. Due to the steric hindrance incurred by the addition of the bulky nonpolar naphthalene group of the dansyl modifier, generally one dansylation was observed at the most terminal phenolic site but a distribution of the dansylated products can be seen in the RICs.

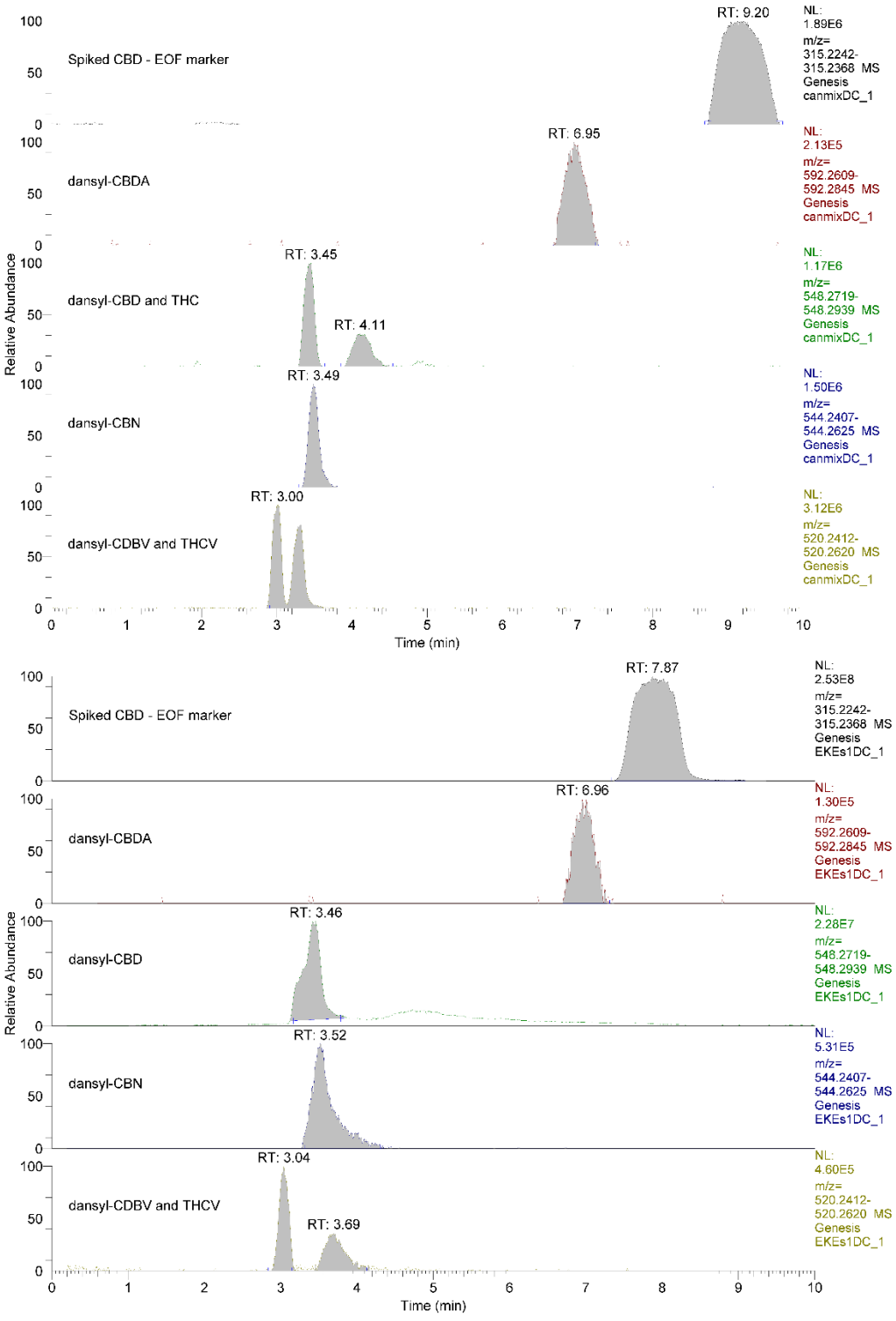

Figure 3. 23 RICs for CBD and dansylated cannabinoid standards (top) and in an ethanol extract (bottom).

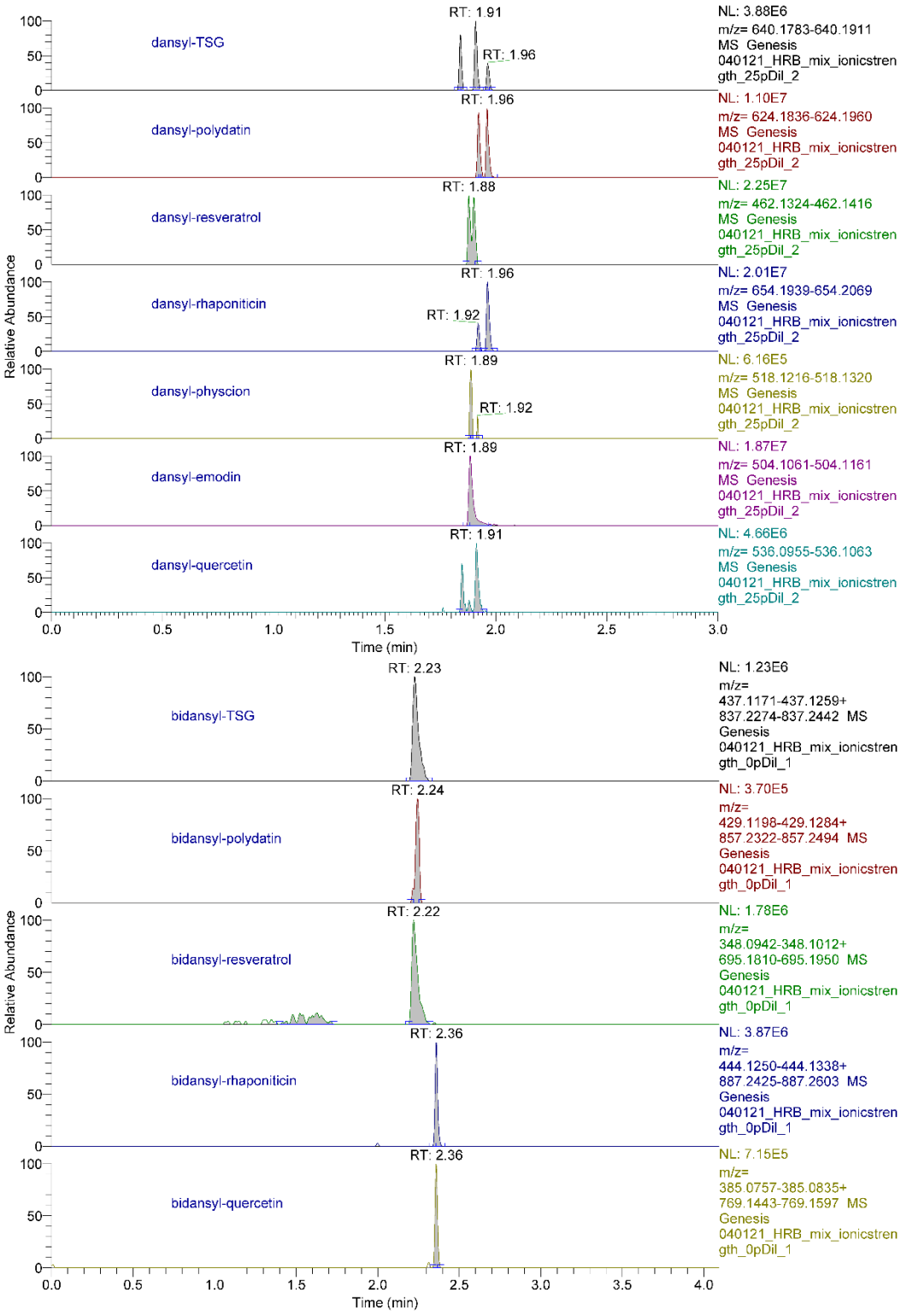

Figure 3. 24 RICs for mono and bi-dansylated polyphenolic standards.

Though adding another layer of complication to the analysis, the fact that they are all baseline resolved from one another despite being very similar structural isomers simplifies the downstream data-processing as no forced chromatographic deconvolution calculations are required, the individual peak area counts can simply be summed for absolute or relative quantitation. When applying the dansylated *polygonum* analytes to the HS chip with the cationic coating, however, the addition of the dansyl group to the stilbenes did not have the same effect that it did for the cannabinoids. In assessing the use of pressure assistance and varying leading electrolyte concentrations (0-100μM), very few conditions resulted in any detectable signals for the dansylated stilbenes. It would appear that they interact strongly with the cationic wall coatings of the HS chips, a feature encountered during the non-dansylated attempts without the addition of the Li^+ to the BGE. This observation provides clear evidence that if this dansylation approach is used for downstream CE-MS applications, the HRB will be a requirement.

In further comparison of the of the HRB and HS chips, as the HRB showed a clear advantage for stilbene analysis, the chips were compared using relatively less conjugated phenolic compounds. Here, the chips were evaluated using dansylated lignin ester monomers and a lignin dimer model compound. Conversely to the application of the HS chips with the stilbenes, the lignin compounds were successfully analyzed using both chips across all applied conditions with the exception of turning off the pressure assist (Figure 2.35). The deactivation of pressure assist was a problem for both chips as stable spray was the limiter for this applications and droplets were repeatedly building up on the chip spray corner, causing ESI spray instability. In further investigations of the most ideal methods for analyzing these dansylated compounds, analytical factors such as peak

duration, peak asymmetry factors, and peak tailing factors were calculated and compared. Also, while theoretical plate counts for CE are not typically used as they are more applicable and better describe true chromatographic methods, the number of theoretical plates were calculated for each chip strictly for comparison of the CE methods. This approach was chosen as it normalizes differences observed between the two chips that could have arisen from the fact that the separation channels are different lengths using the equation:

$$N = 5.54\left(\frac{t}{w_{\frac{1}{2}}}\right)^2 = \mu_{app} \times \frac{V}{2D_m}$$

$$\frac{Theo.\,Plates}{m} = \frac{N \times 100}{sep.\,channel\ length}$$

Figures 3.26 displays a graphical depiction of the changes in peak durations and migration times as a function of chip and electrolyte/organic solvent concentration. Additionally, the changes in the number of theoretical plates for each method is graphically depicted. These results clearly show that the true CE separations using the bare chip outperform the coated chip for this application. Additionally Figure 3.27 shows the asymmetry and tailing factors associated with each method. Again, here ideal conditions can be observed for the HRB chip using 75% diluent with 25% ACN in which both factors come close to 1 - a truly gaussian distributed peak. Note that the high aqueous, high salt condition (right-most points) does not contain a high enough organic solvent composition (0% organic) for these nonpolar analytes and solubility issues to account for the increased variability.

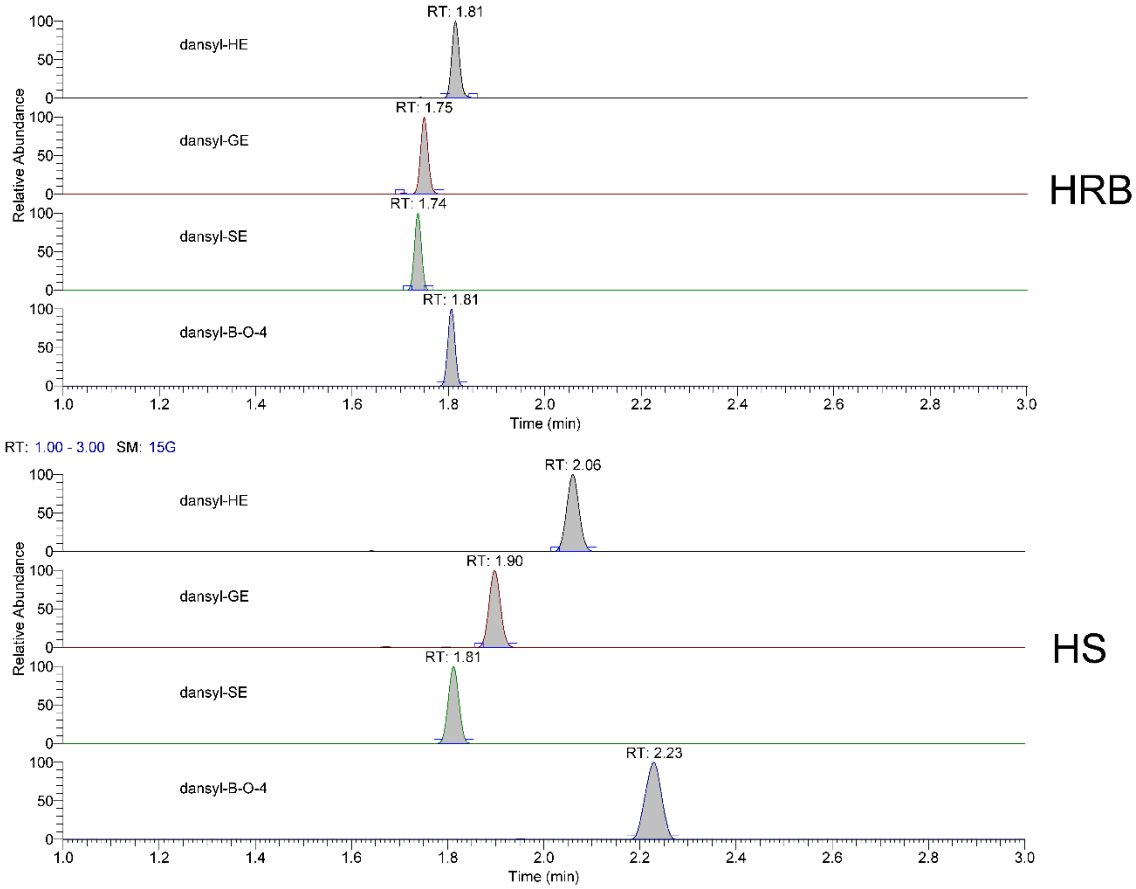

Figure 3. 25 RICs for dansylated-lignin model compounds using the bare long channel chip – HRB (top) and the standard coated chip – HS (bottom).

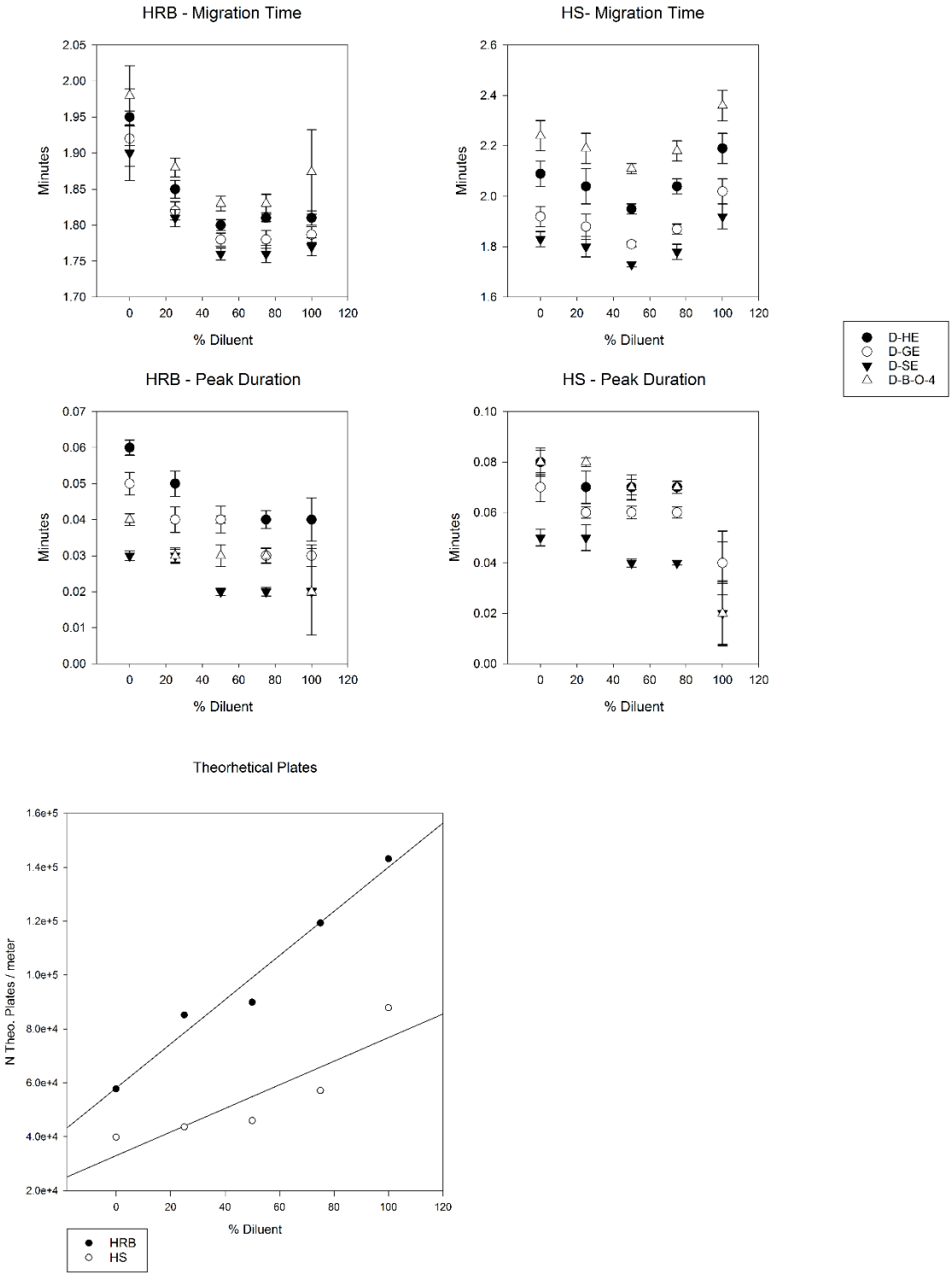

Figure 3. 26 Four charts: Changes in migration time (top) and peak duration (bottom) for dansylated-lignin model compounds using the bare long channel chip – HRB (left) and the standard coated chip – HS (right). Bottom graph: Changes in the number of theoretical plates associated with each chip and varying ionic strengths.

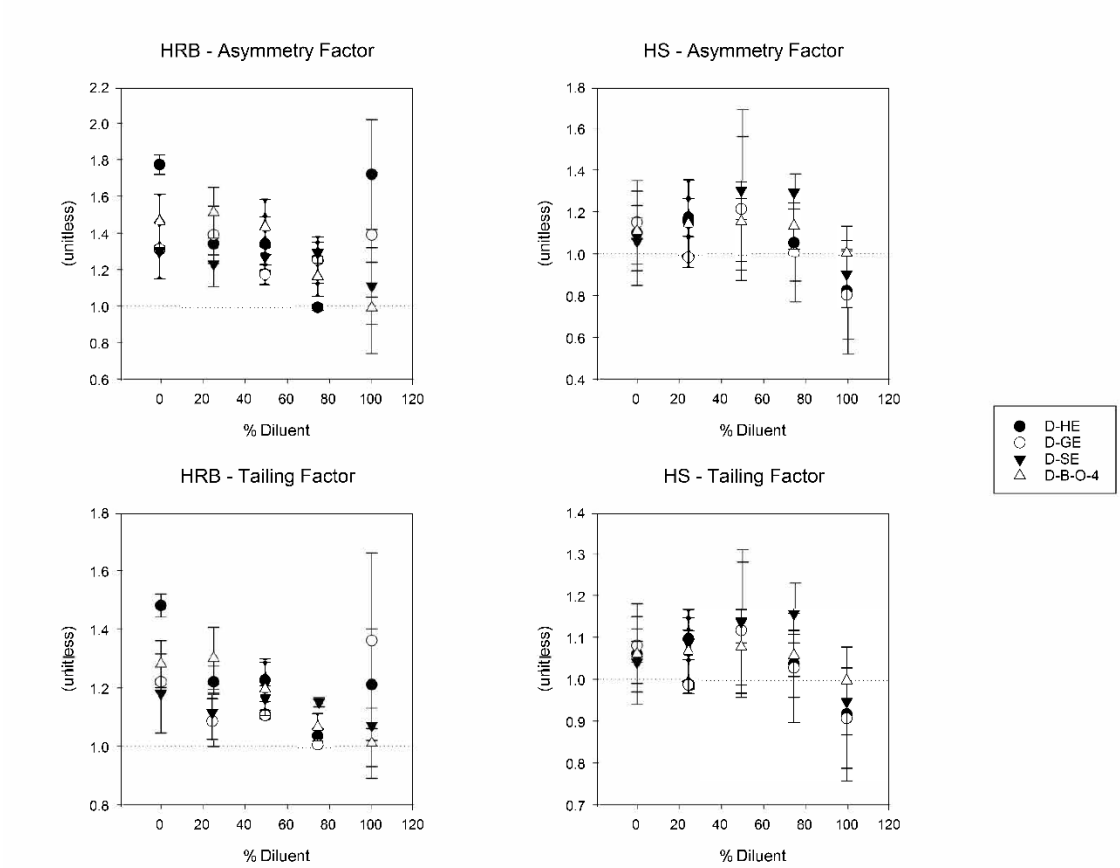

Figure 3. 27 Changes in asymmetry factors (top) and tailing factors (bottom) for dansylated-lignin model compounds using the bare long channel chip – HRB (left) and the standard coated chip – HS (right).

At this concentration, blockages in the separation channels were also observed, furthermore suggesting that this condition is not suitable for analysis. Though *p. multiflorum* hairy root extracts are not yet available to test the dansylation+HRB CZE-MS method, the preliminary results from analyzing dansylated *p. multiflorum* standards and dansylated cannabis extracts suggests that the downstream application should be successful.

Conclusions

In this chapter, the difficulty in the analysis of phenolic secondary metabolites was the primary focus. Unlike the basic nitrogen containing secondary metabolites found in chapter 2, these nonpolar, neutral molecules presented an issue in that the methods primarily used for their analysis, such as GC-MS, HPLC-UV, and even standard UHPLC-MS, can lack sensitivity, accuracy, and can present unusual problems that were not previously encountered. In the first half of this chapter, the hypothesis was that the discrepancy in cannabinoid profiling methods could be understood and either prevented or corrected. It was shown that the current industry standard method, HPLC-UV, lacked the sensitivity to accurately quantify low concentrations of THC in products that were determined to be over the legal limit using other methods. Additionally, the lack of mass spectral detection can lead to coeluting peaks being grouped incorrectly during quantification. The use of GC-MS for profiling, while better suited for these types of molecules, also presented unavoidable issues in that the labile nature of the carboxylic acids on certain cannabinoids, a critical component of the legal-limit equation, resulted in large RSDs and poor precision. Even the use of the more sensitive high-end instrument presented analytical challenges in that source induced degradation was observed. Though the most manageable, provided that temperatures are monitored, this observation raised the need for an alternative method to be developed as all three standard methods were unreliable. In the second part of this chapter, the hypothesis was that certain modifications could allow for the application of capillary electrophoresis for the analysis of *P. multiflorum* extracts. The framework for this alternative method was developed to be applied to both cannabis and *p. multiflorum* extracts. The use of the microfluidic CZE-MS device coupled with dansylation of the analytes and the prototype bare, long channel

chip displayed promising results as a future application once the product is commercially available. Due to restrictions in the number of performable analyses (limit 125 per chip) and the lack of *p. multiflorum* hairy root cultures, testing of the applications could only be applied to cannabis extracts and *p. multiflorum* standards, however, both applications displayed promising results and ideal applicable conditions were determined so that future analyses can be easily performed.

CHAPTER 4. PHARMACOKINETIC AND METABOLOMIC ANALYSIS OF AN ALZHEIMER'S DISEASE THERAPEUTIC IN RAT SERUM VIA MICROFLUIDIC CZE-MS

Introduction

Pharmacokinetic profiles are often used to describe the absorption, distribution, metabolism, and excretion (ADME) of the pharmaceutical therapeutic in question.[115,116,117] Pharmaceutical therapeutics can be administered into the body various ways, with the method and the medium of administration and certain molecular characteristics (ie Lipinski's rule of five) having a significant effect on the ability for it to accumulate in target areas and tissue.[81,115,117] Once administered, they can be absorbed and circulated, however, transportation into to their target tissues require mechanisms to allow them to cross numerous biological obstacles (ie crossing blood-brain barrier). During the absorption and transportation stages, the body can chemically modify or metabolize the therapeutics to make them more easily transported, or, in some cases, increase their efficacy. In most cases, these metabolic reactions produce intermediates with less pharmacologic activity than the parent compound, however, it is also possible that these metabolites can be toxic and lead to an adverse effect.[115,117,118] Following adsorption, distribution, and metabolism, the end product is excreted through the liver, kidneys, skin, lungs, and/or intestines. Pharmacokinetic profiling helps to provide a quantitative description of the behaviors and interactions of therapeutics to better understand how they function, interact, and metabolize.[117] These profiles are developed by analytically monitoring variations in the circulating concentration of the therapeutic of interest as a function of time following administration and are performed as a critical component of clinical and pre-clinical evaluations.[119,120] Method development for the formation of pharmacokinetic profiles typically focuses on high-throughput, highly

sensitive techniques.[33,34] These methods generally employ HPLC coupled to either UV or MS detection and are developed with the primary focus of resolving one or two analytes of interest.[121–123] When involving MS, the industry standard approach utilizes targeted MS/MS analyses using triple quadrupole (QqQ) mass spectrometers due to their sensitivity and specificity.[124–128] Targeted approaches allow for the preceding HPLC methods to be more focused on fast, high-throughput separations at the cost of chromatographic resolution and qualitative aspects, such as primary and secondary metabolite detection or changes in metabolite expression over time.[129,130] While this approach is advantageous for the determination of a potential therapeutic concentration in vivo, the sacrifice of metabolic information can lead to the requirement for further testing at a future stage of development to evaluate changes in metabolism induced by the candidate therapeutic. To address this untargeted analysis, a method for the use of a microfluidic capillary zone electrophoresis (CZE) device, coupled to a mass spectrometer, was developed and evaluated for a metabolomics-inclusive high-throughput pharmacokinetic approach.

The primary focus of this metabolomics-inclusive pharmacokinetic CZE-MS application centers on a potential Alzheimer's disease therapeutic in the preclinical development stage. This therapeutic, BNC-1 (Figure 4.1), was designed by CoPlex Therapeutics LLC (Lexington, KY) and consists of a functionalized naphthyridine and has been shown to reduce amyloid burden and improves markers of synaptic integrity in mouse models (Lovell et al., 2016, US Patent No. 9968574).[131] The hypothesis of this chapter was that the capillary electrophoresis mass spectrometry method could be modified and applied to perform a global, metabolomics-inclusive DMPK analysis. To

test this, serum sample extracts from male and female Sprague Dawley rats, treated with varying doses of BNC-1, were obtained from CoPlex and analyzed using both LC-MS the novel CZE-MS approach. Pharmacokinetic data generated using traditional UHPLC-MS approaches were statistically compared to the CZE-MS approach. Additionally, the metabolomic data obtained from the CZE-MS approach was examined to identify changes in metabolism potentially linked to the use of the therapeutic.

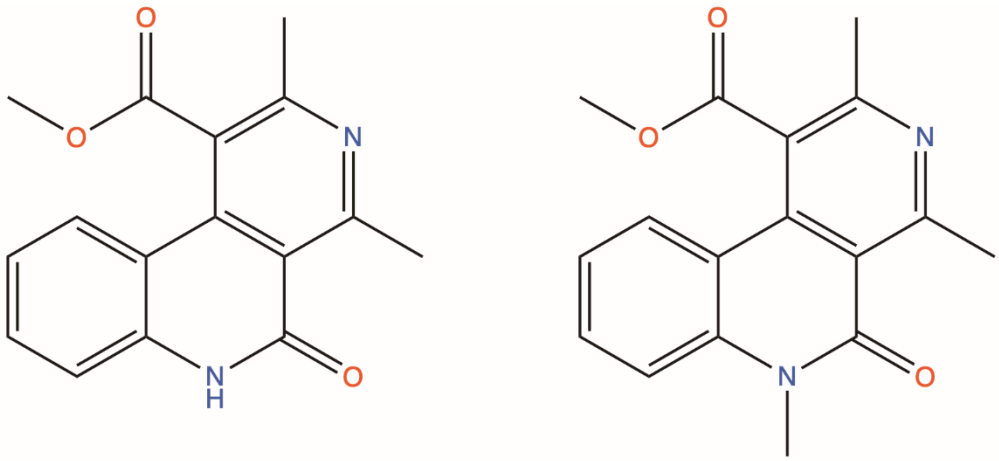

BNC-1
Chemical Formula: $C_{16}H_{14}N_2O_3$
Exact Mass: 282.1004

Internal Standard
Chemical Formula: $C_{17}H_{16}N_2O_3$
Exact Mass: 296.1161

Figure 4. 1 Structures for BNC-1 (2,4-dimethyl-5-oxo-5,6-dihydrobenzo[c][2,7]naphthyridine-1-carboxylic acid, methyl ester) and the internal standard (N-methyl-BNC-1).

Materials, Methods, and Instrumentation

4.1.1 Sample Preparation

Administration of BNC-1 and tail vein blood collection and extraction/sample preaparation was performed by CoPlex Therapeutics as follows: Serum was extracted from the collected blood and provided for analysis. Both male and female Sprague Dawley rats, five each, were treated with 2,4-dimethyl-5-oxo-5,6-dihydrobenzo[c][2,7]naphthyridine-1-carboxylic acid, methyl ester (BNC-1, $C_{16}H_{14}N_2O_3$ – Figure 4.1) by gastric gavage at the following concentrations: 1, 12.5, 25, and 50 mg/kg (additionally, a 5 mg/kg dosage was administered intravenously to rats that did not have the gastric gavage administered). Blood was collected from the tail vein at 0.25, 0.5, 1, 2, 4, 8, 12, and 24 hour intervals by processed into serum by centrifugation. A 50 µL aliquot of serum was diluted with 50 µL internal standard (50 µM stock, N-methyl version of BNC-1 - $C_{16}H_{12}N_2O_4$) in acetonitrile, 50 µL ammonium acetate (500 mM) and 150 µL of acetonitrile, mixed by vortex and centrifuged to remove proteins. Calibration standards were prepared similarly: 50 µL of preconcentrated BNC-1 stock solutions in acetonitrile were diluted with 50 µL internal standard in acetonitrile, 50 µL ammonium acetate (500 mM) and 150 µL of acetonitrile to 0.5, 2, 10, 25, 50, and 100 µM. Quality control spike/duplicate samples were prepared consisting of 50 µL horse serum with 50 µL internal standard in acetonitrile, 50 µL of BNC-1 in acetonitrile (10 µM final concentration), 50 µL ammonium acetate (500 mM) and 150 µL of acetonitrile

4.1.2 UHPLC-MS and Microfluidic CZE-MS analysis

UHPLC-MS analyses were performed by CoPlex Therapeutics as follows: UHPLC separations were performed using a Shimadzu Nexera X2 UHPLC system with a Kromacil EternityXT C18 column (2.5 µm, 2.1x50 mm). Analyses were performed using 5 µL sample injections. The chromatographic separation consisted of solvent A (0.1% formic acid in H2O) and B (0.1% formic acid in ACN) in a gradient flow method at 300 µL/min starting with solvent B at 5% for 2 minutes, increasing linearly to 95% over 10 minutes, being held at 95% for 5 minutes, and then returning to starting conditions for 2 minutes equilibration, 20 minutes in total. UHPLC-MS analyses were performed on a Thermo Scientific Q Exactive Orbitrap Mass Spectrometer (Thermo Fisher Scientific, Waltham, MA, USA). Parameters for the UHPLC-MS analysis consisted of a scan range of m/z 70 to 800, resolution of 140,000, microscans set to 3 (1.7 scans per second), sheath gas flow set to 10 psi and the AGC target was maintained. Electrospray was generated with a 3.0 kV spray voltage and desolvated with a HESI auxiliary gas flow of 4 psi (280 ºC) and an inlet capillary temp of 280 ºC.

For the CZE-MS analysis, a 50 µL aliquot of the treated sample extract, analyzed by UHPLC-MS, was diluted with 50 µL of the 908 Devices metabolites diluent immediately prior to analysis. Capillary zone electrophoresis mass spectral analysis was performed by the authors using the 908 Devices ZipChip interface (ZCI) following the method stated in in Chapter 2, with minor modifications. Briefly, 50µL of each sample was manually transferred to the sample well of a HS chip in the ZCI before analysis. The sample was loaded into the sample channel for 20 seconds as defined by the default HS Metabolites method (5.00 nL injection). Samples were analyzed using the HS

Metabolites background electrolyte (BGE) and method for separation and a field strength of 1000V/cm was applied to the chip for the duration of the 3 minute separation. The samples were recollected from the sample well following analysis and then a sample well washing was performed by the CZE interface for 2 minutes, totaling 6 minutes from injection to washing, per sample. BGE refreshes were performed every 30 minutes. CZE-MS analyses were performed on a Thermo Scientific Q Exactive Orbitrap Mass Spectrometer (Thermo Fisher Scientific, Waltham, MA, USA). The CZE-MS acquisition parameters consist of a full scan range from m/z 70 to 600, resolution of 17,500, microscans set to 1 (8 scans per second), sheath gas flow set to 2.0psi, and a AGC target of 3e6. Additionally, data dependent MS2 (dd-MS2) acquisition was also utilized for metabolite structural elucidation following the microfluidic CZE separation. For dd-MS2 acquisition, the CZE method was modified to employ a voltage gradient starting at 300 V/cm and increasing linearly to 1000 V/cm over 6.00 minutes. All dd-MS2 spectra were acquired using a fixed normalized collision energy (NCE) of 30 and a Top3 filter with a 0.5 minute dynamic exclusion.

4.1.3 Data processing

Resulting data sets from both the UHPLC-MS PK study and the microfluidic CZE-MS PK comparison were processed using MZmine2 following the workflow stated in chapter 2 and in Kelley et al 2019.[66] Briefly, RAW files were directly imported into the processing software. Following importation, the data sets were processed with the following modules: mass detection, ADAP chromatogram builder, chromatogram deconvolution, deisotoping, alignment using the RANSAC aligner with gap-filling, and,

additionally, normalization to the internal standard. Both UHPLC separations and CZE separations were processed using the same modules, however, the time limit parameters for total run time, maximum and minimum peak width, and retention/migration times were adjusted. UHPLC-MS time windows were selected based on the average durations of BNC-1 and the internal standard. CZE-MS time window allowances were selected based on the average duration of the widest peak observed in each separation. Resulting aligned datasets putatively identified using MassBank and Chemspider. Statistical analysis for the comparison of the two methods was performed using Graphpad Prism 8. Pharmacokinetic data was generated using the PKsolver add-in for Microsoft Excel.

Results and Discussion

4.1.4 Method Assessment

4.1.4.1 Pharmacokinetic method comparison

Using data from both the CZE and UHPLC-based methods, the BNC-1 concentration in each rat serum extract was determined. Figure 4.2 displays examples of stacked chromatograms from the UHPLC separations (top) and stacked electropherograms from the CZE separations (bottom) of the first collection time point of the 50 mg/kg dosage (M50-15min). The peaks for BNC-1 can be seen at 3.80 minutes for the UHPLC separations and 1.92 minutes for the CZE separations with the internal standard peaks at 5.41 and 1.77 minutes for each method, respectively. Prior to any chromatographic peak extraction or data processing by MZmine, observable differences in the base peak chromatograms/electropherograms are apparent for each method. This aspect attributed to the nL flow rates employed for the CZE-MS approach compared to

300 µL/min for the UHPLC-MS approach. This reduced baseline greatly aids in post-analysis data processing, especially in determining peak width and noise level parameters for MZmine2. As the only consistently observable peak in the baseline of the UHPLC-MS analysis was internal standard, it was used in determining peak width allowances. Using the ratio of a constant concentration of internal standard and varying concentrations of BNC-1, calibration curves were generated for each method (Figure 4.3A). Calibration standard solutions were generated using both the method described above (50 µL BNC-1 stock solutions, 50 µL IS, 50 µL 500 mM NH_4OAc, and 150 µL ACN) and a second time replacing 50 µL of the ACN with 50 µL of serum to assess for matrix effects. Plotting resulting ratio of BNC-1 and the internal standard using both sample conditions resulted in an R^2=0.9995 implying that, due to the nonpolar nature of BNC-1, the extraction method and presence of serum did not result in any observable ion suppression or other matrix effects. Additionally, recovery of the internal standard was evaluated in comparing the average area counts of the internal standard peaks across all calibration solutions, both with and without serum (n=36) and the internal standard diluted in ACN (n=3) and a recovery of 96±6% was observed. Subsequently, the concentration of BNC-1 was determined in each serum extract without correction. Figure 4.3B displays four examples of the concentration of BNC-1 determined with each method in the serum extracts as a function of time for varying dosages. The difference in administration methods rationalizes the higher BNC-1 serum concentration observed in the 5 mg/kg treatment than that observed in the 25 mg/kg gavage treatment. The apparent C_{max} of BNC-1 was reached between 8 and 12 hours.

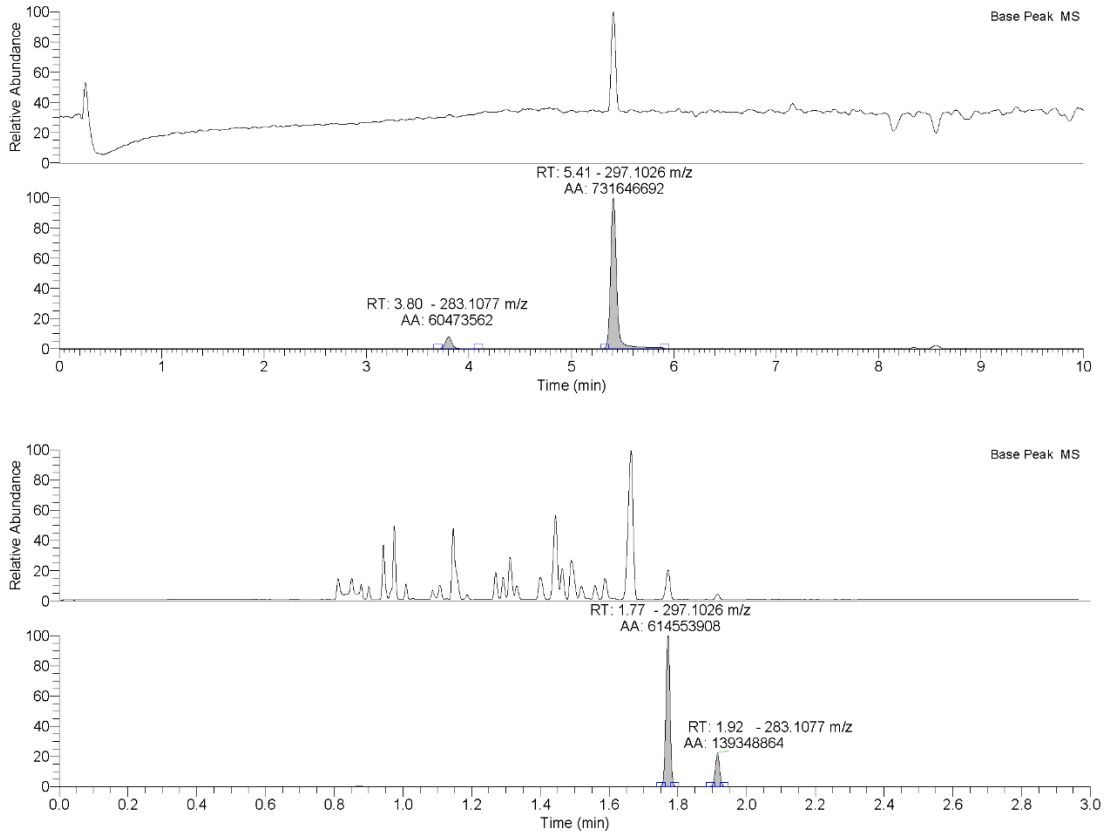

Figure 4. 2 Example of the same sample (male, 50 mg/kg, 15 minute collection time) analyzed using both methods. (Top) UHPLC-MS stacked base peak chromatogram and RIC for BNC-1 (RT: 3.80 min, m/z 283.1077 and the internal standard (RT: 5.41, m/z 297.1026). (Bottom) CZE-MS stacked base peak electropherograms and RIC for the internal standard (RT: 1.77 min, m/z 297.1026) and BNC-1 (RT: 1.92, m/z 283.1077).

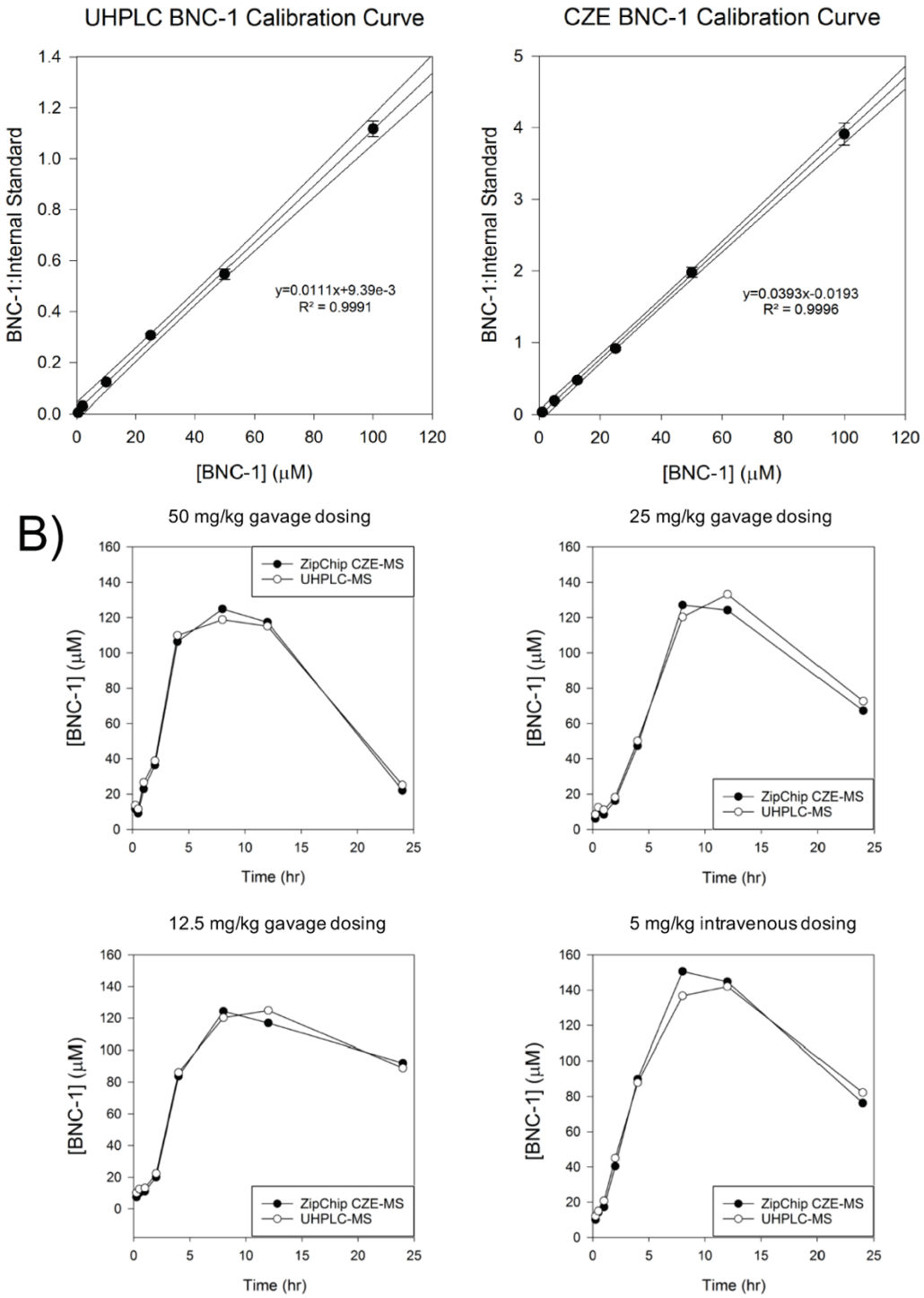

Figure 4. 3 A – Calibration curves generated for UHPLC (right) and CZE (left) separations by analyzing the response ratios from calibration standards containing a fixed concentration of an internal standard and varying concentrations of the target compound, BNC-1. Error bars represent SD from triplicate analyses. B – Four examples of overlaid graphs of calculated BNC-1 concentrations as a function of time using both separation methods.

Using PKsolver, pharmacokinetic data was generated from the [BNC-1] versus time data. An example of the PKsolver data for the 50 mg/kg BNC-1 dosage can be seen in Table 4.1. For cases where the C_{max} was reached at t=12hrs, some PK data could not be calculated as three points indicating the elimination of the therapeutic in serum are required. The largest variations were observed in the calculation of the AUC_{0-t} values, however, in most cases, the RSD was below 20% when comparing the values calculated by both the CZE and UHPLC methods. Additionally, when compared to the UHPLC-MS, the relative error (RE) for the PK results generated via CZE-MS were all below 10% with the only outlier being λ_z (terminal rate constant), at ~20%. Being that this parameter is both small, increasing the impact of small differences (0.10 and 0.12) and directly related to another parameter displaying slight variability, $t_{1/2}$, this observation alone does not discredit the similarity between the results generated using the two vastly different separation methods.

Statistical analyses were performed using GraphPad Prism 8. Regression analysis of the calculated BNC-1 concentrations resulting from both methods displayed significant linearity with an $R^2 = 0.9205$ (Figure 4.4A). A slope of 1.032 (y-axis: UHPLC-MS results and x-axis: CZE-MS) indicates that, while corresponding [BNC-1] calculations generated by each method are similar, the results generated by CZE method are, on average, slightly lower (<5-10 μM variation) than those generated using the UHPLC method, however, only four points fell outside of the confidence interval. This was also observed in comparing the methods using a ratio Bland-Altman plot (Figure 4.4B).

Table 4. 1 Pharmacokinetic data corresponding to the 50 mg/kg dosage resulting from using both separation methods and generated using PKsolver.

Parameter	Unit	CZE	UHPLC	AVERAGE	SD	RSD	RE
T_{max}	h	8	8	8	0	0.00%	0.00%
C_{max}	μM	124.9	118.85	121.88	4.28	3.50%	5.09%
$t_{1/2}$	h	5.99	6.65	6.32	0.47	7.40%	-9.92%
Cl	(mg/kg)/(μM)/h	0.02	0.02	0.02	0	1.50%	0.00%
AUC_{0-t}	μM*h	1969.95	1964.5	1967.23	3.86	0.20%	0.28%
$AUC_{0-\infty}$	μM*h	2160.12	2204.9	2182.51	31.66	1.50%	-2.03%
$AUC_{0-t/0-\infty}$	(unitless)	0.91	0.89	0.9	0.01	1.60%	2.25%
$AUMC_{0-\infty}$	μM*h^2	26048.68	28000.7	27024.69	1380.28	5.10%	-6.97%
$MRT_{0-\infty}$	h	12.06	12.7	12.38	0.45	3.70%	-5.04%
λ_z	1/h	0.12	0.10	0.11	0.01	7.40%	20.00%
V_d	(mg/kg)/(μM)	0.20	0.22	0.21	0.01	5.90%	-9.09%
V_{ss}	(mg/kg)/(μM)	0.28	0.29	0.28	0.01	2.20%	-3.45%

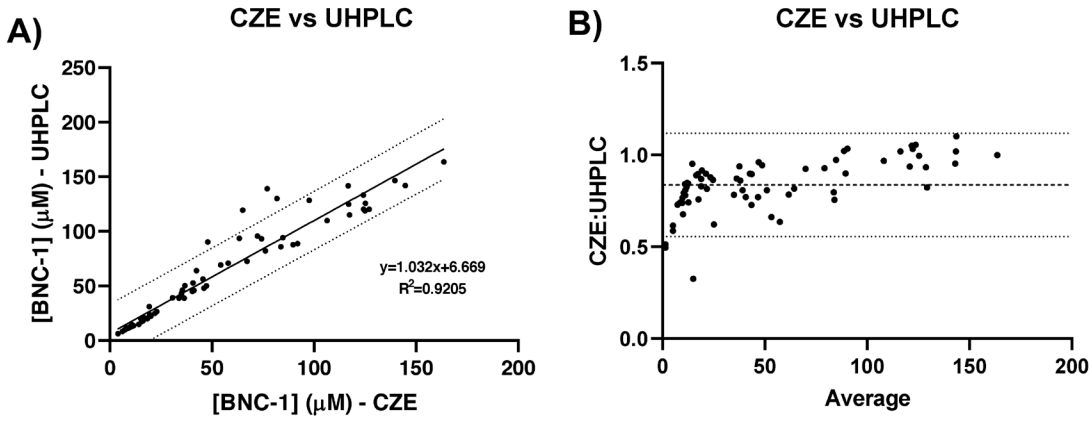

Figure 4. 4 A – Linear regression plot of the serum BNC-1 concentrations resulting from the use of the CZE method plotted against the same samples analyzed using the UHPLC method. B – A ratio Bland-Altman plot comparing the serum BNC-1 concentrations determined using both methods.

Though three data points (~2% of the total data) were observed outside of the limits of agreement and not deemed to be outliers, a strong correlation was observed. The similarity observed in the calculated BNC-1 concentration data suggests that the two methods could be interchangeable for this application without impacting the results of the trial. Furthermore, an additional feature of the microfluidic CZE-MS approach compared to the UHPLC-MS approach is the speed of the separation mechanism. The CZE's employment of transient isotachophoresis (tITP) allows for the separations to be performed in 3 minutes, compared to 10-20 minutes per UHPLC-MS analysis. Depending on the sample injection method applied, the total run times for the CZE-MS analyses range from 4 minutes (active – manual injections) to 6 minutes (passive – autosampler injections) from the time the signal pulse is sent to the instrument to the time that the sample well is washed, 10-15 samples per hour. For the UHPLC-MS analyses, only 2-5 samples could be analyzed per hour once the column equilibration and needle washing times are factored into the total run-time. Given that PK sample sets can often be large (100+), this high throughput aspect would be advantageous.

4.1.4.2 Evaluation of the CZE-MS approach

In an evaluation of the CZE-MS approach, triplicate analysis of a low-dosage (1 mg/kg) serum extract analyzed consecutively with sample well washes between analyses displayed high reproducibility. A maximum RSD of 13% (low: 2%) was observed corresponding to the sample where the BNC-1 serum concentration peaked (t_{max} = 8 hours) during the time course (Figure 4.5). This variation is likely due to the BNC-1 concentration approaching the onset of overloading for the device (~100-200µM, analyte dependent).

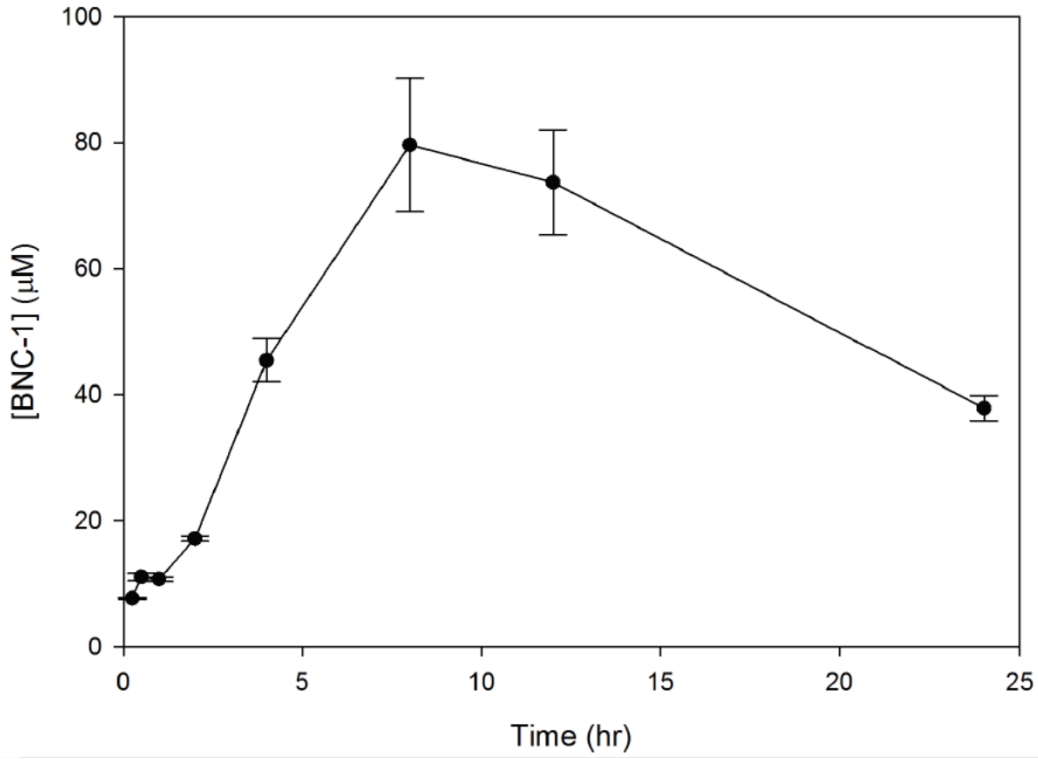

Figure 4. 5 Calculated BNC-1 concentration resulting from triplicate analysis of a serum extract (1 mg/kg) using the CZE approach.

Additionally, both inter-day and intra-day reproducibility were assessed as large sample sets, such as the set analyzed in this work (n=96), can often take an extended period to analyze. Figure 6 displays a stacked extracted electropherogram of the two serum extracts from the same dosage set (50 mg/kg), one determined to have a low BNC-1 concentration (sample collected after 15 min) and one with a high BNC-1 concentration (sample collected after 8 hours), analyzed at time zero – 6A (low) and 6C (high), after 12 hours (data not shown), and 24 hours after the diluted samples were produced and the CZE system was initially primed – 6B (low) and 6D (high). This was performed to assess variation as a function of concentration and time. Calculated concentrations can be seen in Table 4.2. Although resulting calculated concentrations remain consistent (RSD <5%) despite an order of magnitude increase between the two samples, the observed CZE migration times (MT) varied. The BNC-1 peak resulting from samples analyzed on a new chip with fresh BGE eluted at approximately 1.9 min while the same peak eluted at approximately 2.3 min after 24 hours using the same chip and BGE. This is most likely due to degradation of the BGE (consisting of ACN, IPA, H_2O, and formic acid) or sample diluent (MeOH, H_2O, NH_4OAc, and formic acid) as the manufacturer recommended lifetime of the BGE and diluent is 12 hours. Additionally, the cationic wall coating of the chip separation channels and the hydrophobic coating at the spray corner wear over time during analyses, therefore only 125 separations can be performed on each chip. Although a shift in migration is observed, migration of BNC-1 relative to the internal standard (~1.08 minutes) remained constant regardless of concentration or time of analysis.

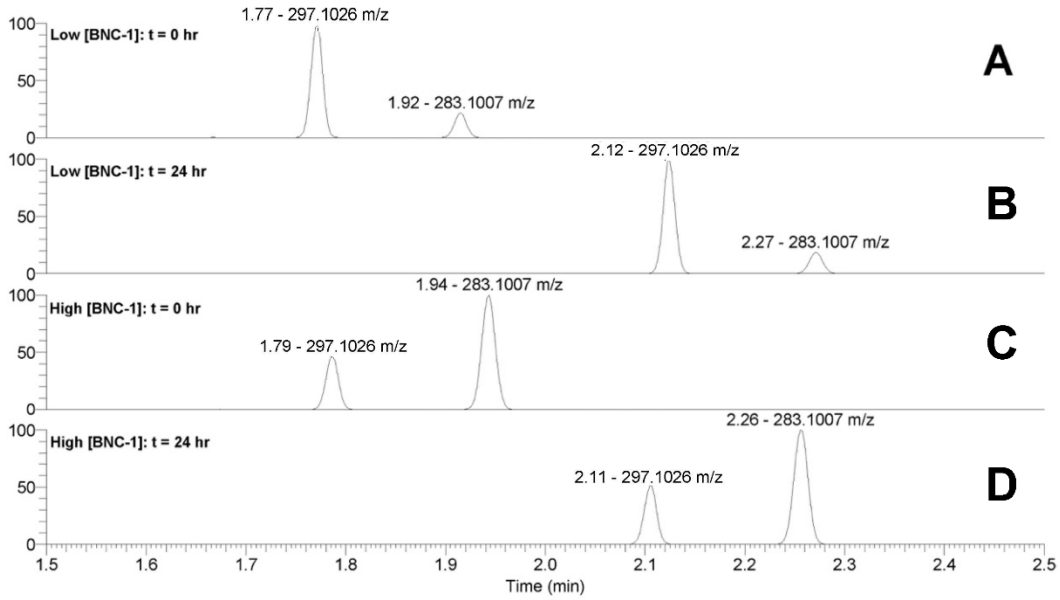

Figure 4. 6 Extracted electropherograms corresponding to a low [BNC-1] sample at two time points (0 and 24 hours 6A-B) and a high [BNC-1] sample at two time points (0 and 24 hours 6C-D).

Table 4. 2 Area counts of BNC-1/internal standard and resulting BNC-1 concentrations corresponding to triplicate analysis of a low concentration serum extract (50 mg/kg dosage, 15 min) and a high concentration serum extract (50 mg/kg dosage, 8 hours) analyzed over twelve hour intervals.

Sample	Time (hours)	BNC-1 Peak Area	Int. Std Peak Area	Ratio	BNC-1 MT	Int Std MT	Rel MT	[BNC-1] (uM)			BNC-1 Rel. MT	
Low [BNC-1]	0	1.39E+08	6.14E+08	0.23	1.92	1.77	1.08	11.88	Average	11.57	Average	1.08
	12	1.89E+08	8.41E+08	0.22	2.07	1.92	1.08	11.74	Stdev	0.43	Stdev	0.01
	24	1.54E+08	7.29E+08	0.21	2.27	2.12	1.07	11.08	RSD	4%	RSD	1%
Sample (time)	Time (hours)	BNC-1 Peak Area	Int. Std Peak Area	Ratio	BNC-1 MT	Int Std MT	Rel MT	[BNC-1] (uM)			BNC-1 Rel. MT	
High [BNC-1]	0	1.55E+09	6.66E+08	2.34	1.94	1.79	1.08	124.49	Average	120.6	Average	1.08
	12	1.62E+09	7.29E+08	2.22	2.06	1.91	1.08	117.65	Stdev	3.52	Stdev	0.01
	24	1.51E+09	6.70E+08	2.25	2.26	2.11	1.07	119.66	RSD	3%	RSD	1%

Due to the consistency in concentration dependent response, no normalization was applied to later samples during the MZmine2 processing in regards to observed response, however, migration time allowance windows were increased to 0.5 minutes to allow for the grouping of similar features despite a difference in MT >10% of the total run time.

4.1.5 Changes in Metabolic Activity

In addition to the monitoring of BNC-1 concentration as a function of time, the CZE-MS method also provided metabolomics data on a number of analytes as a function of [BNC-1] concentration. Using MZmine2, over 80 baseline resolved peaks were detected consistently within the 96-sample data set. The detected features were processed using both the MassBank and Chemspider database tools in MZmine2 and METLIN externally. The final resulting data set comprised of 38 putatively identified metabolites, all 20 amino acids, and 26 features with multiple (n>3) possible identities that would require further experimentation to determine (denoted as their most probable calculated empirical formula). Normalized response changes corresponding to each feature from the t = 15 min mark to the t_{max} can be seen in appendix 5 for the female rats (left columns – denoted as F-dosage) and for the male rats (right columns – denoted as M-dosage). For simplicity, percent changes are expressed as: "-" indicating percent decreases greater than -25% compared to t=15 min, "NC" (no change) indicating percent changes between -25% and +25%, "+" indicating percent increases greater than +25% but less than +100% compared to t=15min, and "+++" indicating increases greater than +100% compared to t=15min. This approach may be useful in providing evidence to how therapeutics affect metabolite expression. For example, m/z 146.1648, putatively identified as spermidine, appears to be down-regulated in eight of the ten rats, regardless of dosage. Spermidine

has been noted in literature to be upregulated in patients with AD.[132–134] Additionally, it has been reported that polyamines, such as spermidine, play a role in amyloid-beta fibrillation and increased MAPK function related to the progression of AD symptoms.[135–138] Preliminary evidence from in vivo and in vitro assays performed by CoPlex Therapeutics involving BNC-1 suggest that the potential therapeutic modulates MAPK activity, specifically TAK1 kinase, also known as MAP3K7.[131,139]

This approach can also be used to evaluate the metabolism of the therapeutic itself. An unidentified metabolite, m/z 299.1028, appeared to be exceptionally increased in all samples where the [BNC-1] reached the C_{max}, and subsequent samples in the time-course, when compared to t=15min, regardless of initial dose. To obtain evidence to identify this metabolite, tandem mass spectrometry was utilized. By employing a voltage gradient method, as discussed in Chapter 2, untargeted MS/MS data-dependent acquisition (DDA) and targeted MS/MS (PRM) experiments could be performed. The usage of voltage gradients allows for slight broadening of the analyte peaks in order to adequately sample each target in the untargeted tandem experiments. The employment of a linear voltage gradient from 300 V/cm to 1000 V/cm over a six-minute run time allowed for an approximate doubling of each peaks' width (ranges from 1.5x to 2.0x). An untargeted approach was chosen to determine if fragment ions or fragmentation patterns observed for other selected precursor masses were in common with those produced by the unidentified metabolite at m/z 299.1028 (putatively calculated as [M+H+] = $C_{16}H_{15}N_2O_4$). In utilizing this method, similar fragmentation patterns were observed for m/z 299.1028 and BNC-1 (Figure 7); BNC-1: m/z 283 → 251(-32), m/z 283 → 223(-60), unidentified metabolite: m/z 299 → 281(loss of H_2O), m/z 281 → 249(-32), and m/z 281

→ 221(-60). This evidence suggests that m/z 299.1028 is most likely an oxidized metabolite of BNC-1, consistent with aromatic hydroxylation.

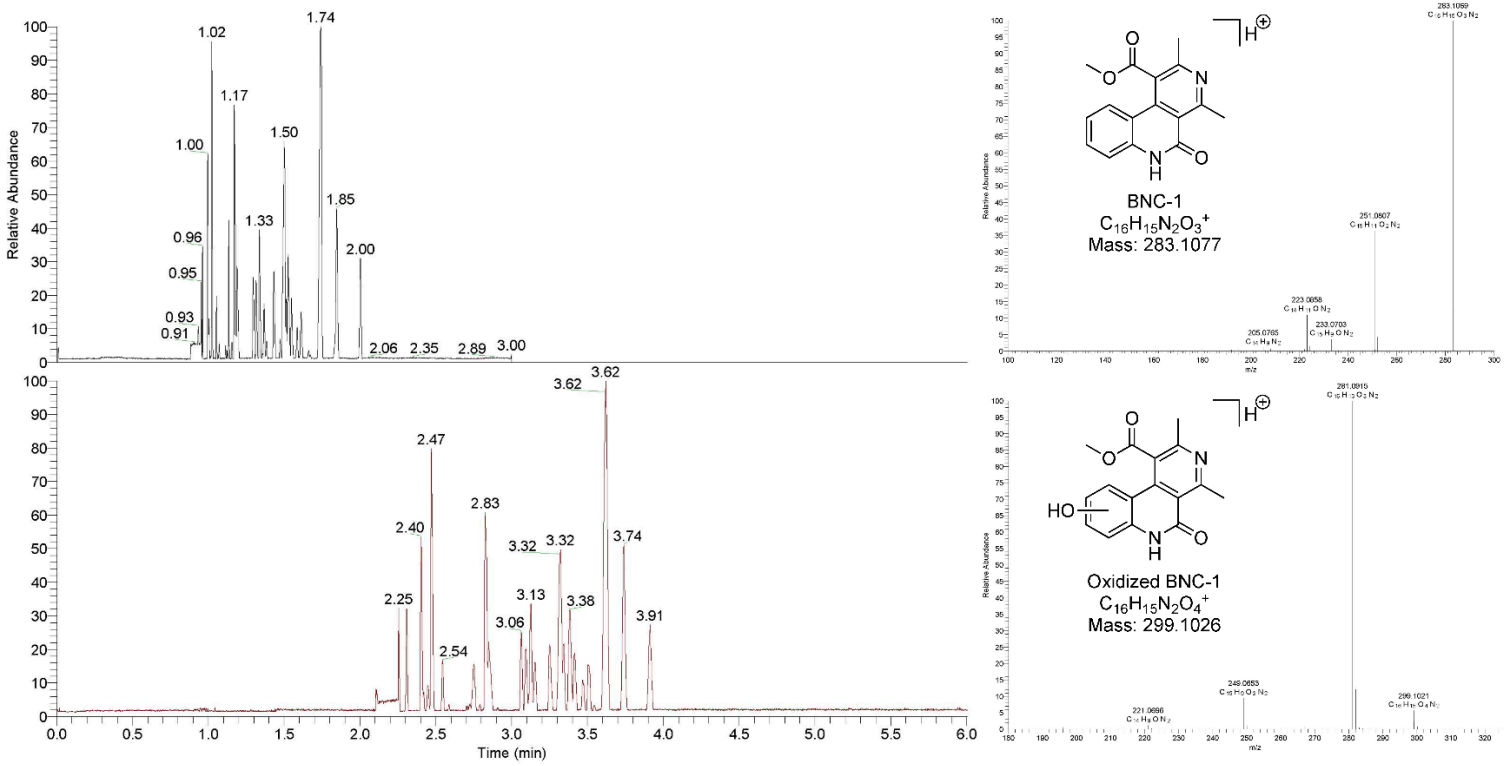

Figure 4. 7 Left - Electropherogram of a set constant voltage (1000 V/cm) CZE-based separation (top) and the same sample analyzed using a voltage gradient (300 V/cm to 1000 V/cm over six minutes - bottom). Right – MS^2 spectra of BNC-1 (top – m/z 283.1069) and the unknown metabolite of interest (bottom – m/z 299.1021).

Conclusions

In this work, the hypothesis was that the capillary electrophoresis mass spectrometry method could be modified and applied to perform a global metabolomics inclusive DMPK analysis. Here, the development and usage of a CZE-MS method for high-throughput pharmacokinetic analysis was compared to a traditional UHPLC-MS analysis method. Traditional approaches heavily rely on streamlining data acquisition at the cost of separation efficiency and usually result in the absence of information pertaining analytes other than the target of interest. The CZE-MS approach provided pharmacokinetic data in approximately six minutes per sample, including sample delivery and transfer line clearing, without sacrificing separation efficiency or limiting the scope of the analyses. Statistical comparison of the pharmacokinetic results generated by both methods suggests that they are interchangeable for this type of analysis. The CZE method proved capable of not only fast and efficient pharmacokinetic analysis, but also highly reproducible results. Both the intra-day and inter-day reproducibly of the CZE-MS method was comparable to that characteristically displayed by UHPLC-MS approaches. Additionally, the CZE method provided metabolomic data alongside the pharmacokinetic experiments that was not present in the UHPLC data set. Further data analysis and mining with processing software like MZmine2 allows for fast comparisons and easy evaluations of large, complex data sets. This aspect can be useful in understanding the primary method of action for a potential therapeutic or in how the target is metabolized. The ease of performing both targeted and untargeted MS^2 experiments to this CZE-based separation is also very advantageous for metabolomics assays.

CHAPTER 5. CONCLUSIONS

Metabolomics mass spectrometry focuses on the analysis of small molecules (<1500 Da) associated with the metabolic processes of an organism. The applications of metabolomics methodologies cover a wide assortment of diverse subjects. Metabolomic profiles can help analysts understand how an organism responds to disease or external stressors, how a potential therapeutic in preclinical trials metabolizes and affects metabolic expression, and what causes certain phenotypic expressions to manifest. While the mass spectral analysis of primary metabolites, like amino acids and nucleic acids, is well defined, the analysis of secondary metabolites, specifically those produced by plants, such as alkaloids and polyphenolic compounds, can be challenging. These challenges arise in the vast, complex diversity of these secondary metabolites, often unique to a specific genus or species. The primary focus of this dissertation was the development of multifaceted metabolomics mass spectrometry methods for the analysis of both primary and secondary metabolites from different biological sources.

The second chapter of this dissertation focused on the bottom-up method development for a metabolomics profiling assay to be applied to a relatively unknown target, *Lobelia cardinalis*. It was previously discovered that extracts from *L. cardinalis* displayed substantial dopamine transporter inhibitory activity. As no recorded history of abuse of this plant has ever been reported, as is the case for many dopamine transporter inhibitors, this discovery presented a promising source for naturally derived cessation-aids to help combat the global substance abuse disorder crisis. Working in tandem with Naprogenix LLC, wild type and mutant *L. cardinalis* extracts were provided for metabolomic profiling. The hypothesis of chapter two was that mutant survivor strains

likely over-expressed novel hDAT inhibitors compared to wild type plants. If this was the case, the novel metabolites would be extracted and purified to be tested individually to verify activity. To test this hypothesis, a metabolomics screening approach was developed and applied. In this work, both liquid chromatography and capillary electrophoresis were applied to determine the best separation method for this application. The analytical complexity attributed to the secondary metabolites observed suggested that the capillary electrophoresis approach was the best option due to increase sensitivity, increased selectivity, reduced sample volume/concentration, and reduced analysis time. Additionally, given that these secondary metabolites were predominantly alkaloids, capillary electrophoresis was suggested as it is ideal for small, positively charged analytes. The application of capillary electrophoretic separations coupled to mass spectrometry was not only applied to characterize wild type *L. cardinalis* and putatively identify secondary metabolites naturally produced, but also to identify changes in the secondary metabolite profile of transgenic plants comparatively. Using the metabolomic information discovered from this analysis, a metabolite was identified and subsequently isolated, characterized, and provided to Naprogenix for preclinical trials. This secondary metabolite, the N-oxide of the main secondary metabolite produced by the plant, lobinaline, exists at concentrations ten to one hundred times lower than its free base counterpart in the plant. Extreme difficulty was encountered when trying to purify the metabolite given its chromatographic similarity to lobinaline during preparative HPLC purification. Utilizing differing physical characteristics of the two metabolites, mainly difference polarity, an extraction method was developed and perfected using xylene to selectively separate lobinaline from the N-oxide, resulting in a hundred-fold enrichment

of the N-oxide. This led to the production of a substantial quantity of the material to be provided to Naprogenix for pharmacological testing. Additionally, a method for the semi-synthetic production of an analytically identical version of the metabolite via N-oxidation using mCPBA was also developed. The impact of this chapter centers around the application of this technology for future pharmaceutical discovery. Despite many of the advances in modern medicine, there is still a plethora of diseases and conditions, especially substance abuse disorders, that plague the world on a regular basis. Since naturally derived pharmaceuticals can potentially treat some of these conditions, like the lead compound discovered in this work and its impact on potentially treating addiction, this metabolomic profiling method is pivotal in streamlining the process of identifying lead compounds for prioritizing and easing the difficult task of purification. Preliminary investigations, performed by Naprogenix, in testing the purified material have been promising in that strong inhibitory activity is being observed, supporting the hypothesis that the upregulated metabolites were likely the source of the activity and that these changes in regulation could be observed using the developed capillary electrophoresis mass spectrometry metabolomic profiling assay. As more than one lead compound was identified, the future developments of this work would be to continue the isolation and purification process of the other prioritized analytes for pharmacological evaluation.

The third chapter of this dissertation focused on two aspects. The first aspect was evaluating the common approaches used for secondary metabolite profiling of *Cannabis* plant extracts and products. The secondary metabolites of the *Cannabis* species, the cannabinoids, have recently been the subject of numerous analytical investigations, as they present many analytical challenges. This aspect analyzed how using different

analytical tools for the same application can lead to different results. Given the legal precedent of the specific application at hand and the tight constraints set to determine such legality, these analytical variations can result in a product being denoted as legal by one lab and illegal by the other, allowing illegal products to enter the consumer market. The hypothesis of this aspect of the chapter was that the sources of variation, specifically intra-laboratory and inter-instrumental variation, could be determined and reduced and, if reduction was not possible, then the mechanisms responsible could at least be understood and accounted for to minimize variation. With the influx of cannabis/hemp products entering the market since the passage of the 2018 KY farm bill, illegal products entering the market has become a common and detrimental issue. An unknowing consumer could risk using these products and potentially losing their careers or facing legal penalties if they were to test positive for these illicit substances. This was the primary motivation behind this aspect of the research. Three methods of varying complexity, HPLC-UV, GC-MS, and UHPLC-MS, modeling the industry standard approaches, were developed and utilized for cannabinoid profiling. Inter-instrumental variations were observed as both potential over- and under-calculation of the cannabinoid concentrations. Interestingly, a previously unreported phenomenon was observed when generating the cannabinoid profiles using the UHPLC-MS method; the temperature-induced formation of an acylium ion and decarboxylation product during the ESI process for the cannabinoid acids. Though no possible instrument temperature variations or solvent compositions where no formation of the degradation products was observed could be determined, the discovery of its formation could lead to better quantitation in the future to prevent illegal products from passing the cannabinoid profiling step. Implementation of temperature monitoring

and multiple ion signal summation when developing the quantitation method was determined to be the best response to the phenomenon. The second aspect of this chapter focused on providing an alternative or ancillary method to perform metabolomics analyses on sources that are already well-characterized. Here, more substantial method evaluations could be performed as a vast wealth of data exists in the literature on this topic. In this specific case, *Polygonum multiflorum* extracts were the analytical subject. This plant produces a vast number of different phenolic compounds, many of which have been suggested to have a degree of pharmacological activity. One particular aspect in focus is the potential use of *p. multiflorum* extracts to treat Parkinson's disease, as it is theorized to reduce alpha synuclein toxicity. Through similar a collaboration described in chapter 2, Naprogenix is in the process of developing a similar plant model to the *L. cardinalis*-hDAT mutants but using *p. multiflorum* and alpha synuclein. The focus of this aspect was to develop a metabolomic database for future characterizations as well as lay down the framework to apply the technology developed in chapter 2 to this application to speed up the discovery and evaluation process, further streamlining the potential target selection and isolation process. Given the impact that Parkinson's disease has on the world population and the current lack of adequate therapies, this application displays extreme importance due to its role and potential impact in the search for future therapeutics. The secondary metabolites of *p. multiflorum* are polyphenolic and not alkaloids, as in chapter 2, therefore applying the capillary electrophoresis method to them was particularly challenging, however the hypothesis was that certain modifications could allow for the application of capillary electrophoresis for the analysis of these extracts. In collaboration with the manufacturer of the capillary electrophoresis device

being utilized, a prototype device was procured to allow for separation of these analytes. Chemical modifications using dansyl chloride and the use of cation-assisted electrophoresis were developed and evaluated against standards and surrogates, given the current lack of the subject plant material. Though the method cannot be tested on actual *P. multiflorum* material currently, successful electrophoretic separations of the dansylated polyphenol standards and dansylated surrogate (*Cannabis extract*) material suggests promising application in the future. The future applications for this chapter are to apply the optimized dansylation and capillary electrophoresis methods to the future extracts. Unfortunately, the capillary electrophoresis device used was a prototype with a constrained number of allotted analyses, so procurement of additional devices is also required for continuation.

The fourth chapter focuses on taking the technology developed in chapters two and three and applying them to another tangential application, drug metabolism pharmacokinetics (DMPK), a critical component of clinical trials. DMPK helps scientists to understand how the potential therapeutics discovered or developed, as was the focus of chapters two and three, interact and metabolize once internalized and processed by an organism. The information obtained in performing DMPK analyses is absolutely critical to understanding and predicting how a drug will not only interact with its intended targets, but also with its unintended targets. The hypothesis of this chapter was that the capillary electrophoresis mass spectrometry method could be modified and applied to perform a global metabolomics inclusive DMPK analysis. In this application, the metabolomics focus was switched from primarily secondary metabolites to primary and secondary metabolites, as well as xenobiotic metabolites. The DMPK results generated

using the capillary electrophoresis mass spectrometry approach were statistically similar to those generated using the standard LC-MS approach, however, extensive metabolomics data was also acquired. By utilizing this developed method, pharmacokinetic profilers can not only streamline the extensive DMPK process, thus streamlining the entrance of much-needed therapeutics into the market, but also easily monitor changes in metabolite expression of both endogenous metabolites and exogenous xenobiotic metabolites linked to the therapeutics themselves. The target of interest in this specific application is an Alzheimer's disease therapeutic that shows a great deal of potential as a prophylactic treatment and halting agent of the disease. Again, another condition that affects millions of people with no reliable treatment. Using this approach, crucial therapeutics like the one in question can be quickly screened and characterized to speed up the arduous process of entering clinical trials.

The research found within this dissertation centering around the usage of mass spectrometry for metabolomics method development displays great adaptability across a number of applications, especially within the drug-discovery and testing process. Here, the development of various methods using capillary electrophoresis mass spectrometry was performed, applicable to the metabolomics-based discovery, quantitation, and evaluation of various, drastically different types of analytes. Capillary electrophoresis, though fairly well known, is under-utilized in both industrial and pharmaceutical industries. Analyses can be difficult to perform when compared to chromatographic methods like HPLC and GC. This has led to capillary electrophoresis being a solution looking for a problem. Through this research, it appears that the problem it is the ideal solution to is high throughput metabolomic mass spectrometry screening. In this work, it

was demonstrated that, not only did the capillary electrophoresis methods generate statistically similar quantitative data to traditional chromatographic approaches, it outperformed in terms of separation efficiency, analysis time, and required sample volume. The low nL flow rates associated with capillary electrophoresis also reduce background noise, easing back-end data processing leading to cleaner, more accurate metabolomic profiles to be generated. As further developments are made in the field of capillary electrophoresis mass spectrometry, it is possible that an industry shift may occur towards the more frequent implementation of these methods for crucial steps in the metabolomics-based drug discovery and evaluation process.

APPENDICES

APPENDIX 1: NORMALIZED AREA COUNTS FOR THE FEATURES DETECTED IN WT, DAT, AND MUTANT *L. CARDINALIS* PLANT EXTRACTS.

Normalized Data set for all 139 features - average area count for m/z 200.2363:					2.00E+08				
row m/z	WT-1	WT-2	WT-3	DAT-1	DAT-2	DAT-3	Mutant-1	Mutant-2	Mutant-3
90.0918	1.728	1.771	1.316	0.706	0.757	0.622	0.815	0.957	0.742
91.0542	1.794	0.847	0.735	2.932	0.579	1.597	2.481	3.145	1.661
97.0079	9.462	20.465	16.211	13.363	16.523	19.122	10.964	16.763	24.292
99.0037	1.196	2.435	2.058	1.302	1.952	2.680	1.187	2.114	3.221
102.0915	12.642	9.273	6.738	12.253	8.813	8.800	11.387	9.687	10.696
102.9705	4.632	17.499	9.649	5.682	13.559	19.904	3.692	8.162	30.668
104.0708	1.592	1.142	0.866	0.634	0.410	0.567	0.459	0.082	0.454
104.1073	2.356	1.436	1.123	4.546	2.418	2.827	2.677	1.541	2.612
105.0036	5.764	9.814	8.382	6.118	8.204	12.292	5.255	9.777	12.460
106.0500	0.468	0.226	0.215	0.442	1.893	2.524	0.320	0.132	0.163
111.0233	8.294	11.457	9.733	10.362	9.416	11.399	10.263	10.660	14.062
113.0190	3.175	3.234	3.222	3.712	2.264	3.118	4.049	2.702	4.007
120.9808	4.545	29.947	18.714	6.086	21.789	32.652	4.452	13.668	43.338
121.0075	4.716	1.906	2.649	3.585	2.590	1.392	5.649	2.716	3.612
122.0812	2.248	0.704	0.567	0.756	0.133	0.196	4.324	1.073	1.742
125.0026	1.704	8.068	6.349	2.267	5.619	6.685	4.364	5.880	8.319
126.9984	1.015	2.466	2.462	1.229	2.018	2.193	1.054	2.392	3.363
132.1015	1.138	1.229	0.672	2.159	1.781	2.388	0.761	0.612	0.578
133.0610	1.400	0.574	0.308	2.529	0.992	1.149	2.967	1.097	1.767
134.9869	3.109	3.956	3.350	3.716	3.524	4.217	3.431	2.631	5.175
136.0426	0.000	0.000	0.000	0.000	13.609	17.726	0.000	0.000	0.000
139.0182	8.566	9.429	7.652	12.969	7.782	8.194	10.354	6.777	9.385
140.1437	0.305	0.206	0.167	3.269	1.805	2.302	0.346	0.152	0.285
141.0139	12.077	8.022	7.750	12.335	5.926	9.598	12.379	6.111	10.559
142.1577	1.205	0.632	0.405	1.332	0.500	0.775	2.167	1.405	2.423
144.0478	25.481	16.857	14.289	18.516	10.959	13.213	34.047	21.760	31.975
144.1383	0.929	0.691	0.535	9.601	6.301	7.589	0.781	0.410	0.668
148.9756	3.144	6.908	3.802	4.237	4.668	7.049	2.872	2.814	8.808

149.0026	43.735	21.255	18.548	53.391	18.030	21.279	24.006	19.510	26.110
151.0541	0.000	0.259	0.627	0.000	1.354	1.861	0.000	2.216	3.579
151.0971	0.965	0.783	0.594	0.545	0.538	0.627	0.732	0.544	0.867
152.9974	7.705	15.315	12.723	11.253	11.632	13.879	9.616	12.353	16.311
155.0299	7.231	4.112	3.000	8.916	3.176	4.331	8.659	2.820	4.622
156.0766	0.311	0.098	0.118	0.181	1.705	1.842	0.417	0.132	0.204
158.1175	0.404	0.241	0.087	0.229	0.106	0.156	1.455	0.874	1.186
158.1539	5.131	3.599	3.473	42.927	27.603	35.305	5.768	3.476	5.557
167.0130	29.913	21.806	19.312	42.521	17.182	21.018	18.762	16.264	22.823
170.1539	0.468	0.316	0.297	0.692	0.331	0.643	1.439	0.496	1.883
172.1692	1.213	1.025	1.047	40.483	28.069	36.687	19.447	13.831	22.302
174.1605	1.969	1.674	1.543	0.808	0.464	0.640	0.013	0.090	0.059
180.1272	0.934	0.985	1.381	2.615	0.788	2.609	4.147	3.283	3.218
181.0289	10.658	5.063	3.944	4.246	4.329	5.028	13.483	3.309	4.540
181.0453	0.141	0.384	0.901	0.138	1.376	2.473	0.217	1.934	2.786
186.1276	4.075	7.167	3.787	36.859	17.513	8.811	18.041	31.881	37.636
186.1277	8.532	3.952	5.938	9.315	21.347	26.559	50.975	11.999	38.745
186.1855	0.100	0.057	0.053	7.632	1.928	6.090	0.558	1.122	1.624
189.0335	0.109	0.869	2.563	0.071	7.093	10.390	0.035	8.807	14.455
193.1356	1.788	1.387	0.265	13.241	6.099	8.246	14.637	11.186	14.036
193.1360	2.220	0.457	0.260	7.844	3.287	1.469	5.621	0.379	2.955
199.0942	4.391	1.553	4.444	3.434	1.263	4.570	8.334	1.342	2.830
200.1253	0.105	0.591	0.506	10.802	8.283	12.192	2.029	2.064	3.297
200.1254	0.526	0.591	0.506	12.012	5.464	11.487	1.936	2.064	3.386
201.0442	0.091	0.094	0.171	1.415	1.393	1.849	1.558	1.453	2.193
201.1500	1.593	1.128	0.353	5.549	2.594	1.639	3.289	2.086	2.448
201.1508	1.643	0.077	0.242	2.504	0.947	1.852	3.361	0.365	1.040
207.0443	0.072	0.408	0.798	0.101	2.305	3.944	0.136	1.785	4.770
213.1099	32.693	41.099	54.816	20.652	18.685	25.870	17.252	41.486	12.591
214.1134	0.608	4.151	3.695	8.954	4.373	2.548	1.839	4.104	2.031
216.0431	0.000	0.000	0.000	0.365	0.142	0.198	3.125	1.704	2.444
216.1569	0.073	1.192	0.879	2.957	2.052	2.299	0.011	1.955	2.712
216.1959	9.662	7.719	6.427	3.031	3.910	2.184	0.450	0.797	1.388
216.1962	0.269	8.105	6.633	6.259	1.801	5.441	0.239	0.797	1.388
219.1357	0.179	0.173	0.375	10.339	4.501	8.786	0.492	0.293	0.820
224.1539	0.256	1.021	1.030	3.122	5.307	7.462	4.938	3.532	5.976

229.1985	3.874	2.783	2.540	11.518	6.751	9.539	18.929	13.287	20.405
230.2113	45.103	33.506	25.683	35.586	13.878	6.021	3.387	14.406	23.443
230.2113	41.613	3.440	0.391	19.957	5.019	27.799	6.640	3.976	5.831
230.2116	35.774	9.463	4.067	8.912	21.184	17.021	19.014	2.677	8.316
232.1524	0.059	0.171	0.095	1.991	0.449	0.557	0.085	0.220	0.289
235.0928	1.931	0.782	0.667	2.213	0.581	0.935	2.390	0.578	1.001
240.1955	2.124	1.448	1.377	1.694	0.929	0.249	3.002	1.609	3.477
242.2830	3.803	0.072	1.222	5.874	0.063	0.916	324.881	212.834	358.452
244.1908	4.354	3.305	3.033	3.190	2.367	7.705	6.866	5.341	24.076
244.1909	0.193	2.637	2.319	8.597	6.009	2.590	20.361	15.593	7.957
244.2268	6.883	22.296	4.917	91.322	25.048	71.450	46.134	68.169	168.396
244.2270	36.450	27.869	23.256	80.592	56.830	33.658	139.165	30.407	50.558
244.2271	18.463	13.233	12.061	32.359	47.246	63.846	25.941	107.265	147.217
245.1883	5.426	2.043	1.149	8.789	1.928	1.033	1.017	2.866	3.632
247.0756	8.402	4.652	3.781	11.253	3.819	4.663	12.009	2.210	5.456
254.2111	0.302	0.126	0.143	0.995	0.192	0.109	7.004	4.500	7.220
256.2269	11.987	46.881	45.641	139.518	88.195	29.752	448.349	325.985	509.560
256.2270	11.987	8.139	18.135	35.645	23.049	112.926	94.704	66.141	368.145
258.2068	1.844	26.814	25.124	23.323	13.409	6.712	4.309	17.925	28.931
259.2076	13.753	0.404	0.564	1.954	0.565	0.289	1.062	0.318	0.725
259.2454	8.178	4.194	2.939	62.951	23.810	31.293	77.747	41.737	89.402
259.6726	0.048	0.237	0.256	3.321	2.383	2.027	16.244	11.602	17.638
260.2224	11.367	7.710	6.315	7.869	4.004	5.017	2.935	1.786	3.288
260.2487	0.187	0.545	0.210	0.343	2.942	4.598	0.516	1.039	8.262
261.0914	5.016	1.535	1.396	7.632	1.571	1.922	3.053	1.668	1.526
270.2428	2.290	1.340	1.398	7.779	4.675	5.728	24.366	22.203	22.171
270.3152	19.125	12.958	9.396	16.507	7.689	13.256	17.929	12.297	16.884
272.2217	14.888	11.080	9.676	15.551	9.744	12.936	41.945	26.808	43.752
273.1904	1.936	0.710	1.231	0.821	0.295	1.851	4.477	0.824	0.625
273.2177	1.913	0.282	0.571	1.351	0.527	1.229	0.747	0.444	1.677
273.2252	2.726	2.281	2.474	3.305	3.723	3.714	9.201	4.462	9.844
273.2617	2.282	0.203	0.751	34.493	21.662	0.385	89.116	0.800	110.284
274.2370	4.639	1.112	0.221	31.875	17.750	22.624	15.687	8.082	15.298
281.1882	0.077	0.032	0.041	0.048	0.145	0.245	0.944	0.035	0.163
282.2791	5.876	3.852	3.562	4.019	2.236	2.815	0.036	0.067	0.123
286.2381	0.674	0.766	0.327	10.925	6.602	7.868	10.193	7.230	13.856

288.2179	6.298	4.589	3.592	0.206	1.347	1.996	0.591	3.651	4.030
288.2529	9.034	6.543	0.122	61.936	37.181	0.648	37.792	26.301	40.748
288.5204	0.613	0.413	0.301	3.639	3.029	3.205	3.934	3.220	4.900
289.2040	0.013	0.349	0.948	0.135	0.487	0.639	4.272	1.780	0.498
289.2561	1.327	0.929	0.973	13.767	7.072	9.935	6.955	4.540	6.417
293.1343	0.012	0.116	0.095	4.578	0.837	2.240	3.889	1.703	2.645
296.2948	0.192	1.050	0.651	2.899	0.415	1.753	0.318	0.052	0.102
299.1612	6.945	5.493	8.938	6.901	3.370	3.356	5.495	1.861	1.350
302.2324	1.471	0.258	0.277	1.261	0.276	0.139	2.265	0.110	0.724
302.2694	0.194	0.034	0.101	3.142	0.276	0.308	0.150	0.196	0.232
306.2129	1.764	0.283	0.025	2.736	1.295	1.679	2.961	0.473	1.360
310.1655	1.184	3.631	0.609	0.408	0.244	0.126	5.171	1.333	1.983
313.1913	0.054	0.011	0.010	0.206	0.308	0.514	6.620	0.260	5.197
322.2371	0.080	0.125	0.145	2.227	0.927	1.352	2.684	1.251	4.133
324.2076	0.000	0.031	0.104	0.000	0.010	0.171	0.013	0.019	2.055
325.1336	7.176	3.407	0.108	1.576	0.122	0.000	0.000	0.000	0.000
344.2389	0.124	0.112	0.111	0.152	2.004	0.313	6.004	6.370	3.525
349.2278	0.354	0.173	0.546	2.744	0.054	2.382	0.142	0.251	0.075
366.3362	0.000	0.000	0.000	0.623	0.220	0.152	4.202	0.190	0.694
367.3323	3.057	0.411	2.091	6.011	3.467	4.374	0.116	0.084	0.184
381.3479	0.131	0.387	0.356	6.180	1.239	0.187	0.070	0.116	0.184
432.2771	0.684	0.637	0.568	6.401	4.587	6.950	5.447	4.606	8.354
451.3899	0.067	0.101	0.040	0.000	0.149	0.110	10.884	4.438	6.723
373.2638, 187.1359	44.100	41.468	36.693	52.606	37.050	46.629	90.543	75.096	103.226
387.2795, 194.1415	942.501	872.394	815.170	1891.060	1524.384	1759.488	2670.708	2308.580	2858.175
399.2822, 200.1446	45.905	33.176	30.042	97.719	60.264	76.876	87.888	58.198	94.319
401.2587, 201.1284	5.141	5.290	3.694	26.461	17.515	25.144	33.295	24.223	40.417
403.2740, 202.1410	46.761	41.434	37.410	222.112	151.634	201.371	278.414	206.729	310.481
415.2749, 208.1415	8.236	7.163	5.850	41.007	25.798	37.216	15.961	11.667	18.680
417.2537, 209.1308	4.012	3.265	2.624	1.622	0.904	1.001	2.186	1.400	2.278
419.2693, 210.1383	0.441	0.362	0.322	3.804	3.460	5.039	5.237	4.932	8.298
130.1595	90.164	69.670	54.757	89.153	55.952	81.086	91.112	63.845	102.822

200.2363	110.668	82.611	73.881	122.000	75.040	107.166	113.176	79.865	135.593
228.1967	46.077	32.804	28.658	108.946	69.950	87.033	161.838	113.509	178.310
242.2115 isomer	55.703	39.533	32.039	107.643	65.919	79.901	213.728	149.076	250.758
242.2115 isomer	35.687	25.427	22.774	59.843	38.608	51.578	136.577	93.104	156.852
242.2115 isomer	196.865	155.823	133.270	317.947	206.694	258.134	748.534	546.598	843.107
258.2437	67.182	47.603	38.916	505.039	313.575	413.151	674.147	474.522	773.172
272.2574	43.757	30.395	28.012	234.213	143.189	195.592	625.380	412.413	681.683

APPENDIX 2: CONFIDENCE INTERVAL CALCULATION FOR ERROR IN LOBINALINE CONCENTRATION FROM CALIBRATION CURVE.

$$\mu_{C_A} = C_A \pm t(s_{C_A})$$

C_A = analyte concentration from the regression equation ($y = b_1x + b_0$)

t = t value based on the desired level of confidence and n–2 degrees of freedom (in this case, at 95% confidence and n-2= 8; t = 2.306)

$$s_{C_A} = \frac{(stdev_{reg})}{b_1}\sqrt{\left(\frac{1}{m}\right) + \left(\frac{1}{n}\right) + \frac{(\bar{Y}-\bar{y})^2}{(b_1)^2\Sigma_i(x_i-\bar{x})^2}}$$

$$(stdev_{reg}) = \sqrt{\frac{\Sigma(y_i-\hat{y}_i)^2}{n-2}}$$

where y_i = average response for the i^{th} standard and $\hat{y}_i$ = the calculated response for that standard using the regression equation

m = number of internal standard replicates

n = number of points in the curve

$\bar{Y}$ = response for analyte in sample

$\bar{y}$ = average response for analyte in all standards

$\Sigma_i(x_i - \bar{x})^2$ = standard sum of squares for concentration range of internal standards.

APPENDIX 3: MS/MS OF PRIORITIZED PEAKS OF INTEREST.

MS/MS spectra for: 1) m/z 387, 2) m/z 403, 3) m/z 419, 4) m/z228, 5) m/z 242-1, 6) m/z 242-2, 7) m/z 242-3, 8) m/z 258, and 9) m/z 272

1) m/z 387

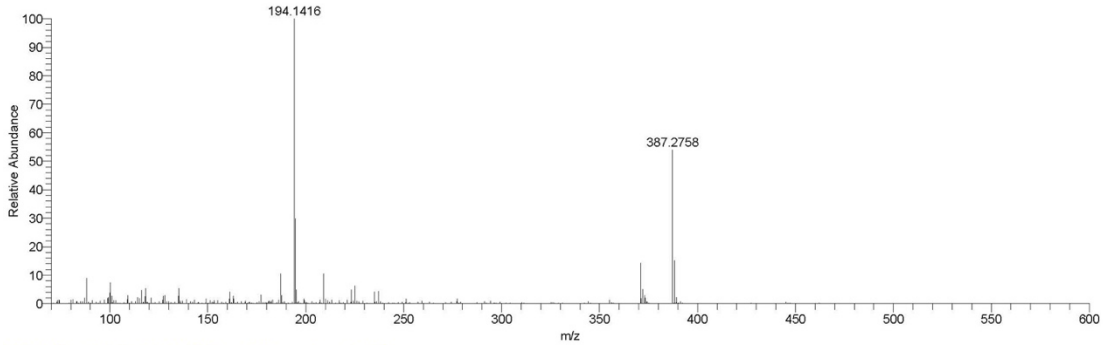

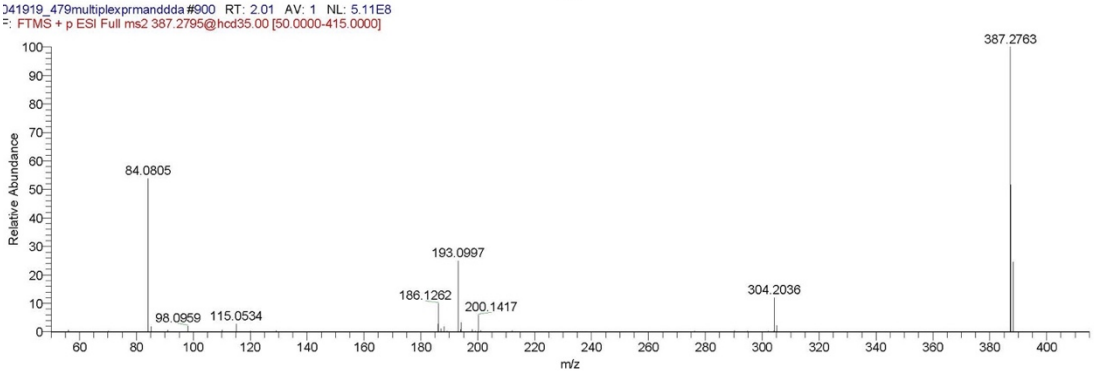

2) m/z 403

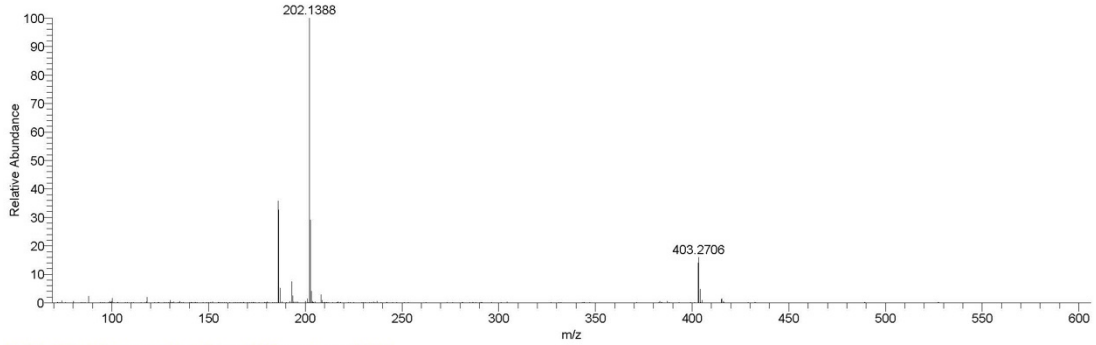

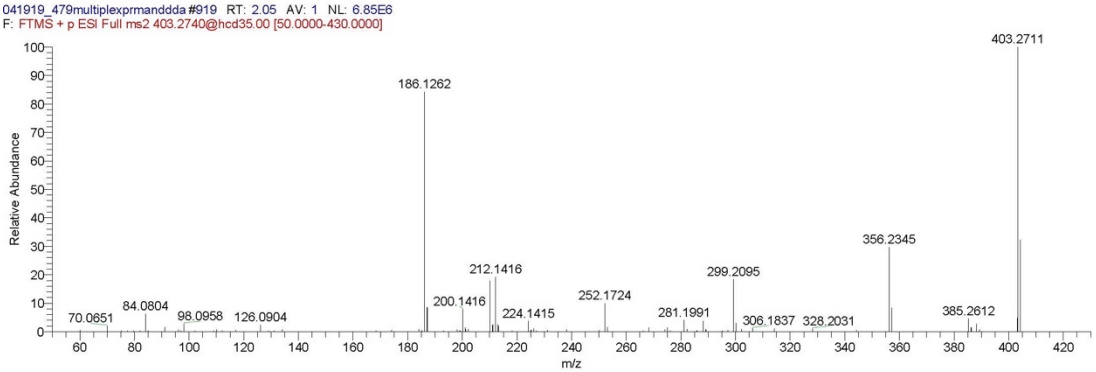

3) m/z 419

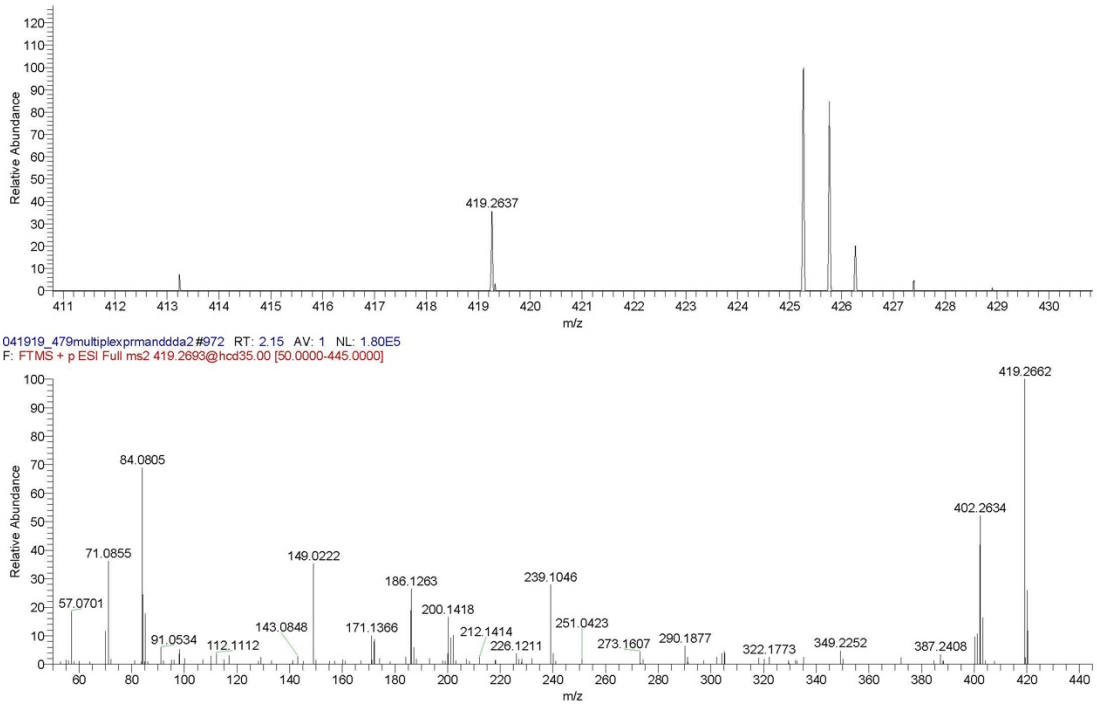

4) m/z 228

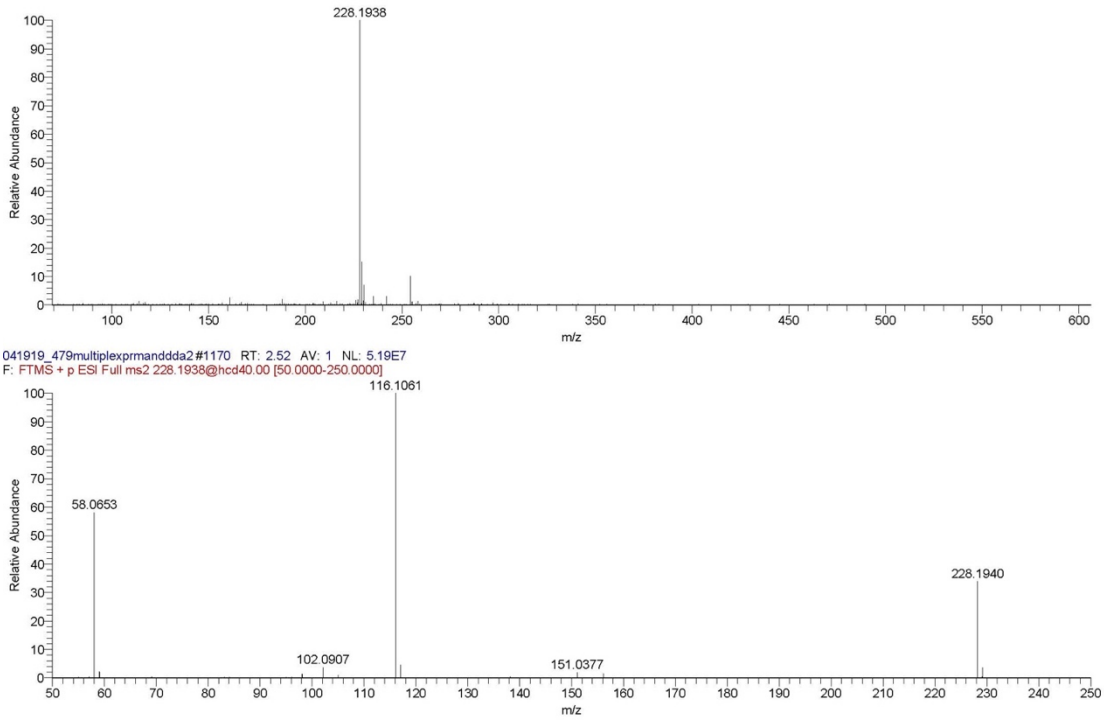

5) m/z 242-1

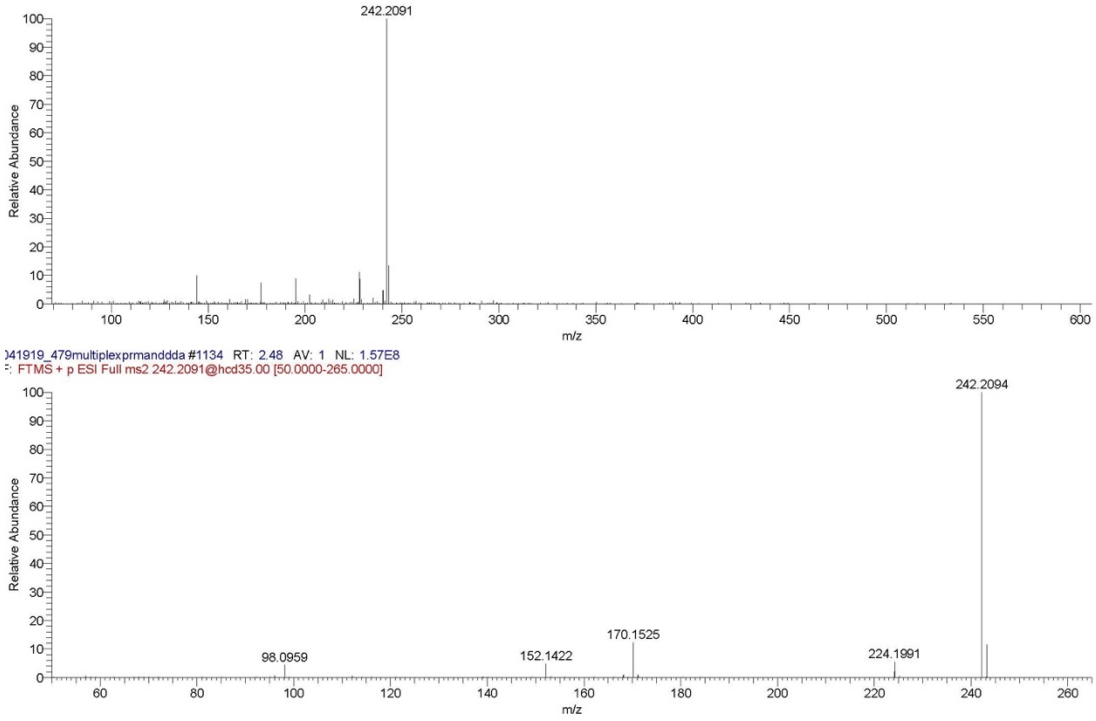

6) m/z 242-2

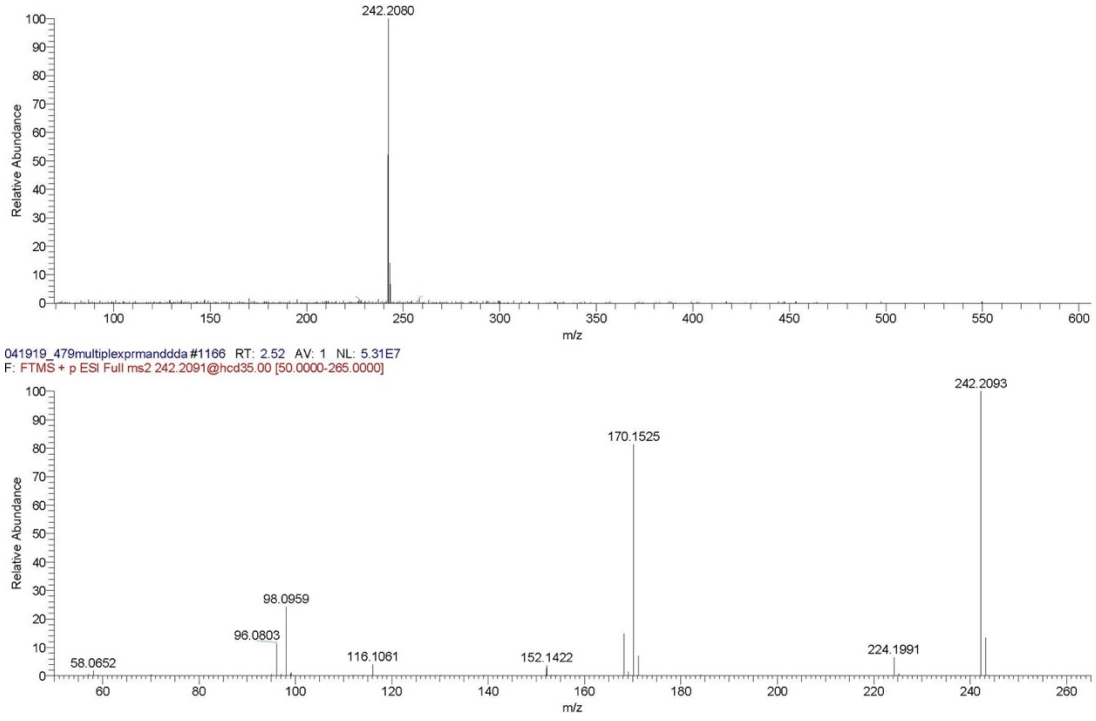

7) m/z 242-3

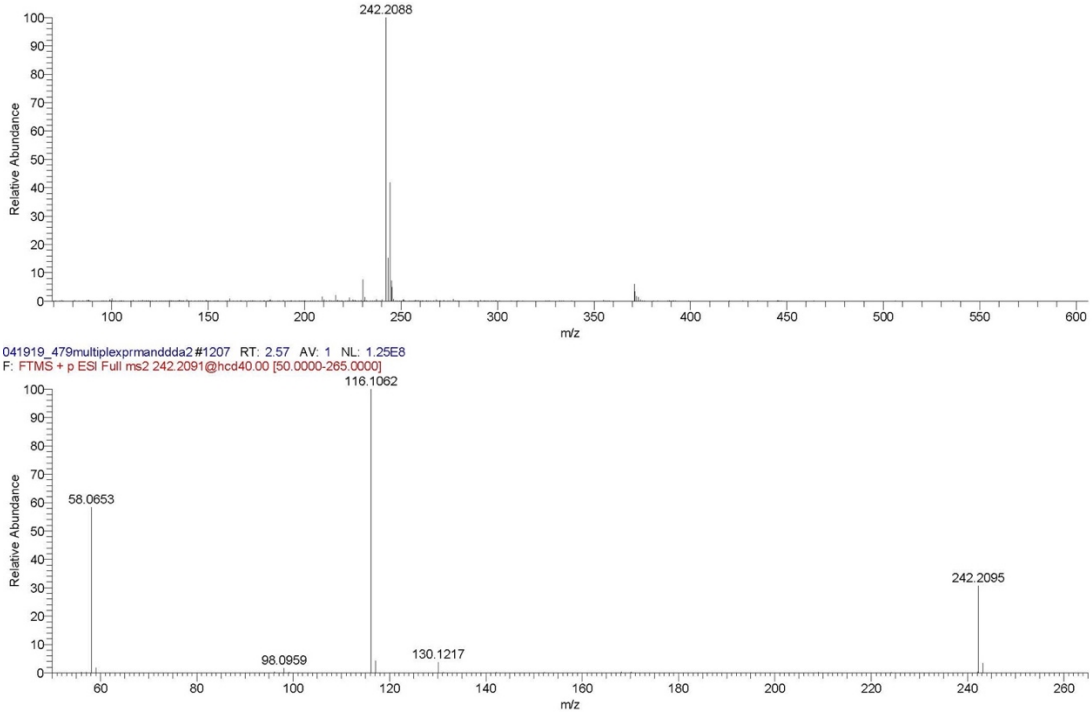

8) m/z 258

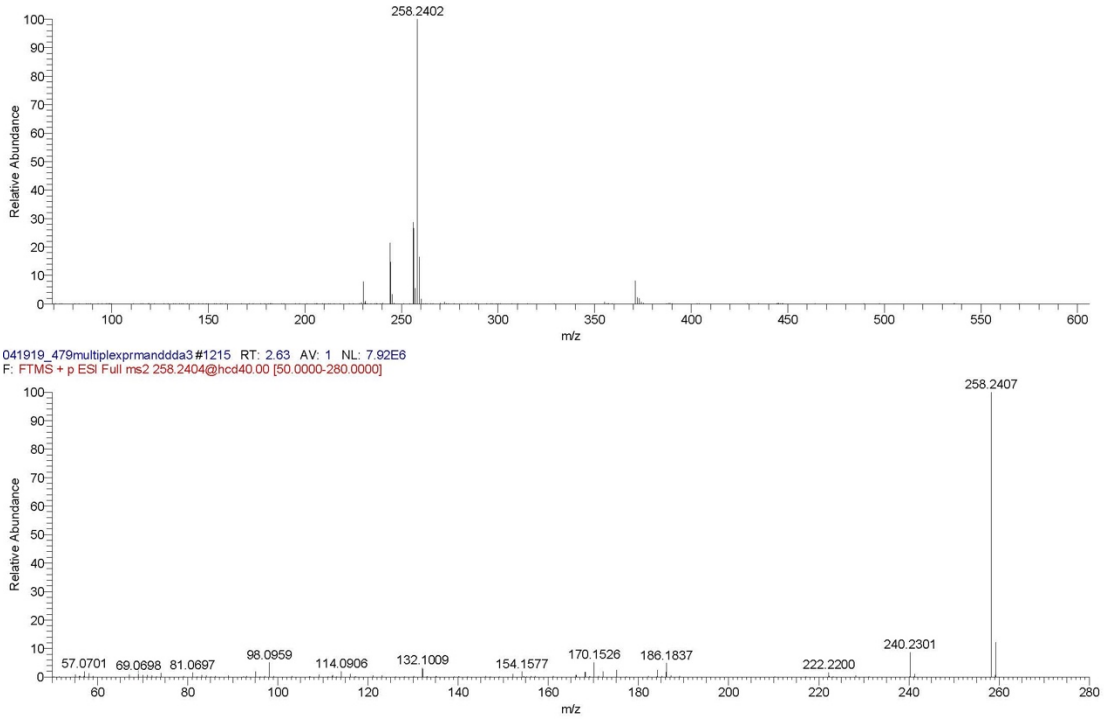

9) m/z 272

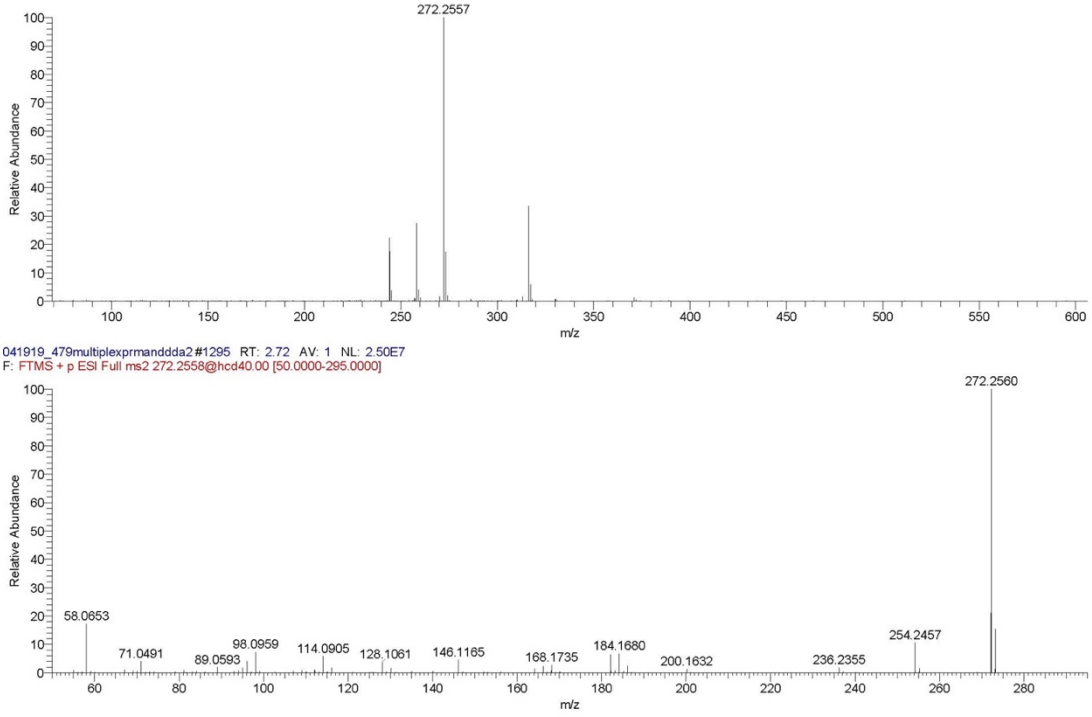
272.2557
Relative Abundance
m/z
041919_479multiplexprmanddda2 #1295 RT: 2.72 AV: 1 NL: 2.50E7
F: FTMS + p ESI Full ms2 272.2558@hcd40.00 [50.0000-295.0000]
272.2560
58.0653
71.0491
89.0593
98.0959
114.0905
128.1061
146.1165
168.1735
184.1680
200.1632
236.2355
254.2457
Relative Abundance
m/z

APPENDIX 4: *POLYGONUM MULTIFLORUM* SECONDARY METABOLITE PEAK LIST

			P. multiflorum 1 (office)							P. multiflorum 2 (greenhouse)						
m/z	RT	row identity (all IDs)	LSR (Mix)	Leaf	Stem	Root	Leaf (rel)	Stem (rel)	Root (rel)	LSR (Mix)	Leaf	Stem	Root	Leaf (rel)	Stem (rel)	Root (rel)
149.0089	*0.23*	Tartaric acid	1.19E+06	1.20E+06	3.31E+05	1.20E+06	44%	12%	44%	3.88E+06	4.92E+05	7.35E+06	2.26E+06	5%	73%	22%
267.0711	*0.24*	Inosine	9.22E+06	6.49E+06	6.31E+06	1.01E+07	28%	28%	44%	6.00E+06	3.67E+06	4.99E+06	7.98E+06	22%	30%	48%
209.0297	*0.24*	D-Glucarate/D-Galactarate	2.93E+06	1.02E+07	2.83E+06	2.47E+06	66%	18%	16%	3.83E+06	1.09E+06	4.87E+06	4.80E+06	10%	45%	45%
237.0608	*0.24*	3-Deoxy-D-manno-octulosonate;Xanthopterin-B2;Ketodeoxyoctonic acid	9.87E+06	2.87E+06	1.41E+07	6.68E+06	12%	60%	28%	1.29E+07	2.91E+06	3.91E+07	2.97E+06	6%	87%	7%
132.0303	*0.24*	Aspartic Acid	1.68E+07	1.04E+07	8.48E+06	2.14E+07	26%	21%	53%	2.85E+07	4.28E+06	1.22E+07	5.73E+07	6%	16%	78%
133.0143	*0.25*	Malic Acid	1.19E+08	5.44E+07	1.20E+08	2.47E+08	13%	28%	59%	2.77E+08	2.27E+07	1.79E+08	5.12E+08	3%	25%	72%
262.0558	*0.25*	C9H13NO8	6.52E+07	3.79E+07	4.32E+07	8.06E+07	23%	27%	50%	2.41E+07	6.64E+06	1.81E+07	4.11E+07	10%	27%	62%
115.0038	*0.25*	Fumaric/Maleic Acid	1.19E+07	7.55E+06	8.58E+06	2.17E+07	20%	23%	57%	3.00E+07	3.29E+06	1.87E+07	6.60E+07	4%	21%	75%
191.0557	*0.25*	Quinic Acid	1.93E+07	6.72E+06	3.87E+07	6.90E+06	13%	74%	13%	9.00E+07	1.49E+07	2.25E+08	7.26E+06	6%	91%	3%
146.0458	*0.25*	Glutamic Acid	9.54E+07	9.79E+07	4.95E+07	9.33E+07	41%	21%	39%	1.22E+08	1.11E+07	2.76E+07	2.57E+08	4%	9%	87%
165.0401	*0.25*	Arabinonic Acid	1.46E+07	1.99E+07	7.95E+06	9.57E+06	53%	21%	26%	2.09E+07	1.05E+07	1.67E+07	1.23E+07	27%	42%	31%
147.0299	*0.26*	D-Arabinono-1,4-lactone	2.05E+07	9.62E+07	6.35E+07	6.00E+07	44%	29%	27%	1.59E+07	1.16E+07	1.35E+07	7.72E+06	35%	41%	24%
195.0505	*0.26*	Gluconic Acid	1.78E+07	7.41E+06	1.13E+07	3.14E+07	15%	23%	63%	2.82E+07	4.10E+06	5.65E+07	1.78E+07	5%	72%	23%
173.0451	*0.26*	Shikimic Acid	6.04E+07	3.64E+07	1.02E+08	4.74E+07	20%	55%	26%	1.11E+08	7.27E+07	2.94E+08	1.07E+07	19%	78%	3%
125.0010	*0.26*	2-Hydroxyethylphosphonate	2.15E+07	2.47E+07	1.37E+07	2.00E+07	42%	23%	34%	7.79E+06	3.81E+06	1.27E+07	1.15E+07	14%	45%	41%
128.0354	*0.26*	4-Oxoproline	3.55E+07	8.28E+06	2.53E+07	4.26E+07	11%	33%	56%	2.61E+07	1.51E+06	2.64E+07	3.99E+07	2%	39%	59%
149.0453	*0.26*	Ribose/Arabinose/Xylose	1.03E+07	1.22E+07	7.70E+06	6.12E+06	47%	30%	24%	1.58E+07	6.65E+06	1.39E+07	1.20E+07	20%	43%	37%
117.0195	*0.26*	Succinate	5.92E+06	4.88E+06	8.87E+06	1.75E+07	16%	28%	56%	8.16E+05	2.57E+06	9.14E+06	8.99E+06	12%	44%	43%
205.0348	*0.26*	2-Methylcitrate	4.36E+06	2.42E+06	3.63E+06	9.17E+06	16%	24%	60%	9.85E+05	3.05E+05	1.91E+06	1.56E+06	8%	51%	41%
319.0660	*0.26*	C16H16O5S	2.06E+04	3.57E+04	1.31E+05	2.23E+05	9%	34%	57%	6.27E+06	4.81E+04	3.29E+06	3.11E+07	0%	10%	90%
251.0764	*0.27*	4'-O-Methylisoflavone	2.60E+06	7.75E+04	1.16E+05	1.27E+07	1%	1%	99%	ND	ND	ND	ND	ND	ND	ND
215.0323	*0.27*	(CI isotope pattern - [M+Cl]-) Likely Fructose/Galactose/Mannose/etc	3.41E+07	4.07E+07	1.80E+07	1.04E+07	59%	26%	15%	8.67E+07	8.38E+07	4.40E+07	1.36E+07	59%	31%	10%
161.0454	*0.27*	2S-hydroxy-Hexanedioic acid	6.14E+06	5.93E+06	5.11E+06	3.86E+06	40%	34%	26%	5.66E+06	2.93E+06	7.63E+06	7.31E+06	16%	43%	41%
129.0195	*0.27*	C5H6O4	8.89E+06	1.85E+07	1.01E+07	1.00E+07	48%	26%	26%	8.78E+06	5.24E+06	6.49E+06	7.56E+06	27%	34%	39%
143.0349	*0.27*	DDMP	5.35E+06	4.91E+06	4.74E+06	4.82E+06	34%	33%	33%	5.16E+06	3.41E+06	6.30E+06	2.65E+06	28%	51%	21%
445.1186	*0.27*	Physcion glucoside	1.36E+06	1.29E+06	5.76E+05	5.46E+05	54%	24%	23%	1.79E+06	1.93E+05	1.77E+06	1.10E+06	6%	58%	36%
225.0609	*0.28*	C14H10O3	7.86E+06	7.86E+06	4.54E+06	2.95E+06	51%	30%	19%	1.69E+07	5.22E+06	3.29E+06	1.26E+06	53%	34%	13%
145.0618	*0.28*	Glutamine	5.16E+07	3.34E+07	7.48E+07	2.81E+07	25%	55%	21%	2.48E+07	6.17E+06	3.30E+07	1.69E+07	11%	59%	30%
379.0816	*0.28*	C21H16O7	3.14E+06	1.27E+06	3.29E+06	6.63E+06	11%	29%	59%	3.30E+07	4.34E+05	3.19E+06	2.18E+07	2%	13%	86%
179.0558	*0.28*	Glucose/Fructose/Galactose	2.82E+07	4.24E+07	3.30E+07	2.06E+07	44%	34%	21%	4.52E+07	3.22E+07	3.17E+07	2.36E+07	37%	36%	27%
125.0245	*0.28*	HMF	3.44E+06	1.49E+06	1.13E+06	3.35E+06	25%	19%	56%	2.23E+06	1.49E+06	1.13E+06	2.50E+06	29%	22%	49%
191.0195	*0.28*	Citric Acid	8.17E+07	3.66E+07	2.14E+07	9.84E+07	23%	14%	63%	2.93E+08	5.81E+06	9.33E+07	5.87E+08	1%	14%	86%
173.0088	*0.28*	Aconitic Acid	9.04E+06	4.27E+06	3.02E+06	6.38E+06	31%	22%	47%	1.26E+07	2.75E+06	4.82E+06	2.24E+07	9%	16%	75%
469.0961	*0.28*	-	3.84E+05	5.03E+03	1.36E+06	3.46E+06	0%	28%	72%	1.83E+07	2.05E+04	2.43E+06	5.12E+07	0%	5%	95%
144.0665	*0.28*	Small Nitrogen containing carboxylic acid (ex. Methyl aminolevuulinate)	1.12E+07	6.91E+06	9.12E+06	8.20E+06	29%	38%	34%	2.82E+06	1.54E+06	2.13E+06	2.54E+06	25%	34%	41%
169.0140	*0.28*	Gallic Acid	6.33E+07	2.44E+06	4.97E+06	1.17E+08	2%	4%	94%	2.78E+07	1.18E+07	1.03E+07	3.59E+07	20%	18%	62%
439.0843	*0.28*	No KEGG match; (C19H20O12) - 3,5-Dihydroxyphenyl 1-O-(6-O-galloyl-beta-D-glucopyranoside)	3.90E+07	4.38E+06	2.53E+07	6.98E+07	4%	25%	70%	5.18E+07	4.34E+05	2.38E+07	7.90E+07	0%	23%	77%
111.0090	*0.29*	C5H4O3	2.34E+06	1.61E+06	9.97E+05	2.19E+06	34%	21%	46%	3.61E+06	1.55E+06	3.17E+06	1.32E+07	9%	18%	74%
387.1133	*0.29*	Multiple methylether flavone	2.98E+07	3.34E+06	9.74E+06	2.42E+07	9%	26%	65%	1.63E+08	3.63E+05	7.33E+06	5.81E+07	1%	11%	88%
683.2246	*0.29*	Maltosylsucrose	1.59E+07	4.44E+05	4.36E+06	3.09E+07	1%	12%	87%	3.87E+07	1.62E+05	3.99E+06	7.02E+07	0%	5%	94%
341.1076	*0.29*	Sucrose/Cellobiose/Maltose	8.68E+07	1.45E+07	5.09E+07	1.38E+08	7%	25%	68%	1.21E+08	1.81E+06	3.19E+07	1.88E+08	1%	14%	85%
147.0662	*0.29*	C6H12O4	9.08E+05	2.81E+05	3.65E+05	1.90E+05	34%	44%	23%	9.29E+06	8.53E+06	7.54E+06	1.02E+07	32%	29%	39%
116.0719	*0.31*	Valine	1.52E+07	6.73E+06	8.17E+06	1.54E+07	22%	27%	51%	1.20E+07	6.62E+05	3.76E+06	1.49E+07	3%	20%	77%
146.0822	*0.31*	4-Hydroxyisoleucine	1.27E+07	3.64E+06	7.09E+06	1.03E+07	17%	34%	49%	1.11E+07	3.25E+05	6.63E+06	5.07E+06	3%	55%	42%
154.0621	*0.36*	Histidine	9.82E+06	2.00E+06	3.86E+06	1.47E+07	10%	19%	71%	3.88E+06	1.73E+05	9.83E+05	7.33E+06	2%	12%	86%
180.0664	*0.37*	Tyrosine	2.30E+07	1.65E+06	5.21E+06	3.14E+07	4%	14%	82%	1.62E+07	8.21E+05	3.94E+06	1.34E+07	5%	22%	74%
130.0874	*0.37*	Leucine/Isoleucine	5.90E+07	2.20E+07	2.14E+07	6.08E+07	21%	21%	58%	2.41E+07	2.59E+06	9.15E+06	1.98E+07	8%	29%	63%
207.0869	*0.37*	No KEGG match; (C8H16O6) - Ethyl beta-D-glucopyranoside	4.09E+07	2.16E+07	1.86E+07	4.43E+07	26%	22%	52%	8.21E+06	9.62E+06	1.31E+07	1.93E+06	39%	53%	8%
337.0919	*0.43*	1-Caffeoyl-4-deoxyquinic acid;4-p-Coumaroylquinic acid;p-Coumaroyl quinic acid;Sodium caffeine benzoate	1.02E+07	6.64E+06	2.98E+06	3.55E+04	69%	31%	0%	8.93E+06	2.45E+07	5.62E+06	1.87E+04	81%	19%	0%
164.0716	*0.72*	Phenylalanine	3.78E+07	1.27E+07	7.35E+06	2.70E+07	27%	16%	57%	6.66E+06	6.98E+05	8.52E+05	2.47E+06	17%	21%	61%
173.1040	*0.75*	Arginine	1.62E+08	1.01E+07	5.36E+07	2.00E+08	4%	20%	76%	2.08E+07	3.09E+05	1.39E+07	6.67E+07	0%	17%	82%
186.1132	*0.78*	8-Amino-7-oxononanoate;(E)-2-Butenyl-4-methyl-threonine	7.38E+07	4.21E+07	2.00E+07	2.06E+07	51%	24%	25%	6.60E+05	6.88E+05	6.52E+05	7.57E+05	33%	31%	36%
257.1135	*0.83*	Possible Stilbene? (3'-O-Methylbatatasin)	7.74E+06	6.29E+03	1.65E+04	3.90E+04	10%	27%	63%	2.21E+06	0.00E+00	1.94E+04	1.74E+04	0%	53%	47%
203.0823	*1.32*	Tryptophan	4.20E+07	9.23E+06	1.14E+07	2.70E+07	19%	24%	57%	1.45E+07	1.67E+06	5.16E+06	1.32E+07	8%	26%	66%
305.0658	*1.63*	Flavanol -(+)-Gallocatechin;(-)-Epigallocatechin	1.51E+07	3.69E+04	2.46E+05	1.19E+06	2%	17%	81%	2.18E+07	2.01E+06	1.07E+06	3.59E+05	58%	31%	10%
577.1343	*3.62*	Proanthrocyanidin	1.61E+07	1.85E+05	2.04E+06	1.22E+07	1%	14%	85%	7.02E+06	4.20E+05	2.21E+06	7.28E+06	4%	22%	73%
329.0869	*3.74*	1-O-Vanilloyl-beta-D-glucose	1.38E+07	2.54E+05	1.86E+05	1.59E+05	42%	31%	27%	1.43E+07	1.63E+07	2.53E+06	1.51E+06	80%	12%	7%
325.0474	*3.84*	(CI isotope pattern - [M+Cl]-) (Epi)catechin	1.41E+07	5.26E+05	5.88E+06	2.29E+07	2%	20%	78%	2.23E+07	3.41E+06	5.55E+06	2.35E+07	11%	17%	72%
121.0296	*3.85*	p-hydroxybenzaldehyde	2.40E+07	7.46E+06	7.79E+06	2.07E+07	21%	22%	58%	8.34E+07	6.38E+06	1.40E+07	1.77E+08	3%	7%	90%
579.1497	*3.86*	6''-p-Coumaroylprunin	1.95E+07	0.00E+00	1.87E+04	4.17E+05	0%	4%	96%	1.68E+07	1.74E+05	1.16E+06	1.52E+07	1%	7%	92%
289.0708	*4.03*	(Epi)catechin	1.52E+07	4.18E+06	1.02E+07	1.41E+07	15%	36%	50%	2.48E+08	2.70E+07	7.40E+07	2.81E+08	7%	19%	74%
691.1719	*4.24*	Dimer of (345.0811) - ionization artifact	3.04E+07	1.28E+07	1.28E+06	3.61E+06	95%	5%	0%	8.33E+07	1.26E+08	1.76E+06	0.00E+00	99%	1%	0%
345.0813	*4.26*	Methyl 6-O-galloyl-beta-D-glucopyranoside	6.88E+08	6.28E+08	1.29E+08	1.51E+07	81%	17%	2%	8.13E+08	1.10E+09	8.60E+07	1.20E+06	93%	7%	0%
727.1481	*4.27*	C32H36O17	1.27E+07	8.89E+06	7.09E+05	7.08E+04	92%	7%	1%	2.98E+07	4.05E+07	1.13E+06	2.63E+04	97%	3%	0%
447.0921	*4.38*	Astragalin	4.07E+05	2.86E+04	3.03E+04	1.78E+05	12%	13%	75%	1.07E+07	1.28E+05	2.70E+06	1.31E+07	1%	17%	82%
517.0978	*4.67*	Emodin-o-malonyl glucoside	4.36E+06	1.45E+06	2.17E+06	4.15E+05	36%	54%	10%	6.68E+03	1.31E+03	0.00E+00	2.40E+03	35%	0%	65%
405.1177	*5.04*	tertrahydroxystilbene (TSG)	3.15E+07	1.42E+05	2.60E+07	6.53E+08	0%	4%	96%	3.29E+08	4.40E+06	1.63E+08	3.40E+08	1%	32%	67%
609.1453	*5.05*	Rutin	1.26E+06	6.99E+05	4.15E+05	1.15E+04	62%	37%	1%	4.05E+05	4.65E+05	1.51E+05	0.00E+00	76%	24%	0%
389.1234	*5.09*	Polydatin	3.40E+06	1.03E+04	8.24E+05	2.65E+06	0%	24%	76%	1.20E+06	3.49E+03	1.77E+05	1.50E+06	0%	11%	89%
463.0855	*5.11*	Hyperin	4.49E+07	3.93E+06	5.19E+06	4.59E+05	41%	54%	5%	7.60E+07	7.54E+07	9.82E+06	1.90E+05	88%	11%	0%
441.0945	*5.16*	(CI isotope pattern - [M+Cl]-) TSG	2.94E+07	1.14E+03	8.68E+06	5.31E+07	0%	14%	86%	3.79E+07	2.78E+05	1.25E+07	3.72E+07	1%	25%	74%
811.2450	*5.16*	Dimer of TSG - ionization artifact	1.44E+08	0.00E+00	1.85E+07	1.67E+08	0%	10%	90%	8.33E+07	1.53E+04	2.87E+07	8.45E+07	0%	25%	75%
167.0348	*5.19*	5-Methoxysalicylic acid	1.16E+07	2.90E+06	3.57E+06	8.93E+06	19%	23%	58%	1.32E+07	1.15E+06	2.62E+06	1.59E+07	6%	13%	81%
557.1290	*5.24*	Piceatannol 4'-galloylglucoside	1.45E+07	0.00E+00	7.98E+04	9.71E+06	0%	1%	99%	6.95E+06	2.65E+04	5.69E+05	6.52E+06	0%	8%	92%
223.0424	*5.36*	Hydroxyanthraquinone	5.74E+06	5.64E+06	1.13E+06	3.09E+04	83%	17%	0%	5.47E+04	3.41E+04	7.62E+03	1.25E+04	63%	14%	23%
447.0919	*5.38*	Astragalin	3.12E+08	2.69E+08	3.57E+07	1.06E+06	88%	12%	0%	1.25E+08	1.74E+08	1.58E+07	3.65E+05	91%	8%	0%
483.0688	*5.38*	(CI isotope pattern - [M+Cl]-) Astragalin	1.74E+07	1.87E+07	2.86E+06	7.43E+04	86%	13%	0%	1.45E+07	1.65E+07	1.84E+06	1.99E+04	90%	10%	0%
507.1129	*5.46*	Flavone glucoside (Tomentin 4'-glucoside)	1.43E+07	7.68E+06	5.13E+05	5.87E+04	93%	6%	1%	1.01E+06	5.21E+05	1.04E+05	3.97E+04	78%	16%	6%
253.0524	*5.47*	Chrysophanol	5.72E+06	2.92E+06	1.77E+05	3.32E+03	94%	6%	0%	1.41E+06	1.65E+06	1.14E+05	3.20E+03	93%	6%	0%
431.0969	*5.63*	Emodin glucoside	1.38E+08	1.49E+08	4.12E+06	4.21E+04	97%	3%	0%	3.74E+07	6.44E+07	2.09E+06	2.13E+04	97%	3%	0%
809.2300	*5.69*	Large molecule, multiple EF possibilities. MS/MS needed	1.16E+07	0.00E+00	1.01E+06	1.98E+07	0%	5%	95%	5.98E+05	0.00E+00	1.97E+05	9.82E+05	0%	17%	83%
404.1101	*5.70*	z=-2 of 809.2286	1.82E+07	0.00E+00	2.34E+06	3.29E+07	0%	7%	93%	1.42E+06	0.00E+00	5.09E+05	2.36E+06	0%	18%	82%
227.0709	*5.87*	Resveratrol	5.46E+06	1.38E+04	1.16E+05	5.02E+06	0%	2%	97%	1.58E+06	1.30E+04	5.19E+04	2.03E+06	1%	2%	97%
263.1295	*5.89*	C15H20O4	8.32E+07	7.68E+07	2.52E+07	7.48E+04	75%	25%	0%	6.49E+04	1.08E+05	9.59E+04	9.78E+04	36%	32%	32%
407.1339	*6.00*	troachrysone-8-O-b-D-glucoside	1.46E+06	2.40E+05	7.77E+05	3.87E+05	17%	55%	28%	5.99E+04	3.90E+04	2.60E+04	1.91E+04	46%	31%	23%
277.1447	*6.10*	Dibutylphthalate	5.46E+07	6.64E+07	1.57E+07	7.94E+05	74%	25%	1%	1.03E+05	1.00E+05	9.88E+04	9.24E+04	34%	34%	32%
285.0395	*6.40*	Quercetin	7.66E+06	4.83E+05	2.69E+06	7.32E+05	12%	69%	19%	6.26E+04	1.12E+03	9.88E+04	1.49E+04	1%	86%	13%
309.1715	*6.45*	C17H26O5	7.03E+07	5.71E+07	2.08E+07	5.55E+06	68%	25%	7%	2.34E+05	4.66E+05	4.52E+05	3.43E+05	37%	36%	27%
311.1679	*6.47*	C20H24O3	8.26E+06	4.98E+06	3.69E+06	4.38E+06	38%	28%	34%	5.37E+04	8.13E+04	7.35E+04	5.85E+04	38%	34%	27%
353.1994	*6.60*	C19H30O6	3.43E+07	3.47E+07	1.51E+07	4.01E+06	65%	28%	7%	7.32E+03	1.09E+04	8.17E+03	8.85E+03	39%	29%	32%
293.1767	*6.63*	Embelin/6-Gingerol (similar)	2.58E+07	2.33E+07	2.68E+07	4.82E+06	42%	49%	9%	4.92E+06	4.34E+06	4.25E+06	4.02E+06	34%	34%	32%
397.2252	*6.67*	C26H34O	1.90E+07	1.94E+07	7.68E+06	2.26E+06	66%	26%	8%	1.37E+03	6.75E+03	5.76E+03	3.34E+03	43%	36%	21%
323.1870	*6.73*	C18H28O5	6.33E+07	6.10E+07	1.74E+07	1.31E+05	78%	22%	0%	1.83E+04	1.12E+04	1.17E+04	1.34E+04	31%	32%	37%
325.1833	*6.73*	C21H26O3	8.07E+06	4.84E+06	3.06E+06	4.69E+06	38%	24%	37%	7.34E+04	9.24E+04	1.08E+05	9.07E+04	32%	37%	31%
367.2132	*6.86*	Phytoprostane variant	3.81E+07	3.55E+07	1.29E+07	8.26E+04	73%	27%	0%	7.19E+03	4.51E+03	2.68E+03	5.49E+03	36%	21%	43%
411.2403	*6.94*	C27H36O	2.15E+07	2.00E+07	6.60E+06	4.94E+04	75%	25%	0%	2.53E+03	0.00E+00	8.38E+02	9.05E+02	0%	48%	52%
461.2663	*7.12*	C29H34O5	2.09E+04	0.00E+00	1.28E+03	7.09E+03	0%	15%	85%	2.25E+07	4.71E+05	9.21E+06	1.89E+07	2%	32%	66%
157.1232	*7.12*	Nonanoic acid	4.84E+07	3.28E+07	3.05E+07	2.91E+07	35%	33%	32%	1.98E+07	1.31E+07	3.20E+07	3.41E+07	17%	40%	43%
473.2809	*7.27*	C29H42O3	9.44E+06	1.16E+07	1.00E+07	8.14E+06	39%	34%	27%	5.10E+03	4.35E+03	4.19E+03	3.69E+03	36%	34%	30%
321.2077	*7.28*	8-Gingerol (similar)	1.14E+07	1.13E+07	3.64E+06	6.16E+05	73%	23%	4%	8.49E+03	5.96E+04	4.26E+04	4.55E+04	40%	29%	31%
287.0917	*7.39*	C16H16O5 - stilbene?	1.42E+07	4.80E+06	2.90E+06	7.11E+05	57%	35%	8%	3.06E+07	1.83E+06	1.28E+07	2.05E+07	5%	36%	58%
463.2821	*7.43*	C23H45O7P	1.60E+04	0.00E+00	0.00E+00	3.42E+03	0%	0%	100%	1.15E+07	3.54E+05	5.19E+06	1.17E+07	2%	30%	68%
171.1388	*8.07*	Decanoic acid	1.42E+08	1.36E+08	1.36E+08	1.26E+08	34%	34%	32%	5.33E+07	4.05E+07	4.03E+07	3.72E+07	34%	34%	32%
269.0443	*8.44*	Emodin/Aloe-Emodin (split)	4.80E+08	1.49E+08	1.49E+08	4.25E+08	21%	21%	59%	1.40E+08	1.15E+07	3.75E+07	1.42E+08	6%	20%	74%
285.0396	*9.02*	6-OH Emodin	2.99E+06	8.80E+04	5.68E+04	1.13E+05	34%	22%	44%	5.44E+04	2.71E+04	1.12E+05	2.33E+05	7%	30%	63%
296.2587	*9.05*	Fatty acid	7.87E+06	1.37E+06	3.74E+06	2.94E+06	17%	46%	37%	ND	ND	ND	ND	ND	ND	ND
509.1228	*9.38*	Anthroquinone dimer? Similar to Palmidin A; Flavonoid Glucoside (Luteolin 7,3'-dimethyl ether 5-glucoside)	5.29E+07	4.50E+07	2.55E+07	7.16E+06	58%	33%	9%	2.68E+07	1.51E+06	1.12E+07	2.34E+07	4%	31%	65%
294.2428	*9.40*	Fatty acid	1.02E+07	8.28E+06	1.05E+07	7.26E+06	32%	40%	28%	9.99E+03	1.37E+04	1.03E+04	1.14E+04	39%	29%	32%
199.1700	*9.89*	Dodecanoic acid	2.64E+07	6.11E+06	5.13E+06	4.67E+06	38%	32%	29%	2.50E+07	1.08E+07	1.08E+07	9.73E+06	35%	34%	31%
283.0604	*10.27*	Physcion	2.51E+07	7.84E+06	1.07E+07	2.30E+07	19%	26%	55%	9.29E+06	1.43E+06	4.29E+06	9.31E+06	9%	29%	62%
586.1348	*10.32*	C31H25N3O7	2.33E+07	1.42E+07	1.13E+07	4.37E+06	48%	38%	15%	9.27E+06	6.75E+05	4.99E+06	6.88E+06	5%	40%	55%
523.1385	*10.39*	Flavanol Glucoside (Barbatoflavan)	1.49E+08	1.15E+08	7.74E+07	9.99E+06	57%	38%	5%	4.08E+07	2.63E+06	1.24E+07	1.53E+07	9%	41%	50%
157.1232	*10.64*	Nonanoic acid	7.66E+06	9.39E+06	1.15E+06	1.63E+06	77%	9%	13%	1.05E+06	9.91E+05	1.02E+06	8.51E+05	35%	36%	30%
277.2164	*10.98*	Octadecatrienoic acid	4.04E+07	1.88E+07	7.75E+06	1.24E+07	48%	20%	32%	1.85E+07	1.38E+07	9.54E+06	3.56E+06	51%	35%	13%
227.2011	*11.17*	Tetradecanoic acid	1.15E+08	7.12E+07	7.00E+07	7.00E+07	34%	33%	33%	5.33E+07	2.68E+07	3.10E+07	2.48E+07	32%	37%	30%
537.1544	*11.62*	Flavone glucoside (similar to PhelLOD/NDensin F)	2.72E+07	1.55E+07	2.45E+07	7.37E+06	33%	52%	16%	4.40E+06	4.68E+05	4.54E+06	5.49E+05	8%	82%	10%
349.2749	*11.64*		8.39E+06	7.33E+06	7.56E+06	9.36E+06	30%	31%	39%	5.02E+07	4.09E+07	4.28E+07	4.15E+07	33%	34%	33%
279.2320	*11.70*		3.24E+08	1.82E+07	6.28E+07	3.76E+08	4%	14%	82%	7.95E+07	2.27E+07	5.30E+07	3.01E+07	21%	50%	28%
253.2166	*11.74*		2.04E+07	1.34E+07	1.37E+07	1.48E+07	32%	33%	35%	8.24E+06	6.37E+06	6.77E+06	5.36E+06	34%	37%	29%
241.2168	*11.82*		9.34E+07	6.60E+07	6.71E+07	7.65E+07	32%	32%	36%	4.89E+07	1.47E+07	1.67E+07	1.47E+07	32%	36%	32%
280.2637	*11.84*	Long chain carboxylic acids	1.28E+07	5.43E+06	1.00E+07	6.10E+06	25%	46%	28%	5.19E+03	3.56E+03	1.56E+03	3.12E+03	43%	19%	38%
267.2321	*12.06*		1.88E+07	8.37E+06	7.48E+06	8.67E+06	34%	31%	35%	6.14E+06	3.68E+06	3.93E+06	3.51E+06	33%	35%	32%
281.2478	*12.48*		2.10E+08	7.70E+07	9.68E+07	2.22E+08	19%	24%	56%	3.74E+07	2.54E+07	2.41E+07	1.26E+07	41%	39%	20%
269.2478	*12.67*		7.49E+06	4.07E+06	3.94E+06	4.41E+06	33%	32%	35%	1.60E+06	9.70E+05	1.16E+06	8.91E+05	32%	38%	29%
393.2768	*12.69*		1.32E+06	2.04E+06	2.13E+06	1.94E+06	33%	35%	32%	1.07E+07	1.12E+07	1.01E+07	1.07E+07	35%	32%	33%
283.2635	*13.44*		1.03E+08	6.52E+07	6.68E+07	7.61E+07	31%	32%	37%	1.26E+07	1.13E+07	8.90E+06	1.18E+07	35%	28%	37%

APPENDIX 5: METABOLOMICS DATA FOR PK ANALYSIS

row m/z	Putative Identity/EF	f-50	f-25	f-12.5	f-5	f-1	m-50	m-25	m-12.5	m-5	m-1
70.0656	1-Pyrroline	-	+	+	NC	+	NC	-	NC	NC	NC
72.0812	Pyrrolidine	NC	+++	+	NC	+++	NC	NC	+	NC	NC
74.0603	C3H7NO	NC	+	+++	-	-	-	-	-	NC	-
80.0499	Pyridine	+	NC	+	-	-	NC	+	+++	NC	+
84.0812	C5H9N	NC	+	+	NC	+	+	+	NC	NC	NC
86.0967	Piperidine	+	+	+	-	+	NC	+	+	+	NC
88.0396	C3H5NO2	+	+++	+	NC	NC	+	+	+	NC	NC
102.0551	C4H7NO2	-	+	+	NC	+	+	+++	+++	NC	NC
104.0708	N-methyl-alanine	NC	+	+	NC	NC	NC	+	+	NC	NC
104.1071	Choline	NC	+++	NC	-	+	+	+++	+++	+	NC
106.0864	C4H11NO2	+++	+++	-	NC	-	NC	-	NC	+++	NC
112.0507	Cytosine	+	+++	+	NC	+	+	-	+	NC	+
114.0662	Creatinine	NC	+	NC	NC	NC	NC	NC	NC	NC	NC
117.0739	C6H12S	-	+	+	NC	+	-	-	NC	NC	NC
118.0651	Glycocyamine	-	+	+	NC	+	NC	+	+	-	NC
118.1222	2-Diethylaminoethanol	-	+++	+++	-	-	+	NC	-	NC	+
119.0898	C6H11S	-	+	+	NC	NC	-	NC	NC	NC	NC
120.0807	Indoline	NC	+++	+	NC	+++	+	+	+	+	NC
123.0442	C7H6O2	NC	+	+	+	NC	-	NC	NC	NC	NC
126.0658	5-Methylcytosine	+	+++	+++	+	NC	+	+	+	+	+
129.0658	5,6-Dihydrothymine	-	NC	NC	-	NC	-	NC	NC	NC	NC
130.0498	4-Oxoproline	-	+	+	NC	NC	-	NC	+	-	NC
130.0861	C6H11NO2	NC	+	+++	NC	+	NC	+	NC	NC	NC
132.0654	Hydroxyproline	NC	+	+	NC	NC	NC	NC	+	NC	+
132.0766	Creatine	+	+++	+	NC	+	+	+++	+	+	NC
133.0802	Ornithine	+	+++	+	NC	+	+	+++	+	+	NC
136.0757	C8H9NO	+	+++	+	NC	NC	NC	NC	NC	NC	+
137.0705	N-methylnicotinamide	NC	+++	NC	NC	+++	+	+	-	NC	+++
138.0547	Aminobenzoic acid	-	+	NC	NC	NC	NC	NC	NC	NC	NC
139.0502	C6H6N2O2	+++	+	+	-	+++	NC	-	-	+	+
144.0808	Naphthylamine	-	+	+	NC	+	NC	NC	+	-	NC
144.1019	C7H13NO2	-	+	NC	NC	NC	NC	NC	+	NC	NC
146.0599	C9H7NO	-	+	+	NC	+	NC	NC	+	-	NC
146.1648	Spermidine	-	-	-	-	-	+	-	-	-	+++
147.0436	C9H6O2	+	+++	+	NC	+	NC	NC	NC	NC	NC
152.0532	C8H9NS	-	+	+	NC	+	NC	+	+	NC	NC
159.0762	4-methylene-glutamine	NC	+++	+	NC	NC	NC	NC	NC	NC	+
159.0912	C10H10N2	-	+	+	NC	+	NC	NC	+	-	NC
160.0756	C10H9NO	-	+	NC	NC	NC	NC	+	NC	NC	NC
160.1330	C8H17NO2	NC	+	+	NC	NC	NC	+	+	NC	NC
162.0763	N-Methyl-glutamate	+	+++	+++	+++	-	NC	NC	NC	-	+++
162.1122	Carnitine	NC	+	+	+	NC	NC	NC	NC	NC	NC
165.0543	C9H8O3	NC	NC	NC	+	-	NC	NC	NC	NC	NC
168.0769	Carbazole	NC	+	+++	+	NC	NC	+	NC	NC	-
170.0595	C4H12NO4P	-	+	+	NC	+	NC	NC	+	-	NC
170.0924	N-methyl-histidine	NC	NC	NC	NC	+	+	+	NC	NC	+
175.1075	N-acetyl-ornithine	NC	+	+++	-	+	+++	+++	+	+	+
177.1018	Canavanine	-	+++	NC	NC	NC	NC	+	NC	-	NC
180.0866	beta-D-Glucosamine	+++	+++	+++	+++	-	-	+	NC	-	+++
188.0703	C11H9NO2	-	+	+	NC	+	NC	NC	+	-	NC
204.1229	Acetyl-Carnitine	NC	+	+	+	NC	-	+++	-	+++	NC
223.0742	C7H14N2O4S	-	NC	NC	-	-	NC	+	NC	-	+
228.0975	Deoxycytidine	+	+++	+++	NC	+	+	+++	+	NC	+
229.1184	C10H16N2O4	+	+++	NC	+	+++	+	+	+	+	+
231.1341	C15H18O2	-	-	NC	+	+	-	-	NC	NC	-
231.1713	Leucine-Valine	NC	+	+	NC	NC	NC	+++	NC	NC	NC
244.0921	Cytidine	+++	NC	NC	+	+	-	+++	+++	-	+++
259.0918	5-methyluridine	-	NC	+	NC	NC	+	+	+++	NC	NC
263.1449	Methionine-Leucine	NC	+++	-	+++	+++	+	+	+	+++	NC
268.1037	Adenosine	-	-	NC	+	+++	+	-	-	+	NC
276.1184	C10H17N3O6	-	NC	+	NC	-	-	-	NC	-	NC
276.1548	C11H21N3O5	+	+	NC	+++	-	+	-	+++	-	+
283.1074	BNC-1	+++	+++	+++	+++	+	+++	+++	+++	+++	+
284.1019	Guanosine	-	+++	+++	+++	+	+++	+++	+++	+++	+
288.2889	C17H37NO2	+	+	-	+++	NC	+	NC	-	+++	-
299.1028	BNC-1 oxidized	+++	+++	+++	+++	+	+++	+++	+++	+++	NC
351.1985	C18H26N2O5	NC	+	-	NC	-	+	NC	+++	NC	+++
Amino Acids		f-50	f-25	f-12.5	f-5	f-1	m-50	m-25	m-12.5	m-5	m-1
76.0397	Glycine	NC	+++	+	NC	NC	+	+	NC	NC	NC
90.0552	Alanine	NC	+	+	NC	+	NC	+	+	NC	NC
106.0499	Serine	+	+++	+++	NC	NC	+	+	+	NC	NC
116.0708	Proline	-	NC	+++	NC	+	-	-	NC	NC	NC
118.0862	Valine	-	+	+	NC	NC	-	NC	NC	NC	NC
120.0654	Threonine	-	+	+	NC	+	+	+++	+	NC	NC
132.1018	Leucine	NC	+++	+++	-	+++	NC	+++	NC	NC	+
132.1018	Isoleucine	+	+	NC	+++	NC	+	NC	+++	NC	-
133.0607	Asparagine	-	+	+	NC	+	+	+	+	-	NC
134.0446	Aspartate	+	+	+	-	NC	+++	+++	+	+	NC
147.0763	Glutamine	-	+	+	NC	NC	NC	NC	+	-	NC
147.1126	Lysine	NC	+	+++	-	+	NC	+	+	NC	NC
148.0603	Glutamate	-	+	NC	-	+	+	+	+	NC	+
150.0582	Methionine	-	+	+	NC	+	NC	+	+	NC	NC
156.0767	Histidine	-	+	+	NC	+	NC	NC	NC	NC	+
166.0861	Phenylalanine	NC	+++	+	NC	+++	NC	+	+	NC	NC
175.1189	Arginine	NC	+	+++	-	+	NC	NC	NC	NC	+
182.0810	Tyrosine	+	+++	+	NC	+	NC	+	NC	NC	+
205.0969	Tryptophan	-	+	+	NC	+	NC	NC	+	-	NC
241.0313	Cystine	NC	NC	-	-	+	-	NC	NC	-	+

REFERENCES

(1) Cragg, G. M.; Newman, D. J. Biodiversity: A Continuing Source of Novel Drug Leads. *Pure Appl. Chem.* **2005**, *77* (1), 7–24. https://doi.org/10.1351/pac200577010007.

(2) Dias, D. A.; Urban, S.; Roessner, U. A Historical Overview of Natural Products in Drug Discovery. *Metabolites* **2012**, *2* (2), 303–336. https://doi.org/10.3390/metabo2020303.

(3) Calixto, J. B. The Role of Natural Products in Modern Drug Discovery.Calixto, J. B. (2019). The Role of Natural Products in Modern Drug Discovery. Anais Da Academia Brasileira de Ciencias, 91, 1–7. Https://Doi.Org/10.1590/0001-3765201920190105. *An. Acad. Bras. Cienc.* **2019**, *91*, 1–7. https://doi.org/10.1590/0001-3765201920190105.Abstract.

(4) Harvey, A. L. Natural Products in Drug Discovery. *Drug Discov. Today* **2008**, *13* (19–20), 894–901. https://doi.org/10.1016/j.drudis.2008.07.004.

(5) Lautié, E.; Russo, O.; Ducrot, P.; Boutin, J. A. Unraveling Plant Natural Chemical Diversity for Drug Discovery Purposes. *Front. Pharmacol.* **2020**, *11* (April), 1–37. https://doi.org/10.3389/fphar.2020.00397.

(6) Li, G.; Lou, H. X. Strategies to Diversify Natural Products for Drug Discovery. *Med. Res. Rev.* **2018**, *38* (4), 1255–1294. https://doi.org/10.1002/med.21474.

(7) Croteau, R.; Kutchan, T. M.; Lewis, N. G. Secondary Metabolites - Chap 24 (Buchanan, Biochem & Mol Biol of Plants 2000). **2000**, 1250–1318.

(8) Vining, L. C. FUNCTIONS OF SECONDARY Structural Complexity of Secondary Metabolites Waste Products. *Annu. Rev. Microbiol.* **1990**, *44*, 395–427.

(9) Sanchez, S.; Demain, A. L. Secondary Metabolites. *Compr. Biotechnol. Second Ed.* **2011**, *1*, 155–167. https://doi.org/10.1016/B978-0-08-088504-9.00018-0.

(10) BENNETT, R. N.; WALLSGROVE, R. M. Secondary Metabolites in Plant Defence Mechanisms. *New Phytol.* **1994**, *127* (4), 617–633. https://doi.org/10.1111/j.1469-8137.1994.tb02968.x.

(11) Bhattacharya, A.; Sood, P.; Citovsky, V. The Roles of Plant Phenolics in Defence and Communication during Agrobacterium and Rhizobium Infection. *Mol. Plant Pathol.* **2010**, *11* (5), 705–719. https://doi.org/10.1111/j.1364-3703.2010.00625.x.

(12) Parsaeimehr, A.; Sargsyan, E.; Vardanyan, A. Expression of Secondary Metabolites in Plants and Their Useful Perspective in Animal Health. *Int. Jounal Bioflux Soc.* **2011**, *3* (2), 129–134.

(13) Williams, D. H.; Stone, M. J.; Hauck, P. R.; Rahman, S. K. Why Are Secondary Metabolites (Natural Products) Biosynthesized. *J. Nat. Prod.* **1989**, *52* (6), 1189–1208. https://doi.org/10.1021/np50066a001.

(14) Demain, A. L.; Fang, A. The Natural Functions of Secondary Metabolites. *Adv. Biochem. Eng. Biotechnol.* **2000**, *69*, 1–39. https://doi.org/10.1007/3-540-44964-7_1.

(15) Demain, A. L. Pharmaceutically Active Secondary Metabolites of Microorganisms. *Appl. Microbiol. Biotechnol.* **1999**, *52* (4), 455–463. https://doi.org/10.1007/s002530051546.

(16) Bourgard, F.; Gravot, A.; Milesi, S.; Gontier, E. Production of Plant Secondary Metabolites: A Historical Perspective. *Plant Sci.* **2001**, *161*, 839–851.

https://doi.org/10.1166/jnn.2008.18298.
(17) Thomford, N. E.; Senthebane, D. A.; Rowe, A.; Munro, D.; Seele, P.; Maroyi, A.; Dzobo, K. Natural Products for Drug Discovery in the 21st Century: Innovations for Novel Drug Discovery. *Int. J. Mol. Sci.* **2018**, *19* (6). https://doi.org/10.3390/ijms19061578.
(18) Muir, R. M.; Ibáñez, A. M.; Uratsu, S. L.; Ingham, E. S.; Leslie, C. A.; McGranahan, G. H.; Batra, N.; Goyal, S.; Joseph, J.; Jemmis, E. D.; Dandekar, A. M. Mechanism of Gallic Acid Biosynthesis in Bacteria (Escherichia Coli) and Walnut (Juglans Regia). *Plant Mol. Biol.* **2011**, *75* (6), 555–565. https://doi.org/10.1007/s11103-011-9739-3.
(19) Lam, K. S. New Aspects of Natural Products in Drug Discovery. *Trends Microbiol.* **2007**, *15* (6), 279–289. https://doi.org/10.1016/j.tim.2007.04.001.
(20) Atanasov, A. G.; Zotchev, S. B.; Dirsch, V. M.; Orhan, I. E.; Banach, M.; Rollinger, J. M.; Barreca, D.; Weckwerth, W.; Bauer, R.; Bayer, E. A.; Majeed, M.; Bishayee, A.; Bochkov, V.; Bonn, G. K.; Braidy, N.; Bucar, F.; Cifuentes, A.; D'Onofrio, G.; Bodkin, M.; Diederich, M.; Dinkova-Kostova, A. T.; Efferth, T.; El Bairi, K.; Arkells, N.; Fan, T. P.; Fiebich, B. L.; Freissmuth, M.; Georgiev, M. I.; Gibbons, S.; Godfrey, K. M.; Gruber, C. W.; Heer, J.; Huber, L. A.; Ibanez, E.; Kijjoa, A.; Kiss, A. K.; Lu, A.; Macias, F. A.; Miller, M. J. S.; Mocan, A.; Müller, R.; Nicoletti, F.; Perry, G.; Pittalà, V.; Rastrelli, L.; Ristow, M.; Russo, G. L.; Silva, A. S.; Schuster, D.; Sheridan, H.; Skalicka-Woźniak, K.; Skaltsounis, L.; Sobarzo-Sánchez, E.; Bredt, D. S.; Stuppner, H.; Sureda, A.; Tzvetkov, N. T.; Vacca, R. A.; Aggarwal, B. B.; Battino, M.; Giampieri, F.; Wink, M.; Wolfender, J. L.; Xiao, J.; Yeung, A. W. K.; Lizard, G.; Popp, M. A.; Heinrich, M.; Berindan-Neagoe, I.; Stadler, M.; Daglia, M.; Verpoorte, R.; Supuran, C. T. Natural Products in Drug Discovery: Advances and Opportunities. *Nat. Rev. Drug Discov.* **2021**, *20* (3), 200–216. https://doi.org/10.1038/s41573-020-00114-z.
(21) Lahlou, M. The Success of Natural Products in Drug Discovery. *Pharmacol. & Pharm.* **2013**, *04* (03), 17–31. https://doi.org/10.4236/pp.2013.43a003.
(22) Newman, D. J.; Cragg, G. M.; Snader, K. M. The Influence of Natural Products upon Drug Discovery. *Nat. Prod. Rep.* **2000**, *17* (3), 215–234. https://doi.org/10.1039/a902202c.
(23) Koehn, F. E.; Carter, G. T. The Evolving Role of Natural Products in Drug Discovery. *Nat. Rev. Drug Discov.* **2005**, *4* (3), 206–220. https://doi.org/10.1038/nrd1657.
(24) Mishra, B. B.; Tiwari, V. K. Natural Products: An Evolving Role in Future Drug Discovery. *Eur. J. Med. Chem.* **2011**, *46* (10), 4769–4807. https://doi.org/10.1016/j.ejmech.2011.07.057.
(25) Panner Selvam, M. K.; Finelli, R.; Agarwal, A.; Henkel, R. Proteomics and Metabolomics — Current and Future Perspectives in Clinical Andrology. *Andrologia* **2021**, *53* (2), 1–18. https://doi.org/10.1111/and.13711.
(26) Zhang, A.; Sun, H.; Wang, P.; Han, Y.; Wang, X. Modern Analytical Techniques in Metabolomics Analysis. *Analyst* **2012**, *137* (2), 293–300. https://doi.org/10.1039/c1an15605e.
(27) Hollywood, K.; Brison, D. R.; Goodacre, R. Metabolomics: Current Technologies and Future Trends. *Proteomics* **2006**, *6* (17), 4716–4723.

https://doi.org/10.1002/pmic.200600106.
(28) Hoffmann, E. de.; Stroobant, V. *Mass spectrometry : principles and applications*; J. Wiley: Chichester, West Sussex, England; Hoboken, NJ, 2007.
(29) Thompson, J. A.; Norris, K. J.; Petersen, D. R. Isolation and Analysis of N-Oxide Metabolites of Tertiary Amines: Quantitation of Nicotine-1′-N-Oxide Formation in Mice. *J. Chromatogr. B Biomed. Sci. Appl.* **1985**, *341* (C), 349–359. https://doi.org/10.1016/S0378-4347(00)84048-7.
(30) McCullagh, J.; Oldham, N. *Mass Spectrometry*; Oxford University Press: Oxford, United Kingdom, 2019.
(31) Skoog, D. A.; Holler, F. J.; Crouch, S. R. *Principles of Instrumental Analysis*; Cengage learning, 2017.
(32) Fenn, J. B.; Mann, M.; Meng, C. K.; Wong, S. F. Electrospray Ionization-Principles and Practice. **1990**, 37–70.
(33) Covey, T.; Thomson, B.; Schneider, B. Atmospheric Pressure Ion Sources. *Mass Spectrom. Rev.* **2009**, *28*, 870–897. https://doi.org/10.1002/mas.
(34) Ahadi, E.; Konermann, L. Ejection of Solvated Ions from Electrosprayed Methanol/Water Nanodroplets Studied by Molecular Dynamics Simulations. *J. Am. Chem. Soc.* **2011**, *133* (24), 9354–9363. https://doi.org/10.1021/ja111492s.
(35) Konermann, L.; Ahadi, E.; Rodriguez, A. D.; Vahidi, S. Unraveling the Mechanism of Electrospray Ionization. *Anal. Chem.* **2013**, *85* (1), 2–9. https://doi.org/10.1021/ac302789c.
(36) Campana, J. E. Elementary Theory of the Quadrupole Mass Filter. *Int. J. Mass Spectrom. Ion Phys.* **1980**, *33* (2), 101–117. https://doi.org/10.1016/0020-7381(80)80042-8.
(37) Titov, V. V. Detailed Study of the Quadrupole Mass Analyzer Operating within the First, Second, and Third (Intermediate) Stability Regions. II. Transmission and Resolution. *J. Am. Soc. Mass Spectrom.* **1998**, *9* (1), 70–87. https://doi.org/10.1016/S1044-0305(97)00194-3.
(38) Yost, R. A. Triple Quadrupole Mass Spectrometry for Direct Mixture Analysis and Structure Elucidation. *Analytical Chemistry*. 1979. https://doi.org/10.1021/ac50048a002.
(39) Makarov, A. Electrostatic Axially Harmonic Orbital Trapping: A High-Performance Technique of Mass Analysis. *Anal. Chem.* **2000**, *72* (6), 1156–1162. https://doi.org/10.1021/ac991131p.
(40) Hu, Q.; Noll, R. J.; Li, H.; Makarov, A.; Hardman, M.; Cooks, R. G. The Orbitrap: A New Mass Spectrometer. *J. Mass Spectrom.* **2005**, *40* (4), 430–443. https://doi.org/10.1002/jms.856.
(41) Nolting, D.; Malek, R.; Makarov, A. Ion Traps in Modern Mass Spectrometry. *Mass Spectrom. Rev.* **2019**, *38* (2), 150–168. https://doi.org/10.1002/mas.21549.
(42) Zubarev, R. A.; Makarov, A. Orbitrap Mass Spectrometry. *Anal. Chem.* **2013**, *85* (11), 5288–5296. https://doi.org/10.1021/ac4001223.
(43) Singh, C.; Zampronio, C. G.; Creese, A. J.; Cooper, H. J. Higher Energy Collision Dissociation (HCD) Product Ion-Triggered Electron Transfer Dissociation (ETD) Mass Spectrometry for the Analysis of N-Linked Glycoproteins. *J. Proteome Res.* **2012**, *11* (9), 4517–4525. https://doi.org/10.1021/pr300257c.
(44) Jedrychowski, M. P.; Huttlin, E. L.; Haas, W.; Sowa, M. E.; Rad, R.; Gygi, S. P.

Evaluation of HCD- and CID-Type Fragmentation within Their Respective Detection Platforms for Murine Phosphoproteomics. *Mol. Cell. Proteomics* **2011**, *10* (12), M111.009910. https://doi.org/10.1074/mcp.M111.009910.

(45) Frese, C. K.; Altelaar, A. F. M.; Hennrich, M. L.; Nolting, D.; Zeller, M.; Griep-Raming, J.; Heck, A. J. R.; Mohammed, S. Improved Peptide Identification by Targeted Fragmentation Using CID, HCD and ETD on an LTQ-Orbitrap Velos. *J. Proteome Res.* **2011**, *10* (5), 2377–2388. https://doi.org/10.1021/pr1011729.

(46) Jora, M.; Burns, A. P.; Ross, R. L.; Lobue, P. A.; Zhao, R.; Palumbo, C. M.; Beal, P. A.; Addepalli, B.; Limbach, P. A. Differentiating Positional Isomers of Nucleoside Modifications by Higher-Energy Collisional Dissociation Mass Spectrometry (HCD MS). *J. Am. Soc. Mass Spectrom.* **2018**, *29* (8), 1–18. https://doi.org/10.1007/s13361-018-1999-6.Differentiating.

(47) Kirkland, J. J. Development of Some Stationary Phases for Reversed-Phase High-Performance Liquid Chromatography. *J. Chromatogr. A* **2004**, *1060* (1-2 SPEC. ISS.), 9–21. https://doi.org/10.1016/j.chroma.2004.10.057.

(48) Manzi, P.; Panfili, G.; Pizzoferrato, L. Normal and Reversed-Phase HPLC for More Complete: Evaluation of Tocopherols, Retinols, Carotenes and Sterols in Dairy Products. *Chromatographia* **1996**, *43* (1–2), 89–93. https://doi.org/10.1007/BF02272829.

(49) Nakajima, K.; Kitazume, S.; Angata, T.; Fujinawa, R.; Ohtsubo, K.; Miyoshi, E.; Taniguchi, N. Simultaneous Determination of Nucleotide Sugars with Ion-Pair Reversed-Phase HPLC. *Glycobiology* **2010**, *20* (7), 865–871. https://doi.org/10.1093/glycob/cwq044.

(50) Rodrigues, A. E. CHROMATOGRAPHY | Convective Transport in Chromatographic Media; Wilson, I. D. B. T.-E. of S. S., Ed.; Academic Press: Oxford, 2000; pp 352–358. https://doi.org/https://doi.org/10.1016/B0-12-226770-2/05501-0.

(51) Shallan, A.; Guijt, R.; Breadmore, M. Capillary Electrophoresis: Basic Principles; Siegel, J. A., Saukko, P. J., Houck, M. M. B. T.-E. of F. S. (Second E., Eds.; Academic Press: Waltham, 2013; pp 549–559. https://doi.org/https://doi.org/10.1016/B978-0-12-382165-2.00241-5.

(52) James, N. Capillary Electrophoresis. **1995**.

(53) Jorgenson, J. W.; Lukacs, K. D. Capillary Zone Electrophoresis. *Science (80-.).* **1983**, *222* (4621), 266–272.

(54) Olivares, J. A.; Nguyen, N. T.; Yonker, C. R.; Smith, R. D. On-Line Mass Spectrometric Detection for Capillary Zone Electrophoresis. *Anal. Chem.* **1987**, *59* (8), 1230–1232. https://doi.org/10.1021/ac00135a034.

(55) Ewing, A.; Wallingford, R.; Olefirowicz. Capillary Electrophoresis Capillary Electrophoresis. *Anal. Chem.* **1989**, *61* (4), 292A-303A.

(56) Schmitt-Kopplin, P.; Frommberger, M. Capillary Electrophoresis - Mass Spectrometry: 15 Years of Developments and Applications. *Electrophoresis* **2003**, *24* (22–23), 3837–3867. https://doi.org/10.1002/elps.200305659.

(57) Hirayama, A.; Abe, H.; Yamaguchi, N.; Tabata, S.; Tomita, M.; Soga, T. Development of a Sheathless CE-ESI-MS Interface. *Electrophoresis* **2018**, *39* (11), 1382–1389. https://doi.org/10.1002/elps.201800017.

(58) Mellors, J. S.; Gorbounov, V.; Ramsey, R. S.; Ramsey, J. M. Fully Integrated

Glass Microfluidic Device for Performing High-Efficiency Capillary Electrophoresis and Electrospray Ionization Mass Spectrometry. *Anal. Chem.* **2008**, *80* (18), 6881–6887. https://doi.org/10.1021/ac800428w.

(59) Chambers, A. G.; Mellors, J. S.; Henley, W. H.; Ramsey, J. M. Monolithic Integration of Two-Dimensional Liquid Chromatography-Capillary Electrophoresis and Electrospray Ionization on a Microfluidic Device. *Anal. Chem.* **2011**, *83* (3), 842–849. https://doi.org/10.1021/ac102437z.

(60) Mellors, J. S.; Black, W. A.; Chambers, A. G.; Starkey, J. A.; Lacher, N. A.; Ramsey, J. M. Hybrid Capillary/Microfluidic System for Comprehensive Online Liquid Chromatography-Capillary Electrophoresis-Electrospray Ionization-Mass Spectrometry. *Anal. Chem.* **2013**, *85* (8), 4100–4106. https://doi.org/10.1021/ac400205a.

(61) Batz, N. G.; Mellors, J. S.; Alarie, J. P.; Ramsey, J. M. Chemical Vapor Deposition of Aminopropyl Silanes in Microfluidic Channels for Highly Efficient Microchip Capillary Electrophoresis-Electrospray Ionization-Mass Spectrometry. *Anal. Chem.* **2014**, *86* (7), 3493–3500. https://doi.org/10.1021/ac404106u.

(62) Khatri, K.; Klein, J. A.; Haserick, J. R.; Leon, D. R.; Costello, C. E.; McComb, M. E.; Zaia, J. Microfluidic Capillary Electrophoresis-Mass Spectrometry for Analysis of Monosaccharides, Oligosaccharides, and Glycopeptides. *Anal. Chem.* **2017**, *89* (12), 6645–6655. https://doi.org/10.1021/acs.analchem.7b00875.

(63) Wang, Y.; Feng, P.; Sosic, Z.; Zang, L. Monitoring Glycosylation Profile and Protein Titer in Cell Culture Samples Using ZipChip CE-MS. *J. Anal. Bioanal. Tech.* **2017**, *08* (02). https://doi.org/10.4172/2155-9872.1000359.

(64) Beri, J.; Kirkwood, K. I.; Muddiman, D. C.; Bereman, M. S. A Novel Integrated Strategy for the Detection and Quantification of the Neurotoxin β-N-Methylamino-l-Alanine in Environmental Samples. *Anal. Bioanal. Chem.* **2018**, *410* (10), 2597–2605. https://doi.org/10.1007/s00216-018-0930-0.

(65) Zhang, Y.; Wang, Y.; Sosic, Z.; Zang, L.; Bergelson, S.; Zhang, W. Identification of Adeno-Associated Virus Capsid Proteins Using ZipChip CE/MS. *Anal. Biochem.* **2018**, *555* (June), 22–25. https://doi.org/10.1016/j.ab.2018.06.006.

(66) Kelley, Z. D.; Rogers, D. T.; Littleton, J. M.; Lynn, B. C. Microfluidic Capillary Zone Electrophoresis Mass Spectrometry Analysis of Alkaloids in Lobelia Cardinalis Transgenic and Mutant Plant Cell Cultures. *Electrophoresis* **2019**, *40* (22), 2921–2928. https://doi.org/10.1002/elps.201900220.

(67) Evans, W. C.; Evans, D. Alkaloids. In *Trease and Evans' Pharmacognosy: Sixteenth Edition*; Evans, W. C., Evans, D., Eds.; W.B. Saunders, 2009; pp 353–415. https://doi.org/10.1016/B978-0-7020-2933-2.00026-5.

(68) Bribi, N. Pharmacological Activity of Alkaloids. A Review. *Asian J. Bot.* **2018**, *1*, 1–6. https://doi.org/10.63019/ajb.v1i2.467.

(69) Nardin, T.; Piasentier, E.; Barnaba, C.; Larcher, R. Alkaloid Profiling of Herbal Drugs Using High Resolution Mass Spectrometry. *Drug Test. Anal.* **2018**, *10* (3), 423–448. https://doi.org/10.1002/dta.2252.

(70) Ziegler, J.; Facchini, P. J. Alkaloid Biosynthesis: Metabolism and Trafficking. *Annu. Rev. Plant Biol.* **2008**, *59*, 735–769. https://doi.org/10.1146/annurev.arplant.59.032607.092730.

(71) Gupta R. N., Spenser, I. D. Biosynthesis of Lobinaline. *Can. J. Chem.* **1971**, *49*,

384–397.
(72) Gupta, R. N., Spenser, I. D. Biosynthesis of Piperidine Alkaloids. *Chem. Commun.* **1966**, *24* (815), 893–894. https://doi.org/10.1039/c2cc35637f.
(73) Oberlies, N. H.; Kim, N.-C.; Brine, D. R.; Collins, B. J.; Handy, R. W.; Sparacino, C. M.; Wani, M. C.; Wall, M. E. Analysis of Herbal Teas Made from the Leaves of Comfrey (Symphytum Officinale): Reduction of N-Oxides Results in Order of Magnitude Increases in the Measurable Concentration of Pyrrolizidine Alkaloids. *Public Health Nutr.* **2004**, *7* (7), 919–924. https://doi.org/10.1079/phn2004624.
(74) Lindigkeit, R.; Biller, A.; Buch, M.; Schiebel, H. M.; Boppré, M.; Hartmann, T. The Two Faces of Pyrrolizidine Alkaloids: The Role of the Tertiary Amine and Its n-Oxide in Chemical Defense of Insects with Acquired Plant Alkaloids. *Eur. J. Biochem.* **1997**, *245* (3), 626–636. https://doi.org/10.1111/j.1432-1033.1997.00626.x.
(75) van de Schans, M. G. M.; Blokland, M. H.; Zoontjes, P. W.; Mulder, P. P. J.; Nielen, M. W. F. Multiple Heart-Cutting Two Dimensional Liquid Chromatography Quadrupole Time-of-Flight Mass Spectrometry of Pyrrolizidine Alkaloids. *J. Chromatogr. A* **2017**, *1503*, 38–48. https://doi.org/10.1016/j.chroma.2017.04.059.
(76) Tian, Y.; Zhang, C.; Guo, M. Comparative Study on Alkaloids and Their Anti-Proliferative Activities from Three Zanthoxylum Species. *BMC Complement. Altern. Med.* **2017**, *17* (1), 1–16. https://doi.org/10.1186/s12906-017-1966-y.
(77) Phillipson, J. D.; Handa, S. S.; El-Dabbas, S. W. N-Oxides of Morphine, Codeine and Thebaine and Their Occurrence in Papaver Species. *Phytochemistry* **1976**, *15* (8), 1297–1301. https://doi.org/10.1016/0031-9422(76)90003-0.
(78) Kopp, T.; Abdel-Tawab, M.; Mizaikoff, B. Extracting and Analyzing Pyrrolizidine Alkaloids in Medicinal Plants: A Review. *Toxins (Basel).* **2020**, *12* (5), 7–10. https://doi.org/10.3390/toxins12050320.
(79) Shen, B. A New Golden Age of Natural Products Drug Discovery. *Cell* **2015**, *163* (6), 1297–1300. https://doi.org/10.1016/j.cell.2015.11.031.A.
(80) Manske, R. Lobinaline, an Alkaloid from Lobelia Cardinalis. *Can. J. Res.* **1938**, *16* (B), 445–448.
(81) Brown, Dustin P. , Rogers, Dennis T. , Pomerleaua, Francois, Siripurapuc, Kirin B. , Kulshresthad, Manish, Gerhardt, Greg A. , and Littleton, J. M. Novel Multifunctional Pharmacology of Lobinaline, the Major Alkaloid from Lobelia Cardinalis. *Fitoterapia* **2016**, *111*, 109–123. https://doi.org/doi:10.1016/j.fitote.2016.04.013.
(82) Brown, D. P.; Rogers, D. T.; Gunjan, S. K.; Gerhardt, G. A.; Littleton, J. M. Target-Directed Discovery and Production of Pharmaceuticals in Transgenic Mutant Plant Cells. *J. Biotechnol.* **2016**, *238*, 9–14. https://doi.org/10.1016/j.jbiotec.2016.09.007.
(83) Felpin, F.-X.; Lebreton, J. History, Chemistry and Biology of Alkaloids from Lobelia Inflata. *Tetrahedron* **2004**, *60* (45), 10127–10153. https://doi.org/10.1016/j.tet.2004.08.010.
(84) St-Pierre A, L. A. and D. P. I. Determination of Piperidine Alkaloids from Indian Tobacco (Lobelia Inflata) Plants and Plant-Derived Products. *Austin Biochem.* **2017**, *2* (2), 1014.

(85) Colau, B.; Hootelé, C. Sedum Alkaloids. V. Sedacrine, the Major Alkaloid of Sedum Acre , and Related Bases . *Can. J. Chem.* **1983**, *61* (3), 470–472. https://doi.org/10.1139/v83-083.
(86) Robison, M.; Pierson, W. G.; Dorfhum, L.; Lambert, B. F.; Lucas, R. A. The Structure of Lobinaline. *Tetrahedron Lett.* **1963**, No. 24, 1513–1519.
(87) Robison, M. M.; Lambert, B. F.; Dorfman, L.; Pierson, W. G. The Stereochemistry and Synthesis of the Lobinaline Ring System. *J. Org. Chem.* **1966**, *31* (10), 3220–3223. https://doi.org/10.1021/jo01348a029.
(88) Robison, M. M.; Pierson, W. G.; Dorfman, L.; Lambert, B. F.; Lucas, R. A. The Skeletal Structure of Lobinaline. *J. Org. Chem.* **1966**, *31* (10), 3206–3213. https://doi.org/10.1021/jo01348a027.
(89) Littleton, J. M. Personal Correspondence. 2021.
(90) Olivon, F.; Grelier, G.; Roussi, F.; Litaudon, M.; Touboul, D. MZmine 2 Data-Preprocessing to Enhance Molecular Networking Reliability. *Anal. Chem.* **2017**, *89* (15), 7836–7840. https://doi.org/10.1021/acs.analchem.7b01563.
(91) Wong, F. C.; Yong, A. L.; Sim, K. M.; Ong, H. C.; Chai, T. T. Proteomic Analysis of Bacterial Expression Profiles Following Exposure to Organic Solvent Flower Extract of Melastoma Candidum D Don (Melastomataceae). *Trop. J. Pharm. Res.* **2014**, *13* (7), 1085–1092. https://doi.org/10.4314/tjpr.v13i7.11.
(92) Li, J.; Zhao, W.; Li, J.; Xia, W.; Lei, L.; Zhao, S. Research Methods to Study Plant Secondary Metabolic Pathways and Their Applications in the Analysis of the Biosynthetic Pathway of Stilbenes from Polygonum Multiflorum -A Review. *Plant Omics* **2014**, *7* (3), 158–165.
(93) Hofmann, T.; Nebehaj, E.; Albert, L. The High-Performance Liquid Chromatography/Multistage Electrospray Mass Spectrometric Investigation and Extraction Optimization of Beech (Fagus Sylvatica L.) Bark Polyphenols. *J. Chromatogr. A* **2015**, *1393*, 96–105. https://doi.org/10.1016/j.chroma.2015.03.030.
(94) Quideau, S.; Deffieux, D.; Douat-Casassus, C.; Pouységu, L. Plant Polyphenols: Chemical Properties, Biological Activities, and Synthesis. *Angew. Chemie - Int. Ed.* **2011**, *50* (3), 586–621. https://doi.org/10.1002/anie.201000044.
(95) Tasioula-Margari, M.; Tsabolatidou, E. Extraction, Separation, and Identification of Phenolic Compounds in Virgin Olive Oil by HPLC-DAD and HPLC-MS. *Antioxidants* **2015**, *4* (3), 548–562. https://doi.org/10.3390/antiox4030548.
(96) Watson, R. R. *Polyphenols in Plants: Isolation, Purification and Extract Preparation*; Elsevier Science, 2018.
(97) Jimenez-Lopez, C.; Pereira, A. G.; Lourenço-Lopes, C.; Garcia-Oliveira, P.; Cassani, L.; Fraga-Corral, M.; Prieto, M. A.; Simal-Gandara, J. Main Bioactive Phenolic Compounds in Marine Algae and Their Mechanisms of Action Supporting Potential Health Benefits. *Food Chem.* **2021**, *341* (September 2020), 128262. https://doi.org/10.1016/j.foodchem.2020.128262.
(98) Liu, Y.; Wang, Q.; Yang, J.; Guo, X.; Liu, W.; Ma, S.; Li, S. Polygonum Multiflorum Thunb.: A Review on Chemical Analysis, Processing Mechanism, Quality Evaluation, and Hepatotoxicity. *Front. Pharmacol.* **2018**, *9* (APR), 1–16. https://doi.org/10.3389/fphar.2018.00364.
(99) Nie, B.; Henion, J.; Ryona, I. The Role of Mass Spectrometry in the Cannabis Industry. *J. Am. Soc. Mass Spectrom.* **2019**, *30* (5), 719–730.

https://doi.org/10.1007/s13361-019-02164-z.
(100) dos Santos, N. A. Analysis of Isomeric Cannabinoid Standards and Cannabis Products by UHPLC-ESI-TWIM-MS.
(101) Berman, P.; Futoran, K.; Lewitus, G. M.; Mukha, D.; Benami, M.; Shlomi, T.; Meiri, D. A New ESI-LC/MS Approach for Comprehensive Metabolic Profiling of Phytocannabinoids in Cannabis. *Sci. Rep.* **2018**, *8* (1), 1–15. https://doi.org/10.1038/s41598-018-32651-4.
(102) McRae, G.; Melanson, J. E. Quantitative Determination and Validation of 17 Cannabinoids in Cannabis and Hemp Using Liquid Chromatography-Tandem Mass Spectrometry. *Anal. Bioanal. Chem.* **2020**, *412* (27), 7381–7393. https://doi.org/10.1007/s00216-020-02862-8.
(103) Maralikova, B.; Weinmann, W. Simultaneous Determination of Δ9 - Tetrahydrocannabinol, 11-Hydroxy- Δ9 -Tetrahydrocannabinol and 11 -nor-9-Carboxy- Δ9 - Tetrahydrocannabinol in Human Plasma by High-Performance Liquid Chromatography/Tandem Mass Spectrometry. *J. Mass Spectrom.* **2004**, *39* (5), 526–531. https://doi.org/10.1002/jms.616.
(104) Christinat, N.; Savoy, M. C.; Mottier, P. Development, Validation and Application of a LC-MS/MS Method for Quantification of 15 Cannabinoids in Food. *Food Chem.* **2020**, *318* (October 2019), 126469. https://doi.org/10.1016/j.foodchem.2020.126469.
(105) Cardenia, V.; Gallina Toschi, T.; Scappini, S.; Rubino, R. C.; Rodriguez-Estrada, M. T. Development and Validation of a Fast Gas Chromatography/Mass Spectrometry Method for the Determination of Cannabinoids in Cannabis Sativa L. *J. Food Drug Anal.* **2018**, *26* (4), 1283–1292. https://doi.org/10.1016/j.jfda.2018.06.001.
(106) Comeau, Z. J.; Boileau, N. T.; Lee, T.; Melville, O. A.; Rice, N. A.; Troung, Y.; Harris, C. S.; Lessard, B. H.; Shuhendler, A. J. On-the-Spot Detection and Speciation of Cannabinoids Using Organic Thin-Film Transistors. *ACS Sensors* **2019**, *4* (10), 2706–2715. https://doi.org/10.1021/acssensors.9b01150.
(107) Bounda, G.-A.; Feng, Y. U. Review of Clinical Studies of Polygonum Multiflorum Thunb. and Its Isolated Bioactive Compounds. *Pharmacognosy Res.* **2015**, *7* (3), 225–236. https://doi.org/10.4103/0974-8490.157957.
(108) Li, X.; Matsumoto, K.; Murakami, Y.; Tezuka, Y.; Wu, Y.; Kadota, S. Neuroprotective Effects of Polygonum Multiflorum on Nigrostriatal Dopaminergic Degeneration Induced by Paraquat and Maneb in Mice. *Pharmacol. Biochem. Behav.* **2005**, *82* (2), 345–352. https://doi.org/10.1016/j.pbb.2005.09.004.
(109) Zhang, L.; Chen, J. Biological Effects of Tetrahydroxystilbene Glucoside: An Active Component of a Rhizome Extracted from Polygonum Multiflorum. *Oxid. Med. Cell. Longev.* **2018**, *2018*. https://doi.org/10.1155/2018/3641960.
(110) Meurer, E. C.; Sabino, A. A.; Eberlin, M. N. Ionic Transacetalization with Acylium Ions: A Class-Selective and Structurally Diagnostic Reaction for Cyclic Acetals Performed under Unique Electrospray and Atmospheric Pressure Chemical Ionization in-Source Ion-Molecule Reaction Conditions. *Anal. Chem.* **2003**, *75* (17), 4701–4709. https://doi.org/10.1021/ac0344384.
(111) Middlemiss, N. E.; Harrison, A. G. The Structure and Fragmentation of Protonated Carboxylic Acids in the Gas Phase. *Can. J. Chem.* **1979**, *57* (21), 2827–2833.

https://doi.org/10.1139/v79-459.
(112) Kingston, D. G. I.; Hobrock, B. W.; Bursey, M. M.; Bursey, J. T. Intramolecular Hydrogen Transfer in Mass Spectra. III. Rearrangements Involving the Loss of Small Neutral Molecules. *Chem. Rev.* **1975**, *75* (6), 693–730. https://doi.org/10.1021/cr60298a002.
(113) Shi, H.; Wang, Y.; Hua, R. Acid-Catalyzed Carboxylic Acid Esterification and Ester Hydrolysis Mechanism: Acylium Ion as a Sharing Active Intermediate via a Spontaneous Trimolecular Reaction Based on Density Functional Theory Calculation and Supported by Electrospray Ionization-Mass. *Phys. Chem. Chem. Phys.* **2015**, *17* (45), 30279–30291. https://doi.org/10.1039/c5cp02914g.
(114) Lee, P. D.; Chang, Y. J.; Lin, K. L.; Chang, Y. Z. Simultaneous Determination of Δ 9-Tetrahydrocannabinol and 11-nor-9-Carboxy-Δ 9-Tetrahydrocannabinol in Oral Fluid Using Isotope Dilution Liquid Chromatography Tandem Mass Spectrometry. *Anal. Bioanal. Chem.* **2012**, *402* (2), 851–859. https://doi.org/10.1007/s00216-011-5439-8.
(115) Chen, N.; Zhou, S.; Palmisano, M. Clinical Pharmacokinetics and Pharmacodynamics of Lenalidomide. *Clin. Pharmacokinet.* **2017**, *56* (2), 139–152. https://doi.org/10.1007/s40262-016-0432-1.
(116) Lucas, C. J.; Galettis, P.; Schneider, J. The Pharmacokinetics and the Pharmacodynamics of Cannabinoids. *Br. J. Clin. Pharmacol.* **2018**, *84* (11), 2477–2482. https://doi.org/10.1111/bcp.13710.
(117) Backes, W. L. *Pharmacokinetics*; 2007.
(118) Lea-Henry, T. N.; Carland, J. E.; Stocker, S. L.; Sevastos, J.; Roberts, D. M. Clinical Pharmacokinetics in Kidney Disease: Fundamental Principles. *Clin. J. Am. Soc. Nephrol.* **2018**, *13* (7), 1085–1095. https://doi.org/10.2215/CJN.00340118.
(119) Roberts, S. A. High-Throughput Screening Approaches for Investigating Drug Metabolism and Pharmacokinetics. *Xenobiotica* **2001**, *31* (8–9), 557–589. https://doi.org/10.1080/00498250110060978.
(120) Sharma, A.; Thavathiru, E.; Benbrook, D. M.; City, O.; Health, O.; City, O. Plasma : Application to Pharmacokinetics Study. **2018**. https://doi.org/10.7243/2050-120X-6-2.Bioanalytical.
(121) Mao, Y.; Zhang, X.; Zhang, X.; Lu, G. Development of an HPLC Method for the Determination of Salidroside in Beagle Dog Plasma after Administration of Salidroside Injection: Application to a Pharmacokinetics Study. *J. Sep. Sci.* **2007**, *30* (18), 3218–3222. https://doi.org/10.1002/jssc.200700273.
(122) Gu, Y. Determination of 5-Fluorouracil in Human Plasma by High-Performance Liquid Chromatography (HPLC). *Trans. Tianjin Univ.* **2010**, *6*, 167–173. https://doi.org/10.1007/s12209.
(123) Ranjan, O. P.; Nayak, U. Y.; Reddy, M. S.; Dengale, S. J.; Musmade, P. B.; Udupa, N. Development and Validation of RP-HPLC Method with Ultraviolet Detection for Estimation of Montelukast in Rabbit Plasma: Application to Preclinical Pharmacokinetics. *J. Young Pharm.* **2013**, *5* (4), 133–138. https://doi.org/10.1016/j.jyp.2013.10.006.
(124) Ocque, A. J.; Hagler, C. E.; DiFrancesco, R.; Lombardo, J.; Morse, G. D. Development and Validation of an Assay to Measure Cannabidiol and Δ9-

Tetrahydrocannabinol in Human EDTA Plasma by UHPLC-MS/MS. *J. Chromatogr. B Anal. Technol. Biomed. Life Sci.* **2019**, *1112* (January), 56–60. https://doi.org/10.1016/j.jchromb.2019.03.002.

(125) Lin, Q.; Zhang, Q.; Song, X.; Gong, T.; Sun, X.; Zhang, Z. Novel LC-MS/MS Method for Analyzing Imperialine in Rat Plasma: Development, Validation, and Application to Pharmacokinetics. *J. Chromatogr. B, Anal. Technol. Biomed. life Sci.* **2013**, *938*, 51–59. https://doi.org/10.1016/j.jchromb.2013.08.033.

(126) Dubey, R.; Ghosh, M. Simultaneous Determination and Pharmacokinetic Study of Losartan, Losartan Carboxylic Acid, Ramipril, Ramiprilat, and Hydrochlorothiazide in Rat Plasma by a Liquid Chromatography/Tandem Mass Spectrometry Method. *Sci. Pharm.* **2015**, *83* (1), 107–124. https://doi.org/10.3797/scipharm.1410-15.

(127) Goldwirt, L.; Zahr, N.; Farinotti, R.; Fernandez, C. Development of a New UPLC-MSMS Method for the Determination of Temozolomide in Mice: Application to Plasma Pharmacokinetics and Brain Distribution Study. *Biomed. Chromatogr.* **2013**, *27* (7), 889–893. https://doi.org/10.1002/bmc.2877.

(128) Ananthula, S.; Janagam, D. R.; Jamalapuram, S.; Johnson, J. R.; Mandrell, T. D.; Lowe, T. L. Development and Validation of Sensitive LC/MS/MS Method for Quantitative Bioanalysis of Levonorgestrel in Rat Plasma and Application to Pharmacokinetics Study. *J. Chromatogr. B Anal. Technol. Biomed. Life Sci.* **2015**, *1003*, 47–53. https://doi.org/10.1016/j.jchromb.2015.09.006.

(129) Xie, L.; Liu, X.; Zhu, X.; Xu, Y.; Peng, S.; Sun, K.; Cai, H.; Dai, Q.; Wang, C.; Zhou, Q.; Cai, B. Development of an UHPLC-MS/MS Method for Comparative Pharmacokinetics of Nine Anthraquinones in Rats and Application to Dosage Conversion between Different Semen Cassiae Forms. *J. Pharm. Biomed. Anal.* **2019**, *174*, 696–706. https://doi.org/https://doi.org/10.1016/j.jpba.2019.07.001.

(130) Patel, P. N.; Kalariya, P. D.; Swamy, C. V.; Gananadhamu, S.; Srinivas, R. Quantitation of Acotiamide in Rat Plasma by UHPLC-Q-TOF-MS: Method Development, Validation and Application to Pharmacokinetics. *Biomed. Chromatogr.* **2016**, *30* (3), 363–368. https://doi.org/10.1002/bmc.3555.

(131) Lovell, M. A.; Lynn, B. C.; Fister, S.; Bradley-Whitman, M.; Murphy, M. P.; Beckett, T. L.; Norris, C. M. A Novel Small Molecule Modulator of Amyloid Pathology. *J. Alzheimer's Dis.* **2016**, *53* (1), 273–287. https://doi.org/10.3233/JAD-151160.

(132) Yatin, S. M.; Yatin, M.; Aulick, T.; Ain, K. B.; Butterfield, D. A. Alzheimer's Amyloid β-Peptide Associated Free Radicals Increase Rat Embryonic Neuronal Polyamine Uptake and Ornithine Decarboxylase Activity: Protective Effect of Vitamin E. *Neurosci. Lett.* **1999**, *263* (1), 17–20. https://doi.org/10.1016/S0304-3940(99)00101-9.

(133) Morrison, L. D.; Kish, S. J. Brain Polyamine Levels Are Altered in Alzheimer's Disease. *Neurosci. Lett.* **1995**, *197* (1), 5–8. https://doi.org/10.1016/0304-3940(95)11881-V.

(134) Sandusky-Beltran, L. A.; Kovalenko, A.; Ma, C.; Calahatian, J. I. T.; Placides, D. S.; Watler, M. D.; Hunt, J. B.; Darling, A. L.; Baker, J. D.; Blair, L. J.; Martin, M. D.; Fontaine, S. N.; Dickey, C. A.; Lussier, A. L.; Weeber, E. J.; Selenica, M. L. B.; Nash, K. R.; Gordon, M. N.; Morgan, D.; Lee, D. C. Spermidine/Spermine-N

1-Acetyltransferase Ablation Impacts Tauopathy-Induced Polyamine Stress Response. *Alzheimer's Res. Ther.* **2019**, *11* (1), 1–24. https://doi.org/10.1186/s13195-019-0507-y.
(135) Stark, F.; Pfannstiel, J.; Klaiber, I.; Raabe, T. Protein Kinase CK2 Links Polyamine Metabolism to MAPK Signalling in Drosophila. *Cell. Signal.* **2011**, *23* (5), 876–882. https://doi.org/10.1016/j.cellsig.2011.01.013.
(136) Guerra, G. P.; Rubin, M. A.; Mello, C. F. Modulation of Learning and Memory by Natural Polyamines. *Pharmacol. Res.* **2016**, *112*, 99–118. https://doi.org/10.1016/j.phrs.2016.03.023.
(137) Luo, J.; Yu, C. H.; Yu, H.; Borstnar, R.; Kamerlin, S. C. L.; Gräslund, A.; Abrahams, J. P.; Wärmländer, S. K. T. S. Cellular Polyamines Promote Amyloid-Beta (Aβ) Peptide Fibrillation and Modulate the Aggregation Pathways. *ACS Chem. Neurosci.* **2013**, *4* (3), 454–462. https://doi.org/10.1021/cn300170x.
(138) Minois, N.; Carmona-Gutierrez, D.; Madeo, F. Polyamines in Aging and Disease. *Aging (Albany. NY).* **2011**, *3* (8), 1–17. https://doi.org/0.18632/aging.100361.
(139) Lovell, M. A.; Lynn, B. C. Personal Correspondence. 2020.

VITA

Zachary Kelley was born and raised in Altoona, Pennsylvania. Zachary earned a B.A. in Biochemistry from Duquesne University in Pittsburgh, PA in 2016. While at Duquesne, he was granted the opportunity to enroll in the undergraduate research program and was a member of Dr. Michael Cascio's research group. He continued his studies at the University of Kentucky working under Dr. Bert C. Lynn towards a PhD in Analytical Chemistry. He is a member of the American Society for Mass Spectrometry.

Publications:

1. **Kelley, Z. D**.; Rogers, D. T.; Littleton, J. M.; Lynn, B. C. Microfluidic Capillary Zone Electrophoresis Mass Spectrometry Analysis of Alkaloids in Lobelia Cardinalis Transgenic and Mutant Plant Cell Cultures. *Electrophoresis* **2019**, 40 (22), 2921–2928. https://doi.org/10.1002/elps.201900220.
2. **Kelley, Z. D**.; Lovell, M. A.; Lynn, B. C.; Pharmacokinetic and Metabolic Analysis of an Alzheimer's Disease Therapeutic in Rat Serum Via Microfluidic CZE-MS. *Biomedical Chromatography* (in review)
3. Rogers, D. T.; Pomerleau, F.; **Kelley, Z. D.**; Brown, D.; Lynn, B. C.; Gerhart, G. A.; Littleton, J. Target-directed Evolution of Novel Inhibitors of the Dopamine Transporter in *Lobelia Cardinalis* Hairy Root Cultures. (In-progress)
4. **Kelley, Z. D.**; Lynn, B. C. Temperature Dependent Ionization Source-induced Degradation of the Carboxylic Acid Cannabinoids. (In-progress)

Presentations:

1. Poster presentation (March 2018) – 2018 Naff Symposium – “Evaluation of the 908devices microfluidic ZipChip for CE-MS analysis of lobelia cardinalis alkaloids”.
2. Poster presentation (June 2018) – Drug Discovery and Development Colloquium - “Evaluation of the 908devices microfluidic ZipChip for CE-MS analysis of lobelia cardinalis alkaloids”.
3. Poster presentation (June 2019) – ASMS Annual Meeting - Pharmacokinetic analysis of an Alzheimer's disease therapeutic in rat serum via the 908 Devices ZipChip CZE-MS.
4. Webinar – C&EN: Advanced Characterization of Intact Biotherapeutics using CE-MS, https://cen.acs.org/media/webinar/908devices_082819.html.
5. Poster presentation (June 2020) – ASMS Annual Meeting - An In-depth Evaluation of Accuracy in Cannabis Potency Testing Methods.